Isolation and characterization of compounds from seeds of *Pongamia pinnata* L.

A thesis submitted by

ANUMA SINGH

For the award of degree of

Doctor of Philosophy

Indian Institute of Technology Guwahati
Guwahati-781039, Assam, India

DECEMBER 2018

INDIAN INSTITUTE OF TECHNOLOGY GUWAHATI
Department of Biosciences and Bioengineering
Guwahati - 781039

STATEMENT

I do hereby declare that the matter embodied in this thesis is the final result of investigations carried out by me in the Department of Biosciences and Bioengineering, Indian Institute of Technology Guwahati, India, under the guidance of Prof. Latha Rangan.

In keeping with the general practice of reporting scientific observations, due acknowledgments have been made wherever the work prescribed is based on the findings of other investigators.

Anuma Singh

December, 2018

ANUMA SINGH

INDIAN INSTITUTE OF TECHNOLOGY GUWAHATI
Department of Biosciences and Bioengineering
Guwahati - 781039

December 2018

CERTIFICATE

It is certified that the work described in this thesis, entitled **"Isolation and characterization of compounds from seeds of *Pongamia pinnata* L."** done by Ms. Anuma Singh for the award of the degree of Doctor of Philosophy. It is an authentic record of the results obtained from the research work carried out under my supervision in the Department of Biosciences and Bioengineering, Indian Institute of Technology Guwahati, India, and this work has not been submitted elsewhere for a degree.

Prof. Latha Rangan

Professor

(Thesis Supervisor)

Dedicated to my beloved parents

ACKNOWLEDGMENT

First and foremost I am genuinely thankful to Prof. Latha Rangan, my thesis supervisor for her continuous guidance and support throughout my doctoral research. I would also like to thank Prof. R. Swaminathan for his constructive advice and for sharing his expertise in spectroscopic data interpretation. I sincerely thank my doctoral committee, Prof. V.V. Dasu (Former chairman), Prof. K. Pakshirajan (Chairman), Dr. S. Senthilkumar (Member) and Dr. A.B. Kunnumakkara (Member) for their support and fruitful suggestions throughout the year. I wish to acknowledge the help provided by Prof. A. Khare (Department of Physics) and Dr. A.N. Panda (Department of Chemistry) with regard to the problems related to vibrational spectroscopy. My special thanks to all the staffs of the Department of Biosciences and Bioengineering for extending their help and support directly or indirectly.

I want to express my sincere gratitude to Department of Biosciences and Bioengineering, Central Instruments Facility (CIF) and Government of India, Ministry of Human Resource Development (MHRD) for the financial support provided to me during my doctoral career.

I would like to thank my labmates who kept me motivated by their constant encouragement. I knew they are always there whenever I needed someone to talk. I would also like to thank my friends who are always my stress buster and always support me during the ups and downs of my life.

I thank my parents for being very supportive of my career and giving me the strength to achieve whatever I have ever wished and always encouraging me to do better. I would also like to thank my brothers and sister for being always there for me and always motivating me to keep going.

December, 2018

(ANUMA SINGH)

CONTENT

3. EXTRACTION, ISOLATION, AND PURIFICATION OF COMPOUNDS FROM SEEDS OF *P. pinnata*

4. STRUCTURAL CHARACTERIZATION OF COMPOUNDS AND CORRELATION OF ITS VIBRATIONAL ASSIGNMENT WITH DENSITY FUNCTIONAL THEORY (DFT)

6. BIOACTIVITY OF CRUDE EXTRACT AND PURIFIED COMPOUNDS AGAINST BACTERIA

GRAPHICAL ABSTRACT

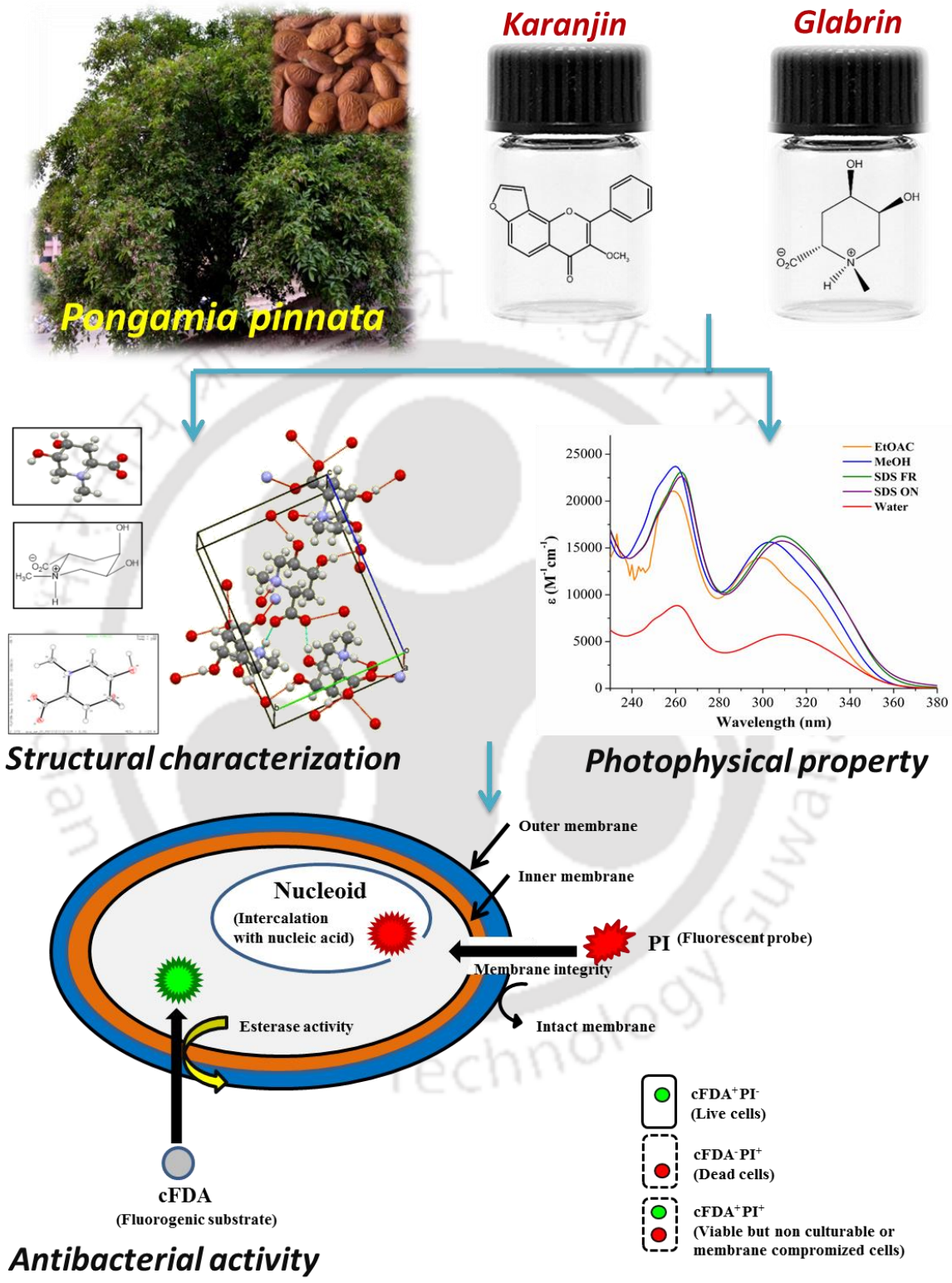

ABSTRACT

The current investigation was aimed at the utilization of *Pongamia pinnata* L. seeds as a gold mine for procuring medicinally important products with diverse pharmacological properties. It also deals with the development of novel methods for the isolation and characterization of compounds from the seed oil. Structural elucidation was carried out via HRMS, FTIR, XRD, NMR, Raman spectroscopy and thermogravimetric studies. Density functional theory (DFT) has also been used to calculate vibrational spectra of isolated compounds (Karanjin and Glabrin) with sufficiently high accuracy. The photophysical property of Karanjin in different microenvironments was also studied as a function of the solvatochromic parameters. The physicochemical parameters of the compound were determined by *in silico* drug-likeness property, and molecular docking against bacteria revealed their potential as highly functionalized and medicinally useful compounds. The potency of seed crude extracts and purified compounds were assessed against pathogenic indicators. The antibacterial action was evaluated by multiparametric flow cytometry, supported by Raman scattering, cell leakage analysis and FESEM imaging that revealed complex patterns of probable cell wall leakage and cell disruption. Current work gave additional scientific support to the mode of antibacterial action of Karanjin and Glabrin as depicted using fluorescent probes indicating its utility as a potential pharmacophore.

ABBREVIATIONS

CASTp	Computed atlas of surface topography of proteins
CC	Column chromatography
CCDC	Cambridge crystallographic database centre
CFD	Constant fraction discriminator
cFDA	Carboxyfluorescein diacetate
CMC	Critical micellar concentration
CPT	Candidate plus tree
DCM	Dichloromethane
DEPT	Distortionless enhancement by polarization transfer
DFT	Density functional theory
DMF	Dimethylformamide
ESI	Electrospray ionization
EtOAc	Ethyl acetate
FC	Flow cytometry
FESEM	Field emission scanning electron microscopy
FTIR	Fourier transform infrared spectroscopy
HPLC	High-performance liquid chromatography
HRMS	High-resolution mass spectrometry
IRF	Instrument response function
I_{SS}	Steady-state intensity
MCA	Multichannel analyzer
MeOH	Methanol
MIC	Minimal inhibitory concentration

MO	Molecular orbitals
NATA	N-acetyl-L-tryptophanamide
NGPP	North Guwahati *Pongamia pinnata*
NMR	Nuclear magnetic resonance
OD	Optical density
PBS	Phosphate buffer saline
PDB	Protein data bank
PI	Propidium iodide
RIR	Restrict internal rotation
RT	Retention time
SDS	Sodium dodecyl sulfate
TAC	Time to amplitude converter
TCSPC	Time-correlated single photon counting
TGA	Thermogravimetric analysis
TLC	Thin layer chromatography
XRD	X-ray diffraction

Abbreviations for intensities of ^{1}H NMR signals

d - doublet	s - singlet
dd - doublet of doublet	t - triplet
Hz - Hertz	m - multiplet

UNITS

h	hour
min	minute
s	second
ns	nanosecond
g	gram
mL	milliliter
mM	millimolar
mg	milligram
mg/mL	milligram/milliliter
v/v	volume/volume
w/v	weight/volume
µM	micromolar
°C	degree celsius
A.U.	arbitrary unit
Å	angstrom
pH	negative log H^+ ion
$M^{-1}cm^{-1}$	molar/centimeter
D	Debye
rpm	revolution per minute

LIST OF FIGURES

LIST OF TABLES

Introduction

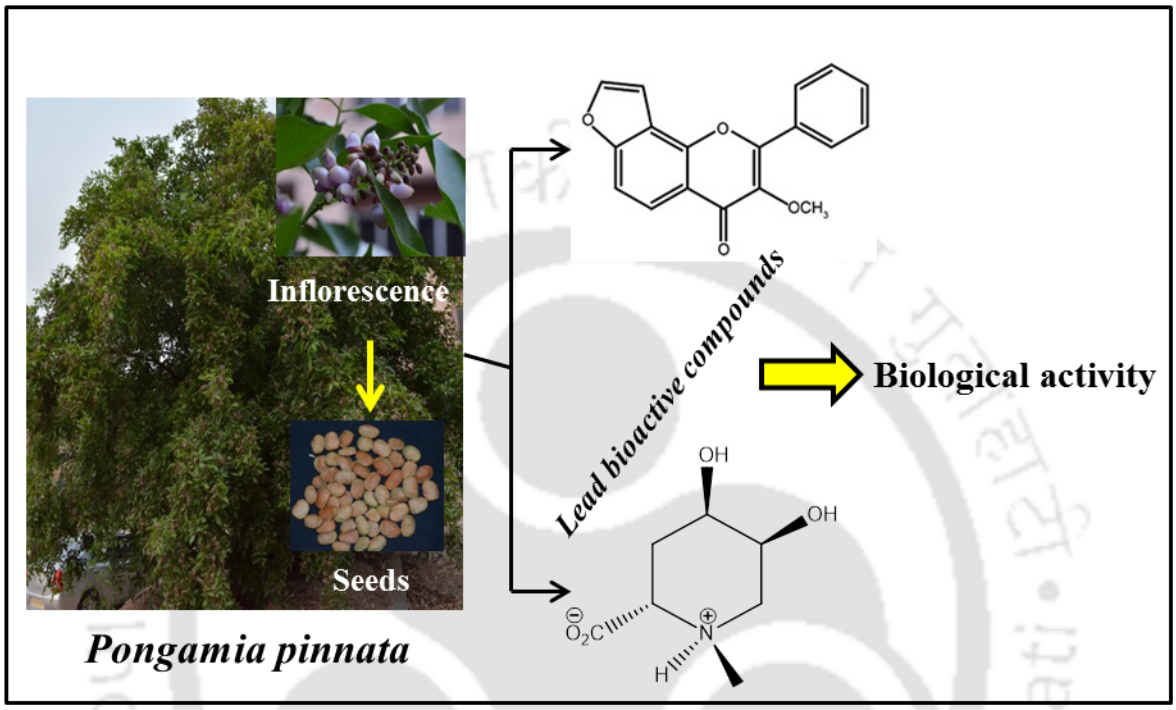

The chapter describes brief background on the natural product and highlights its emerging role as important pharmacophore for the treatment of various diseases. Further, it describes the importance of the specific objectives of the thesis work.

Chapter 1

Introduction

Medicinal plants are an important source of traditional medicine and remedy to cure various human health problems. Plant-based traditional medicines are gaining popularity due to its availability (Taylor, 2013) and lesser side effects (Philomena, 2011; Kazemipoor et al., 2012). Medicinal plants have played a leading role in providing drugs or template for drugs and have been an important part of ancient traditional medicine system such as Chinese, Ayurveda, and Egyptian, many of which are still in use even today. Approximately 25% of modern medicine and 75% of new drugs developed against infectious diseases originate from natural sources (Bedoya et al., 2009; Clardy and Walsh, 2004; Newman and Cragg, 2007) and are inspired by natural product chemistry due to its great diversity of chemical scaffolds. Mostly, natural products are secondary metabolites produced besides the primary biosynthetic and metabolic routes associated with plant growth and development and are capable of eliciting pharmacological and toxicological effects in man and animals. According to earlier reports, only 6% of existing plant species have been investigated pharmacologically and only 15% phytochemically so far (Verpoorte, 2000; Fabricant and Farnsworth, 2001; Cragg and Newman, 2013). Less than 10% of the world's total biodiversity has been evaluated for different biological activities; however, many natural compounds are still unexplored due to the difficulties involved with large-scale extraction (Cragg and Newman, 2005). Advanced spectroscopic and analytical techniques are used in the natural product drug discovery for understanding its complex chemical structure. It also improves the speed of compound isolation and structure elucidation process and also addresses the suitability and specificity of the biological activity of natural products.

Therefore, ethnopharmacological knowledge has promoted further investigation of plant-based secondary metabolites with potential pharmacological effect to enhance the probability of success in the new drug-finding process.

Many research groups have investigated Leguminaceae or Fabaceae due to its versatile nature and high medicinal value. Legumes are known for their nitrogen-fixing ability and repository for vast variety of secondary metabolites. The main metabolites of legume include alkaloids (Yasuda et al., 2002), terpenoids (Saleem, 2009), flavonoids (Balabhadrapathruni et al., 2000; Horn-Ross et al., 2002), tannins (Molan et al., 2000), non-protein amino acids (Bergan et al., 2001) etc., exhibiting biological and pharmacological effects.

Pongamia pinnata (L.) Pierre (Synonyms: Indian Beech Tree, Honge Tree, Pongam Tree, *Millettia pinnata*, *Derris indica*, *Pongamia glabra*) is an important pioneer of second-generation sustainable biofuel crop due to its high oil content in seeds (Scott et al., 2008; Kesari and Rangan, 2010). It is a perennial multipurpose legume which grows on marginal land attributed with the nitrogen-fixing capability (Calica, 2017) and pharmacological properties (Muthu et al., 2006). All parts of this plant have been frequently used as traditional medicine in the treatment and prevention of various infectious diseases. *Pongamia* seed oil is used to treat diseases such as scabies, leprosy, pile, ulcer, chronic fever, lever pain, and lumbago. Pharmacological studies have revealed that various types of preparation, extracts, and single compound of *Pongamia* exhibits broad spectrum of biological activities such as antioxidant, antimicrobial, anti-inflammatory, and anti-diabetic, etc (Al Muqurrabun et al., 2013).

Therefore, the present study was undertaken with the objective to isolate organic solvent extracts from seeds of candidate plus tree (CPT) of *P. pinnata* followed by isolation, purification and structural characterization of useful compound(s). Structure

and photophysical property of the compounds were investigated in different microenvironments. Further, the efficacy of the crude extracts and purified compounds were studied towards antibacterial activity in the perspective of herbal therapeutics.

1.1. Objectives

The present study involves the isolation and structural characterization of compound(s) from seeds of candidate plus tree (CPT) of *P. pinnata* based on the background study, its role and importance in medicinal and therapeutic applications. Solvents with different dielectric constants were used to investigate the photophysical properties of the compound. Changes in UV-Visible spectra, fluorescence emission, and fluorescence mean lifetime as a function of the solvatochromic parameters were also studied. Further, the biological efficacy of the compounds towards the development of herbal therapeutics was investigated. The specific objectives are:

1) Extraction, isolation, and purification of compounds from the seeds of *P. pinnata.*

2) Structural characterization of compounds and correlation of its vibrational assignment with density functional theory (DFT).

3) UV-Visible absorbance and fluorescence spectra of Karanjin in different solvents and solvent mixture.

4) Bioactivity of crude extract and purified compounds against bacteria.

Chapter 2

Literature Review

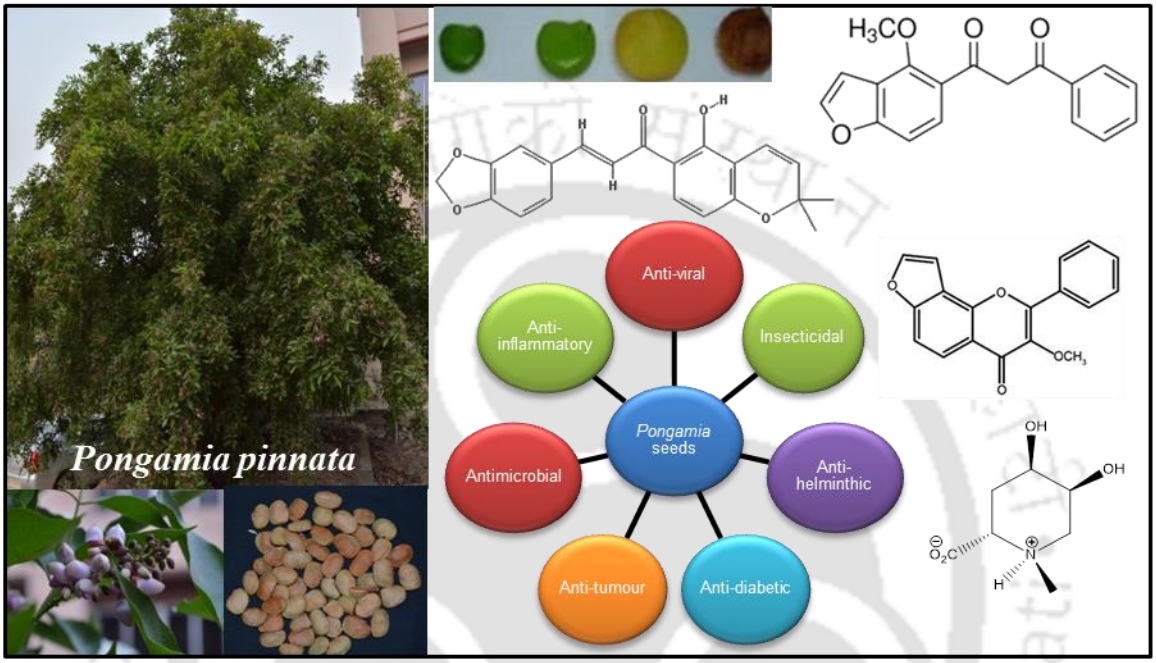

The chapter describes history and current status of natural product as traditional and pharmacological remedy. This information further illustrates the importance of *Pongamia* seeds and its bioactive compounds in towards biological activity.

Chapter 2

Literature Review

2.1. Introduction

Plant-based medicine is the principal source of the drug in different traditional medicinal system that has been passed orally from generation to generation. The World Health Organization (WHO) has estimated that over 65% of the world's population still depends on the plant product as curative agent to improve the health (Cragg et al., 2009). In Europe and North America, the knowledge of traditional healing system has led to an increasing interest in herbal medicine (Tyler, 2000). These herbal medicine has been incorporated into so-called 'alternative,' 'complementary,' 'holistic' medical system and also called as 'phytomedicine'. In India, about 70% of the modern drugs are from natural resources, and many synthetic analogs have been prepared from the prototype inspired from the plant (Sen et al., 2011; Pan et al., 2014).

Advancement in chemical analysis has allowed researchers to extract and modify active ingredients from plants. The efficacy and effectiveness of these products have been demonstrated using modern technological and scientific tools which have aided in the treatment of various acute and chronic infectious diseases. Therefore, the search for novel therapeutic agent continues for an effective medication for treating/curing deadly diseases either by direct therapeutic effect after semisynthetic modification or by new synthesis of chemicals based on the natural product model. Natural products from medicinal plants are hub of structurally diverse array of pharmacologically active compounds that have proved to be indispensable for the cure of deadly diseases or as lead structure for novel pharmaceuticals (Newmann et al., 2000).

2.2. History of herbal medicine

History of medicine dates back practically to the existence of human civilization. Human has always been dependent on the natural resources especially plants for their primary healthcare. This knowledge of herbal medicine for curing ailments or disease has been passed orally through generations. Historically, majority of new drugs have been synthesized or inspired by natural products due to their excellent chemical scaffold.

One of the earliest record of medical documents '*Papyrus Ebers*' wrote by Egyptians around 1500 BC, documented around 700 plant-based remedies (**Table 2.1**). A similar record of herbal study '*Shennong Bencaojing*' was written by the Chinese Emperor Shen Nong around 2000 BC, contains information about 300 plants.

Before the 20th century, crude extract of plants, animals, and minerals represented the only medication available to treat human and domestic animal illness. With advancement in the field of chemistry, plants were intensively examined for their utility aspect as it relates to medicines (Phillipson, 2001). In 1804, 'morphine' was purified from opium by Serturner and found that it has analgesic and sedative effects (Lockemann and Serturner, 1951). After this discovery, other scientists started to seek "active principles" of medicinal plants. Two French scientists, Caventou and Pelletier isolated quinine from Cinchona bark or Peruvian bark in 1820 and made a notable breakthrough in the history of herbal medicine (Borchardt, 1996). Subsequent years later, scientists discovered narcotine (1817), caffeine (1821) and atropine (1831).

Table 2.1 History of natural product medicine (Source: Sarkar et al., 2006).

Period	Type	Description
>3000 BC	Ayurveda Chinese Traditional Medicine	Introduced medicinal properties of plant and other natural products
1550 BC	Ebers Papyrus	Present a large number of crude drug from natural sources (e.g., castor seeds and gum Arabic)
460-377 BC	Hippocrates	Describe several plants and animals that can be the source of medicine
370-287 BC	Theophrastus	Describe several plants and animals that can be the source of medicine
23-79 AD	Pliny the Elder	Describe several plants and animals that can be the source of medicine
60-80 AD	Dioscorides	Describe several plants and animals that can be the source of medicine
131-200 AD	Galen	Practiced botanical medicine (Galenicals) and made them popular in the west
15th Century	Krauterbuch	Presented information and pictures of medicinal plants

The structural elucidation and characterization of natural products geared up after morphine structure was determined in 1923 (Gulland and Robinson, 1923), quinine's structure in 1908 (Rabe, 1908) and cocaine in 1898 (Willstatter and Muller, 1898). In 1956, morphine was first synthesized by Gates and Tschudi and encouraged other scientist towards the synthesis of natural products (Gates and Tschudi, 1956). The 20th century has revolutionized entirely the idea of using the extracts as drug and target mediated by specific interactions with biological macromolecules. It has led the scientists to conclude that individual active compound in extract are responsible for biological activity of the drug (Lahlou, 2013). This concept eventually led to the beginning of a new era in pharmacology that is to use the pure isolated chemical towards treatment of diseases.

Several plant-based natural products have been isolated after the onset of World War II and are found to be promising till date. Few notable were the discovery of 'reserpine' from *Rauwolfia serpentina* roots (used as a potent tranquilizer), anticancer drug

'vinblastin' and 'vincristine' from *Catharanthus roseus* (Phillipsons, 2001). Other remarkable achievements were the discovery of 'Camptothecin' and 'Taxol' which are regarded as lifesaving drugs in cancer therapy (Oberlies and Kroll, 2004). Many natural products and their derivatives are still in use to combat various infectious and non-infectious diseases and are regarded as potent antibacterial, anticancerous agents (Butler, 2008; Newman and Cragg, 2012).

2.3. The downfall in herbal drug research

Crude extracts obtained from various parts of the plant are fractionated to isolate main active ingredients and tested for their biological activity. Bioassays can be conducted at multiple steps during the entire procedure. Regardless of several achievement and advancement, natural product drug discovery is rather time-consuming, tedious and laborious. Other factors that hinder the progress are instability of compounds, separation, and unreliability of bioassay (Beutler, 2009). These problems have indeed reduced the scope of drug discovery by mainstream pharmaceutical companies. Loss of interest by pharmaceutical companies has led to the downfall of plant-based drug discovery. However, with the emergence of microbial resistance and continuous advancement in analytical techniques, plant-based natural products have attracted attention and gaining popularity due to its fewer side effects and flexibility of their chemical structures. Several alternative approaches such as high throughput screening of compounds or combinatorial techniques are also being explored in efforts to improve the extraction speed and efficiency in natural products drug discovery (Ertl et al., 2008).

2.4. Plant secondary metabolites

The plant kingdom has a vast diversity of bioactive compounds that are the primary sources of various therapeutic or pharmacologically active agent for combating different

infectious disease (Clardy and Walsh, 2004; Newman and Cragg, 2007). Plant synthesizes both primary and secondary metabolites to cope and sustain in different environmental conditions. Primary metabolites are compounds produced by the plant, such as, amino acid, nucleic acid, lipid, etc that are directly involved in its growth and development. On the other hand, secondary metabolites are regarded as products of biochemical processes capable of eliciting pharmacological and toxicological effects in living organism. Important functions of secondary metabolite produced by plants are:

1. Protection against biotic (predators or pathogens) and combating abiotic stress (UV radiation, physical or chemical barrier, etc.)
2. Endogenous regulators of plant growth hormone
3. Commercial purposes (dyes, essential oil, flavoring agent, pesticide, pharmaceutical, tanning agent, perfume or cosmetic item, etc.)

Based on their biosynthetic origin, secondary metabolites have been classified into three major categories as shown in **Figure 2.1**.

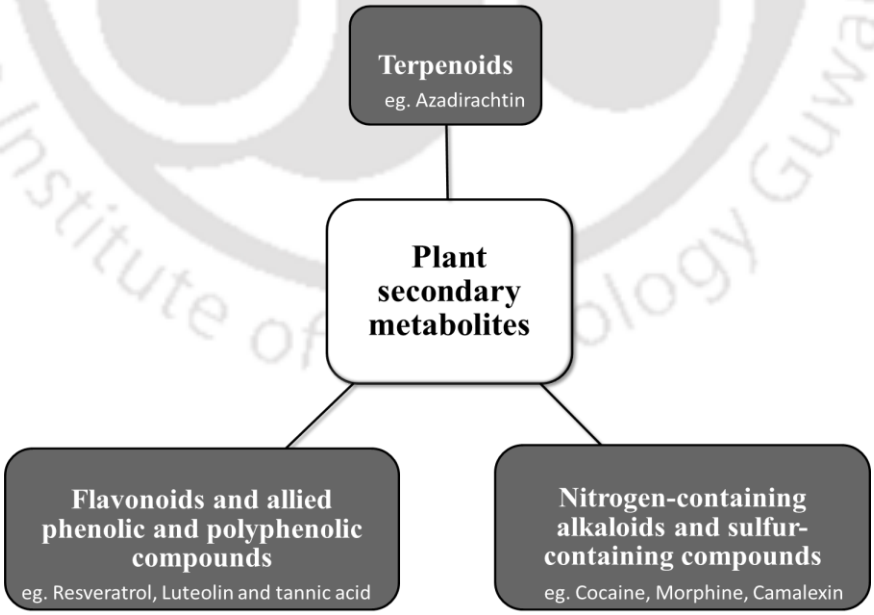

Figure 2.1 different classes of plant secondary metabolites.

2.4.1. Terpenoids: Terpenoids constitute the largest class of plant secondary metabolites and have garnered a lot of attention because of their important physiological function (i.e., hormone, aliphatic membrane anchor, membrane structure stabilization, etc), and for ecological role (i.e., defense, insect/animal attractant) (Kempinski et al., 2015). Besides, the role of terpenoids in pharmaceutical sector and industry is well known (i.e., flavors, fragrance, and medicines) (Schwab et al., 2008; Niehaus et al., 2011; Shelar, 2011).

2.4.2. Phenolic compounds: Plants produce a variety of secondary compounds that are naturally occurring phenolic compounds, occurring both in free state and as glycosides. The diverse functions include their role in plant physiology, protection against stress and structural integrity (Bhattacharya et al., 2010). Subcategories of plant phenolic compounds are colored pigments (i.e., carotenoid and flavonoid) and phenolic polymers (i.e., phenolic acid, lignin, and tannin). Flavonoids are naturally occurring polyphenolic compounds that are an integral part of the plant defense mechanism. They are secondary metabolites, which share a common carbon skeleton of diphenylpropanes (C6-C3-C6). The carbon skeleton includes two aromatic carbon ring, a benzopyran, and the benzene ring. Furthermore, based on the degree of oxidation of the benzopyran ring, the hydroxylation pattern of the ring structure and substitution in the 3-position, flavonoids are further divided into 6 subgroups, namely the flavone, flavan-3-ol, flavon-3-ol, flavanone, isoflavone, and anthocyanidin (Pandey and Kumar, 2013). Flavonoids are widely distributed secondary metabolites with different metabolic functions in plant. It act as signal molecule (Peer and Murphy, 2006), phytoalexins (McNally et al., 2003), detoxifying agents (Michalak, 2006), stimulants for germination of spores (Bagga and Straney, 2000), in seed germination (Shirley, 1998), as UV-filters (Lanot and Morris, 2005), towards temperature acclimatization (Kaplan et al., 2004), in drought resistance

(Hernandez et al., 2004), as pollinator attractants (Iwashina, 2003) and allelochemical agents (Duke, 2007) among many others.

Flavonoids are generally photochemically inert as indicated by their reported use as photosensitizers, photoquenchers and ultraviolet absorption filters (Monici et al., 1993). The backbone polyphenol structure of flavonoids makes them very sensitive to changes in their surroundings, thereby, altering the solubility, hydrophobicity, and spectroscopic properties of the compound and leading to changes in their biological activity. Molecular structure like planarity, rigidity, conjugation, substituent, etc also play an essential role in the absorption and emission behavior of the flavonoids and control its photophysical properties in the ground as well as excited state (Voicescu et al., 2014).

2.4.3. Nitrogen-containing alkaloids and sulfur-containing compounds: A large variety of plant secondary metabolites have nitrogen as part of their structure. Nitrogen-containing compounds are mainly derived from amino acids like tyrosine, lysine, tryptophan and aspartic acid; impart defensive role against herbivores and pathogen attack (Summons et al., 2006). Included in this category are well-known as alkaloids and cyanogenic glycosides. Alkaloids are used as narcotic, in pharmaceutical industry, and as poison (Hesse, 2002). Commonly used plant-derived alkaloids as drug include vincristine, vinblastine, and camptothecin used as anticancer; morphine and codeine as analgesic and scopolamine as a sedative (Crozier et al., 2010). Moreover, many plants also contain unusual amino acids, called non-protein amino acids for defense purpose. Over 250 non-protein amino acids have been identified in the plant kingdom and are noteworthy in many ways as an intermediate in biosynthetic pathway and for their role as a pharmacological compound (Swain, 1977). For example, L-5-hydroxytryptophan is the precursor of serotonin in the human brain, and accounts for 14% of dry seed weight

obtained from *Griffonia* species (Bell and Fellows, 1966; Bell et al., 1976). Similarly, L-3,4-dihydroxyphenylalanine (L-DOPA) serves as a precursor of dopamine in the brain and constitute about 6-9% of the dry seed weight of *Mucuna pruriens*. It has been widely used as a drug for the treatment of Parkinson's disease (Damodaran and Ramaswamy, 1937). L-Homoarginine (2-amino-6-guanidinohexanoic acid) is isolated from *Lathyrus* species (Bell, 1962; Rao et al., 1963) and its identical synthetic compound is used as a substrate for rat liver arginase (Stevens and Bush, 1950). About 42 non-protein amino acids have been isolated from *Vicieae* species (Lambein et al., 1990).

Sulfur-containing secondary metabolites are rather unusual plant constituents. They play an important role in plant-pest interactions and constitute a major chemical defense in the plant belonging to Brassicaceae, Alliaceae, and Asteraceae family (Halkier and Gershenzon, 2006). Brassicaceae plants have evolved the ability to synthesize a wide range of sulfur-containing secondary metabolites, including glucosinolates and indole-type phytoalexins (Bednarek, 2012). *Allium sativum* (garlic) is widely known for its sulfur-containing component endowed with health-promoting benefits, and its medicinal properties known since ancient time (Venditti and Bianco, 2018). Typical example of sulfur-containing secondary metabolite is thiophenes from *Tagetes* species that exhibit a wide range of antimicrobial and antiherbivore activities (Wink, 2015).

2.5. Flavonoids and their biological activity

Various studies have shown that flavonoids exhibit a wide range of biological and pharmacological activities such as anti-oxidant (Pietta, 2000), antibacterial (Kanwal et al., 2015), anti-cancer (Kandaswami et al., 2005), anti-inflammatory (Pan et al., 2014), anti-hyperglycemic (Akansha et al., 2010), anti-viral (Vargas et al., 2015),

hepatoprotective activity (Tapas et al., 2008), etc. **Table 2.2** shows various flavonoids isolated from different plants capable of eliciting pharmacological action.

Table 2.2 Flavonoids isolated from different plants.

Plant	Compound	Biological activity	Reference
Rosa sempervirens	quercetin, quercetin-3-rhamnoside, quercetin-3-xyloside and quercetin-3-galactoside	Antioxidant activity Antibacterial activity	Bitis et al., 2017
Rosa agrestis	diosmetin, kaempherol, quercetin, kaempherol 3-glucoside, quercetin 3-rhamnoside, quercetin 3-xyloside and quercetin 3-galactoside	Antioxidant activity	Bitis et al., 2010
Chrysanthemum morifolium	Diosmetin	Anticancer activity	Androutsopoulos et al., 2009; Androutsopoulos et al., 2013; Liu et al., 2016
Dianthus versicolor	Diosmetin	Treatment of liver problems	Obmann et al., 2011
Ampelopsis grossedentata	Dihydromyricetin	Anticancer activity	Wu et al., 2013
Xylosma longifolium	kaempferol-3β-xylopyranoside-4'-α-rhamnoside	Antibacterial activity	Parveen M, Ghalib, 2012
Malus sylvestris	Phloretin	Antibacterial activity	Hunter and Hull, 1993
Camellia sinensis	Theaflavin	Antibacterial activity	Vijaya et al., 1995
Camellia sinensis	Catechins	Antiviral activity	Keating and O'Kennedy, 1997
Millettia thonningii	Alpinumisoflavone	Anthelmintic activity	Perrett et al., 1995
Podocarpus nagi	Totarol	Antibacterial activity	Kubo et al., 1994
Swertia franchetiana	Swertifrancheside	Antiviral activity	Pengsuparp et al., 1995
Passiflora caerulea	5,7-dihydroxyflavone	Antiviral activity	Critchfield et al., 1996; Mani and Natesan, 2018
Passiflora caerulea	Chrysin	Anticancerous activity	Karthikeyan, 2013; Yu et al., 2013; Liu et al., 2013; Yang et al., 2014; Lirdprapamongkol et al., 2013; Kasala et al., 2016
Passiflora caerulea	Chrysin	Antiinflammatory activity	Cho et al., 2004; Rehman et al., 2014
Passiflora caerulea	Chrysin	Antioxidant activity	Woodman and Chan, 2004
Passiflora caerulea	Chrysin	Antiproliferative activity	Lo et al., 2012
Passiflora caerulea	Chrysin	Neuroprotective	Mehri et al., 2014; Zhang et al., 2015; Souza et al., 2015
Passiflora caerulea	Chrysin	Antidiabetic	Rani et al., 2016
Justicia wynaadensis	3,3′,4′-Trihydroxyflavone	Antibacterial activity	Dsouza and Braz, 2018
Myristica fragrans	3′,4′,7-trihydroxyflavone	Antibacterial activity	Dzotam et al., 2018
Morus mongolica	Morusin	Antinociceptive activity	Chi et al., 2001; Cheon et al., 2000
Theobroma cacao	(-)-epicatechin and (+)-catechin	Immunomodulatory activity	Ramiro et al., 2005
Waltheria indica	(-)-epicatechin, quercetin, and tiliroside	Anti-inflammatory activity	Rao et al., 2005
Caesalpinia pulcherrima	2´-hydroxy-2, 3, 4´, 6´- tetramethoxy chalcone	Immunomodulatory activity	Madagundi et al., 2012

2.6. Identification and structural elucidation of bioactive compounds

The premier step to study natural product chemistry from plant resources are isolation, characterization and biological evaluation of bioactive compounds. Study of natural products and therapeutic drug design has encouraged the development of separation techniques and spectroscopic approaches for structure elucidation. Mainstream analytical methods used by the researchers for elucidation and characterization of compounds mainly involve spectroscopic and chromatographic techniques (Sasidharan et al., 2011). Compound from natural sources can absorb light due to its molecular structure which can be studied by spectroscopic techniques such as UV-Visible spectroscopy, fluorescence spectroscopy, mass spectrometry, vibrational spectroscopy, nuclear magnetic resonance (NMR). Compound with crystalline nature is often subjected to X-ray diffraction (XRD) technique for determination of its absolute configuration (Kong and Wang, 2013). Therefore, spectroscopy is a powerful technique to analyze, identify and characterize compound at the molecular and atomic level.

2.7. Leguminaceae (Fabaceae)

Fabaceae (peas or bean) is the third largest land plant family and easily recognized by their characteristic flower, fruit (legume) and their alternate compound stipulated leaves. Legumes also act as a host for *Rhizobium* for efficient nitrogen fixation. Legumes are economically and culturally important plants due to their extraordinary diversity and abundance. They also provide wood resource and dye, resin, insecticide, fibre, fodder, etc (Isely, 1982). They are well-known as edible crops and for the chemical compound with medicinal property (Graham and Vance, 2003). With regard to medicinal use, variety of chemically active constituents, such as tannin, flavonoid, alkaloid, and terpene often found in members of this family. These secondary metabolites are chemical with a

high level of biological activity and are used extensively in the treatment of a wide variety of human ailments.

2.8. *Pongamia pinnata*

Pongamia pinnata (L.) Pierre (Synonyms: Indian Beech Tree, Honge Tree, Pongam Tree, *Millettia pinnata*, *Cytisus pinnatus* L, *Derris indica*, *Pongamia glabra*) is a perennial multipurpose legume with the nitrogen-fixing capability and medicinal properties. The plant is native to India and can be grown on marginal land with no direct competition with the food crops. It can thrive in areas having an annual rainfall ranging from 500 to 2500 mm and the maximum temperature range from 27°C to 38°C and minimum 1°C to 16°C (Sangwan et al., 2010). Mature trees can withstand waterlogging, slight frost, and high salinity. It is used to control soil erosion and binding dunes because of its dense network of lateral roots and thick long tap root making it drought tolerant. It is well known for its high seed oil, and almost all the plant parts are widely used for various purposes (**Figure 2.2**). *Pongamia* can be successfully propagated through seeds and cuttings (Handa et al., 2005; Singh et al., 2005; Kesari et al., 2010). The viability of the seed is up to one year.

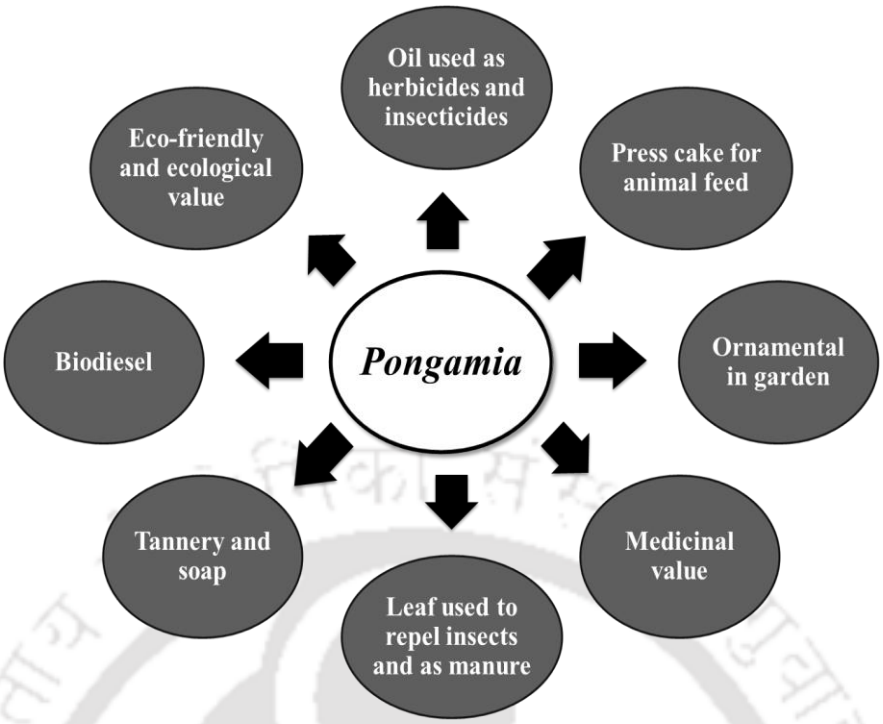

Figure 2.2 Important uses of *Pongamia pinnata.*

Historically, *Pongamia* has been used as a folk medicinal plant, particularly in Ayurveda and Siddha system of Indian medicine. All parts of this plant have been used to treat various diseases as listed in **Table 2.3** and **Table 2.4**. Due to its multiple utility, *Pongamia* has gained much attention from scientists and has undoubtedly encouraged them towards the development of potential therapeutics.

Table 2.3 Traditional use of *Pongamia* (Source: Al Muqarrabun et al., 2013).

Part	Medicinal use	Reference
Whole part	Snakebite treatment of tumor, pile, skin disease, wound, and ulcer	Kirtikar and Basu, 1987; Tanaka et al., 1992; Rout et al., 2009; Pavithra et al., 2010
Fruit	Abdominal tumor, anthelmintic	Hartwell, 1967; Kirtikar and Basu, 1987
Flower	Diabetes	Kirtikar and Basu, 1987; Badole and Bodhankar, 2009a
Seed/ Seed oil	Keratitis, urinary discharge, pile, ulcer, chronic fever, rheumatism, leucoderma, lumbago, Scabies, leprosy, bronchitis, whooping cough, chronic skin diseases, wound treatment, chronic fever, hypertension, liver pain	Nadkarni, 1954; Kirtikar and Basu, 1987; Ghani, 1998; Ayyanar and Ignacimuthu, 2009; Warrier et al., 1993; Prasad and Reshmi, 2003
Leaf	Rheumatism, gonorrhea, skin disease, fever, pile, scabies, anthelmintic, diarrhea, dyspepsia, flatulence, glycosuria, antiseptic, blood purifier, wound treatment	Chopra et al., 1993; Nadkarni, 1954; Satyavati et al., 1987; Warrier et al., 1993; Bandaranayake, 1998; Kirtikar and Basu, 1987; Ayyanar and Ignacimuthu, 2009; Ambasta et al., 1992; Oommen et al., 2000; Brijesh et al., 2006
Stem/ Bark	Diabetes, malaria, bleeding pile, beriberi, anthelmintic, hemorrhoid, ophthalmopathy, vaginopathy, skin disease, genatalia, sinus, stomach pain, intestine disorder, wound treatment	Aiman, 1970; Bhargava, 1983; Kirtikar and Basu, 1987; Bandaranayake, 1998; Joy et al., 1998; Carcache-Blanco et al., 2003; Khare, 2004; Ayyanar and Ignacimuthu, 2009
Root	Wound and gastric treatment, gonorrhea, cleaning gums, teeth and ulcer, vaginal and skin diseases	Muthu et al., 2006

Table 2.4 Biological activity of *Pongamia*.

Plant part	Biological activity
Flower	• Antioxidant (Anuradha and Krishnamoorthy, 2011) • Anti-diabetic (Punitha and Manoharan, 2006; Punitha et al., 2006)
Fruit	• Antioxidant (Bhatia et al., 2008) • Antibacterial (Shoba and Thomas, 2001)
Leaf	• Antioxidant (Essa and Subramanian, 2006) • Antibacterial (Arote et al., 2009; Bajpai et al., 2009; Chandrashekar and Prasanna, 2010; Brijesh et al., 2006; Khan et al., 2006) • Antiviral (Brijesh et al., 2006; Rameshthangam and Ramasamy, 2007) • Anti-parasite (Brijesh et al., 2006; Simonsen et al., 2001) • Anti-inflammatory (Srinivasan et al., 2001) • Anti-convulsant (Manigauha et al., 2009; Manigauha and Patel, 2010) • Anti-diabetic (Lanjhiyana et al., 2011; Sikarwar and Patil, 2012) • Anti-hyperammnonemic (Essa et al., 2005) • Cytotoxicity (George et al., 2010) • Insecticidal (Deshmukhe et al., 2009; Samuel et al., 2009; Kumar et al., 2006) • Immune-modulatory (Manikannan et al., 2011) • Anti-convulsant (Manigauha et al., 2009) • Anti-ulcer (Giri et al., 2010)
Root	• Antioxidant (Raghavendra et al., 2007; Patil et al., 2010) • Antibacterial (Khan et al., 2006) • Anti-inflammatory (Patil et al., 2010) • Anti-diabetic (Rao et al., 2009)
Seed and seed oil	• Antioxidant (Vadivel and Biesalski, 2011) • Antibacterial (Wagh et al., 2007; Kesari et al., 2010) • Antifungal (Wagh et al., 2007; Kesari et al., 2010) • Antiviral (Elanchezhiyan et al., 1993) • Anti-inflammatory (Prabha et al., 2009) • Anthelmintic (Nirmal et al., 2007) • Insecticidal (Kumar et al., 2006; Singh, 2007; Parmar, 1977) • Treatment of rheumatic arthritis (Tanaka et al., 1992; Carcache et al., 2003) • Anti-pyretic (Warrier et al., 1993) • Hypoglycemic and hypolipidemic activity (Semalty et al., 2012)
Stem/Stem Bark	• Anti-inflammatory (Badole et al., 2012, 2013; Sagar et al., 2010; Giri et al., 2010) • Anti-diabetic (Badole and Bodhankar, 2009a; Badole and Bodhankar, 2009b) • Anti-pyretic (Philip and Sharma, 1997)

2.9. *Pongamia* seed

Historically, *Pongamia* has been used in India and its neighboring region as a source of traditional medicine, animal fodder, green manure, timber, fish poison, and fuel (Scott et al., 2008). It is also a pioneer of second-generation sustainable biofuel crop for its high oil seed production. Pods are smooth, oblique oblong to ellipsoid, flattened but slightly swollen, slightly curved with short, curved point (beaked), brown, thick-walled, thick leathery to subwoody, hard, indehiscent, 1-2 seeded, short-stalked. Seed oil is an important asset of this tree and has been used as lamp oil, in soap making, and as a lubricant for many years. Seeds have 19% moisture, 27.5% fatty oil, 17.4% protein, 6.6% starch, 7.3% crude fibre and 2.4% ash. The seed contains 40% non-edible oil and the remaining protein-rich (30%) by-product that can be used as feed supplement for animal and biogas production (Vismaya et al., 2010). The composition of seed may greatly vary due to various factors, like genotype, climatic condition, and method of crude extraction. The crude seed oil of this plant can be used as a fuel for cooking and lighting tradtional lamps. Also, oil is used as lubricant, pesticide and in soap making industry. It has also been used against ulcer, chronic fever, rheumatoid arthritis, and leprosy (Sangwan et al., 2010) owing to its medicinal property. Therapeutic activity of the seed oil is mainly because of the presence of various types of secondary metabolites, such as Karanjin, kanjone, pongaglabrone, pongapin, furanoflavone, etc. (Al Muqurrabun et al., 2013). Several compounds have been reported from this plant, such as terpenoids, flavonoids, steroids, amino acids derivative, disaccharides, fatty acids and esters, etc (**Table 2.5**).

Table 2.5 Bioactive compounds isolated and characterized from *Pongamia* seeds.

Compound	Type	Reference
Karanjin	Furanoflavone	Limaye, 1925; Talapatra et al., 1980; Pathak et al., 1983a; Saha et al., 1991;Tanaka et al., 1992
Kanjone	Furanoflavone	Aneja et al., 1963; Talapatra et al., 1980; Pathak et al., 1983a
Pongaglabrone	Furanoflavone	Khanna and Seshadri, 1963; Pathak et al., 1983a; Tanaka et al., 1992
Pongapin	Furanoflavone	Row, 1952; Pathak et al., 1983a; Saha et al, 1991; Tanaka et al., 1992; Minakawa et al., 2010
Pongaflavone/karanjachromene	Chromenoflavone	Lakhsmi et al., 1974; Rashid et al., 2008
Isopongachromene	Chromenoflavone	Pathak et al., 1983a
Gamatin	Isofuranoflavone	Khanna and Seshadri, 1963
Pongamol	Furanochalcone	Talapatra et al., 1980; Pathak et al., 1983a; Tanaka et al., 1992; Minakawa et al., 2010
Obovatachalcone, Glabrachalcone	Chromenochalcone	Pathak et al., 1983b
Glabrachromene II	Chromenochalcone	Li et al., 2006
β-sitosterol, Stigmasterol	Sterol	Shameel et al., 1996
β-sitosterylacetate, Stigmasteryl acetate	Sterol acetate	Shameel et al., 1996
β-sitosterol-3-O-β-D-galactoside, Stigmasterol-3-O-β-D-galactoside	Sterol glycoside	Shameel et al., 1996
Methylkarranjic acid	Aromatic carboxylic acid	Baki et al., 2007
Glabrin	Amino acid	Rao and Rao, 1941
Sucrose	Disaccharide	Shameel et al., 1996
Palmitic acid	Fatty acid	Bala et al., 2011
Stearic acid	Fatty acid	Carcache-Blanco et al., 2003; Bala et al., 2011
Eicosanoic acid, Behenic acid, Lignoceric acid, Oleic acid, 11-eicosenoic acid, Erucic acid, Linoleic acid, Linolenic acid	Fatty acid	Bala et al., 2011
Tridecylate, Palmitate, Stearate, Heptadecylenate, Oleate, Linoleate	Fatty acid methyl ester	Shameel et al., 1996

Based on the literature survey, it is concluded that secondary metabolites from *Pongamia* seed might represent a fascinating library for critical ingredients towards its pharmaceutical application which in turn can be used to treat a wide range of health disorder, disease, and ailments.

Chapter 3

Extraction, isolation, and purification of bioactive compounds from the seeds of *P. pinnata*

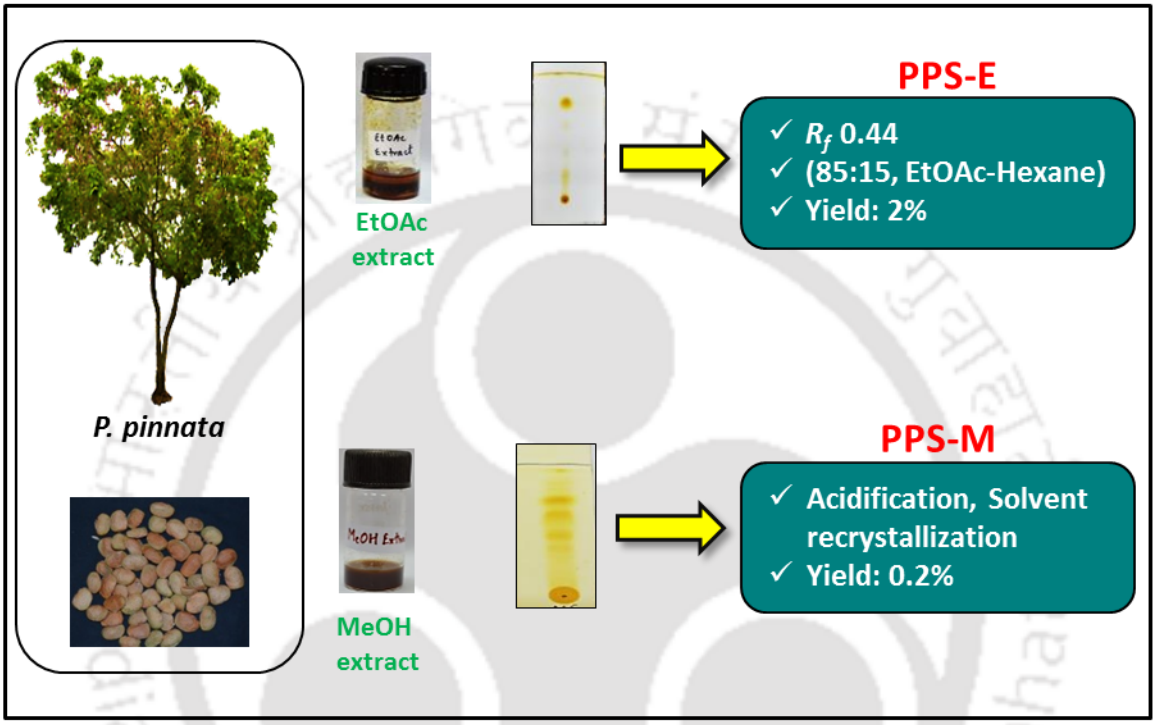

The chapter describes the development of novel and rapid method for the isolation of analytically pure compound from organic crude extract of seeds with an emphasis on achieving higher yield.

Chapter 3

Extraction, isolation, and purification of compounds from seeds of *P. pinnata*

3.1. Introduction

India is a rich abode to medicinal plants, which include more than 2000 species and primarily used in Ayurveda, Unani and Siddha form of system of medicine. Unfortunately, chemical and pharmacological aspects have been explored for only a few of them (Gupta et al., 2005). Since time immemorial, human beings have been using plant and their various parts for the treatment of a large number of disease and ailments. An assessment by the World Health Organization (WHO) revealed that about 65% of the world's populations depend mainly on traditional herbal medicine for their primary health care (Cragg et al., 2009). Different constituents of crude extract of medicinal plant affect the health of an organism through complex and multi-targeted interactions (Wang et al., 2005). Several compounds have been isolated from the medicinal plant, such as terpenoid, flavonoid, steroid, amino acid derivative, disaccharide, fatty acid and ester with various pharmacological properties. For the efficient extraction of compound, plant material is often exposed to high-temperature conditions. Therefore, the physical property like thermal stability of crude extract is an important parameter for judging its quality and lifetime over a range of temperatures. The thermoanalytical study such as thermogravimetric analysis (TGA), differential thermogravimetric analysis (DTG) and differential thermal analysis (DTA) are used to understand the thermal lifetime and decomposition profile of organic crude extract and purified fraction during storage (Mannina et al., 1999).

Pongamia is a legume known for its traditional use and medicinal property. Seeds contain about 28-34% oil with a high percentage of polyunsaturated fatty acids (Sarma et al., 2005; Kesari et al., 2008). After oil extraction, seed cake is used as a green manure as it is rich in protein and nitrogen (Sangwan et al., 2010). The composition of seeds may vary due to various factors, such as genotype, time of harvesting, climatic conditions and method of crude extraction which leads to the variation in the chemical content of the crude extract and their relative composition. Many natural products have been isolated and extensively studied for their biological and pharmacological properties. All parts of this plant are used as a source of traditional medicine such as Ayurveda and Unani. It has been used as a drug for the treatment of tumor, pile, skin disease, wound and ulcer (Sangwan et al., 2010; Al Muqurrabun et al., 2013). Seed oil is used for the treatment of various inflammatory and infectious diseases, such as leucoderma, leprosy, lumbago and muscular and articular rheumatism (Mahli et al., 1989; Singh and Pandey, 1996; Khare, 2004).

Therefore, the current chapter is focussed on the extraction of crude extracts from the mature seeds of *P. pinnata* and studying its physical properties.

3.2. Materials and methods

3.2.1. Sample collection

Ten candidate plus trees (CPTs) of *P. pinnata* were identified based on vegetative and reproductive traits; NGPP 26, NGPP 27, NGPP 28, NGPP 29, NGPP 30, NGPP 46, NGPP 47, NGPP 48, NGPP 49 and NGPP 50 as described by Kesari et al. (2008). Out of which NGPP 46 (North Guwahati *P. pinnata*) was found to be the superior genotype in terms of its pod-seed character having high oil content and was selected for all future studies. The seeds of NGPP 46 were collected from Indian Institute of Technology

Guwahati (IITG) campus (26°12.476'N to 91°41.965'E) during May 2013-July 2013. The mature pods (brown color) were harvested and seeds cleaned and dried in the shade for few days before extraction of oil.

3.2.2. Preparation of the organic extract

Several commonly used techniques for procurement of plant crude extract are maceration, percolation, decoction, ultrasound-assisted extraction, microwave-assisted extraction, etc. Extraction by hot solvent using Soxhlet apparatus gives significantly higher yield with little investment. Therefore in the present study, dried seeds (50 g) of *P. pinnata* were grounded into a fine powder to increase the contact surface between the sample and extracting solvent. It was then subjected for hot organic solvent extraction for 6 h in Soxhlet apparatus. The sequential extraction of the same sample (50 g) was done according to the polarity strength (300 mL) by increasing polarity gradient starting with non-polar (n-hexane), semi-polar (ethyl acetate, EtOAc) and polar (methanol, MeOH) solvents in the ratio of 1:6 (w/v; seed to solvent ratio) as per the procedure of Kesari et al. (2010). After each step of extraction, the sample was dried completely to remove left over solvents before proceeding with next round of extraction. All solvents and reagents used were of HPLC grade (Merck, India). Extracts obtained were concentrated and dried by *BUCHI R-210 rotatory evaporator*, Switzerland and stored at 4^{o}C for further analysis. The schematic representation of the extraction of organic crude extracts is depicted in **Figure 3.1**.

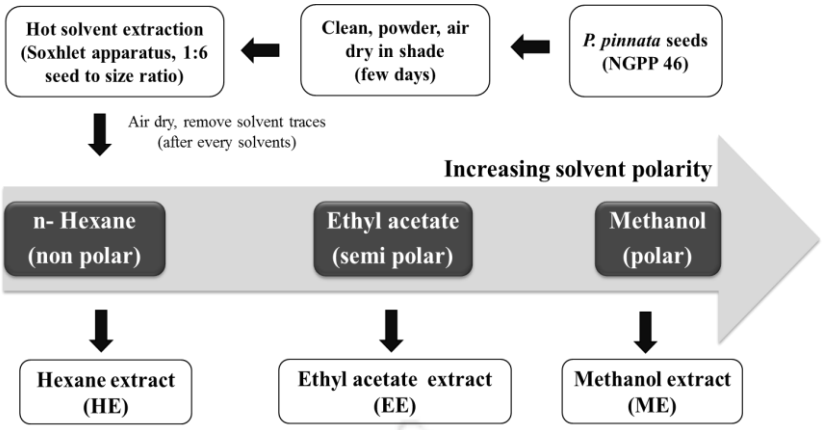

Figure 3.1 Scheme for the extraction of crude extracts from the seeds of *P. pinnata*. Seeds were subjected to hot solvents with different polarity using Soxhlet apparatus. Three crude extracts (HE, EE and ME) were obtained and stored for further study.

3.2.3. Thin layer chromatography (TLC) of crude extract

Thin layer chromatography (TLC) was done on pre-coated silica gel 60 F254 (0.25 mm, Merck, Germany). Crude extracts were diluted in EtOAc, and 10 µL was loaded on TLC plates. The mobile phase optimization was done with different percentage of n-hexane and EtOAc. The samples were allowed to run in a chromatographic chamber saturated with volatile binary solvent of the mobile phase. The individual spot on the plate was visualized under UV and iodine fume. Retardation factor (R_f) of each spot on TLC plates were noted down. After a series of optimization (solvents to be used as mobile phase), crude extracts were subjected to column chromatography and solvent extraction.

3.2.4. Thermal stability of crude extract

About 3 mg of crude extracts were placed in platinum TGA sample holder for thermal analysis using the *Hitachi model STA7200 Thermal Analysis System*. The high purity nitrogen (99.9%) gas was used as purge gas maintaining the flow rate of 50 mL/min. Analysis was performed between 40°C to 700°C with a heating rate of 10°C/min (Gill, 1992).

3.2.5. Isolation of compounds

Due to the high abundance of fatty acids in HE fraction, compound isolation was carried forward only to EE and ME fractions. For the isolation of compound from organic crude extracts (EE and ME), various analytical techniques were used. The isolated fractions were then further purified (TLC, analytical and preparative) and characterized. The schematic representation of isolation of compound from crude extract is depicted in **Figure 3.2**.

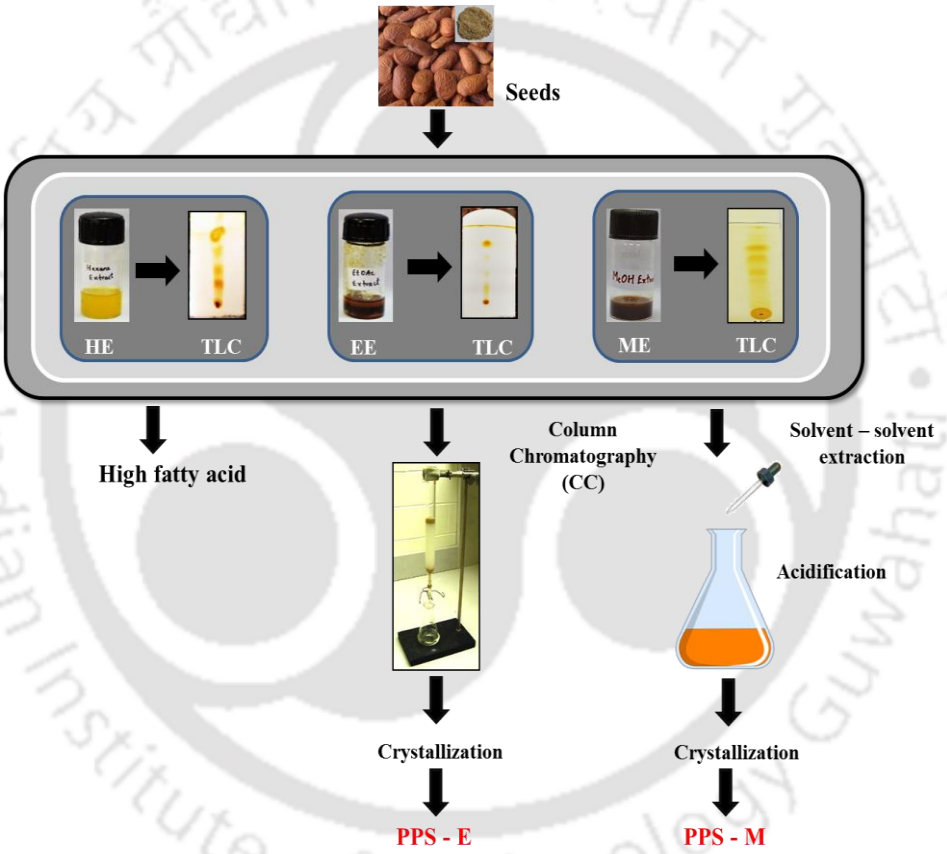

Figure 3.2 Scheme for compound isolation from seed extracts of *P. pinnata*. Seed extracts were subjected to thin layer chromatography (TLC) before column chromatography (CC) and solvent extraction.

3.2.5.1. Isolation and purification of the compound from EtOAc crude extract

The glass column (3 × 50 cm) was sealed with cotton at the end of the column. The column was then filled with slurry of silica gel (80 g, 60-120 mesh, Merck India) in n-

hexane. Initially, 2 g of EE was dissolved in a minimum volume of dichloromethane (DCM), and dry silica gel was added further to form sample slurry. After evaporating DCM completely, sample slurry was loaded onto the packed silica column. Silica column was washed with 100 mL n-hexane. The column was eluted slowly at the rate of 1 mL/min and was collected in test tubes with appropriate labeling. Gradient elution with EtOAc and hexane (v/v) were used as a mobile phase for elution of different fractions. From EE, one major fraction was collected when mobile phase reached at 15:85 (EtOAc-hexane, v/v) and a small aliquot (10 µL) was loaded on TLC plate and visualized under UV light and iodine fume. Fractions having similar R_f values were pooled together and concentrated using rotatory evaporator leaving behind the pure fraction named as PPS-E. It was then allowed to precipitate in EtOAc to obtain crystals, washed with hexane and stored in an amber glass vial. Further, the fractions obtained were checked in TLC with the appropriate solvent system to confirm its purity. High-performance liquid chromatography (HPLC) was carried as a part of purity assessment.

HPLC analysis was done using *Shimadzu's HPLC system* with degassing unit (DGU 20ASR), autosampler (SIL 20AHT and liquid chromatogram (LC 20AD) system. The chromatographic purification of PPS-E was achieved with Enable C-18G column having i.d. of 250 × 4.6 mm and 5 µm particle size. The eluted fraction obtained from column chromatography (10 mg/mL) was dissolved in MeOH: water (80:20) and filtered through a syringe filter (0.45 µm). Sample injection volume was 10 µL, and isocratic elution was done at a flow rate of 1.5 mL/min. The program was run for 30 min with UV/Vis Detector (SPD-20A) set at wavelength 264 nm (Prabhu et al., 2002). Data was procured and processed using Shimadzu lab solutions. All the readings were taken in duplicate. Finally, the pure fractions were filtered, concentrated by a rotatory evaporator and stored at 4°C for further study.

3.2.5.2. Isolation and purification of the compound from MeOH crude extract

Defatted methanolic crude extract (ME) (50 g) was homogenized in 0.01 N HCl (100 mL) for 8 min. The solution was centrifuged for 20 min at 4°C, and the supernatant was collected. Deproteination was carried out by addition of ethanol and the mixture was allowed to stand for 20 min at 4°C. The precipitate was then further separated by centrifugation. Subsequently, the supernatant was dried using rotatory evaporator and stored at -20°C. For further purification, the residue was re-extracted in 0.01 N HCl and compound was obtained by preparative TLC using methanol as mobile phase. The fraction was collected and then re-dissolved in water and was allowed to settle for complete precipitation. Brown crystals were obtained and stored. Preparative TLC was done to obtain an analytically pure compound and to get away the impurities.

A thick layer of silica gel slurry (SRL, India) containing 13% $CaSO_4.1/2H_2O$ as a binder was made on thin glass plates (15 × 25 cm) and air dried in hot air oven (80°C) for 2 h. The mixed fraction (30 µL) was loaded, and the plates were allowed to run in a chromatographic chamber saturated with methanol as mobile phase. The plates were taken out and were allowed to dry at room temperature for an hour. The fractions were scraped out from the plates and washed with EtOAc. The solvent collected after washing was filtered, pooled together and concentrated using rotatory evaporator. The fraction was then air dried and stored at 4°C for further characterization.

3.3. Results and discussion

3.3.1. Plant material

Healthy and matured seeds were collected from Candidate plus tree (CPT) NGPP 46 and used for organic crude extraction and isolation of compounds.

3.3.2. Preparation of the organic extract

Three organic crude extracts were obtained after fractionation based on their solubility in organic solvent. These extracts were named as HE, EE and ME with yield percentage of 32.42, 4.75 and 11.24, respectively (**Table 3.1**). After each step of extraction, approximately 170-200 mL of solvent was recovered using rotatory evaporator.

Table 3.1 Optimization of yield-related parameters for extraction of organic extract from *P. pinnata* seeds using Soxhlet apparatus.

Parameter	*HE	*EE	*ME
Sample weight (g)	50	50	50
Solvent volume (ml)	300	300	300
Time for 1st cycle (min)	30	40	50
Time for next cycle (min)	15	22	36
No. of cycle	9	8	7
Total time	1 h 46 min	2 h 12 min	2 h 20 min
Solvent recovery (%)	73.60	59.33	60.02
The weight of crude extracts obtained	16.21 g	2.37 g	5.62 g
Yield (%)	32.42	4.75	11.24
Colour	Light shining yellow	Dark brown	Dark brown
Smell	Light oily	Bitter almond	Bitter sugary

***HE:** hexane crude extract, ***EE:** EtOAc crude extract and ***ME:** MeOH crude extract

3.3.3. Thermal stability of crude extract

In the current study, thermal property of organic crude extract is monitored as a function of temperature. **Figure 3.3** shows thermogram and DTA curve obtained upon plotting the data for HE, EE and ME with increasing temperature on the x-axis and the decreasing sample weight (as a percentage) on the y-axis.

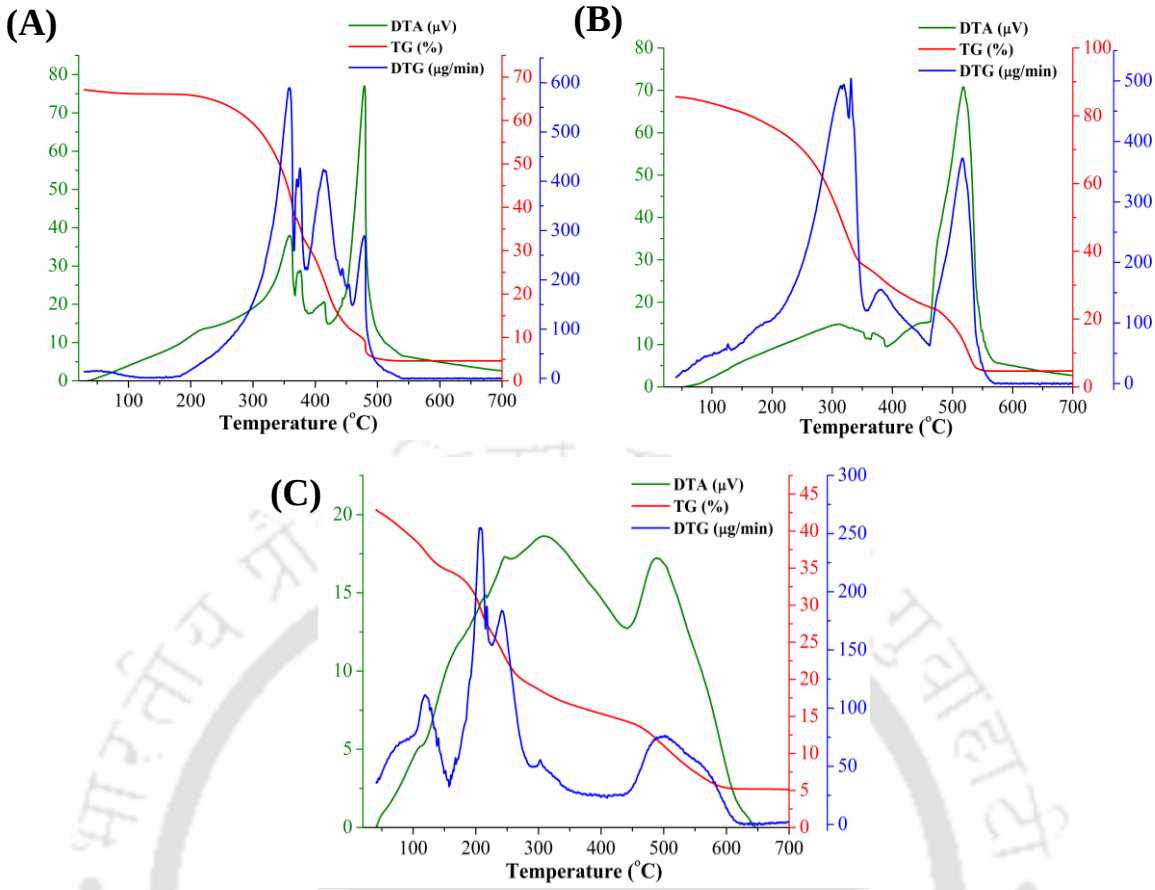

Figure 3.3 The thermoanalytical analysis representing TGA, DTG, and DTA of organic crude extracts. (**A**) HE; (**B**) EE and (**C**) ME.

From the TG curve, the descending thermal curve of HE indicates weight loss that occurred around 220°C with complete decomposition at 480°C (**Figure 3.3 A**). On the other hand, weight loss of EE and ME occurs at around 150°C and 100°C along with complete degradation at 540°C and 600°C, respectively (**Figure 3.3 B** and **C**). Degradation is completed at 560°C, leaving a residue of 5-10%, corresponding to the content of the inorganic material or mineral salts. The mass loss at this stage corresponds to 90-95% of the original mass. Moreover, all crude extracts show one exothermic peak at a temperature range 400-450°C as evident from the corresponding DTA curve.

In DTG curve, it can be seen more clearly that the thermal decomposition of seed crude extract occurred in three steps, with loss of initial mass at the range of approximately 200-380°C. This mass loss is due to evaporation of moisture (Santos et

al., 2012) and decomposition of polyunsaturated fatty acids leading to devolatization of light volatile content owing to heating at high temperature. The second degradation occurs at 380-480°C due to decomposition of monounsaturated fatty acids in HE and EE. The third step of degradation occurs at 450-580°C which corresponds to the degradation of saturated fatty acids (Gouveia de Souza et al., 2004; Pena Muniz et al., 2015). Therefore, the result obtained from thermogram of crude extract clearly shows its stability towards high temperature which is an essential and determining parameter during its extraction, processing, and storage.

3.3.4. Isolation and purification of compound(s)

3.3.4.1. Isolation and purification of the compound from EtOAc crude extract

The major compound isolated from EE by column chromatography was named as PPS-E with R_f value of 0.44 in 15:85 (EtOAc: hexane, v/v) (**Figure 3.4**). After crystallization, the colorless needle-shaped crystals (melting point of 158ºC) were obtained. The process of recovery through crystallization was very efficient in achieving a yield of pure crystals up to approximately 2%.

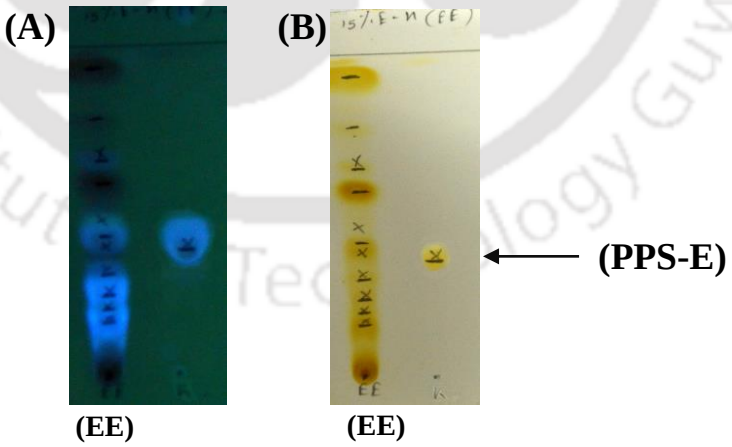

Figure 3.4 TLC images of PPS-E with EtOAc crude extract (EE) observed under (**A**) UV light and (**B**) iodine chamber.

The fraction PPS-E is UV active fraction (λ = 360 nm), thus, to ascertain the purity of compound analytical HPLC was performed using UV detector. Chromatogram of the compound displayed a single peak at retention time of 17.65 min revealing its high purity which can be used for further characterization as shown in **Figure 3.5**.

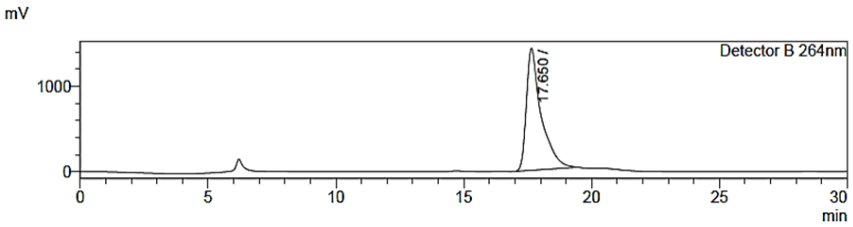

Figure 3.5 HPLC chromatogram of PPS-E.

3.3.4.2. Isolation and purification of the compound from MeOH crude extract

Compound was also isolated from ME by solvent extraction. After crystallization, brown crystals with melting point of 280°C were obtained and named as PPS-M. The fraction PPS-M was further purified by preparative TLC using methanol as mobile phase. After a series of recrystallization and preparative TLC, the yield of pure crystals obtained was 0.2% and was stored in an amber glass vial and so were the crystals PPS-M gives a blue color with ninhydrin. It is known that ninhydrin reaction is very sensitive test for amino acids as it gives positive reaction due to the presence of the free amino group at α position to free carboxylic acid group. The pure compound was kept at 4ºC for its structural characterization.

3.4. Conclusion

In this chapter, seed crude extracts were obtained by hot solvent extraction method using Soxhlet extractor. Two major compounds, PPS-E and PPS-M, were isolated from EE and ME respectively. Compounds obtained by a simple extraction step using different solvents and purified. The procedure employed is efficient and cost effective in getting analytically pure compounds for further characterization. Moreover, the thermoanalytical method was considered to be versatile technique to study the thermal degradation profile of crude extracts revealing its stability over a range of temperature.

Chapter 4

Structural characterization of compounds and correlation of its vibrational assignment with density functional theory (DFT)

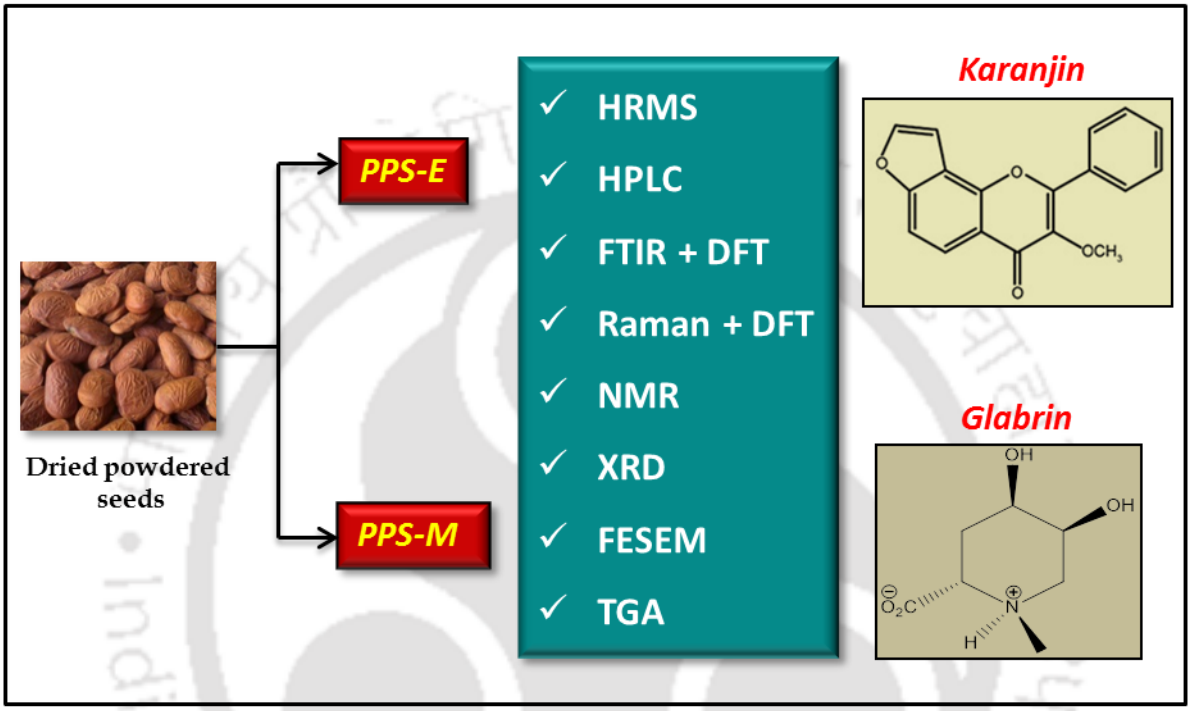

The chapter describes the structural characterization of two bioactive compounds isolated from matured seeds of *P. pinnata* using various analytical and spectroscopic techniques.

Chapter 4

Structural characterization of compounds and correlation of its vibrational assignment with density functional theory (DFT)

4.1. Introduction

Medicinal plants produce number of diverse and beneficial phytochemicals used largely to circumvent certain diseases or disorders. According to Bernhoft (2010), bioactive compounds are secondary plant metabolites produced as products of sidetrack molecules capable of eliciting pharmacological and toxicological effects in human. *Pongamia* is a multipurpose medicinal plant well known for its traditional and pharmacological properties. Different classes of phytochemicals have been reported from various parts of *Pongamia*, such as flavonoids (Ghufran et al., 2004; Yadav et al., 2004; Li et al., 2006), terpenoids (Talapatra et al.,1982; Carcache-Blanco et al., 2003; Shameel et al.,1996), steroids (Talapatra et al., 1982; Shameel et al., 1996), etc. Extracts, and single compound from *Pongamia* exhibits broad spectrum of biological activities such as antimicrobial, antioxidant, anti-inflammatory, anti-diabetic activity, etc (Al Muqurrabun et al., 2013). The seed oil of *Pongamia* contains 5-6% of flavonoid such as Karanjin, kanjone, pongaglabrone, pongapin, out of which the main constituent is Karanjin.

The traditional way of studying natural product includes fractionation of crude mixture or extract, separation and isolation of the individual component using chromatography. The chemical structure of the isolated and purified fraction is elucidated with one or more hypothesised structures and verified with the experimental spectra of the compound. Identification and characterization of the compound often involve different spectroscopic methods which have developed into a mainstream

analytical technique for the elucidation of molecular structure. Various techniques have been used for characterization due to their easy implementation, intrinsic sensitivity, and non-destructive nature (Webb, 2005). The techniques often involve mass spectrometry, vibrational spectroscopy, NMR and XRD (Steinbeck, 2004; Clardy and Walsh, 2004; Exarchou et al., 2005). NMR is known to be a widely used technique for structural elucidation of natural products (Breton and Reynolds, 2013). The structure elucidated by NMR can be further supported and validated by mass spectrometry (Beynon, 1959) and vibrational spectroscopy like FTIR and Raman spectroscopy (Abraham et al., 2003). Infrared and Raman spectroscopy have found an increasing value as applied to *in situ* detection, identification and analysis of vibrational assignments of a compound which can be compared with the computational density functional theory (DFT). DFT appears to represent an excellent method for calculating vibrational spectra with sufficiently high accuracy (Zhu et al., 2000; Pandey et al., 2014). Moreover, few natural products are crystalline for which single crystal XRD is the most promising technique for absolute configuration determination (Kong and Wang, 2013).

Two compounds were isolated and purified from seeds of *P. pinnata,* namely PPS-E and PPS-M and identified as furanoflavonoid and cyclic amino acid, respectively as described in previous chapter. Therefore, this chapter focus is on the structural characterization of the identified compounds. Also, the theoretical calculation of molecular vibrational frequencies of compound has been carried out to obtain a deeper understanding of the vibrational spectra.

4.2. Materials and methods

4.2.1. High-resolution mass spectrometry (HRMS)

About 1 mg crystals of PPS-E and PPS-M were dissolved in 5 mL of methanol (HPLC grade). The solution was used for recording spectra on *Agilent Accurate-Mass Q-TOF LC/MS 6520* by electrospray ionization method (ESI-HRMS). The flow rate was set at 0.2 mL/min for a total run time of 30 min. Diode array was used as a detector, and the ESI probe served as positive and negative ion mode in the analysis.

4.2.2. High-performance liquid chromatography (HPLC)

The purified fraction PPS-E was subjected to HPLC analysis for its identification. It was done using *Shimadzu's* HPLC system with degassing unit (DGU 20ASR), autosampler (SIL 20AHT and liquid chromatogram (LC 20AD). The chromatographic separation was achieved with Enable C-18G column (i.d. 250 × 4.6 mm; 5 µm particle size). Karanjin standard (Sigma, India) stock of 1 mg/mL was prepared in MeOH: water (80:20) from which the working concentrations of Karanjin were made at 0.1, 0.2, 0.3 and 0.4 mg/mL. The eluted fraction (PPS-E) obtained from column chromatography (10 mg/mL) was dissolved in MeOH: water (80:20) and filtered through a syringe filter (0.45 µm). Sample injection volume was 10 µL, and isocratic elution was done at a flow rate of 1.5 mL/min. The program was run for 30 min, and Karanjin was detected using UV/Visible Detector (SPD-20A) set at wavelength 264 nm (Prabhu et al., 2002). Data was procured and processed using Shimadzu lab solutions. All readings were taken in a duplicate manner.

4.2.3. Fourier transform infrared spectroscopy (FTIR) and density functional theory (DFT)

About 1 mg crystal of isolated fractions of PPS-E and PPS-M, were crushed along with dry potassium bromide (HiMedia, IR grade) to obtained pellets. FTIR spectra of the compound were recorded with *Perkin Elmer Fourier Transform Infrared spectrophotometer*, Germany in the range of 600 to 2000 cm^{-1}.

Ab initio electronic structure calculations of PPS-E and PPS-M were carried out using the Gaussian 09 software (Frish et al., 2004). For PPS-E, calculation was carried out at B3LYP/6-311G (D, P) level to determine the vibrational and rotational modes in the sample. On the other hand, the Onsager dipole-sphere model was used for PPS-M zwitterion calculation. At first, a geometry optimisation was carried out at B3LYP/6-31G (D, P) level. For the self-consistent reaction field (SCRF) calculation, the cavity radius to be used in the vibrational studies was determined by carrying out a set of calculations with various radii within 3.0 to 4.5 Å and then the radius producing the best agreement with the experimental results was used. Recorded experimental data of PPS-E and PPS-M from FITR were correlated with reference to DFT, and the raw vibrational frequencies were scaled by 0.97.

4.2.4. Raman spectroscopy and density functional theory (DFT)

Raman spectrum of the pure isolated crystal of PPS-E was recorded by *Horiba LabRAM HR* spectrometer in the backscattering mode using Argon-ion laser at wavelength 514 nm as the excitation source at room temperature (Canamares et al., 2009). Spectral data generated as Raman signal was taken from the sample at specific wavenumbers (200 to 2,000 cm^{-1}). Recorded experimental data from Raman spectroscopy was correlated with

reference to DFT (B3LYP/6-311G (D, P) calculation using Gaussian 09 software (Frish et al., 2004).

4.2.5. Nuclear magnetic resonance (NMR)

One dimension spectral analysis of PPS-E was carried out by dissolving 5 mg of the compound in 600 µL $CDCl_3$ and transferred to 5 mm NMR tube. Spectra were acquired on a *Bruker 600 MHz* (at 298 K). Solvent residual proton resonance and carbon resonance ($CDCl_3$: δ (^{1}H) 7.26 ppm; δ (^{13}C) 76.70 ppm) were used for calibration along with tetramethylsilane (TMS) as an internal reference. ^{1}H and ^{13}C spectral chemical shifts and coupling constants (*J* values) were expressed in δ and Hz, respectively and number of protons: signals were characterized as s (singlet), d (doublet), t (triplet), m (multiplet). Pulse angle employed in distortionless enhancement by polarization transfer (DEPT) experiment was 135º. NMR was controlled by the software TopSpin 2.1.

4.2.6. X-ray diffraction (XRD)

The detailed structures of PPS-E and PPS-M were elucidated and confirmed by single crystal XRD *CrysAlisPro Agilent Technologies,* Germany. A saturated solution of the compound prepared by dissolving 2 mg of sample in 10 mL of DCM to obtain crystals. A single pure crystal of PPS-E and PPS-M were selected, washed for impurities and subjected on Eos diffractometer (SuperNova, Single source at offset) with MoKα radiation (λ = 0.7107 Å) in φ and ω scan modes set at the temperature of 25ºC during data collection. Absorption correction was based on multiple and symmetry-equivalent reflections in the data set using the SADABS program (Sheldrick, 2004). The structure was solved with the help of Superflip and refined with SHELXL-97 (Sheldrick, 1997) and Olex2 (Dolomanav et al., 2009) softwares.

4.2.7. Field transmission scanning electron microscopy (FESEM)

The shape and size of PPS-E and PPS-M were examined by capturing its image using *Carl Zeiss Ultra 55, Sigma* field emission scanning electron microscopy (FESEM). For this, crystals were washed with hexane to remove impurity from the surface and gold coated.

4.2.8. Thermal gravimetric analysis (TGA)

About 3 mg of PPS-E was placed in platinum TGA sample holder for thermal analysis using the *Hitachi model STA7200 Thermal Analysis System*, USA. The high purity nitrogen (99.9%) was used as purge gas by maintaining the flow rate of 50 mL/min. Analysis was performed between 30°C to 700°C with a heating rate of 10°C/min.

4.3. Results and discussion

4.3.1. Identification of PPS-E

Colourless needle-shaped crystals were isolated from EE by column chromatography using EtOAc-hexane eluent system (15:85, v/v) with R_f value of 0.44 (yield 2%, melting point 158ºC). The HRMS confirmed mass of the compound with molecular formula of $C_{18}H_{12}O_4$. The m/z of the isolated compound in positive mode $[M+H]^+$ is 293.087 (**Figure 4.1**), and exact molecular mass is 292.0808 that matched well with the reported mass of karanjin (Katekhaye et al., 2012) (**Figure 4.2**).

HRMS spectrum

MS data showed parent molecular ion peak at 293.087.

Theoretical value $[M+H]^+ = 293.0808$

Observed value $[M+H]^+ = 293.087$

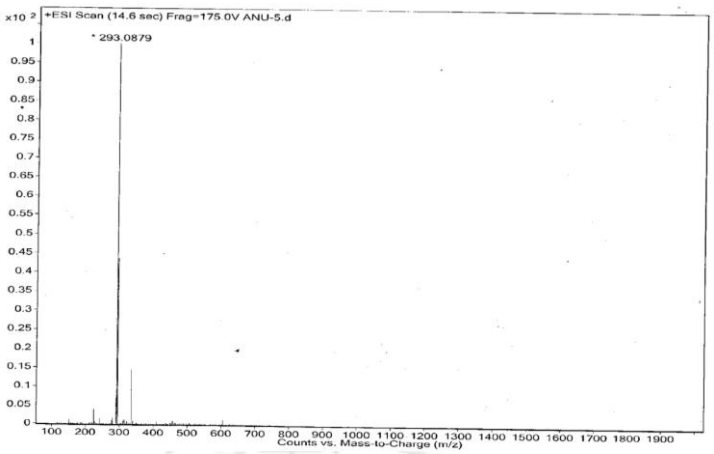

Figure 4.1 Mass spectrum of PPS-E isolated from seeds of *P. pinnata*.

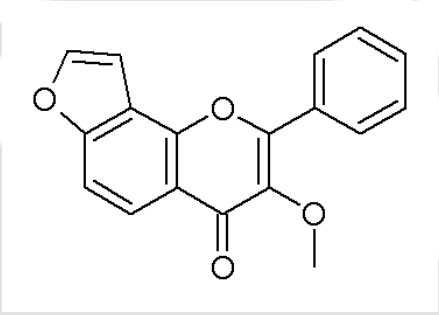

Figure 4.2 Structure of Karanjin (IUPAC: 3-methoxy-2-phenylfuro [2,3-h]chromen-4-one).

Analytical HPLC with UV detector was performed to ascertain the purity of isolated compound (**Figure 4.3**) as it offers high sensitivity (Li et al., 2004) and also because majority of flavonoids are believed to have UV absorbance (Cannell, 1998). The compound showed retention time of 17.68 min and 98% purity when compared with standard Karanjin as evident from HPLC chromatogram (**Figure 4.3 A**). The relative standard deviation for retention time and peak area is less than 0.04% and 1.24% respectively. Therefore, the isolated compound, PPS-E is confirmed to be a furanoflavone named as Karanjin (IUPAC: 3-methoxy-2-phenylfuro [2,3-h]chromen-4-one). Earlier report with regard to Karanjin isolation from the seeds varied from 1 to 1.5% depending upon the geographical site of the collection. The maximum purity was reported to be 80% as evaluated by HPLC (Vismaya et al., 2010). The relative

abundance of Karanjin in different crude extracts were found to be highest in EE and least in ME as Karanjin is semi-polar (**Figure 4.3 B**). Compound was further validated and confirmed by various spectroscopic techniques.

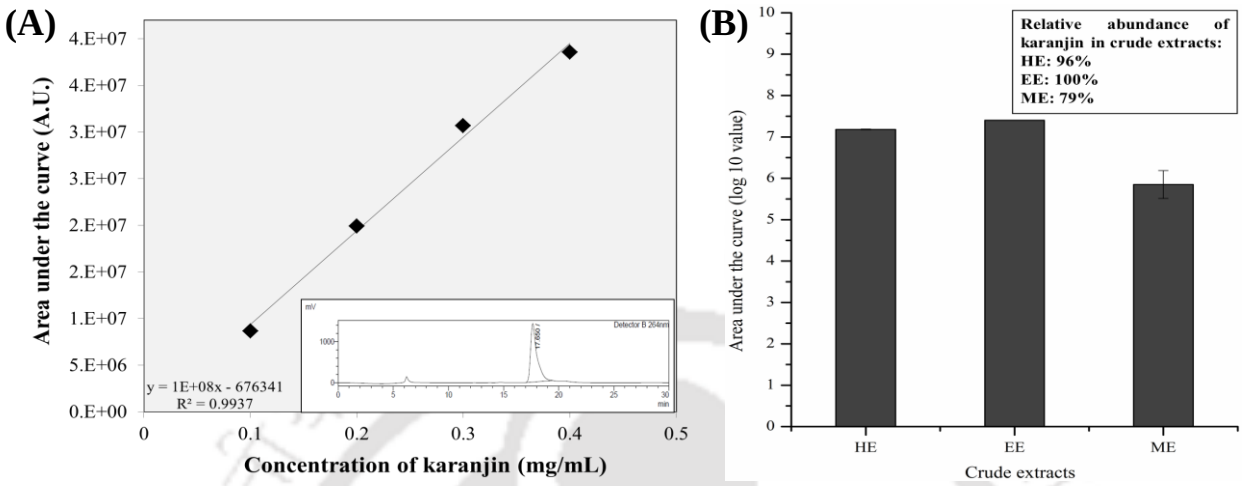

Figure 4.3 Purification of Karanjin (**A**) HPLC chromatogram, inset depicts single peak of an isolated compound, PPS-E and (**B**) Relative abundance of Karanjin in different crude extracts.

4.3.1.1. Fourier transform infrared spectroscopy (FTIR)

Infrared (IR) is most useful in providing information about the presence or absence of specific functional groups. FTIR spectrum of Karanjin crystal was recorded and used to compare with DFT carried out with Gaussian 09 software, at B3LYP/6-311G (D,P) level (**Figure 4.4**). Prominent peaks from experimental FTIR match well with the calculated DFT value (**Figure 4.4 A**). As seen, the C=O stretching vibration appears as a prominent mode in the FTIR spectrum at 1624 cm^{-1}. The peak at 1405 cm^{-1} gives the information that the compound comprise important -CH_3 functional group and recorded spectra is in good agreement with the calculated value at 1408 cm^{-1} (**Figure 4.4 B**). The prominent peak is primarily due to the butterfly motion in -CH_3 group present in Karanjin molecule as suggested by Pandey et al. (2014). In the experimental spectrum, another peak appeared at 756 cm^{-1} because the geometry of the molecule is out of the plane and it is well matching with the calculated value at 757 cm^{-1}. Some of the vibrational peaks at

958, 1019, 1035, 1132, 1164, 1227, 1260, 1285, 1332, 1227 and 1463 cm^{-1} are due to the presence of -C-C-H vibration in aromatic rings of Karanjin. Other peaks at 1285 and 1373 cm^{-1} are showing the deformation in the aromatic rings. Almost all the peaks matched well with the calculated DFT values.

(A)

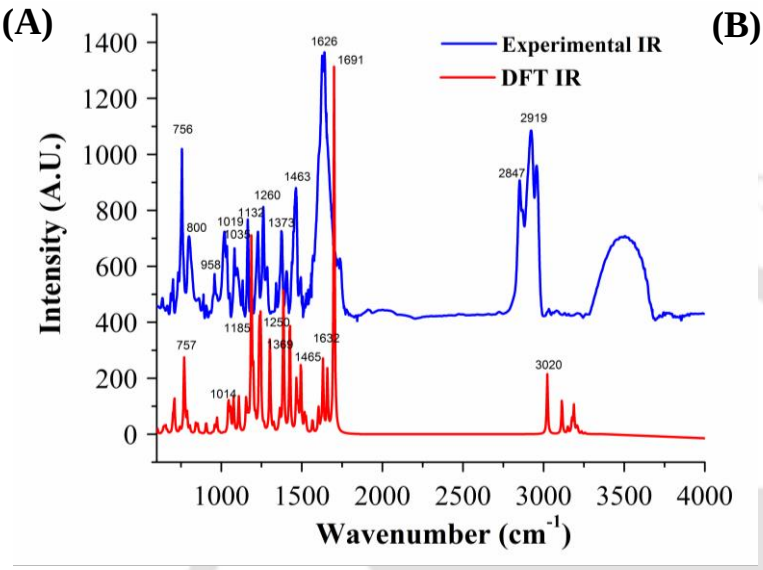

(B)

IR Exp. (cm^{-1})	DFT Cal. (cm^{-1})
756	757
958	951
1019	1014
1035	1034
1132	1140
1164	1164
1227	1214
1260	1250
1285	1273
1373	1369
1405	1408
1463	1465
1626	1632

Figure 4.4 FTIR spectra of Karanjin (**A**) Comparison of calculated vibrational frequency with experimental FTIR spectra and (**B**) Values of vibrational frequency.

4.3.1.2. Raman Spectroscopy

Raman spectrum of pure Karanjin crystal was recorded and was used to compare with the DFT carried out with Gaussian 09 software, at B3LYP/6-311G (D, P) level (**Figure 4.5**). The scaled theoretical wavenumbers are in perfect agreement with the experimental values of pure Karanjin crystal (**Figure 4.5 A**). The prominent peaks observed at 1605 cm^{-1} and 1627 cm^{-1} are due to strong C=O stretching of flavone ring (Canamares et al., 2009), and these peaks are in good agreement with the calculated values such as 1610 and 1631 cm^{-1}, respectively (**Figure 4.5 B**). The peak at 1372 cm^{-1} present in the spectrum is due to the presence of $-CH_3$ group. Another intense peak at 1005 cm^{-1} is due to the trigonal stretching of flavone B ring. Furthermore, peaks at 1191, 1285 and 1530 cm^{-1} are involved in the bending of the CH plane. All these observed peaks in the Raman

spectrum of Karanjin matched well with three flavonoids like chrysin, apigenin and leutin and some flavone (Canamares et al., 2009; Corredor et al., 2009). Few additional peaks at 1022, 1341 and 1438 cm^{-1} are because of the CH vibration in the furan ring and are nearly in agreement with DFT calculation.

(A)

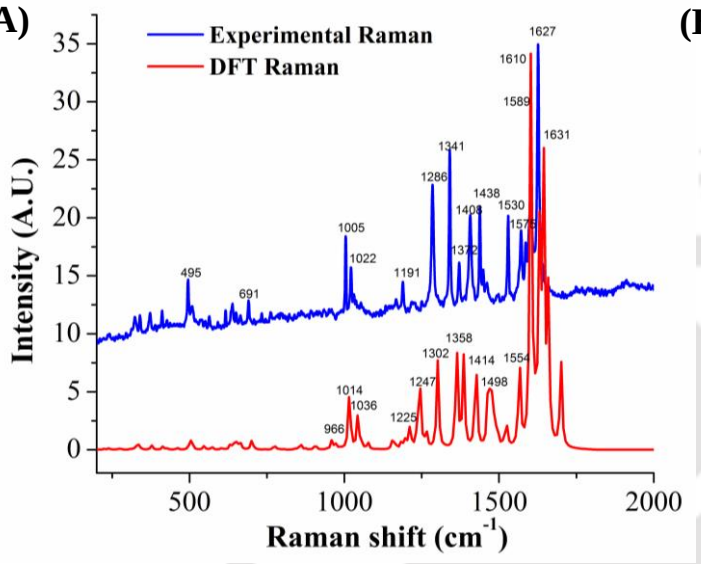

(B)

Raman Exp. (cm^{-1})	DFT Cal. (cm^{-1})
327	301
495	-
691	679
1005	966
1022	1036
1191	-
1286	1225
1341	1302
1372	1358
1408	1414
1438	1498
1530	1554
1575	1589
1605	1610
1627	1631

Figure 4.5 Raman spectra of Karanjin (**A**) Comparison of calculated vibrational frequency with experimental Raman spectra and (**B**) Values of vibrational frequency.

4.3.1.3. Nuclear magnetic resonance (NMR)

One dimensional NMR spectra of Karanjin acquired and analyzed for its structural characterization (**Figure 4.6**). ^{1}H Spectral data (**Figure 4.6 A** and **B**) of pure Karanjin revealed the presence of characteristic signal of furan ring as δH/δC at δ 8.151 (d, J = 1.8 Hz, H_5)/145.92 (C_5) and at δH/δC at δ 7.17 (d, J = 1.8 Hz, H_{15})/104.44 (C_{15}). The signal at 7.57-7.53 (4H, multiplet) indicated amono-substituted aromatic ring of Karanjin. ^{13}C spectral data showed the presence of a carbonyl carbon in flavonoid moiety at 175.26 and a prominent methoxyl carbon at 60.4 (**Figure 4.6 C**). Two carbon at 145.9 and 158.3 and two more tertiary carbon at 150.15 and 155.04 indicate aromatic carbon linked to an oxygen atom in a furanoflavonoid molecule. Amono-substituted aromatic ring is shown

at δ 131.19, 128.84 (one carbon), 128.86 (two carbons) and 128.5 (two carbons). Also, the ^{13}C spectrum of Karanjin contain four more signal for aromatic carbon at δ 122.09, 110.19, 119.9 and 117.2 along with a signal at 142.04 for the carbon attached to the methoxyl group. With the help of the DEPT experiment, CH, CH_2 and CH_3 groups can be easily differentiated by variation of the selection angle parameter (the tip angle of the final ^1H pulse). Angle 135° gives all CH and CH_3 in a phase opposite to CH_2. DEPT spectra showed signals for CH and CH_3 carbons accounting for 10 carbon as a result of transfer of proton magnetization onto the directly bound carbon in the molecule (**Figure 4.6 D**). From ^1H and ^{13}C spectral assignment along with DEPT spectral data, it could be inferred that annealation of the furan and flavonoid rings is at C2/C13 and C4/C12 positions, and phenyl ring substitution at C3 (C7) position, respectively (**Table 4.1**).

(A)

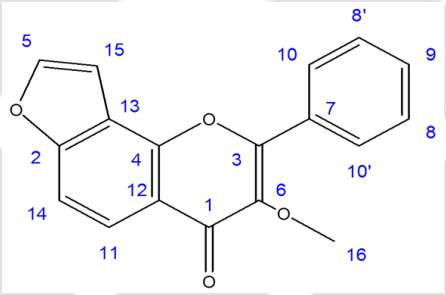

(B)

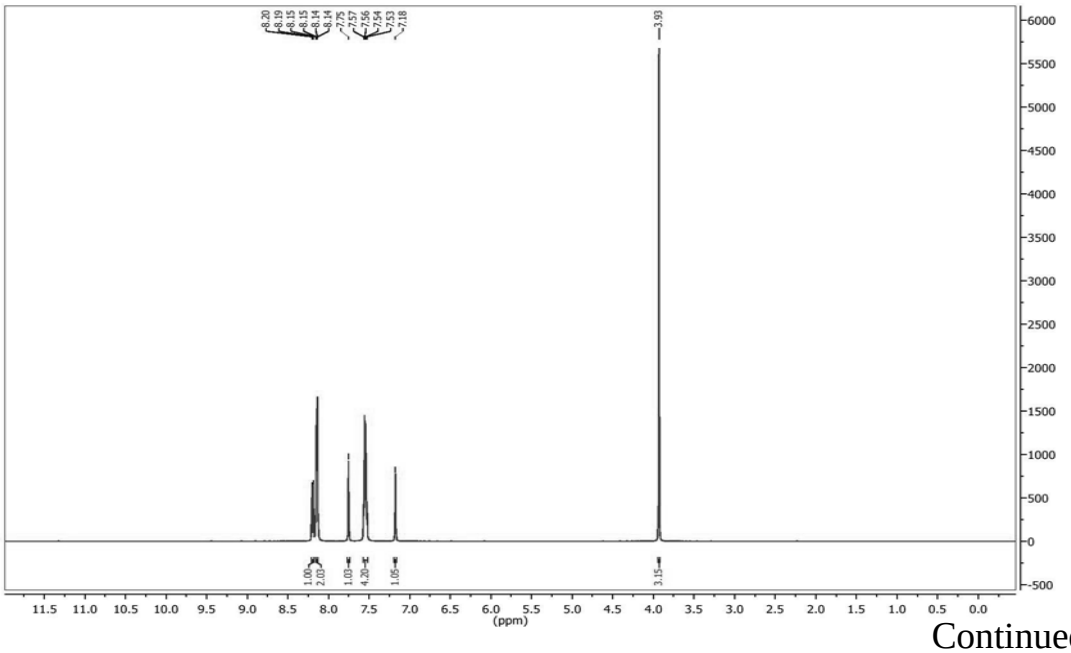

Continued..

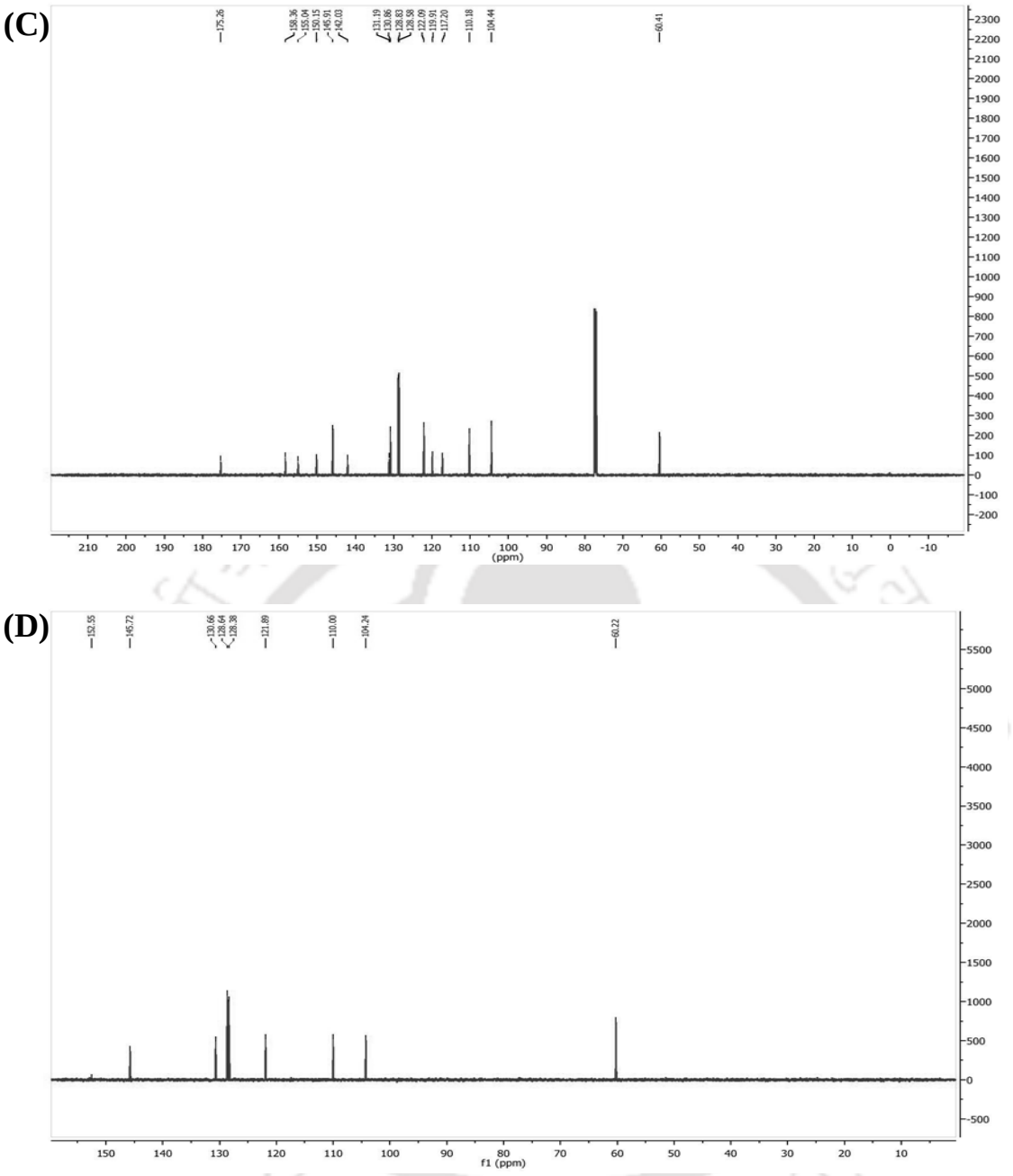

Figure 4.6 NMR spectra of Karanjin (**A**) Atom nomenclature; (**B**) ^{1}H; (**C**) ^{13}C and (**D**) DEPT 135°.

Table 4.1 NMR (^{1}H and ^{13}C) spectral data of Karanjin (δ in ppm).

Atom no.	^{1}H (δ, *J* in Hz)		^{13}C	
	Isolated	**Reported***	**Isolated**	**Reported***
1			175.26	174.7
2			158.37	157.8
3			155.04	154.5
4			150.15	149.6
5	8.151 d (1.8)	7.78 d (2)	145.92	145.4
6			142.04	141.5
7			131.19	130.7
8	7.544 m	7.60 m	130.86	128.3
9			128.84	130.3
10	7.759 d (1.8)	8.17 m	128.58	128.0
11	8.206 d (9)	8.22 d (8.5)	122.09	121.6
12			119.91	119.4
13			117.20	116.7
14			110.91	109.7
15	7.179 d (1.8)	7.20 d (2)	104.44	103.9
16	3.933 s	3.85 s	60.40	59.9

* Vismaya et al., 2010.

4.3.1.4. X-ray Diffraction (XRD)

Single-crystal X-ray diffraction determines atom position in three-dimensional space. Various chemical and physical properties of Karanjin crystal are listed in **Table 4.2**. Chemical structure, ball-stick model, crystal packing, and ellipsoid plot of the molecular structure of Karanjin as obtained from X-ray diffraction technique and mercury software respectively is shown in **Figure 4.7 (A-D)**. There is no formation of hydrogen bond within the crystal unit cell (**Figure 4.7 C**). Due to antibonding repulsion, the phenyl ring of Karanjin is slightly shifted above the plane (**Figure 4.7 D**) to minimise its surface energy (Pandey et al., 2014). The ground state optimised geometry was found to be non-planar. The refined structure was deposited to Cambridge Crystallographic Database Centre (CCDC) with ID number 1422898.

(http://www.ccdc.cam.ac.uk/Community/Depositastructure/Pages/DepositaStructure.aspx).

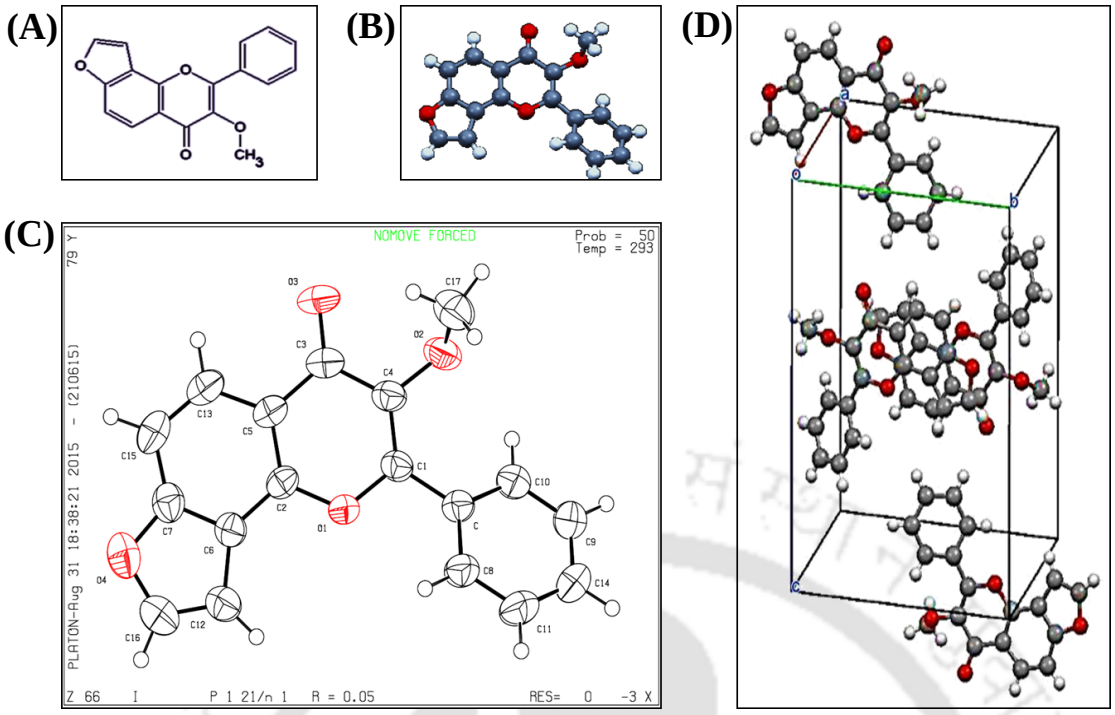

Figure 4.7 Perspective view of Karanjin. (**A**) Chemical structure; (**B**) Structure ball and stick model; (**C**) Ellipsoid plot of molecular structure and (**D**) Crystal packing in the unit cell.

Table 4.2 Crystal data of Karanjin.

Parameters	Karanjin
Empirical formula	$C_{18}H_{12}O_4$
Formula weight	292.0879
Crystal habit	Needle
Colour	Colourless
Crystal system	Monoclinic
Space group	P21/n
Temperature, T	296 K
Wavelength, λ(Å)	0.7107
Volume, V ($Å^3$)	1400.29
Cell formula unit Z	4
Calculated density, Mg m^{-3}	2.065
Unit cell dimensions	a=7.2020(6) Å, b=11.2867(9) Å, c=17.5318 (17) Å α=90.00(7)°, γ=90.00(7)°,β=100.707(6)°
Completeness to θ	99% (θ = 25.00°)
Refinement method	SHELXL-97 (Sheldrick, 1997), Olex2

4.3.1.5. Field emission scanning electron microscopy (FESEM)

FESEM image of Karanjin shows that it is needle-shaped crystal having sharp edges (**Figure 4.8**) Size of the crystal obtained after purification and crystallization is in the range of 0.1-0.5 mm.

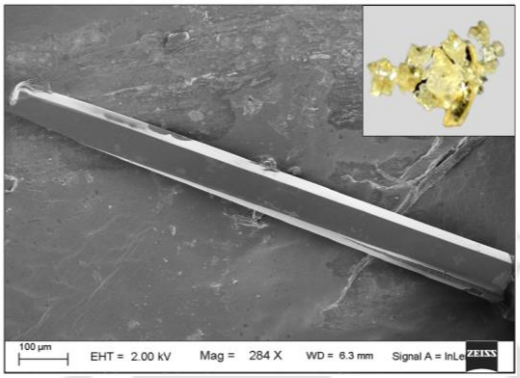

Figure 4.8 FESEM image of Karanjin (inset: crystals after recrystallization).

4.3.1.6. Thermoanalytical analysis

Thermoanalytical analysis (TGA, DTG and DTA) of Karanjin was done (**Figure 4.9**). Crystal is brought quickly up to the desired temperature (isothermal procedure), and weight of the sample is monitored during thermal decomposition. The DTA profile of Karanjin shows exothermic peaks at 150-300°C and 320-620°C. From the TG curve of Karanjin under nitrogen purge gas, a continuous mass loss was observed from 200-300°C leaving approximately 2% of original mass at 450°C depicting homogeneous degradation behaviour of flavanone. Karanjin is completely decomposed at this temperature in which -OCH_3 being the weakest bond tends to be decomposed first. The TG profile of Karanjin showed one decomposition step which resembled the thermal degradation of quercetin (Moreira et al., 2002). Thermal analysis is recognized as an essential technique to understand the thermal stability of flavonoid because of its simplicity, high efficiency, and easy curve analysis (Ferreira et al., 2017).

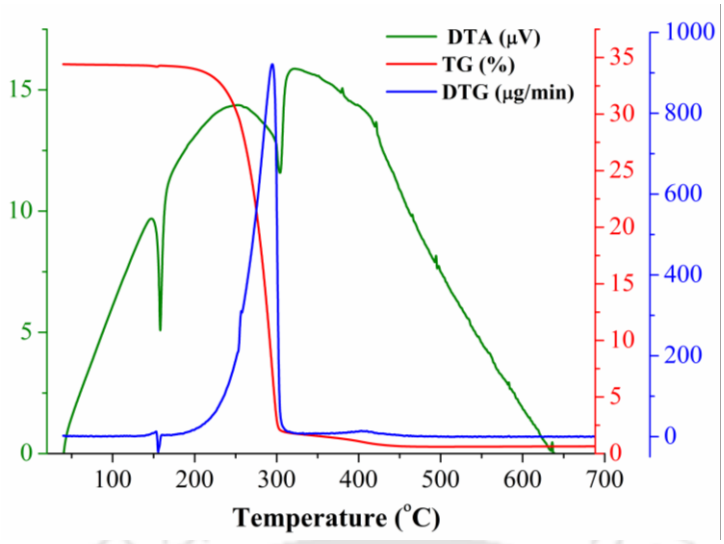

Figure 4.9 Thermogram curve of Karanjin.

4.3.2. Identification of PPS-M

Brown crystals (PPS-M) were isolated and purified from ME by solvent extraction (yield 0.2%, melting point 280ºC). The HRMS confirmed mass of compound with molecular formula $C_7H_{14}NO_4$. The m/z of the compound in positive $[M+H]^+$ and negative mode $[M+H]^-$ are 176.0914 and 174.0777, respectively (**Figure 4.10**). The molecular mass was found to be 175.0845 and matched well with the reported mass value of glabrin (**Figure 4.11**) (Rao and Rao, 1941). Earlier reports with regard to Glabrin isolation from the seeds varied from 0.04 to 0.1% depending upon the geographical site of collection (Rao and Rao, 1941; Chandel et al., 2005). Also, the process for procurement of Glabrin was tedious and time-consuming. However, in the current protocol, the pure compound has been achieved by a simple extraction step followed by purification with solvents. Glabrin was validated and confirmed by spectroscopic techniques viz; FTIR, FESEM and XRD which are primary tools utilised by researchers in structural elucidation;

HRMS spectrum

MS data showed parent molecular ion peak at 175.0845.

Theoretical value $[M+H]^+$ = 176.0914

Theoretical value $[M+H]^-$ = 174.0777

Observed value = 175.0845

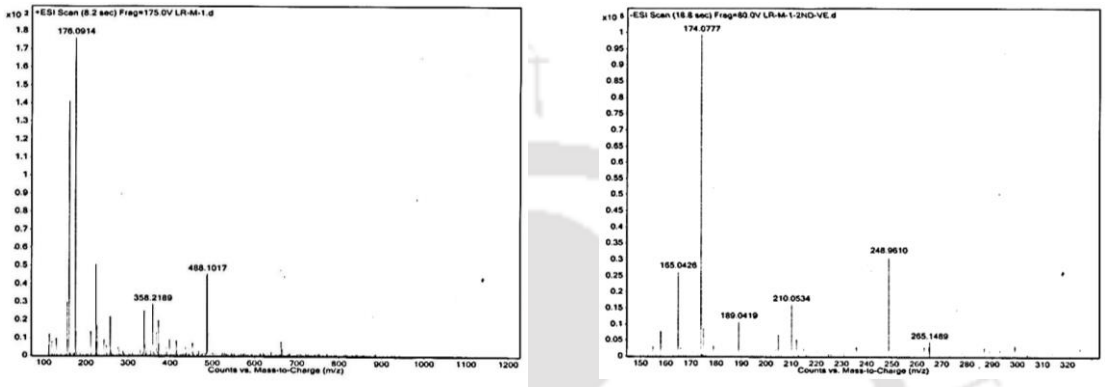

Figure 4.10 Mass spectrum of PPS-M isolated from seeds of *P. pinnata*.

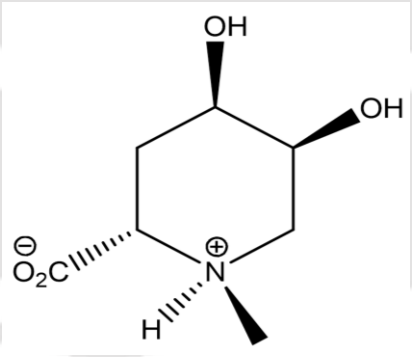

Figure 4.11 Structure of Glabrin (IUPAC: 4,5-dihydroxy-1-methylpiperidine-2-carboxylic acid).

4.3.2.1. Fourier transform infrared spectroscopy (FTIR)

The infrared spectrum encodes a lot of important information on amino acid like protonation state, charge, H-bond formation, and conformational freedom. According to the 3N-6 rule (with N the number of atoms), glabrin has 69 normal modes. In the present work, the vibrational spectrum of Glabrin has been obtained and compared with the result obtained from DFT calculation (**Figure 4.12**). DFT is considered to be a good tool

for the band assignment of zwitterionic amino acids (Fischer et al., 2005; Chowdhry et al., 2008). In the spectrum, we observed the vibration mode near low-frequency region (around 750-1040 cm^{-1}). This region represents the stretching and bending vibrations of C-C skeletal, C-H bending and C-N stretching (Fischer et al., 2005). The position of the N-H bending appeared at 1402 cm^{-1} in the experimental spectrum, while the corresponding peak from DFT appeared at 1404 cm^{-1}. Glabrin has a strong band near 1619 cm^{-1} indicating the existence of the asymmetric ionic carboxyl mode of vibration (Blom et al., 2007). The carbonyl stretch of a carboxylic acid moiety is one of the most significant band in the IR spectra of amino acids. The band at 2949 cm^{-1} in the spectrum corresponds to C-H stretching of CH_2. The vibrational mode of O-H and N-H groups appear as a single broadband with strong intensity at 3314 cm^{-1} in IR spectrum (**Table 4.3**). However, the stretching vibration of O-H groups showed strong and sharp peaks at 3443 and 3508 cm^{-1}. The N-H stretching band was observed at high-frequency region approximately at 3338 cm^{-1} in DFT calculation. Our FTIR absorption study reveals that the spectrum of Glabrin is very particular and they can serve as a fingerprint for the compound.

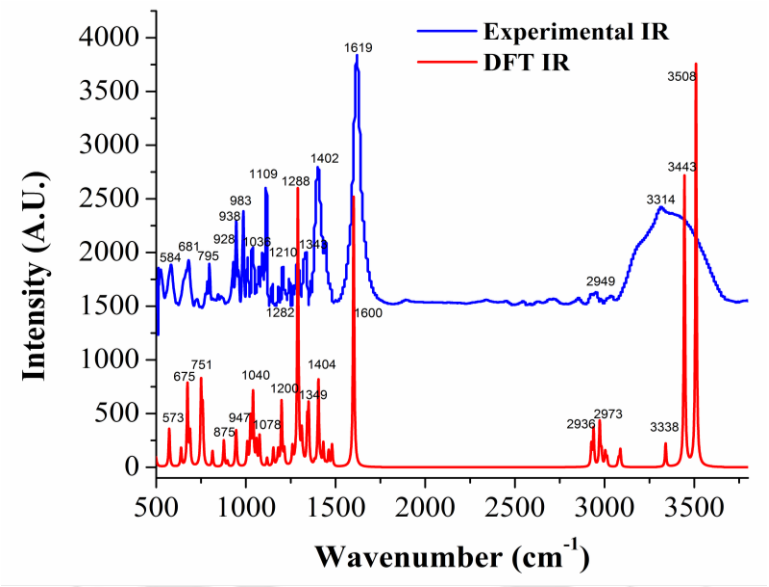

Figure 4.12 Comparison of calculated vibrational frequency and experimental FTIR spectra of Glabrin.

Table 4.3 Experimental IR frequency of Glabrin and theoretical calculation using DFT along with their respective assignment of bond vibrations.

Sr. No.	IR Exp. (cm^{-1})	DFT Cal. (cm^{-1})	Assignments
1	681	675	OH bending
2	795	751	C-C bending
3	938	947	C-C bending and C-C stretching
4	1036	1040	C-C bending and C-N stretching
5	1109	1078	C-OH stretching and N-H bending
6	1210	1200	C-H bending
7	1282	1288	C-C stretching and C-H bending
8	1343	1349	C-H bending
9	1402	1404	N-H bending
10	1619	1600	Asymmetric COO stretching
11	2949	2936	Symmetric CH_2 Stretching
12	-	2973	Asymmetric CH_2 stretching
		3338	NH stretching
13	3314	3443	OH stretching
		3508	OH stretching

4.3.2.2. X-ray diffraction (XRD)

Single-crystal X-ray diffraction can be used to determine, confirm, or complete molecular structure routinely and unambiguously, thereby, establish conformation and relative stereochemistry and even conformation of the compound. Ball-stick model, chair

conformation, ellipsoid plot, and crystal packing of Glabrin were obtained from X-ray Diffraction technique and mercury software respectively as shown in **Figure 4.13 (A-D)**. From XRD data, there is the formation of both intra- and inter-molecular hydrogen bonds within the crystal unit cell. The compound exhibited the chair conformation indicates the stability of the compound. Various chemical and physical properties of Glabrin crystal are listed in **Table 4.4**.

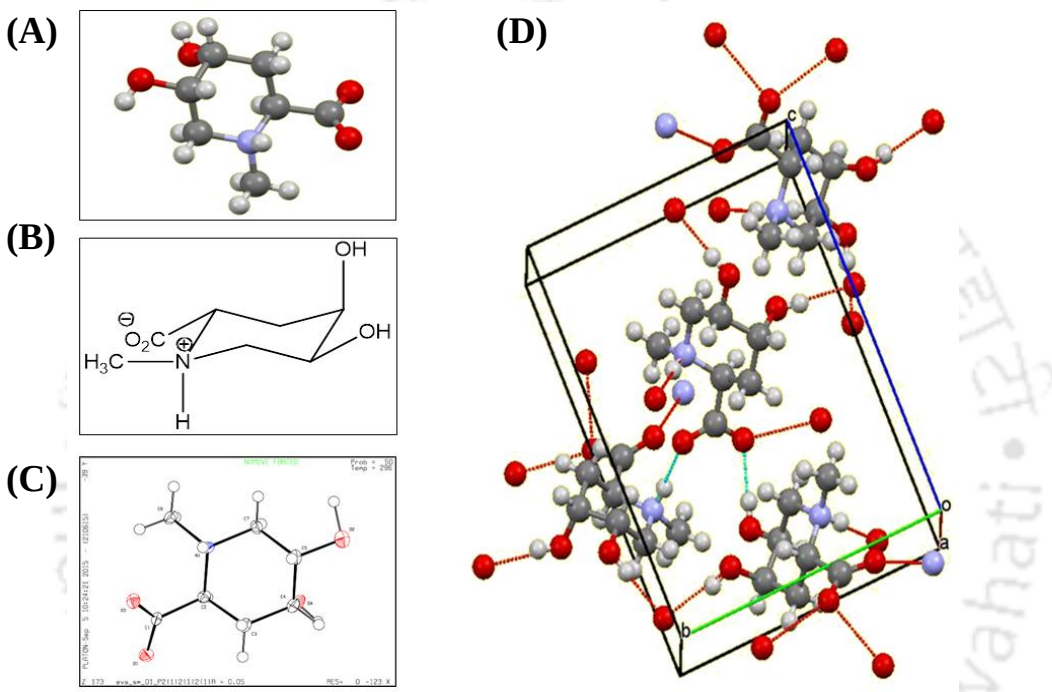

Figure 4.13 Structure of Glabrin. (**A**) Ball and stick model; (**B**) Chair conformation; (**C**) Ellipsoid plot of molecular structure and (**D**) Crystal packing in the unit cell.

Table 4.4 XRD data of Glabrin.

Parameters	Glabrin
Empirical formula	$C_7H_{14}NO_4$
Formula weight	175.0845
Crystal habit	Rectangular plates
Colour	Brown
Crystal system	Orthorhombic
Space group	P 21 21 21
Temperature, T	296 K
Wavelength, λ(Å)	0.7107
Volume, V ($Å^3$)	765.2(2)
Cell formula unit Z	4
Calculated density, Mg m^{-3}	1.495
Unit cell dimensions	a= 6.1799(10)Å, b= 9.5894(17)Å, c= 12.912(2)Å α= 90.00°, γ= 90.00°, β= 90.00°
Completeness to *θ*	99% (θ = 28.80°)
Refinement method	SHELXL-97 (Sheldrick, 1997), Olex2

4.3.2.3. Field emission scanning electron microscope (FESEM)

Figure 4.14 shows the FESEM image of a Glabrin crystal having sharp edges. Size of the crystal obtained after purification and crystallisation is in the range of 0.1-0.6 mm.

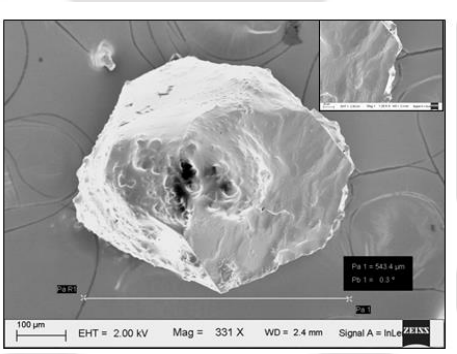

Figure 4.14 FESEM image of Glabrin, inset surface topography of crystal.

4.4. Conclusion

In this chapter, two compounds (PPS-E and PPS-M) were characterized using various analytical and spectroscopic techniques. Theoretical vibrational assignment of compounds showed good agreement when compared with experimental values. PPS-E and PPS-M have been characterized and identified as a furanoflavone namely Karanjin (IUPAC: 3-methoxy-2-phenylfuro [2,3-h]chromen-4-one) and cyclic amino acid as Glabrin (IUPAC: 4,5-dihydroxy-1-methylpiperidine-2-carboxylic acid).

Chapter 5

UV-Visible absorption and fluorescence spectra of Karanjin in different solvents and solvent mixture

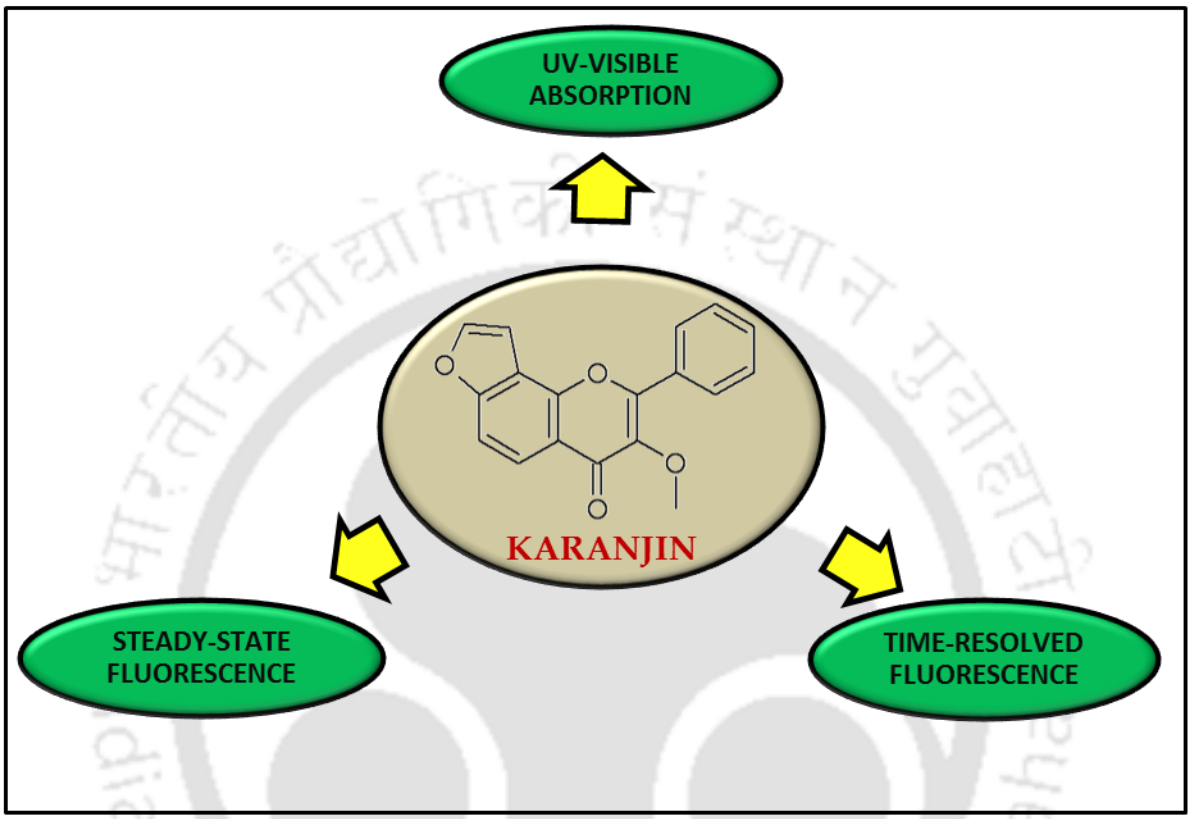

This chapter describes UV-Visible absorption and fluorescence spectroscopy investigation of Karanjin.

Chapter 5

UV-Visible absorption and fluorescence spectra of Karanjin in different solvents and solvent mixture

5.1. Introduction

Flavonoids (C6-C3-C6 backbone) are secondary metabolites abundantly present in the plant tissues. They have attracted attention because of their versatile health benefits (Pandey and Kumar, 2013). The conjugated ring structure in flavonoids makes them sensitive to changes in their immediate surroundings, thereby altering their photophysical properties and photobiological behavior. Aromatic groups present in all flavonoids contribute to their UV absorption in the 250 nm region, while certain flavonoids contain carbonyl groups that absorb light in 300 nm region. Thus, the molecular structure of flavonoids like planarity, conjugation, and substituents play an essential role in their photostability and photophysical properties (Sisa et al., 2010; Voicescu et al., 2014). However, investigating the spectroscopic properties of these bioactive compounds *in vivo* is difficult in a biological system. Therefore, many biological mimetic conditions such as aqueous-organic and micellar systems are often considered for research purposes (Liu et al., 2009).

The characterization of the biologically active natural products is mainly done by UV-Visible (Posokhov et al., 2005; Fain et al., 2006; Anouar et al., 2014) and fluorescence spectroscopy (Dunford et al., 2003; Sengupta et al., 2005; Bi et al., 2006; Sun et al., 2008; Donovalova et al., 2012) owing to their high specificity and sensitivity. The solvent environment surrounding the probe is an important factor for understanding its photophysical properties that in turn depends on the polarity and ability of the probe

to form hydrogen bonds with solvents. The change of solvent affects the ground and excited states differently, and these changes are important to study the overall effects of the solute-solvent interactions. These interactions can be used in monitoring the microenvironment in various neat solvents and solvent mixtures (Zhao et al., 2010; Sancho et al., 2011). Many studies have been done on solvatochromism of fluorescent molecules in aqueous solutions and organic solvents using UV-Visible absorption and fluorescence techniques (Satpati et al., 2005; Gustavsson et al., 2007; Liu et al., 2013).

On the other hand, the amphiphilic species like sodium dodecyl sulfate (SDS) in water lead to the spontaneous self-assembly of surfactant to form micelles in the solution. Critical micellar concentration (CMC) is the minimum concentration of the surfactant at which micelle formation occurs. Micelles are being accompanied by complex and interesting physicochemical phenomena and owing to their basic structural similarity with the membrane; they have been one of the most exploited membrane mimetic agents (Fendler, 1980; Tulumello and Deber, 2009). It is one of the central research topics in colloid science for its useful practical applications in technology processes. The solvation dynamics in heterogeneous microenvironments like micelles mostly arise due to the restricted movement of the confined water molecules and their characteristic properties that are largely different from that of the bulk water (Bhattacharyya and Bagchi, 2000) and therefore, make it one of the interesting subjects of intense research in recent years.

Biophysical techniques like UV-Visible spectroscopy and fluorescence spectroscopy have always been the primary research tool for understanding the photophysical property of the fluorophore. When the continuous radiation passes through a chromophore, a portion of the radiation is absorbed by the molecule. As a result of this absorption, the electrons in chromophore are excited from the ground vibrational level,

S_0 (low energy) to higher vibrational levels, S_1 or S_2 (high energy) in a very short span of time (10^{-15} s) (**Figure 5.1**). The energy difference between these two states in the transition is exactly equal to the energy of absorbed radiation which can be represented as an absorption spectrum.

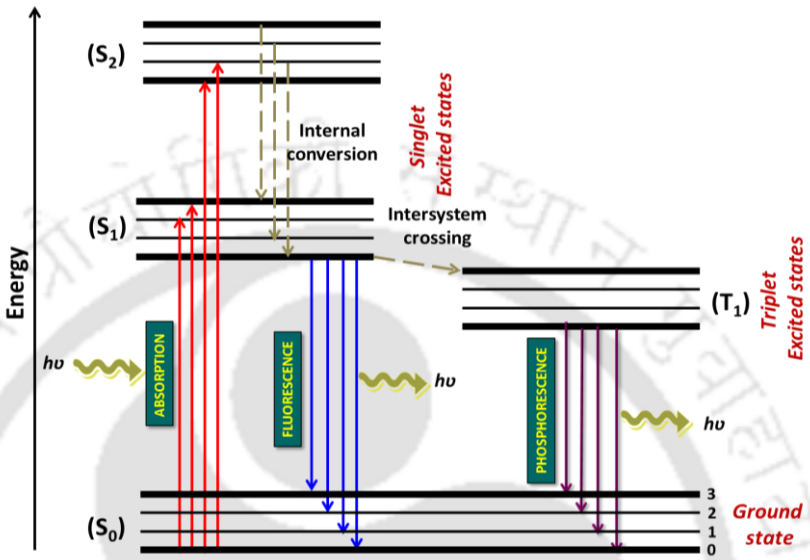

Figure 5.1 Jablonski diagram.

Here: $h\upsilon$ is a generic term for photon energy with h = Planck's constant (6.63×10^{-34} Js) and υ = frequency of light.

UV-Visible spectroscopy follows Beer-Lambert law stating that absorbance of the analyte is directly proportional to its concentration and pathlength of sample cell as per the **equation 1.1.**

$$A = \log I_0/I = \varepsilon cl \qquad (1.1)$$

where, A = absorbance, I_0 = intensity of incident light, I = intensity of transmitted light, ϵ = molar extinction coefficient or molar absorptivity ($M^{-1}cm^{-1}$), c = molar concentration of sample (M) and l = pathlength of sample cell (cm).

Moreover, several physical parameters define the strength of a molecule to absorb radiation, such as molar extinction coefficients (ϵ), transition dipole moments (μ)

and oscillator strengths (*f*). Compound with higher ϵ value shows higher absorption capacity at a given wavelength. It is an intrinsic property of the compound and particularly useful in a spectroscopic study in dthe etermination of the concentration of the compound of interest. Moreover, knowledge of molar absorptivity of the compound will certainly assist in its quantification in biological samples (Trela and Waterhouse, 1996).

Transition dipole moment is the electric dipole moment that measures the coupling between molecular orbitals associated with the transition between excited state and ground state. Determination of ground (Ψ_a) and excited (Ψ_b) state dipole moments is important as it gives information about the change in electronic distribution upon excitation. According to quantum mechanics, the light absorptivity of a molecule depends on its transition dipole moment, i.e., a larger transition dipole moment indicates stronger absorptivity. It is calculated using **equation 1.2**.

$$\textbf{Dipole strength} = |\langle \Psi_b | \underset{\sim}{\mu} | \Psi_a \rangle|^2 = 9.18 \times 10^{-3} \int \frac{\varepsilon(\upsilon)}{\upsilon} d\upsilon \qquad \textbf{(1.2)}$$

where, Ψ_a = wavefunction of the ground state, Ψ_b = wavefunction of the excited state, $\underset{\sim}{\mu}$ = transition dipole moment operator, $\epsilon(\upsilon)$ = molar extinction coefficient as a function of frequency (Hz).

Oscillator strength is a dimensionless parameter that expresses the probability and absorption strength of electromagnetic radiation in transitions between energy levels of an atom or molecule (Radwan, 2007). For spin allowed electronic transitions, oscillator strengths generally fall in the range of $1 > f > 0$. It is calculated by following **equation 1.3**.

$$f = 4.32 \times 10^{-9} \int \varepsilon(\bar{\upsilon}) d\bar{\upsilon} \qquad \textbf{(1.3)}$$

where, *f* = oscillator strength, $\epsilon(\bar{\upsilon})$ = molar absorption as function of wavenumber (cm^{-1}).

Following the absorption of radiation, electron stays in singlet excited state only for a very short period of time (few nanoseconds or less) and return to ground state. Therefore, the extra energy is often lost through the emission of light or luminescence process. Luminescence is the emission of light from the molecule and broadly divided into two categories fluorescence and phosphorescence depending on its excited state electronic transitions. A molecule in the S_1 state can return to S_0 by the emission of photons called 'fluorescence' and generally occurs in 10^{-9} s. Excited molecule can also relax to ground state via first triplet state (T_1) by undergoing intersystem crossing and spin conversion (**Figure 5.1**). The emission from T_1 is termed as 'phosphorescence,' and the emission is shifted to longer wavelength relative to the fluorescence. The wavelength of the excitation radiation is always shorter than the emission radiation. The difference between the peak wavelengths of absorption and emission of the fluorophore is called 'Stokes shift' and highly sensitive to the immediate environment around the fluorophore.

The fluorescence of the molecule can be measured by two different techniques, namely: steady-state and time-resolved. Steady-state fluorescence measurement is performed with continuous illumination of light, and the emission intensity is recorded as a function of wavelength. Time-resolved measurement is used for recording fluorescence intensity decay kinetics when the sample is exposed to a short pulse of light. The decay is fitted to a kinetic model to extract decay parameters.

The fluorescence decay kinetics rate constant is one of the most important characteristics of a fluorophore because it defines the time window of observation of the dynamic phenomenon. The fluorescence lifetime (τ) is defined by the average time the molecule spends in the excited state before return to the ground state. There are two methods of measuring fluorescence lifetime: frequency-domain and time-domain. In the frequency-domain method, the sample is excited with sinusoidally modulated light, and

the emission is delayed in time relative to the excitation. This delay is measured as a phase shift (φ) which can be used to calculate the decay time (Lakowicz, 1999).

In the time-domain method, the sample is excited with an ultra-short pulse of light and the fluorescence lifetime can be obtained from the time taken for the intensity to decrease to 1/*e* of its initial value or from the slope of the plot of log *I*(*t*) versus *t* (**equation 1.4**).

$$I(t) = I_0 e^{-t/\tau} \qquad \textbf{(1.4)}$$

where, I_0 = intensity at time $t = 0$ and τ = decay time

Equation 1.4 is based on the assumption that the fluorescence decay follows a single exponential. For example, N-acetyl-L-Tryptophanamide (NATA) in water showed single exponential decay upon fitting and displaying a single lifetime of 2.88 ns (**Figure 5.2**).

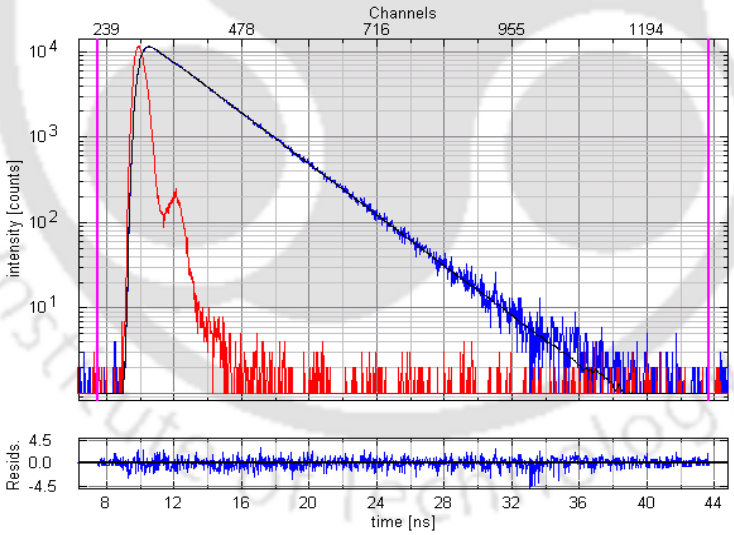

Figure 5.2 Time-resolved fluorescence intensity decay of NATA in water (λ_{ex} = 280 nm, λ_{em} = 350 nm). The image shows instrument response function (red), measured decay curve (blue) and fitted curve (black).
Results: τ = 2.88 ns; reduced χ^2 = 1.065; lower panel: residual plot (Source: GmbH, 2018).

However, several fluorophores do not always follow the above equation as it may possess several conformational states of different lifetime. For higher order or multiexponential decays, intensity decay can be fitted according to **equation 1.5**.

$$I(t) = \sum_{i=1}^{n} \alpha_i e^{-t/\tau} \quad ; \qquad \sum \alpha_i = 1.0 \qquad \textbf{(1.5)}$$

where, n = 1, 2 or 3; α_i = individual fractional contributions and τ_i = their individual lifetimes.

In the case of multiexponential decays, mean lifetime (τ_m) can be defined as:

$$\tau_m = \sum_i \alpha_i \tau_i \qquad \textbf{(1.6)}$$

where, τ_m is proportional to the area under the fluorescence intensity decay curve.

For example, hydroxyquinoline showed bi-exponential decay function displaying mean lifetimes of 3.328 ns in 100% dimethylformamide (DMF) and 5.275 ns in 99% Water-1% DMF mixture (**Figure 5.3**).

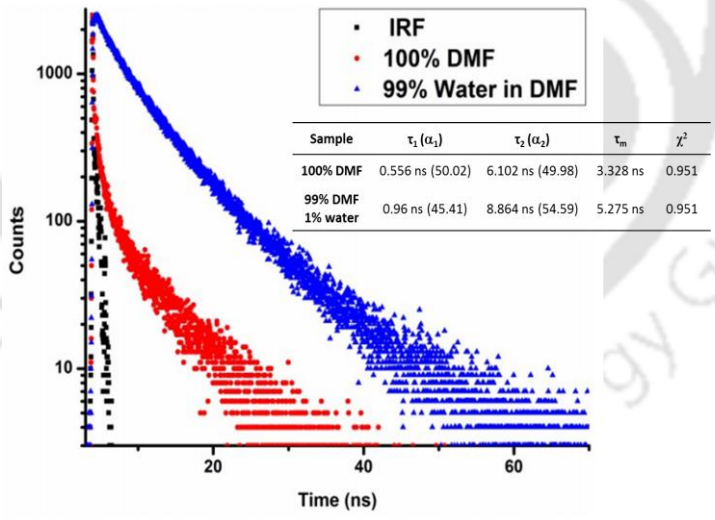

Sample	τ_1 (α_1)	τ_2 (α_2)	τ_m	χ^2
100% DMF	0.556 ns (50.02)	6.102 ns (49.98)	3.328 ns	0.951
99% DMF 1% water	0.96 ns (45.41)	8.864 ns (54.59)	5.275 ns	0.951

Figure 5.3 Time-resolved fluorescence intensity decay profiles of hydroxyquinoline (β-NN) in DMF. The image shows the instrument response function (black), β-NN in 100% DMF (red; λ_{ex}= 375 nm, λ_{em} = 430 nm), β-NN in 99% Water-1% DMF mixture (blue; λ_{ex}= 375 nm, λ_{em} = 500 nm).

Results: Bi-exponential decays with average lifetimes of 3.328 ns in 100% DMF and 5.275 ns in 99% Water-1% DMF mixture (Source: Meher et al., 2016).

One of the most powerful techniques used for measuring fluorescence decay kinetics in time-domain is time-correlated single photon counting (TCSPC) due to its powerful electronics, high repetition rate, and picosecond laser light source. In this technique, the sample is repetitively excited with pulsed light source serving as a start signal. This signal is used to trigger the voltage ramp of the 'time to amplitude converter (TAC).' The voltage ramp is stopped when the detector detects fluorescence photon (stop signal) by the sample. The time difference between these start-stop signals provides an output voltage by TAC which then converted digitally to time by a multichannel analyzer (MCA) and stored. After many repetitive pulses, MCA builds a histogram plot of counts versus time. This histogram represents the fluorescence intensity decay (**Figure 5.4**).

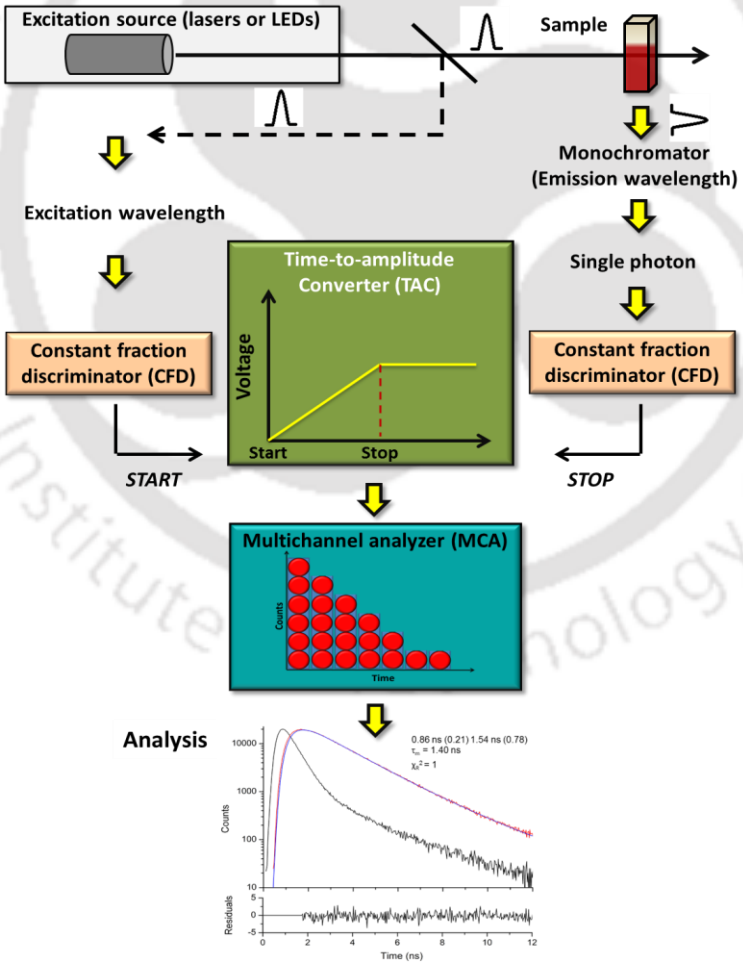

Figure 5.4 Schematic representation of TCSPC setup.

An instrument response function (IRF) or lamp function reflects the distribution of photons from the excitation pulse in a non-fluorescent scattering media or zero lifetime samples. The experiment often starts with a standard sample with known single exponential decays kinetics to test the performance of the instrument (Lampert et al., 1983). The lifetime is extracted using curve fitting software based on the application of Marquardt's algorithm for non-linear least squares analysis (Bevington, 1969; Berezin and Achilefu, 2010). Careful examination of the deviations between the experimental and fitted data comprises of graphical techniques such as weighted residuals or autocorrelation function and numerical statistical test like the reduced value of χ^2 (χ_R^2) which indicates goodness of the fit (Grinvald and Steinberg, 1974). Moreover, fluorescence lifetime has also been used to measure the excited state kinetics of the molecule making it a suitable technique to monitor dynamic changes in the fluorophore's environment (Voicescu et al., 2014; Lemos et al., 2015).

On the other hand, the relationship between steady state intensity (I_{ss}) and time-resolved measurements can be expressed as follows (**equation 1.7**).

$$\mathbf{I_{ss}} \propto \int_0^\infty \boldsymbol{I_0}\, \boldsymbol{e^{-t/\tau}}\, \boldsymbol{dt} = \boldsymbol{I_0\tau} \qquad \textbf{(1.7)}$$

For multiexponential decays, it can be expressed as (**equation 1.8**).

$$\mathbf{I_{ss}} \propto \int_0^\infty \boldsymbol{\alpha_i}\, \boldsymbol{e^{-t/\tau_i}}\, \boldsymbol{dt} = \boldsymbol{\Sigma \alpha_i \tau_i} \qquad \textbf{(1.8)}$$

where, I_{SS} = steady-state fluorescence intensity. Here, it is clear that steady-state intensity is proportional to the lifetime.

Photophysical characterization of various flavonoids, such as 3-hydroxyflavone (Sarkar and Sengupta, 1991), 3,5,7-trihydroxy-8,4′-dimethoxyflavone (Kumar et al., 2001), coumarins (Evale et al., 2009), 7-hydroxyflavone (Sancho et al., 2011), quercetin

(Park et al., 2013; Hofener et al., 2013), formononetin (Dunford et al., 2003), etc have been carried out in various aqueous and organic solvents. Numerous studies of flavonoids investigated using UV-Visible and fluorescence spectroscopy are summarized in **Table 5.1**. However, very limited literature regarding fluorescence lifetime measurement of flavonoids is available.

Table 5.1 Photophysical properties of the flavonoids. Parentheses indicate the solvents used in the experiments.

Sr. No.	Flavonoid	Absorbance Data	Fluorescence data	Quantum yield (ϕ)	Lifetime (τ_m)	Reference
1	Robinetin	λ_{max} = 359 nm (water); 366 nm (MeOH); 356 nm (EtOAc)	Ex 370 nm λ_{max} = 490 nm (MeOH); 424 nm (EtOAc)	-	-	Guharay and Sengupta, 1997
2	2-(2-benzo [b] furanyl) 3-hydroxychromone	λ_{max} = 336 nm (EtOH); 358 nm (CH_3CN)	Ex 450 nm λ_{max} = 544 nm (EtOH); 542 nm (CH_3CN)	0.12 (EtOH); 0.18 (CH_3CN)	-	Klymchenko et al., 2001
3	3-Hydroxyflavone	λ_{max} = 394 nm (EtOAc); 410 nm (water)	Ex 410 nm λ_{max} = 475 nm (EtOAc); 554 nm (water)	0.03 (EtOAc); 0.003 (water)	-	Klymchenko et al., 2002
4	**A)** Flavone **B)** 7-Hydroxyflavone	**A)** λ_{max} = 294 nm (MeOH) **B)** λ_{max} = 308 nm (MeOH)	-	-	-	Sancho et al., 2011
5	**A)** Fisetin **B)** Apigenin **C)** Quercetin **D)** Kaempferol **E)** Morin	**A)** λ_{max} = 365 nm (MeOH-water) **B)** λ_{max} = 338 nm (MeOH-water) **C)** λ_{max} = 372 nm (MeOH-water) **D)** λ_{max} = 366 nm (MeOH-water) **E)** λ_{max} = 357 nm (MeOH-water)	**A)** Ex 377 nm λ_{max} = 470 nm (MeOH-water) **B)** Ex 390 nm λ_{max} = 524 nm (MeOH-water) **C)** Ex 425 nm λ_{max} = 484 nm (MeOH-water) **D)** Ex 426 nm λ_{max} = 484 nm (MeOH-water) **E)** Ex 417 nm λ_{max} = 490 nm (MeOH-water)	-	-	Hofener et al., 2013

Continued..

Sr. No.	Flavonoid	Absorbance Data	Fluorescence data	Quantum yield (ϕ)	Lifetime (τ_m)	Reference
6	**A)** Quercetin **B)** Apigenin	**A)** λ_{max} = 370 and 257 nm (MeOH-water); 335 and 265 nm (CH_3CN-water) **B)** λ_{max} = 370 and 255 nm (MeOH-water); 320 and 270 nm (CH_3CN-water)	**A)** Ex 320 nm λ_{max} = 381 nm (MeOH); 376 nm (CH_3CN) **B)** Ex 325 nm λ_{max} = 395 nm (MeOH); 395 nm (CH_3CN)	**A)** 23.7×10^{-3} (MeOH); 20.9×10^{-3} (CH_3CN) **B)** 9.78×10^{-3} (MeOH); 17.7×10^{-3} (CH_3CN)	**A)** Ex 337 nm 3.34 ns (MeOH); 4.81 ns (CH_3CN) **B)** Ex 337 nm 2.67 ns (MeOH); 4 ns (CH_3CN)	Park et al., 2013
7	Flavonoid crude extract from *Syngonanthus nitens*	λ_{max} = 330 nm (isopropanol and water); 340 nm (DMSO, propylene glycol and MeOH)	Ex 375 nm λ_{max} = 435 nm (acetone, isopropyl and MeOH); 460 nm (water); 488 nm (DMSO)	-	Ex 375 nm 0.5, 1.8 and 5.6 ns (solvent not mentioned)	Berlim et al., 2018
8	Artepillin C	λ_{max} = 291 nm (citrate-phosphate)	Ex 310 nm λ_{max} = 400 nm (aqueous, pH 7)	-	Ex 296 nm 0.18 ns (aqueous, pH 7)	Camuri et al., 2018

Karanjin, a furanoflavonoid (3-methoxy-2-phenylfuro[2,3-h] chromen-4-one) isolated from *Pongamia pinnata*, is the most widely studied flavonoid due to its vast biological and therapeutic activities (**Figure 5.5**).

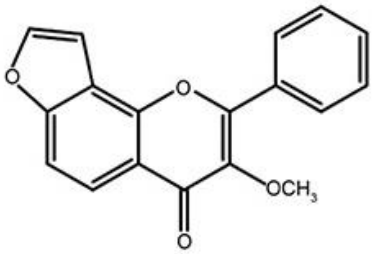

Figure 5.5 Structure of Karanjin (IUPAC: 3-methoxy-2-phenylfuro[2,3-h]chromen-4-one).

Flavonoid like Karanjin is characterized by fully unsaturated rings in a single conjugated system with furan ring, phenyl, and methoxyl as substituent groups. Christoff et al., (1996) have also shown the significant changes in the photophysical and photochemical behavior of the flavones upon introduction of a methoxyl group in the molecule. It is, therefore, important to know the local microenvironmental influence on the photophysics of Karanjin for understanding its biological activities.

This chapter describes the measurement of spectral parameters related to intrinsic UV-Visible absorption and fluorescence of Karanjin. The high analytical sensitivity and specificity of fluorescence provides advantages over other physical techniques and offers a powerful approach for understanding the photophysical and photochemical features of the flavonoid in different microenvironments at physiologically relevant concentrations (micromole range), from both qualitative and quantitative perspectives.

5.2. Materials and methods

5.2.1. Compound and solvent

Karanjin was isolated and purified by the protocol described earlier in the previous chapter. Karanjin with 98% purity was used for the investigation of all spectroscopic

studies in different solvents, such as EtOAc, MeOH, water, and glycerol. All solvents used were HPLC grade, purchased from Spectrochem (India). Surfactant like SDS was purchased from Sigma-Aldrich, India (L4509). The micellar surfactant solutions (20 mM) were prepared in deionized water. Two sets of sample-surfactant solutions were used; freshly prepared sample-surfactant solution and the sample incubated in surfactant solution overnight (~12 h) at room temperature (22-25°C) labeled as SDS FR and SDS ON, respectively. N-acetyl-L-tryptophanamide (NATA, ε = 5,690 $M^{-1}cm^{-1}$ at 280 nm) was purchased from Sigma-Aldrich, India (A6501) and was prepared in deionized water (Milli Q, Millipore). The solutions were allowed to equilibrate to ambient conditions before any data acquisition.

5.2.2. UV-Visible spectroscopy of Karanjin

5.2.2.1. Absorption spectra of Karanjin in different solvent

Absorption spectra of Karanjin were recorded with *Perkin Elmer Lambda 25 spectrophotometer* using quartz cuvettes of 1 cm pathlength in the range of 230 to 400 nm. Solvents used in this study are neat (EtOAc, MeOH, water, and SDS) and binary solvent mixtures (water-MeOH and glycerol-MeOH). Blank consisted of the solvents used for respective samples. A certain amount of Karanjin (10, 20, 30, 40 and 50 µM) dissolved in neat solvents were used to calculate the molar extinction coefficient (ϵ, $M^{-1}cm^{-1}$) of the compound. Absorbance values were plotted against different concentrations of Karanjin used to obtain slopes indicating ϵ in respective conditions. All the experiments were repeated multiple times.

5.2.2.2. Transition dipole moment and oscillator strength determination

Absorption spectra of Karanjin (50 μM) in different solvents were recorded by UV-Visible spectrophotometer in the range of 230-400 nm. Transition dipole moment and oscillator strength of Karanjin in different solvents were determined experimentally by integration of the absorption peak from respective UV-Visible spectra. The wavelengths were rescaled in terms of respective wavenumbers ($\bar{\upsilon}$) and frequency (υ) as needed.

Equation 1.2 was used for the calculation of transition dipole moment, where $\varepsilon(\upsilon)$ is the molar extinction coefficient as a function of frequency (Hz). A graph was plotted, and area under the peak (ε/υ VS υ) was then integrated from λ_{230} to λ_{400}. The values obtained from the graph was used to obtain transition dipole moments of Karanjin in different solvents based on the equation.

Equation 1.3 was used for the calculation of oscillator strengths of Karanjin in different solvents. A graph was plotted between ε and $\bar{\upsilon}$ and area under the peak (ε VS $\bar{\upsilon}$) was then integrated from λ_{230} to λ_{400}. The values obtained from the graph was used to obtain oscillator strengths of Karanjin in different solvents based on the equation.

5.2.2.3. Critical micellar concentration (CMC) determination

Surfactant selected for this study is SDS, and its concentration in the aqueous system varied from 0.5 to 22 mM. The concentration of Karanjin was kept constant (20 μM) throughout the experiment. The absorbance at 263 and 309 nm were plotted as a function of SDS concentration. According to the simplest approach (Williams et al., 1995), the intersection of two straight lines obtained from absorption spectra at different surfactant concentration, which are smaller (pre-micellar range) and higher (post-micellar range) gives the value of CMC of SDS in water.

5.2.3. Steady-state fluorescence investigation of Karanjin

Fluorescence spectra of Karanjin in different solvents were recorded with *Fluoromax 4 fluorescence spectrofluorometer* at room temperature (22-25°C). Quartz cuvettes of 1 cm pathlength were used for all experiments. Fluorescence emission spectra of Karanjin (1 µM) in different neat media (MeOH, SDS FR, SDS ON, and water) excited at 260, 295, 305 and 340 nm were collected. The long pass filter with 305 nm cut-off was used to suppress 520 nm peak in the spectra when the sample is excited with 260 nm. Spectra of Karanjin (1, 5 and 20 µM for water-MeOH; 10 µM for glycerol-water and glycerol-MeOH solvent mixtures) were also recorded. Excitation wavelength (λ_{ex}) used was according to the excitation maxima (λ_{em}) of Karanjin in respective solvents. All the fluorescence data were recorded in the range of 320-600 nm in multiple scans. Appropriate blanks were subtracted from the respective experimental data recorded in the same conditions. All the fluorescence spectra were recorded with constant slit widths (excitation and emission slits are 1 and 10 nm, respectively). Integrated fluorescence intensity was computed by calculating the area under emission spectrum. Stokes shifts of Karanjin in different solvents were also calculated using absorption spectra, and steady-state fluorescence emission spectra excited at 260, 295, 305 and 340 nm and were presented as absorbance maxima, emission maxima and Stokes shift (in terms of $\Delta\lambda$, nm and $\Delta\bar{\upsilon}$, cm^{-1}).

5.2.4. Time-resolved fluorescence investigation of Karanjin

Time-resolved fluorescence intensity decay measurements were carried out with *Horiba DeltaPro* instrument with time-correlated single photon counting (TCSPC) technique, using 295 and 340 nm pulsed LED excitation source (Horiba DeltaDiode, DD 295 and DD 340, UK) at room temperature (22-25°C). Karanjin (1 µM) was dissolved in

different solvents (MeOH, SDS FR, SDS ON, and water). The fluorescence decays were collected at a time resolution of 0.028 ns/channel and acquired in 4096 channels. The peak count for a single decay was fixed at 20,000 and 10,000 for 295 and 340 nm excitations respectively. Pulse widths of 295 and 340 nm excitations were 0.8 and 0.75 ns, respectively. The instrument response function (IRF) was obtained at both excitations (295 and 340 nm) using a dilute colloidal suspension of chalk and recorded before the acquisition of all the samples. Fluorescence intensity decay data was analyzed by iterative reconvolution technique using PERI software written by Prof. Periasamy to extract decay parameters (Swaminathan et al., 1994a; Swaminathan et al., 1994b). The goodness of the fit was judged by reduced χ^2 values (χ_R^2) and visual inspection of randomness of the weighted residuals along with autocorrelation functions among the data channels.

5.3. Results

5.3.1. UV-Visible spectroscopy of Karanjin

5.3.1.1. Absorption spectra of Karanjin in neat solvent

The UV-Visible absorption spectra of Karanjin (50 μM) contain two main absorption bands around 261 nm (band I, S_0-S_2 transition) and 309 nm (band II, S_0-S_1 transition) as shown in **Figure 5.6**. The absorption spectrum of Karanjin is similar to the spectrum obtained by Arshad et al. (2013). The spectrum showed band I has higher absorbance than band II in all the samples. The absorption maxima of Karanjin in different solvents are shown in **Table 5.2**. The spectra show absorption maxima around 259-263 nm (band I) and 299-309 nm (band II) with a shift of the maxima with respect to the dielectric constants of solvents used. Karanjin in non-polar solvent like EtOAc has λ_{max} at 259 and 299 nm. The band at 259 nm in EtOAc shows a significantly less red shift with an

increase in polarity. The band at 299 nm in EtOAc shows a higher red shift with an increase in solvent polarity. However, the absorbance of Karanjin in water decreases as compared to other solvents with λ_{max} at 261 and 309 nm. Karanjin dissolved in micellar solutions (SDS FR and SDS ON) has absorption maxima at 263 and 309 nm. There is no difference between the absorption maxima and the absorbance when the sample is dissolved in freshly prepared and overnight incubated SDS solution. It showed that UV-Visible absorbance property of Karanjin in micellar solution is independent of the time required for the sample incubation. The less pronounced red shift of λ_{max} in the absorption spectra observed in all the solvents indicates that the ground-state energy distribution is not affected to a greater extent possibly due to the less polar nature of Karanjin in the ground state than in the excited state (Husain et al., 2012).

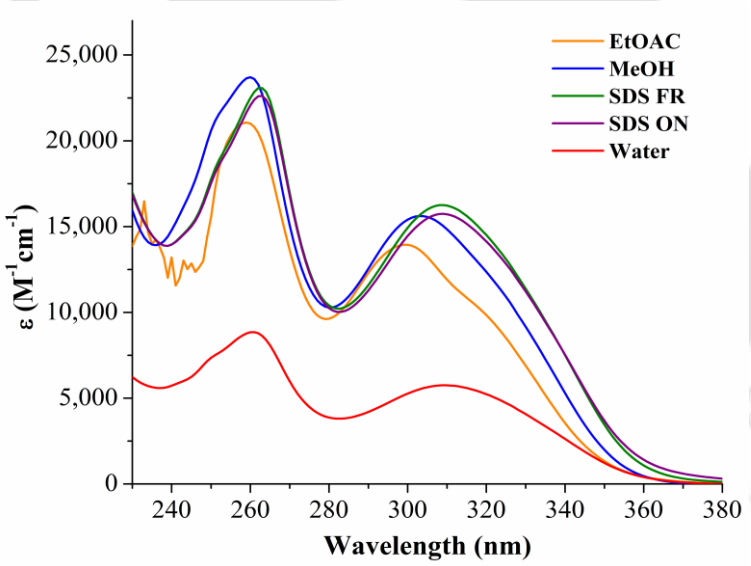

Figure 5.6 Absorbance spectra of Karanjin (50 µM) in different solvents (EtOAc, MeOH, water, SDS freshly prepared and SDS overnight incubated).

5.3.1.2. Molar extinction coefficient of Karanjin

In the current study, the molar extinction coefficients of Karanjin were determined and compared in different solvents (**Figure 5.7** and **Table 5.2**). Extinction coefficients of Karanjin dissolved in different solvents are higher in the band I than band II. It also

showed a linear relationship with the sample concentration and followed Beer-Lambert's law (**Figure 5.7 A** and **B**). Extinction coefficient found to vary with the polarity of solvent; Karanjin in MeOH has the highest extinction coefficient followed by SDS and EtOAc (**Figure 5.7 C**). At λ_{max1}, Karanjin dissolved in MeOH has the highest extinction coefficient (ε = 23,947 $M^{-1}cm^{-1}$) and least when Karanjin is dissolved water (ε = 6,350 $M^{-1}cm^{-1}$). Karanjin dissolved in aqueous SDS micellar solutions (SDS FR and SDS ON) showed the insignificant difference in extinction coefficient at λ_{max1}. At λ_{max2}, Karanjin dissolved in SDS FR has the highest extinction coefficient of (ε = 16,103 $M^{-1}cm^{-1}$) and least when Karanjin is dissolved water (ε = 4,113 $M^{-1}cm^{-1}$). Karanjin dissolved in a non-polar solvent like EtOAc also showed comparatively high extinction coefficient of 21,840 and 14,586 $M^{-1}cm^{-1}$ at λ_{max1} and λ_{max2}, respectively.

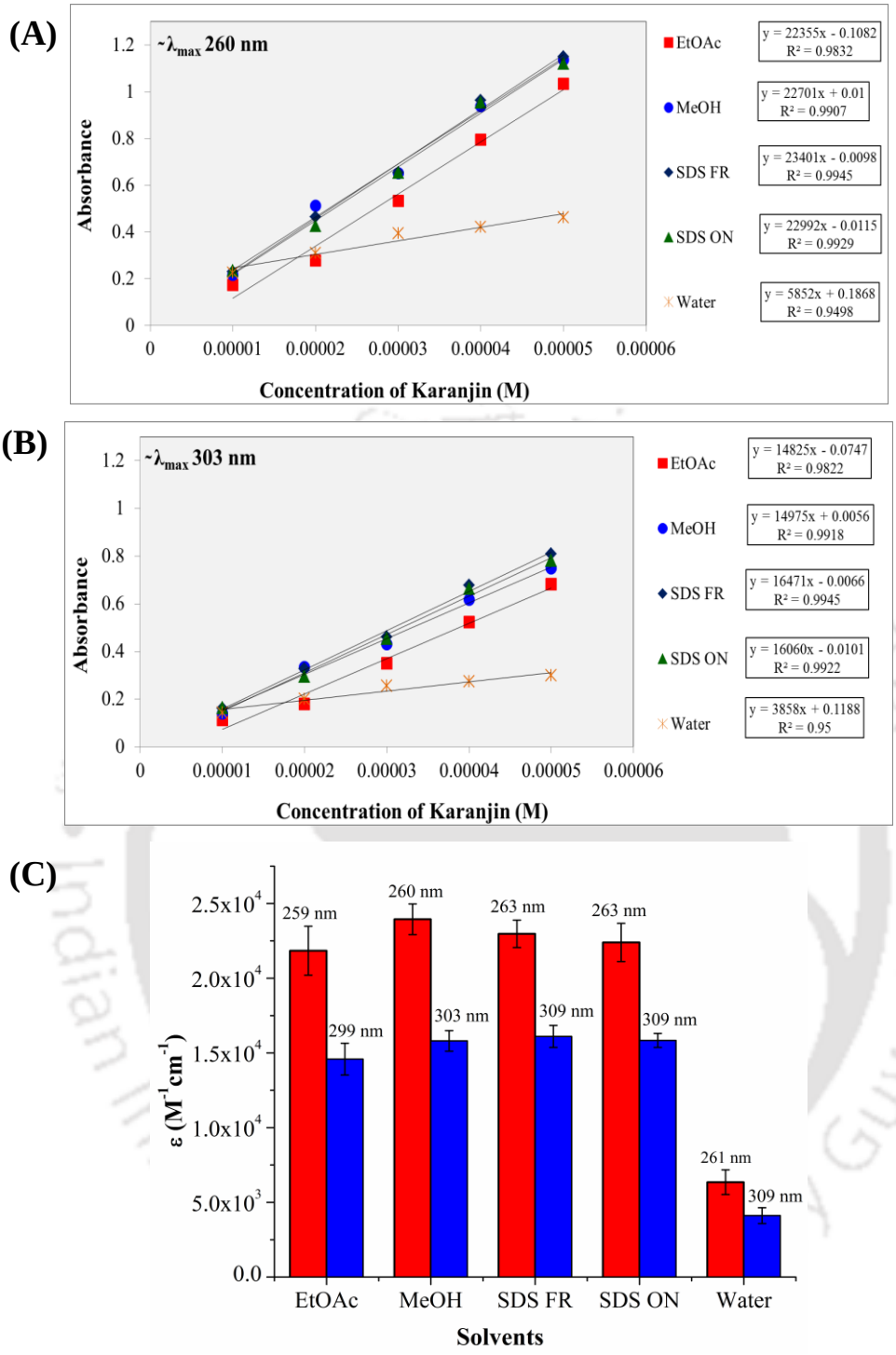

Figure 5.7 Molar extinction coefficients calculation of Karanjin in different solvents at two absorption maxima. (**A**) ~λ_{max} 260 nm (band I); (**B**) ~λ_{max} 303 nm (band II) and (**C**) Comparison of the averages of molar extinction coefficient determined at two different maxima.

Table 5.2 λ_{max} and molar extinction coefficient of Karanjin in different solvents, at two different wavelength maxima. Molar extinction coefficient values reported are the averages of multiple measurements (n = 4 times) using different concentrations of Karanjin (10-50 μM); as shown in Figure 5.7.

Solvent	Refractive index (25°C)	Dielectric constant (25°C)	λ_{max1} (nm)	Є at λ_{max1} ($M^{-1}cm^{-1}$)	λ_{max2} (nm)	Є at λ_{max2} ($M^{-1}cm^{-1}$)
EtOAc	1.375	6	259	21,840 ± 163	299	14,586 ± 106
MeOH	1.331	33	260	23,947 ± 102	303	15,805 ± 689
SDS FR	1.335	-	263	22,971 ± 916	309	16,103 ± 735
SDS ON	1.335	-	263	22,395 ± 127	309	15,835 ± 468
Water	1.333	79	261	6,350 ± 824	309	4,113 ± 530

5.3.1.3. Absorption study in solvent mixture

The solvent effects on the electronic absorption spectra of Karanjin in binary mixtures were also investigated (**Figure 5.8**), and the data were tabulated along with the absorbance ratio between both wavelength maxima (A_{261}/A_{309}) (**Table 5.3** and **5.4**). Karanjin was dissolved in the binary mixtures that were made with an increasing percentage of water in MeOH mixture and glycerol in MeOH mixture. The spectral pattern of the Karanjin (20 μM) in water-MeOH mixtures fluctuates up to 70% volume fraction of water and then reveals a transition that abruptly decreases till it reaches 90% fraction of water. For 10 μM Karanjin, this transition occurs late at 80-90% fraction of water which might be attributed due to the decrease in solubility with an increase in water fraction (**Figure 5.8 A**). In MeOH-glycerol mixture, however, A_{261} decreases with increasing glycerol percentage till 80% but shows an increase from 80-90%. A_{309} shows nearly constant value with increasing glycerol percentage till 80% but shows an increase from 80-90% like A_{261} (**Figure 5.8 B**).

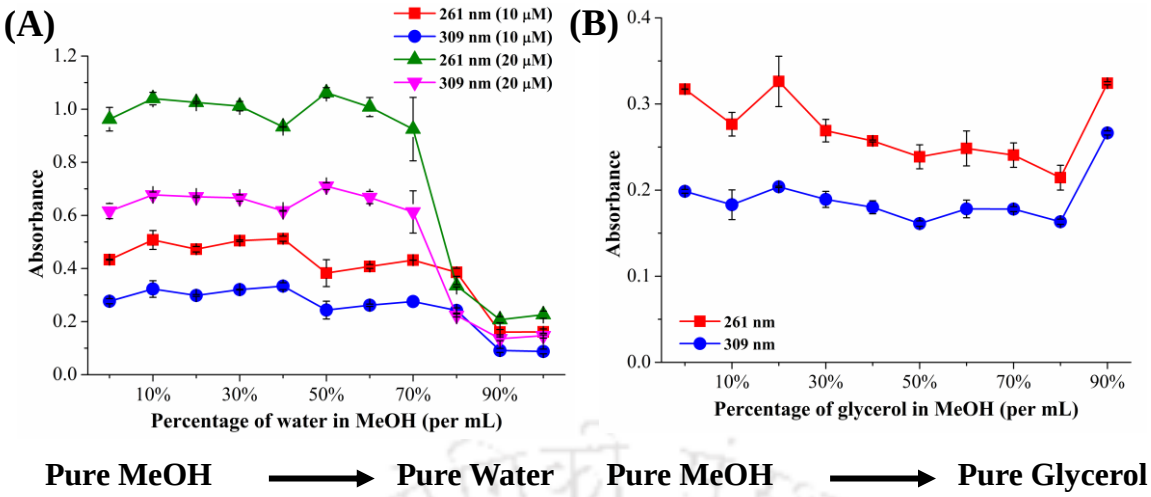

Figure 5.8 The absorbance spectrum of Karanjin in different percentages of (**A**) Water in MeOH (0-100%) at 10 and 20 μM Karanjin; (**B**) Glycerol in MeOH (0-90%) at 10 μM Karanjin. The absorbance of Karanjin in 100% glycerol is not shown.

Table 5.3 Absorbance data of Karanjin (10 and 20 μM) in water-MeOH solvents; as shown in Figure 5.8A.

Percentage of water in MeOH (per mL)	λ_{261} (nm)		λ_{309} (nm)		Absorbance Ratio (261/309)	
	10 μM	20 μM	10 μM	20 μM	10 μM	20 μM
0%	0.43	0.96	0.27	0.61	1.56	1.56
10%	0.5	1.04	0.32	0.67	1.57	1.53
20%	0.47	1.02	0.29	0.67	1.58	1.53
30%	0.5	1.01	0.32	0.66	1.57	1.51
40%	0.51	0.93	0.33	0.61	1.53	1.51
50%	0.38	1.06	0.24	0.71	1.57	1.49
60%	0.4	1	0.26	0.66	1.55	1.51
70%	0.43	0.92	0.27	0.61	1.56	1.5
80%	0.38	0.33	0.24	0.22	1.59	1.5
90%	0.16	0.2	0.09	0.13	1.75	1.53
100%	0.16	0.22	0.08	0.14	1.84	1.53

Table 5.4 Absorbance data of Karanjin (10 μM) in glycerol-MeOH solvents; as shown in Figure 5.8B.

Percentage of glycerol in MeOH (per mL)	λ_{261} (nm)	λ_{309} (nm)	Absorbance Ratio (261/309)
0%	0.31	0.19	1.59
10%	0.27	0.18	1.51
20%	0.32	0.20	1.60
30%	0.26	0.18	1.42
40%	0.25	0.18	1.42
50%	0.23	0.16	1.48
60%	0.24	0.17	1.39
70%	0.24	0.17	1.35
80%	0.21	0.16	1.31
90%	0.32	0.26	1.21

5.3.1.4. Transition dipole moment and oscillator strength

Transition dipole moment measures the transition from one state to another; which occurs when the radiation field connects the two states and represents all atomic and molecular parameters related to the "strength" of the transition. Transition dipole moments of Karanjin in different solvents were calculated (**Table 5.5**). Karanjin in SDS FR and SDS ON have high transition dipole moments of 7.47 and 7.43 Debyes (or D), respectively, followed by Karanjin in MeOH with transition dipole moment of 7.35 Debyes. Karanjin in water has the least transition dipole moment of 4.56 Debyes.

The oscillator strength characterizes the intensity of a transition between excited and ground states of the molecule. Oscillator strengths of Karanjin in different solvents were calculated and tabulated in **Table 5.5**. From the experimental data, Karanjin has high oscillator strengths of 0.94 and 0.93 in SDS FR and SDS ON, respectively, followed by Karanjin in MeOH with an oscillator strength of 0.92. Karanjin in water has the least oscillator strength of 0.35.

Table 5.5 Transition dipole moments and oscillator strengths of Karanjin (50 μM) in different solvents.

Solvents	Transition dipole moment (Debyes)	Oscillator strength
EtOAc	6.83	0.80
MeOH	7.35	0.92
SDS FR	7.47	0.94
SDS ON	7.43	0.93
Water	4.56	0.35

5.3.1.5. CMC determination

CMC of SDS in water in the presence of Karanjin (20 μM) was determined as a function of surfactant concentration at room temperature (~23°C) (**Figure 5.9**). The linear regression analysis for the concentration dependence of these absorbance bands reveals that it obeyed Lambert-Beer's law for the surfactant concentration range studied up to 9 μM [SDS]. **Figure 5.9 A** represents a plot between the absorbance recorded at two different absorption maxima wavelengths (λ_{263} and λ_{309} nm) and different concentrations of surfactant. A change of slope in the plot between absorbance at absorption maximum and surfactant concentration is observed when micelles start to form, and the CMC value can be obtained from the intersection. Interestingly, breakpoints clearly showed the CMC values of the SDS solution in the presence of Karanjin at 9.77 and 9.89 mM when the absorbance spectra are taken at 263 and 309 nm, respectively (**Figure 5.9 B** and **C**). There is a very small peak shift (2 nm) or broadening in the absorption spectra. Karanjin being water insoluble molecule is likely to locate near the hydrophobic core of micelles when the surfactant concentration is above the CMC (**Figure 5.10**). At post-micellization, the addition of the surfactant only increases the number of free micelles in the sample-surfactant solution that can be explained by the constant value of absorbance beyond the CMC.

However, many researchers have reported CMC of SDS in water to be in the range of 7-8.7 mM (**Table 5.6**). Many factors such as addition of electrolytes (Benito et al., 1997), buffer pH (Lin et al., 1996), temperature (Garidel et al., 2000), ionic strength of the aqueous solution (Emerson and Holtzer, 1965; Garidel et al., 2000) presence of additives (Lin et al., 2001), etc., make the CMC of SDS different from that determined in pure water. CMC value of surfactants under different environmental conditions is important for a number of different biological and chemical processes.

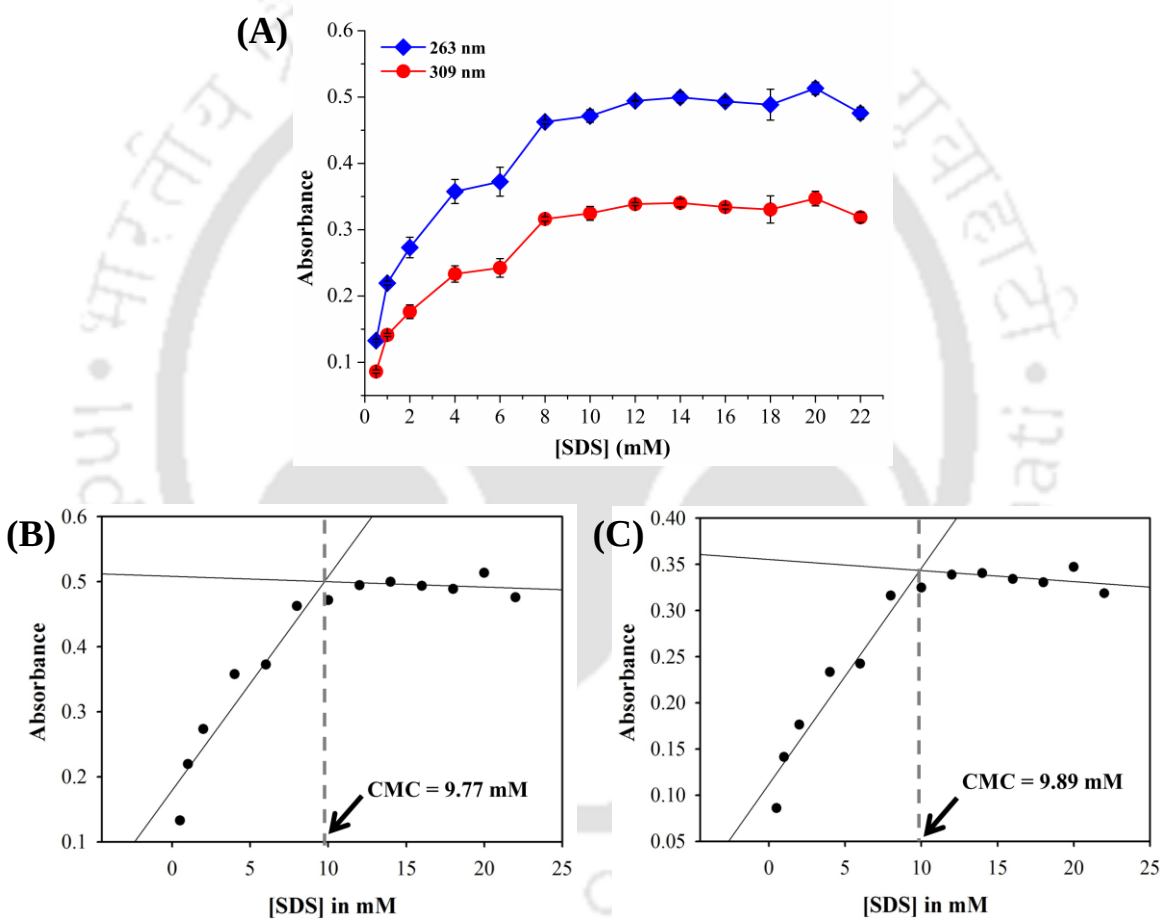

Figure 5.9 CMC determination of SDS in water in the presence of Karanjin (20 µM). (**A**) Absorption spectra at 263 and 309 nm; (**B**) 263 nm and (**C**) 309 nm.

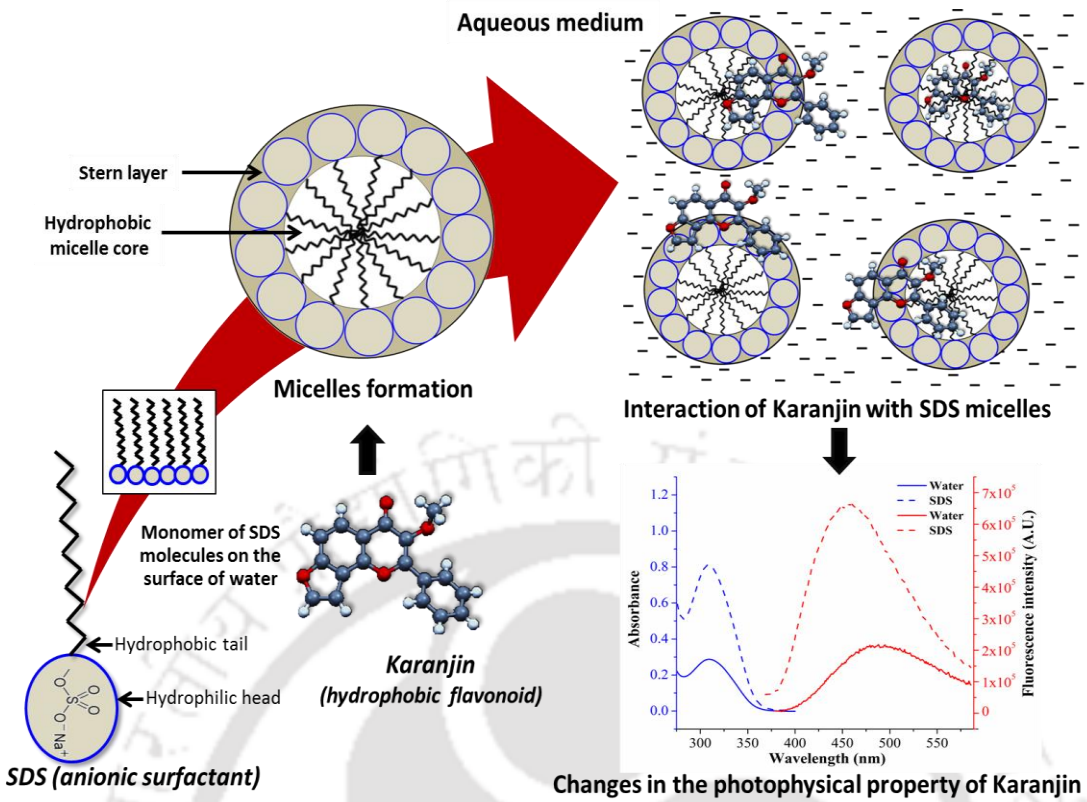

Figure 5.10 SDS micellization in water encapsulating Karanjin.

Table 5.6 CMC values of SDS in water determined by various methods (at 25°C).

CMC determination methods	CMC (mM)	References
Conductometry	8	Marcolongo and Mirenda, 2011
	8.2	Cirin et al., 2012
	7.2	Schick, 1964
Surface tension measurement	9	Bahri et al., 2006
	8.2	Cirin et al., 2012
Speed of sound measurement	8.72	Junquera et al., 1994
Bipolar pulse conductance	8.5	Hammond et al., 1980
Pyrene fluorescence probe	7.4	Dominguez et al., 1997
	8.1	Aguiar et al., 2003
Capillary electrophoresis	8.3	Cifuentes et al., 1997
	8.1	Stanley et al., 2009
Absorbance	7	Beyaz et al., 2004
	8.1	Demissie and Duraisamy, 2016
Fiber-optic refractive index sensing	8.1	Tan et al., 2010

5.3.2. Steady-state fluorescence investigation of Karanjin

5.3.2.1. Steady-state fluorescence study of Karanjin in neat solvent

Fluorescence spectra of Karanjin (1 μM) in different solvents are obtained by excitation at 260 and 305 nm (**Figure 5.11**). The fluorescence intensity, area under the emission curves and λ_{max} at respective excitations are summarized in **Table 5.7** for two bands: Band I (320-370 nm) and Band II (370-590 nm).

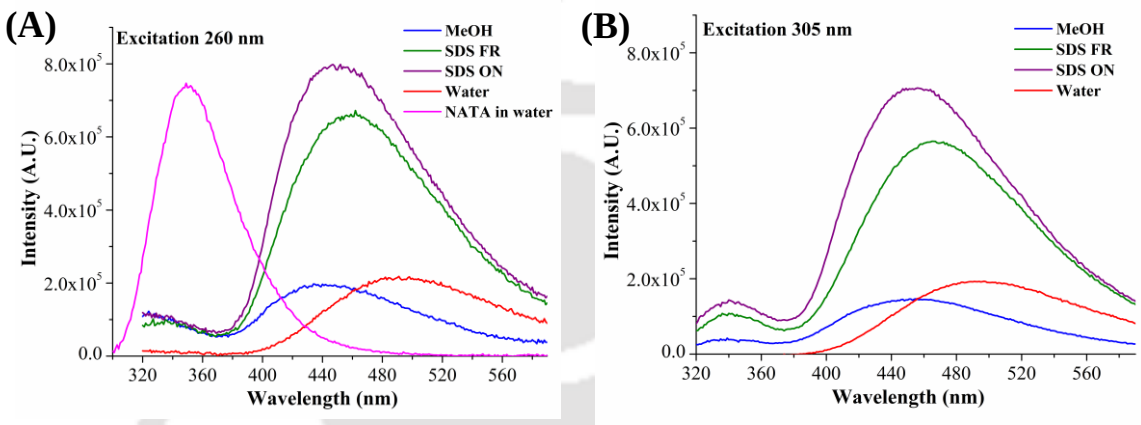

Figure 5.11 Steady-state fluorescence emission spectra of Karanjin (1 μM) excited at (**A**) 260 nm and (**B**) 305 nm in different solvents as indicated. The emission spectrum of NATA in water (1 μM) excited at 260 nm is shown as control (Alston et al., 2004).

Table 5.7 Steady-state fluorescence parameters of Karanjin (1μM) in different solvents excited at 260 and 305 nm; as shown in Figure 5.11. The area under the emission curve of NATA in water (λ_{300}- λ_{500} nm) is shown in the first table. *NA - not applicable.

Band I: 320-370 nm

Solvent/Excitation	Maximum Intensity (A.U.)		Area under the curve (A.U.)		λ_{max} (nm)	
	260 nm	305 nm	260 nm	305 nm	260 nm	305 nm
MeOH	1.2×10^5	3.8×10^4	4.3×10^6	1.6×10^6	324	341
SDS FR	1.0×10^5	1×10^5	3.9×10^6	4.4×10^6	327	340
SDS ON	1.1×10^5	1.4×10^5	4.6×10^6	5.9×10^6	329	340
Water	1.6×10^4	$<10^2$	5×10^5	$<10^2$	325	340
NATA	7.3×10^5	*NA	5×10^7	NA	350	NA

Continued..

Band II: 370-590 nm

Solvent/Excitation	Maximum Intensity (A.U.)		Area under the curve (A.U.)		λ_{max} (nm)	
	260 nm	305 nm	260 nm	305 nm	260 nm	305 nm
MeOH	1.9×10^5	1.4×10^5	2.5×10^5	1.9×10^7	434	455
SDS FR	6.6×10^5	5.6×10^5	8.4×10^7	7.3×10^7	459	465
SDS ON	7.9×10^5	7×10^5	1×10^8	9.1×10^7	456	456
Water	2.1×10^5	1.9×10^5	2.7×10^5	2.4×10^7	491	491

Karanjin showed two emission peaks in all the solvents at both excitations except Karanjin in water at 305 nm excitation (**Figure 5.11**). These peaks are labeled as band I and band II in the region 320-370 nm and 370-590 nm respectively. For both emission bands, Karanjin dissolved in SDS ON has highest fluorescence intensity and yield followed by SDS FR at both 260 and 305 nm excitations (**Table 5.7**). For band I, Karanjin dissolved in water has least fluorescence intensity (~10^4) and yield (~10^5) at λ_{ex} = 260 nm, however, emission peak is absent at λ_{ex} = 305 nm. The band I of Karanjin dissolved in MeOH has less fluorescence intensity and yield at 305 nm excitations. At 260 nm excitation, its intensity and yield are comparable to SDS ON. For band II, Karanjin dissolved in MeOH has the least fluorescence intensity and yield at both 260 and 305 nm excitations followed by water. Band II is found to be more sensitive to the polarity of the solvent than the band I.

The solvatochromic shift of Karanjin is observed with an increase in the polarity of the solvents. The polarity of solvents leads to remarkable changes in the shape of the fluorescence emission spectra and shifts the emission maxima to a longer wavelength. For band II, the emission maxima of Karanjin in water for both excitations (260 and 305 nm) are at 491 nm, while for MeOH they are at 434 and 455 nm respectively. Significant differences in emission maxima are observed in the band I also. The difference in spectral λ_{em} when Karanjin dissolved in pure water, and pure MeOH is evident when

excited at two different wavelengths. For band II, the spectra exhibited a huge blue shift of ~57 nm at λ_{ex} = 260 nm compared to water, whereas the spectra exhibited a blue shift of ~36 nm at λ_{ex} = 305 nm. The huge Stokes shift of emission maxima of all Karanjin samples could be due to the marked difference between the excited state and the ground state dipole moment of Karanjin, resulting in a stronger interaction with polar solvents in the excited state. Interestingly, fluorescence emission was not observed when Karanjin is dissolved in EtOAc (data not shown).

5.3.2.2. Stokes shift

The magnitude of the Stokes shift is dependent on the fluorophore and its environment. Stokes shift in different solvents has been determined from the absorption and Band II of fluorescence emission spectra of Karanjin (**Figure 5.12**). The fluorescence of Karanjin exhibits large Stokes shift in water and SDS, and the magnitude of these shifts increase with solvent polarity from MeOH to water. Karanjin in MeOH showed least Stokes shift of 174 and 152 nm at 260 and 305 nm excitations, respectively. The Stokes shift is represented as wavenumber difference ($\Delta\bar{\upsilon}$, cm^{-1}) as shown in **Table 5.8** to reflect the difference in absorption/emission maxima in terms of energy. The largest Stokes shift of 230 and 182 nm when Karanjin dissolved in water excited at 260 and 305 nm, respectively. The huge Stokes shift of Karanjin in pa olar protic solvent like water indicates a large change in dipole moment of Karanjin in the excited state compared to the ground state. Substantial Stokes shifts might be due to the dynamic process of the solvent molecules to reorient themselves around the newly created excited state dipole which lowers its energy and shifts emission to longer wavelength (often called as solvent relaxation occurs in 10^{-10} s) (Lakowicz, 1999). The magnitude of these shifts increase

with solvent polarity due to large solvent relaxation of polar solvents like water. Such large Stokes shifts hint at the presence of a charge transfer state in Karanjin.

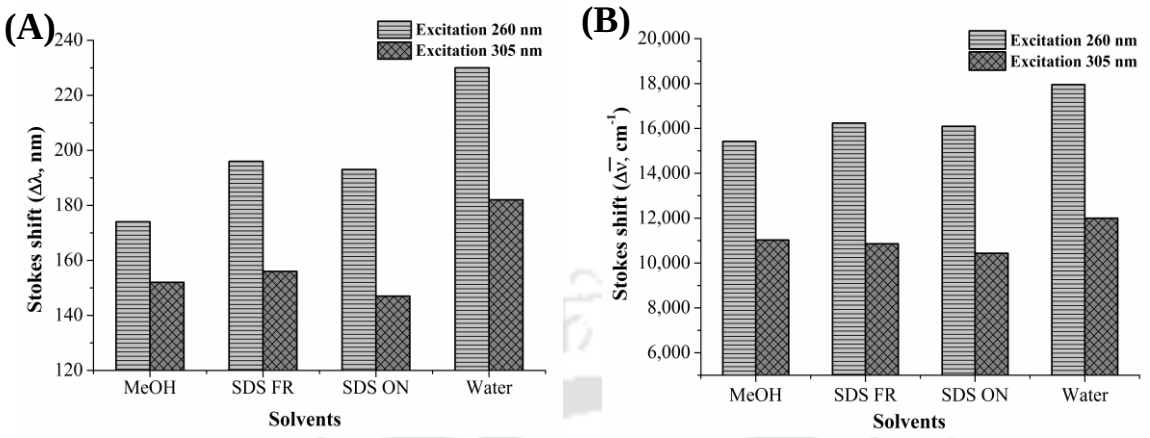

Figure 5.12 Stokes shift of Karanjin (1μM) in different neat solvents excited at 260 and 305 nm. Stokes shift expressed as (**A**) Δλ, nm and (**B**) $\Delta\bar{\upsilon}$, cm^{-1}.

Table 5.8 Absorbance maxima (λ_{abs}), emission maxima (λ_{em}) and Stokes shifts of Karanjin (1μM) in different solvents excited at 295 and 305 nm; as shown in Figure 5.12.

Solvents	Excitation - 260 nm				Excitation - 305 nm			
	λ_{abs} (nm)	λ_{em} (nm)	Stokes shift		λ_{abs} (nm)	λ_{em} (nm)	Stokes shift	
			Δλ (nm)	$\Delta\bar{\upsilon}$ (cm^{-1})			Δλ (nm)	$\Delta\bar{\upsilon}$ (cm^{-1})
MeOH	260	434	174	15,420	303	455	152	11,025
SDS FR	263	459	196	16,236	309	465	156	10,857
SDS ON	263	456	193	16,093	309	456	147	10,433
Water	261	491	230	17,948	309	491	182	11,996

5.3.2.3. Steady-state fluorescence study of Karanjin in solvent mixture

5.3.2.3.1. Glycerol in MeOH

To restrict internal rotation (RIR), the viscosity of the media has been incorporated into this study. As the viscosity strongly perturbs the RIR process, viscosity dependent studies will substantiate the RIR hypothesis. The normalized maximum fluorescence intensity of Karanjin in different percentages of glycerol in MeOH (with glycerol as 0 to 100%, per mL) excited at 260 and 305 nm are shown in **Figure 5.13**. The emission

intensity increases with an increase in the percentage of glycerol. This increase is also accompanied by an increase in emission λ_{max}. The emission maxima peak is at 459 nm in pure MeOH (0% glycerol) and shifts to 478 nm in pure glycerol (0% water) at excitation 260 nm (**Figure 5.13 A**). Similarly, the emission maxima peak is at 455 nm in pure MeOH and shifts to 471 nm in pure glycerol at excitation 305 nm (**Figure 5.13 B**). The gradual addition of glycerol increases the viscosity of the medium, and consequently, fluorescence intensity also increases.

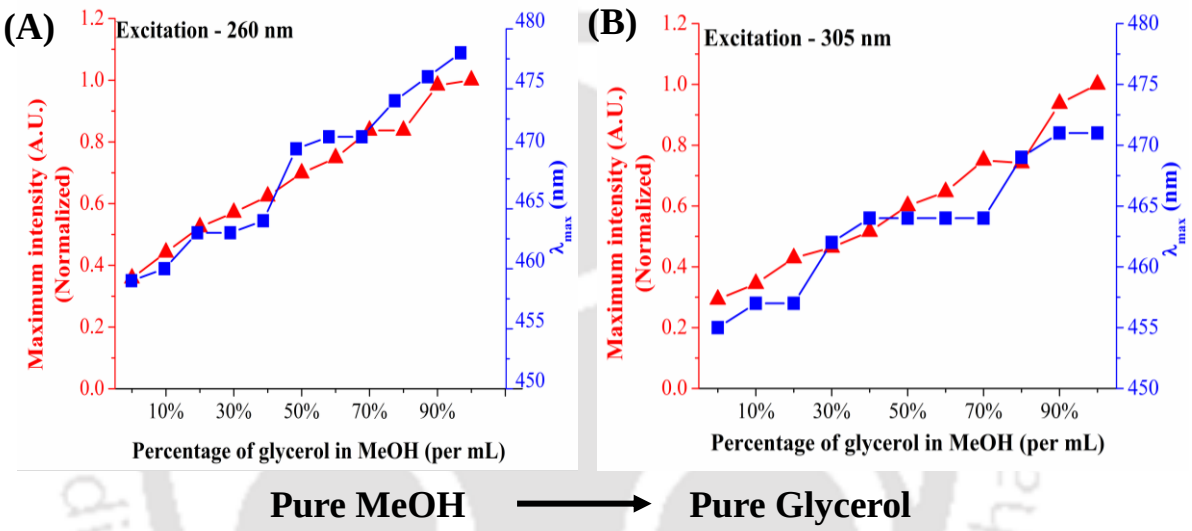

Figure 5.13 Steady-state fluorescence emission spectra of Karanjin (10 μM) in different percentage of glycerol in MeOH excited at (**A**) 260 nm and (**B**) 305 nm. Emission acquisition range: 420-560 nm.

The percentage values indicate the volume percentage of glycerol in MeOH solution (v/v). The condition with highest maximum intensity was normalized to unity. Maximum intensity at other conditions was normalized with respect to this value.

5.3.2.3.2. Glycerol in water

The fluorescence emission spectra of Karanjin in the glycerol-water binary solvent was excited at 260 and 305 nm as shown in **Figure 5.14**. The fluorescence intensity increases with the increase in the percentage of glycerol in aqueous solutions. λ_{max} of Karanjin is observed at 494 nm in pure water (0% glycerol) has blue shifted to 476 nm when Karanjin is dissolved in pure glycerol (0% water) (**Figure 5.14 A** and **B**).

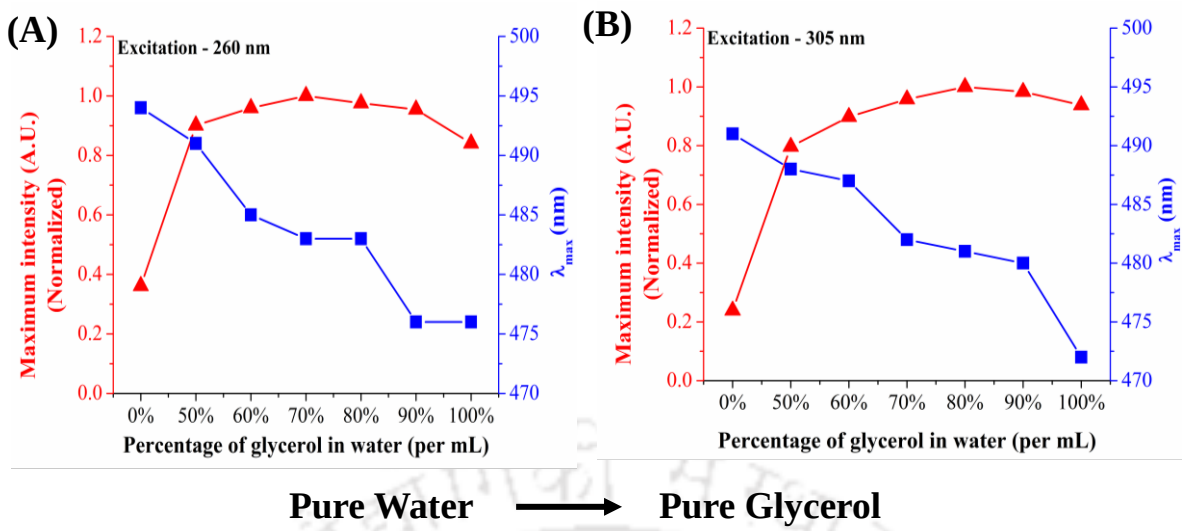

Figure 5.14 Steady-state fluorescence spectra of Karanjin (10 μM) in glycerol-water excited at (**A**) 260 nm and (**B**) 305 nm. Emission acquisition range: 420-560 nm. Other conditions are similar to Figure 5.13.

5.3.2.3.3. Water in MeOH

Fluorescence spectra of Karanjin (1, 5 and 20 μM) in different MeOH-water mixtures were obtained by excitation at 261 and 309 nm. The area under the emission curves of each spectrum was calculated. Fluorescence intensity, area under the emission curves and λ_{max} values were plotted against the different percentage of water in the methanolic solution as shown in **Figure 5.15**. The fluorescence intensity of Karanjin showed bell-shaped where the intensity increases up to 50% volume fraction of water and then gradually decreases till it reaches 100% fraction of water (**Figure 5.15 A and B**). Similarly, fluorescence yield showed bell-shaped curve at both 261 and 305 nm excitations (**Figure 5.15 C and D**). At 20 μM Karanjin, the fluorescence intensity and yield drop in a similar manner as absorbance with an increase in the percentage of water in MeOH solutions (70-90%) as shown in **Figure 5.8** and **Table 5.3**. The emission spectra showed that the gradual addition of water as cosolvent increases the polarity of the mixtures. The continuous red shift in λ_{max} is observed with increase water fraction in the mixture at both 261 and 305 nm excitations except at high concentration (20 μM)

where λ_{max} remains almost constant (**Figure 5.15 E and F**). This shift might be attributed due to more solvent relaxation when water is a major solvent component.

Intensity

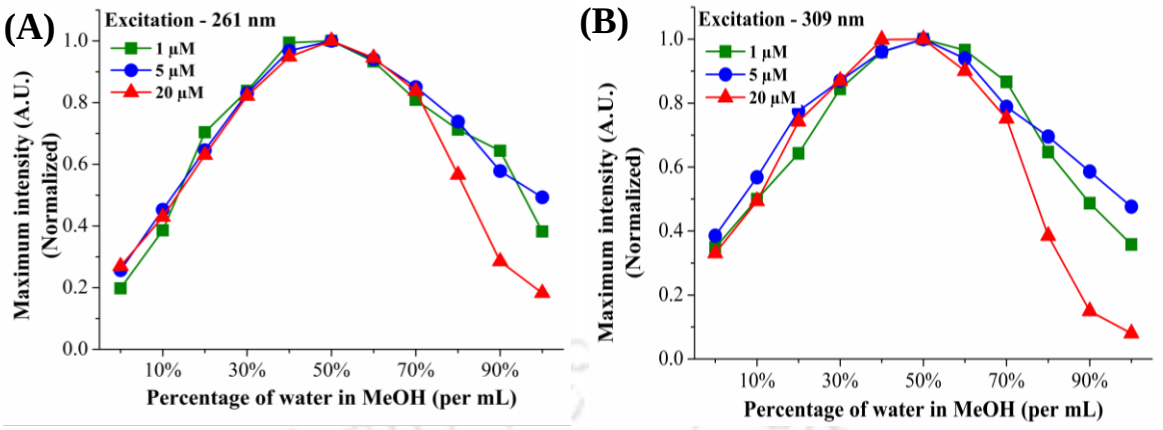

Area under the curve

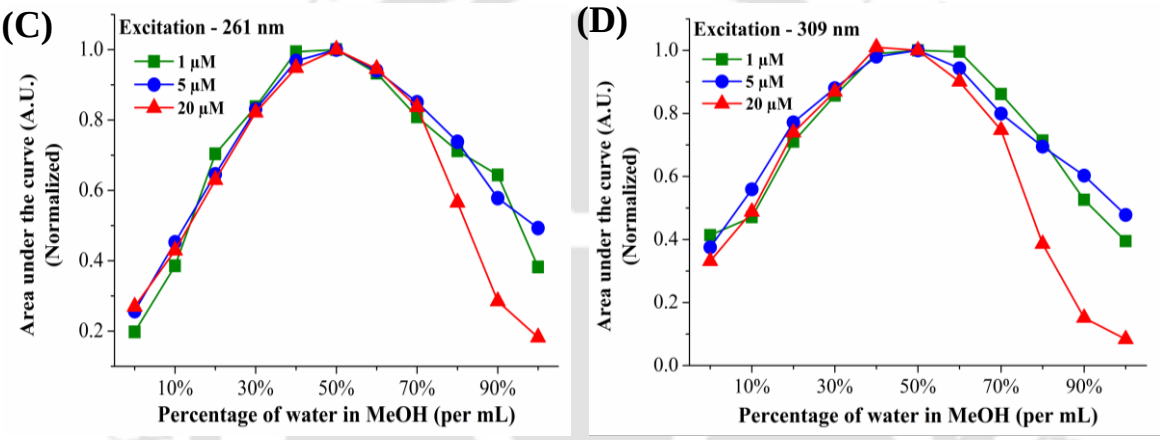

λ_{max}

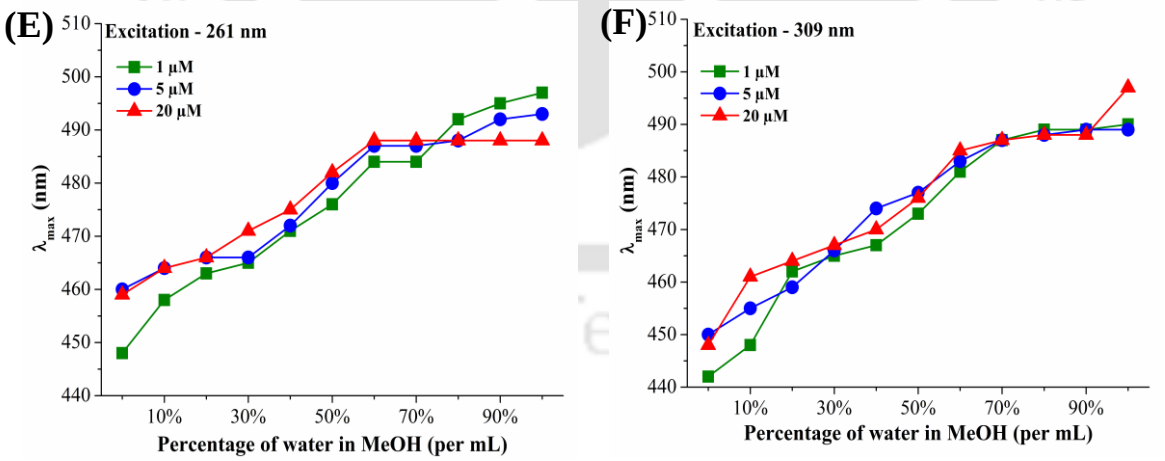

Figure 5.15 Steady-state fluorescence study of Karanjin (1, 5 and 20 µm) excited at 261 and 309 nm representing fluorescence intensity (**A** and **B**), area under the curve (**C** and **D**) and λ_{max} (**E** and **F**), on the gradual addition of water to MeOH solutions. Emission acquisition range: 420-560 nm. Other conditions are similar to Figure 5.13.

5.3.3. Time-resolved fluorescence investigation of Karanjin

5.3.3.1. Steady-state fluorescence study of Karanjin

Steady-state fluorescence emission spectra of Karanjin in different solvents were acquired after excitation with 295 and 340 nm (**Figure 5.16**). These excitations and conditions of acquiring are similar to that of TCSPC measurement. Areas under the emission curves (λ_{380}-λ_{580}) for each condition were calculated. Fluorescence intensity, area under the curve, λ_{max} and Stokes shift are summarized in **Table 5.9** and **Table 5.10**.

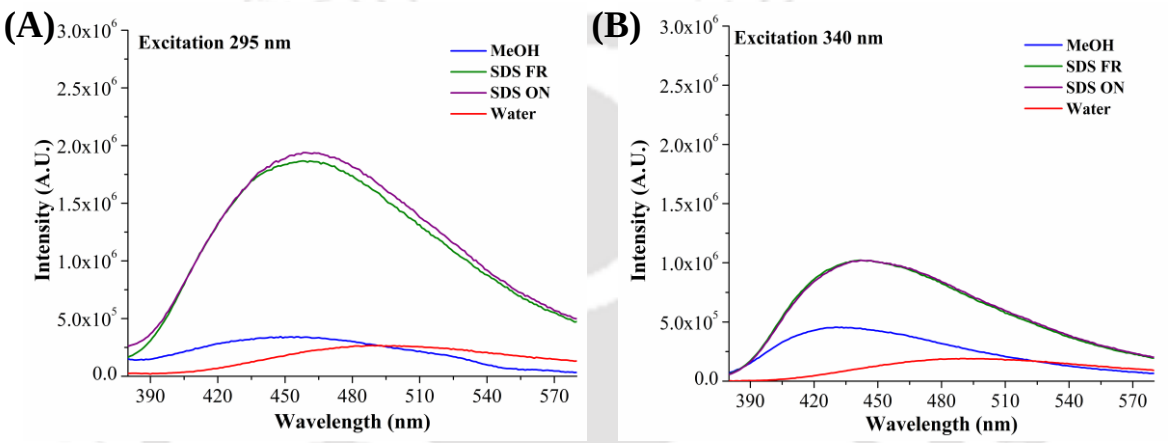

Figure 5.16 Steady-state fluorescence study of Karanjin (1 μM) in different solvents excited at (**A**) 295 nm and (**B**) 340 nm.

Table 5.9 Steady-state fluorescence parameters of Karanjin (1μM) in neat solvents excited at 295 and 340 nm (TCSPC study); as shown in Figure 5.16.

Solvent/ Excitation	Intensity (A.U.)		Area under the curve (A.U.)		λ_{max} (nm)	
	295 nm	340 nm	295 nm	340 nm	295 nm	340 nm
MeOH	3.3×10^5	4.5×10^5	4.2×10^7	5.1×10^7	454	430
SDS FR	1.8×10^6	1×10^6	2.3×10^8	1.2×10^8	459	442
SFS ON	1.9×10^6	1×10^6	2.4×10^8	1.2×10^8	459	442
Water	2.5×10^5	1.9×10^5	3.3×10^7	2.3×10^7	502	489

Table 5.10 Stroke shifts of Karanjin (1μM) in neat solvents excited at 295 and 340 nm; as shown in Figure 5.16.

Solvent/ Excitation	Stokes shifts (nm)			
	295 nm		340 nm	
	Δλ (nm)	$\Delta\bar{\upsilon}$ (cm^{-1})	Δλ (nm)	$\Delta\bar{\upsilon}$ (cm^{-1})
MeOH	194	16,435	127	9,748
SDS FR	196	16,236	133	9,738
SDS ON	196	16,236	133	9,738
Water	241	18,394	180	11,913

5.3.3.2. Time-resolved fluorescence study of Karanjin

Fluorescence lifetime is an intrinsic property of a fluorophore and often affiliated with an energetically unstable state. It can be sensitive to a variety of internal factors (fluorophore structure and orientation) and external factors (temperature, polarity, and interactions with the solvent molecule in solution) (Berezin and Achilefu, 2010). Detailed information about the fluorophore can be extracted and renders fluorescence lifetime as a separate yet complementary method to traditional fluorescence intensity measurements.

To corroborate the results found in steady-state fluorescence analysis (**Figure 5.17** and **Table 5.9**), fluorescence lifetime studies of Karanjin in several solvents were performed. Karanjin shows bi-exponential decay in all the solvents upon fitting as shown in **Figure 5.17** (ex 295 nm) and **5.18** (ex 340 nm). For bi-exponential fluorescence intensity decays, two parameters become important, namely the individual lifetimes of each component (τ_1 and τ_2) and their fractional contributions (α_1 and α_2). Karanjin has two lifetimes: one short-lived and long-lived species. Since there is no fluorescence emission observed when Karanjin is dissolved in EtOAc solvent, mean lifetime measurement becomes impossible. Figures also showed the random distributions of

weighted residuals values obtained in fitting the raw decay data of Karanjin in different solvents.

The mean fluorescence lifetime (τ_m) of Karanjin in different solvent system ranges from 1.31 to 2.09 ns and 1.36 to 3.48 ns when excited at 295 (**Figure 5.17)** and 340 nm (**Figure 5.18**) respectively. At 295 nm excitation, Karanjin in SDS FR and SDS ON have τ_m of 2.09 ns (τ_1 = 1.56 ns, α_1 = 0.81; τ_2 = 4.34 ns, α_2 = 0.19) and 2.05 ns (τ_1 = 1.49 ns, α_1 = 0.78; τ_2 = 4.11 ns, α_2 = 0.21), respectively. On the other hand, Karanjin in MeOH showed least τ_m of 1.31 ns (τ_1 = 1.29 ns, α_1 = 0.99; τ_2 = 4.86 ns, α_2 = 0.021), followed by τ_m of 1.40 ns (τ_1 = 0.86 ns, α_1 = 0.21; τ_2 = 1.54 ns, α_2 = 0.78) when Karanjin is dissolved in water. Similarly, at 340 nm excitation Karanjin in SDS FR and SDS ON solution showed long mean lifetime of 3.27 ns (τ_1 = 2.19 ns, α_1 = 0.40; τ_2 = 3.98 ns, α_2 = 0.60) and 3.48 ns (τ_1 = 3.22 ns, α_1 = 0.90; τ_2 = 6.06 ns, α_2 = 0.09), respectively. However, Karanjin in MeOH has the least τ_m of 1.36 ns (τ_1 = 1.20 ns, α_1 = 0.89; τ_2 = 2.56 ns, α_2 = 0.11) followed by Karanjin in water with τ_m of 1.39 ns (τ_1 = 1.79 ns, α_1 = 0.73; τ_2 = 0.26 ns, α_2 = 0.27). Good fit of the fluorescence decay data are observed and judged by reduced χ^2 values of respective conditions. The decay parameters, average fluorescence lifetimes and χ_R^2 values are listed in **Table 5.11**. A fairly good linear relationship (R^2 = 0.98 at ex 295 nm; R^2 = 0.93 at ex 340 nm) is found between area under the emission curve obtained from steady-state fluorescence study and mean lifetime obtained from TCSPC data as shown in **Figure 5.19**.

(A)

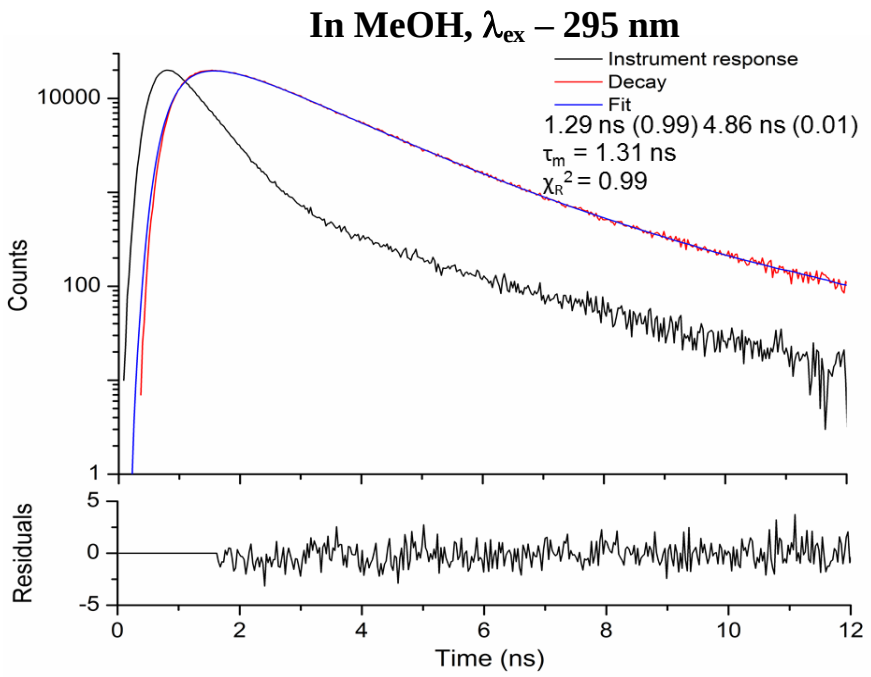

(B)

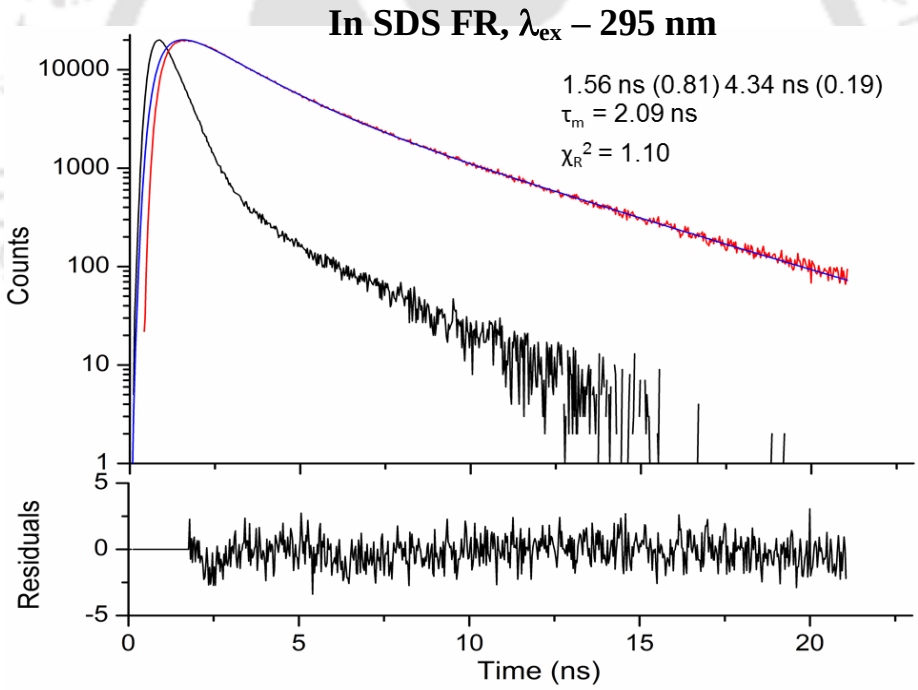

Continued..

(C)

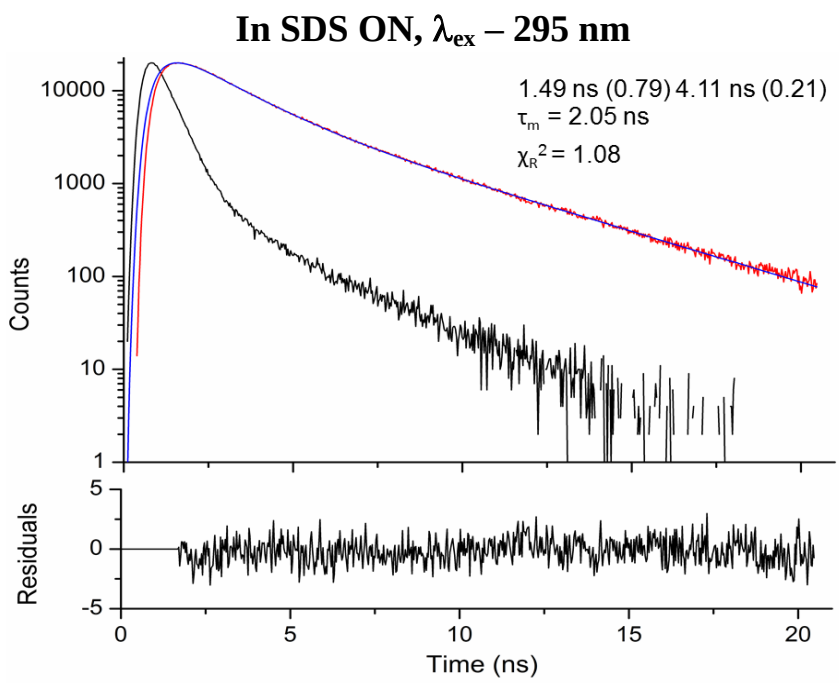

(D)

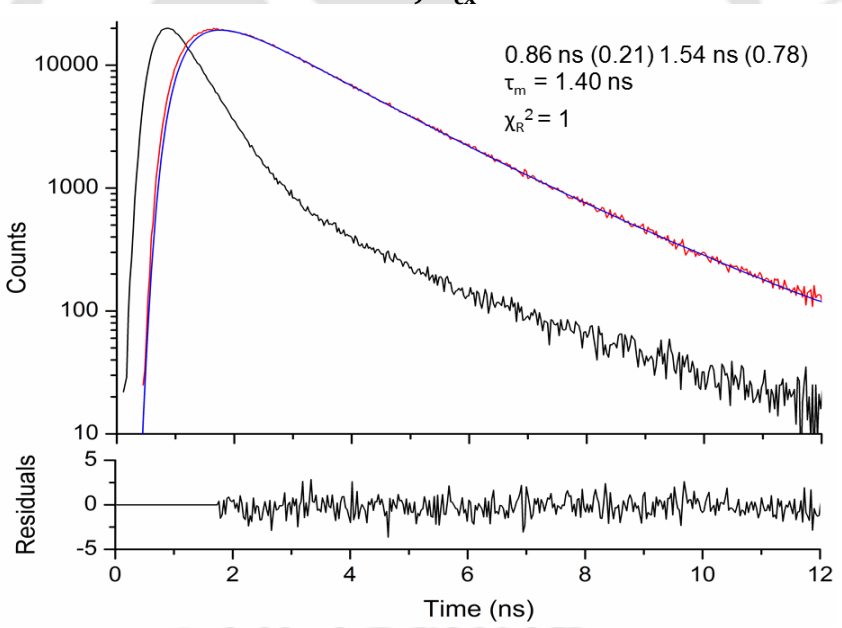

Figure 5.17 Fluorescence intensity decays of Karanjin (1μM) in different solvents excited at 295 nm using TCSPC. (**A**) MeOH; (**B**) SDS FR; (**C**) SDS ON and (**D**) Water.

(A) **In MeOH, λ_{ex} – 340 nm**

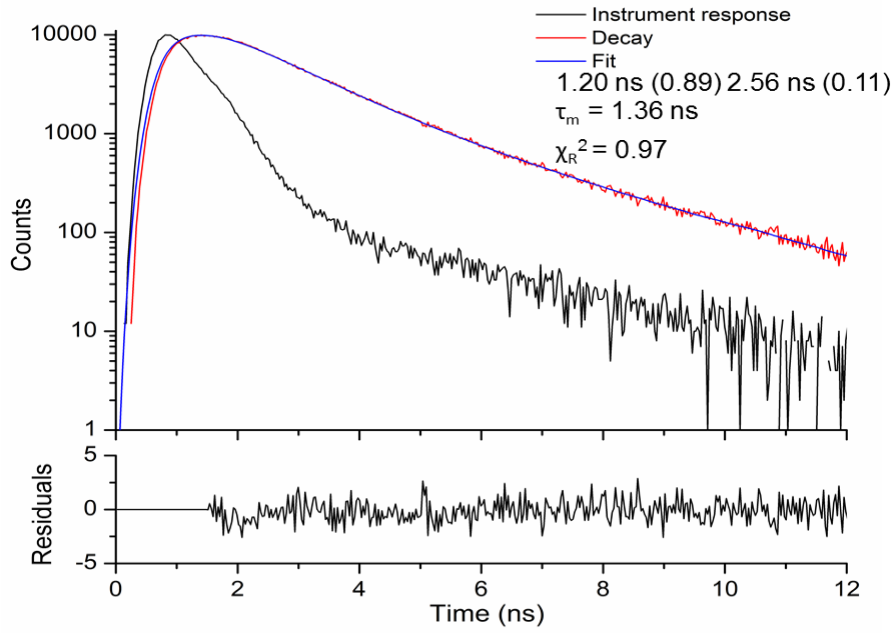

(B) **In SDS FR, λ_{ex} – 340 nm**

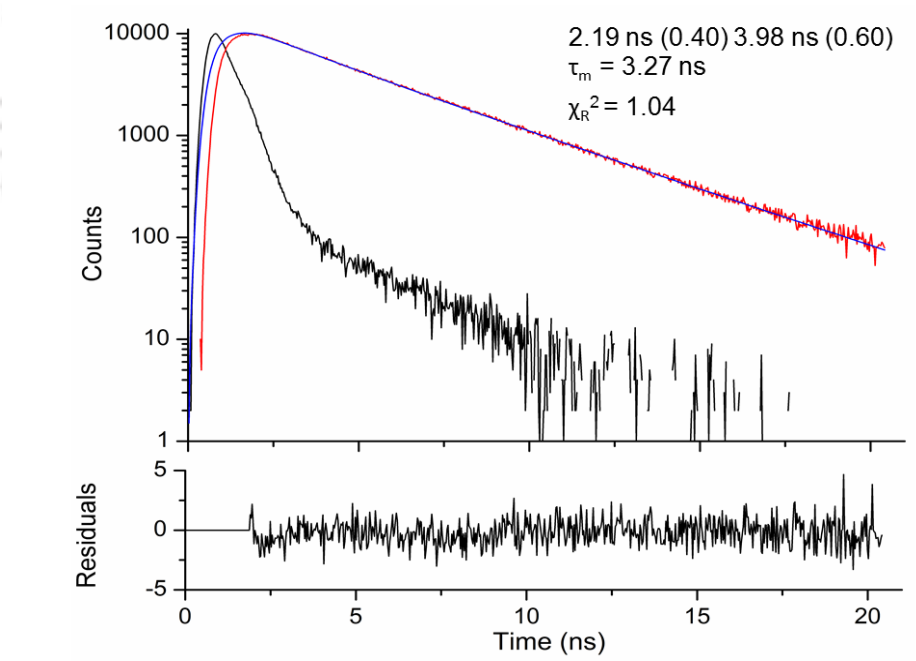

Continued..

(C) **In SDS ON, λ_{ex} – 340 nm**

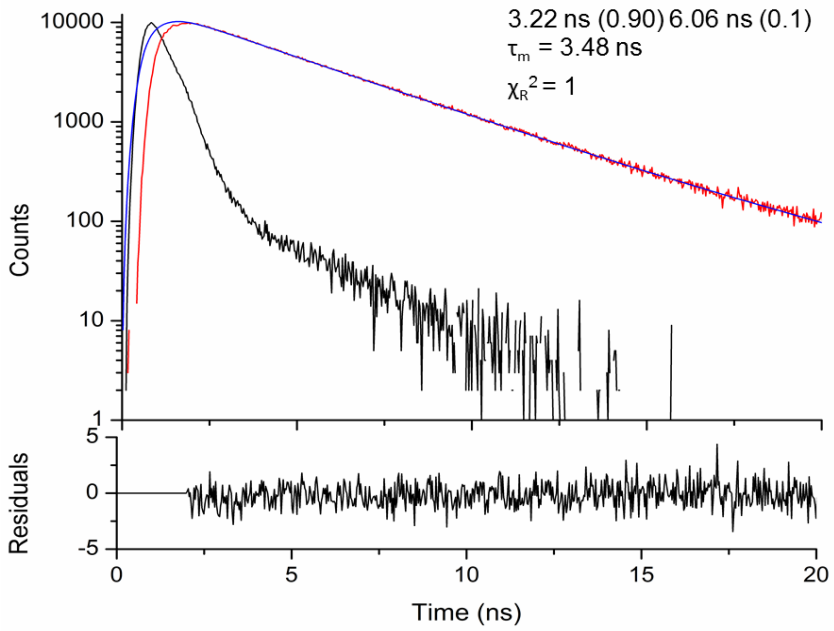

(D) **In Water, λ_{ex} – 340 nm**

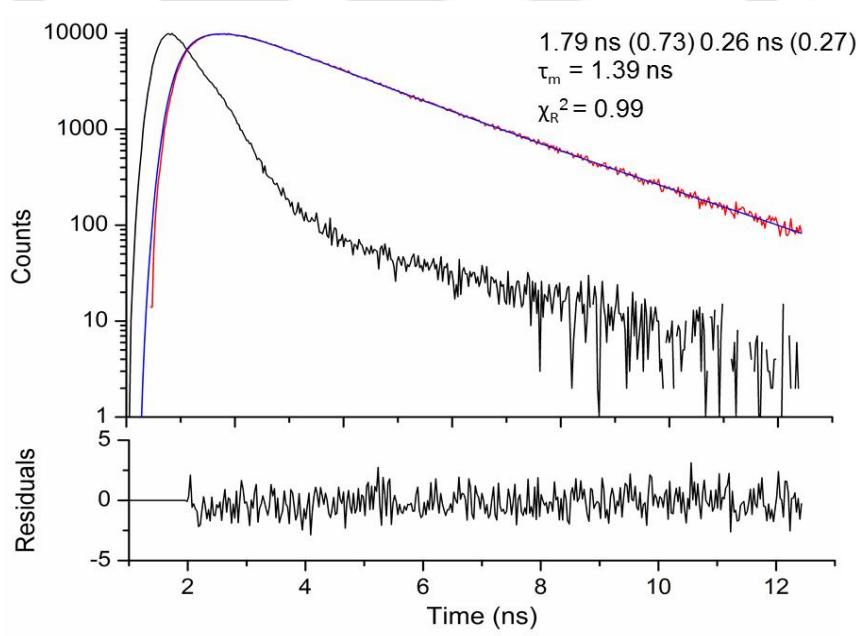

Figure 5.18 Fluorescence intensity decays of Karanjin (1μM) in different solvents excited at 340 nm using TCSPC. (**A**) MeOH; (**B**) SDS FR; (**C**) SDS ON and (**D**) Water.

Table 5.11 Bi-exponential fit function parameters for the fluorescence decay of Karanjin (1 μM) in different solvents; as shown in Figure 5.17 and 5.18. (Temperature: 22-25°C) $\tau_m = \Sigma\alpha_i\tau_i$

Excitation	Solvent	α_1	τ_1 (ns)	α_2	τ_2 (ns)	τ_m (ns)	χ_R^2
295 nm	MeOH	0.99	1.29	0.01	4.86	1.31	0.99
	SDS FR	0.81	1.56	0.19	4.34	2.09	1.1
	SDS ON	0.78	1.49	0.21	4.11	2.05	1.08
	Water	0.21	0.86	0.78	1.54	1.40	1
340 nm	MeOH	0.89	1.20	0.11	2.56	1.36	0.97
	SDS FR	0.40	2.19	0.60	3.98	3.27	1.04
	SDS ON	0.90	3.22	0.09	6.06	3.48	1
	Water	0.73	1.79	0.27	0.26	1.39	0.99

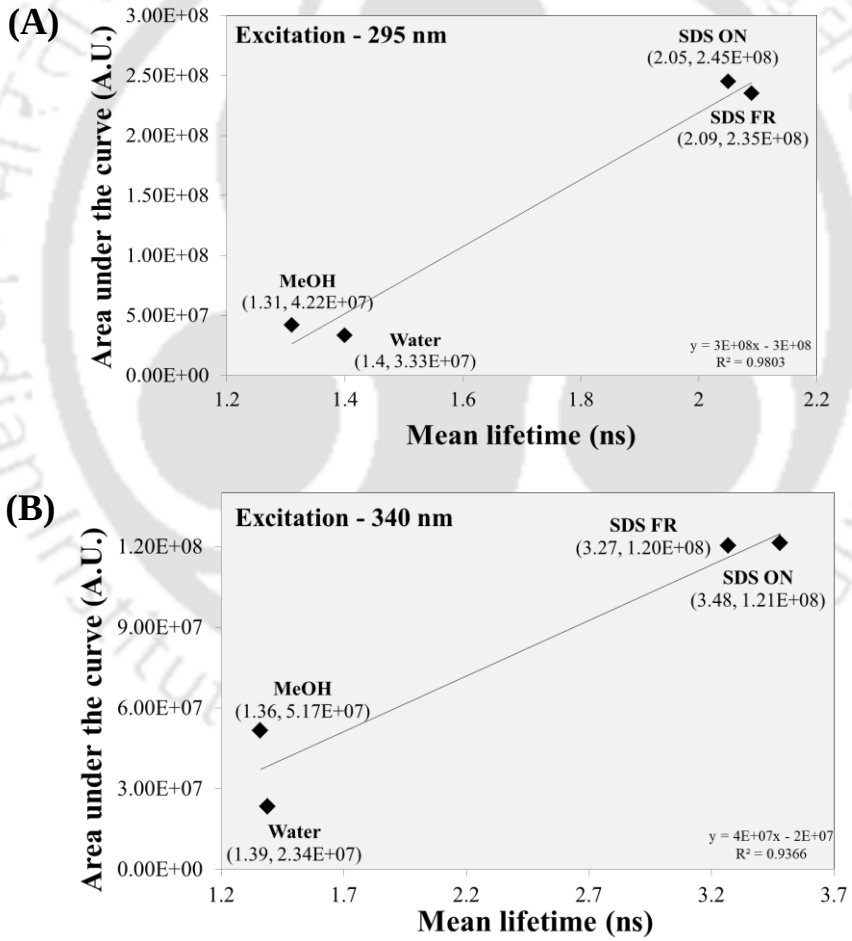

Figure 5.19 Correlation of area under the curve obtained from steady-state fluorescence and mean lifetimes from TCSPC of Karanjin excited at (**A**) 295 nm and (**B**) 340 nm.

5.4. Discussion

5.4.1. UV-Visible absorption of Karanjin

5.4.1.1. Absorption spectra of Karanjin and its molar extinction coefficient in neat solvent

Karanjin exhibits different spectroscopic characteristics depending upon the properties of the solubilizing media. Solvatochromic shifts of the ground and excited states of Karanjin were analyzed by monitoring the absorption spectra regarding the solute-solvent and solvent-solvent interactions. From UV-Visible absorption data, it is evident that absorption property of Karanjin exhibit strong dependences on solvent characteristics. Karanjin showed two major absorption bands *viz*., band I (around 261 nm) and band II (around 309 nm) which arise due to cinnamoyl and benzoyl moiety of the flavonoid, respectively (**Figure 5.6**) (Zsila et al., 2003). The observed spectral features indicate the microenvironment immediately surrounding the probe. Variations in the position, intensity, and shape of the absorption spectra can be direct measures of the specific interactions between the solute and solvent molecules. At the S_0 state, the phenyl linkage substituent of Karanjin has an anti-bonding characteristic. This inter-ring bond in Karanjin has some π bonding characteristics due to the conjugation of π electrons, therefore exhibiting π-π^* transition (260 nm) (Kumar et al., 2001). Karanjin in EtOAc and MeOH was observed to have high absorbance and ε as shown in **Figure 5.6** and **5.7**. It may be due to their predominantly monomeric nature and least degree of aggregate formation in the solution. The low absorbance of Karanjin in water when it is compared to other solvents might be attributed due to aggregate formation. **Table 5.2** showed a small red shift in λ_{max} compared to EtOAc when Karanjin is dissolved in MeOH which shifts further in aqueous micellar media. This shift can be described by the solvent ability to form hydrogen bonds. The carbonyl group of Karanjin acting as hydrogen bond

acceptors is responsible for the intermolecular hydrogen bond formation with protic solvents like MeOH and water (Liu et al., 2013). The dimerization of fluorophores and formation of higher order aggregates in water can be a factor for changes in the extinction coefficients.

On the other hand, the enhanced absorbance and ε values of Karanjin dissolved in micellar solutions of SDS may be due to a predominantly monomeric form of Karanjin in micellar media. It is likely that Karanjin is buried inside and sufficiently shielded from water in the presence of SDS micelles. It may explain the increase in ε that is similar to EtOAc and MeOH in the presence of SDS micelles.

5.4.1.2. Absorption spectra of Karanjin in binary solvent

Absorbance spectra of Karanjin dissolved in different solvent mixtures were obtained (**Figure 5.8**), and absorbance data were also tabulated as shown in **Table 5.3** and **5.4**. Different percentages of cosolvents (water and glycerol) were used to study the absorbance pattern of Karanjin in mixed solvents. The important factor in mixed solvents is preferential solvation and commonly results from specific and non-specific interactions. From the experimental data, the absorbance of Karanjin fluctuates in mixed solvents due to continuous change in the polarity of the surroundings. There is not much change in the absorbance till 70% of cosolvent (water and glycerol). Karanjin concentration-dependent transition is seen at 80-90% (10 μM) and 70-90% (20 μM) in water-MeOH mixtures. On the other hand, no significant change is observed in glycerol-MeOH mixtures.

5.4.1.3. Transition dipole moment and oscillator strength of Karanjin

The transition dipole moment measures the coupling between molecular orbitals (MOs) involved during light absorption and their substantial spatial overlapping of electron

densities in the involved orbitals (Liu et al., 2013). The solute-solvent interaction can induce changes in the electronic structure and dipole moment of the solutes. Changes in the dipole moment alter the electrostatic interaction with the solvent in the ground and excited state, with a shift in the absorption maximum (λ_{max}). The less pronounced absorption shift (**Table 5.2**) with solvent as compared to emission shift (**Table 5.7**) implies that the ground-state energy distribution is not affected to a greater extent, possibly due to the less polar nature of the dye in the ground-state rather than in the excited state. Karanjin dissolved in MeOH, and SDS micelles have found to have high transition dipole moments and oscillator strengths whereas water has the least as shown in **Table 5.5**. The values obtained by calculating oscillator strength indicate that the electronic transition S_0-S_1 is a strongly allowed transition. Generally, the oscillator strength of an electronic transition of a compound in a series of solvents increases with an increase in solvent polarity (Ahmed et al., 2016). However, in our experiment, we found the oscillator strengths increase with increase in polarity of the solvents except in water due to a decrease in solubility of Karanjin in water at a relatively high concentration (50 μM) used in the calculation.

5.4.1.4. CMC of SDS in water in the presence of Karanjin

Literature shows that SDS has been extensively used and acts as an excellent tool to decipher the extent and dynamics of various excited-state processes in an inhomogeneous environment (Sarangi and Basu, 2011). The increase in absorbance when Karanjin is dissolved in SDS might be correlated to the formation of micelles till it reaches CMC values (CMC of SDS in pure water as reported to be around 7-8.7 mM; **Table 5.6**). To verify this, we have monitored the micelle formation by observing an increase in the absorbance values. This value remains constant after ~9 mM and after

that, indicating the formation of SDS micelles in the presence of Karanjin (**Figure 5.9**). The increase in absorbance values with an increase in the surfactant concentration is regarded to be caused by the flavonoid molecules penetration into the micelles. Several molecular interactions such as hydrophobic interactions, electrostatic interactions, hydrogen bonds, π-stacking, and Van der Waals forces are typical examples of the intermolecular forces that dominate the interactions of the probe with surfactant molecules (Naeem et al., 2000; Karukstis et al., 2010; Dezhampanah and Firouzi, 2012). These interactions of Karanjin with SDS micelles are responsible for the changes in the photophysical property of the compound and thereby, affecting the absorbance property of Karanjin. In the pre-micellar region, monomers of SDS molecule interact with the Karanjin to form ion association complexes, while in the post-micellar region, Karanjin molecules are likely to be localized inside the micelles as the ε and fluorescence properties appear closes to non-polar media. SDS micelles allow the penetration of Karanjin within the apolar or hydrophobic micellar phase, resulting in monomeric Karanjin to reside inside the core of SDS micelles or micellar surface as represented in **Figure 5.10**. The location and orientation of Karanjin within the micellar micro-environment depend on both compound's structure and charges on surfactant head groups. **Figure 5.6** shows the absorption spectrum of Karanjin dissolved in aqueous surfactant solutions similar to spectrum dissolved in a polar solvent like MeOH which one can assume that Karanjin is situated in the moderately polar Stern layer of micelles (Tehrani-Bagha and Holmberg, 2013). Moreover, according to Hirose and Sepulveda (1981), the compound having a phenyl residue like Karanjin can lie parallel to the surface of the micelle with some of the methylene groups (CH_2) of the alkyl chain lying on the surface and the rest immersed in the micelle. A similar result has also been reported by Liu and Guo (2005) that the phenyl ring of Morin slightly deviates from the

planarity like Karanjin is shown to interact with non-anionic micelles. Several research works were done to solubilize flavonoid inside SDS micelles and understanding the interaction between the flavonoid and surfactant (Foti et al., 1996; Naseem et al., 2004; Buchweitz et al., 2016).

5.4.2. Steady-state fluorescence investigation of Karanjin

5.4.2.1. Steady-state fluorescence of Karanjin in neat solvent

From steady-state fluorescence data, Karanjin showed spectral differences with respect to the polarity of the solvents. **Figure 5.11** showed that Karanjin dissolved in SDS micelles have the highest fluorescence yield owing to the relatively confined and rigid microenvironment of the micellar hydrophobic core than neat solvents like MeOH and water. Karanjin dissolved in freshly prepared micellar solution (SDS FR) has similar fluorescence yield while Karanjin is dissolved in overnight incubated solution (SDS ON) revealed the spontaneous SDS micelles formation and subsequently encapsulation of Karanjin inside micelles. **Figure 5.11** and **Table 5.7** revealed the presence of two emission bands of Karanjin at both 260 and 305 nm excitations. The presence of band I (λ_{320}- λ_{370} nm) and band II (λ_{370}- λ_{590}) nm presumably indicate the existence of locally excited emission and charge transfer bands respectively. It is well known that the bands due to local transitions are solvent insensitive, whereas the charge transfer bands are sensitive to environmental changes (Sherif, 1997).

The solvent relaxation effect results in the reduction of excited state energy levels relative to those of the ground states. Consequently, it showed a red shift in λ_{max} when Karanjin is dissolved in polar solvents like water, therefore, decreasing energy gap between the energy states. This stabilization varies with an increase in polarity of the solvents (Liu et al., 2013). Sengupta and Kasha (1979) had earlier recognized that

molecular structural and electronic features, which affect the orientation of the plane of the phenyl ring would influence the basicity of the carbonyl group of flavanone. It is important to notice that the relative intensities of long and short wavelength emissions change accordingly to the nature of the solvent with the excitation energy.

5.4.2.2. Stokes shift

The effects of specific (hydrogen bonding) and non-specific solvent interactions on the electronic absorption spectra are often interpreted in terms of Stokes shift. From the experimental data as shown in **Figure 5.12** and **Table 5.8**, Karanjin showed large Stokes shift in the range of 15,420-17,948 $cm^{-1}$and 10,433-11,996 cm^{-1} when excited at 260 and 305 nm, respectively. The most substantial Stokes shifts of Karanjin in water observed are a result of extensive stabilization of excited states by polar solvent molecules that can reorient about the dipole of excited Karanjin in liquid solution (Dunford et al., 2003). Due to large change in electron density distribution during the electronic transition, a large Stokes shift is observed. Moreover, intermolecular hydrogen bonding interaction between the fluorophore and the solvent molecules can also play an important role in stabilizing these excited states in MeOH and water solutions. The values of the Stokes shift are indicative of the charge transfer transition. Large Stokes shift helps to minimize the self-quenching effect; a greater separation of the excitation-emission wavelengths and also boosts the signal-to-noise ratio in bioimaging applications (Lakowicz, 2006).

5.4.2.3. Steady-state fluorescence of Karanjin in solvent mixture

5.4.2.3.1. Glycerol in MeOH

The behavior of a solute in a neat solvent is known to be very different from the behavior in mixed binary solvent systems. Fluorophore like Karanjin is sensitive to the physical properties of the solvent surrounding the fluorophore. Viscosity is one the important

physical parameter for the investigation of the photophysical property of the molecule. In a viscous environment like glycerol, the intramolecular rotation is slowed down, and the non-radiative decay of Karanjin is consequently suppressed. Thus, both the fluorescence intensity and yield of Karanjin can be correlated to the viscosity of the surrounding environment. The fluorescence intensity increases about ~2.5 fold with the increase in glycerol percentage as a cosolvent in the solution (**Figure 5.13**). This increase is quite small compared to ~100 fold rise as seen in probes like Thioflavin T (Friedhoff et al., 1998).

5.4.2.3.2. Glycerol in water

The fluorescence emission spectrum shifts of Karanjin in different percentage of glycerol in water (**Figure 5.14**) might be due to change in polarity of the microenvironment. However, the change in fluorescence intensity of the flexible molecules like Karanjin also depends on the constraint imposed by the media. The constrained microenvironment of Karanjin restricted the internal motions of the molecule that lead to the enhancement of the fluorescence emission intensity as recorded in glycerol-water (Dash et al., 2013). The sensitivity of emission spectra on solvent polarity suggests that strong dipole moment changes occur between S_0 and S_1 of Karanjin. In the presence of glycerol, the dipolar reorientation of the solvent cage around the excited fluorophores will be inhibited, and this results in a dramatic blue shift of the fluorescence band due to the emission from the unrelaxed, Franck-Condon excited state. Moreover, according to Egorov et al. (2011), the presence of water increases the overall mobility of glycerol, while glycerol slows the movement of water. In other words, the gradual addition of glycerol as cosolvent increases the viscosity of the medium and consequently, solvation

time also increases leading to blue shifted of λ_{max}. A similar observation was observed in flavonoid Fisetin and reported by Guharay et al. (1999).

5.4.2.3.3. Water in MeOH

Karanjin was dissolved in different percentages of water in methanolic solution as shown in **Figure 5.15**. Solvatochromic studies assume complete solvation of the compound. For an aqueous methanolic solution, the initial rapid increase in fluorescence intensity and yield is explained by the increased hydrogen bonded interaction as more and more water molecules replace the MeOH molecules in the microenvironment. However, at a higher percentage of water owing to the strong self-association of water molecules the background consists mainly of associated water clusters and these interact with the water molecules in the solvation shell, decreasing the hydrogen bonding ability of bare water molecules (Banerjee et al., 1995). Thus, the observed value of fluorescence intensity and yield of Karanjin at a high percentage of water tends to decrease. Also, the decrease in fluorescence is consistent with a decrease in absorbance (**Figure 5.8**).

The important factor in mixed solvents is preferential solvation. The solute-solvent and solvent-solvent interactions are more complicated in the case of mixed solvents than in pure solvents. This is due to the composition of the cybotactic region of the solution, which is different from the bulk solvent. Preferential solvation commonly results from specific and non-specific interactions. The non-specific interactions may also cause that one of the components of the binary mixtures prefers a molecule of the same type in its neighborhood, leading to the formation of self-association of the fluorophore (Sasirekha et al., 2008). However, aggregation is possible for Karanjin, even at a low concentration up to 5 μM. Karanjin readily forms crystal upon addition of water

due to its hydrophobicity. Formation of higher order Karanjin aggregates or crystals upon addition of water is confirmed by microscopic images (40X) (**Figure 5.20**).

Furthermore, water provides the hydrophobicity for molecular aggregation may lead to quenching at a higher percentage (>50% water) of water fractions.

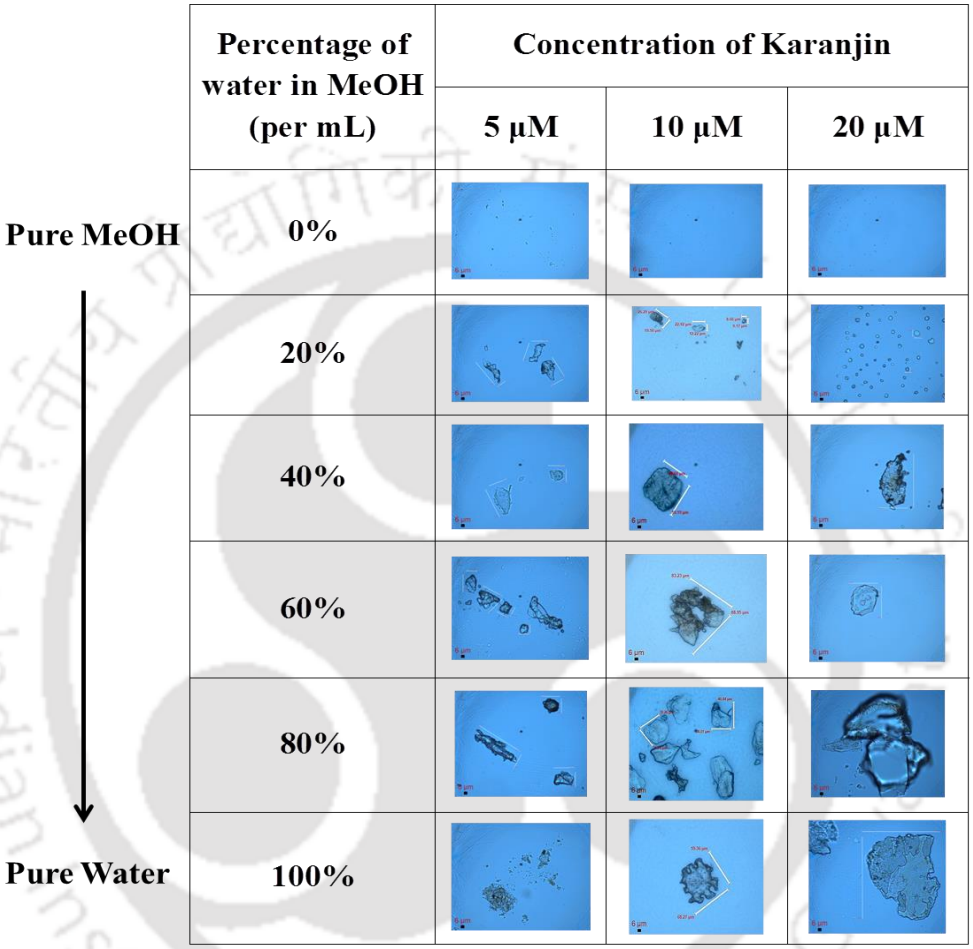

Figure 5.20 Bright-field microscopic image (40X) of Karanjin in different percentage of water in MeOH at various concentrations (**A**) 5 µM; (**B**) 10 µM and (**C**) 20 µM. Magnification bar: 6 µm; Microscope: *Olympus CX 31, India.*

Change in the fluorescence intensity may be attributed to the fact that aggregation is much more facile at higher water contents and the emission is probably only observed from the molecules attached at the surface of these highly aggregated particles, which results in a drop of original fluorescence of the aggregated structure. Our experimental

findings give interesting insights into the hydrogen bonding effects of the solvent on the fluorescence emission of Karanjin.

5.4.3. Time-resolved fluorescence investigation of Karanjin

Time-resolved fluorescence lifetime measurements were carried out for Karanjin in different solvents excited at 295 and 340 nm. TCSPC technique helps in obtaining more information about the intrinsic property of Karanjin in its local environment by providing its fluorescence lifetimes in any particular conditions. The fluorescence emission spectra of Karanjin obtained from steady-state fluorescence experiment (**Figure 5.16**) were also correlated with its mean lifetime obtained from TCSPC data. Karanjin in different neat solvents was excited at two excitations; viz., 295 and 340 nm and fluorescence decays were collected as shown in **Figure 5.17** and **5.18** respectively. Lifetime data of Karanjin demonstrated bi-exponential decays. From this data, Karanjin showed two conformations represented by two lifetimes (τ_1 and τ_2) with their respective fractional distributions (α_1 and α_2). Differences in lifetimes of the fluorophore are due to the differential degrees of solvent relaxation around the fluorophore in the distinct region of a confined environment (Varma et al., 2015). The bi-exponential decays found in all solvents might be due to the presence of presumably two different types of hydrogen-bonded complexes formed between Karanjin and solvent molecules. Significant changes in the lifetime were observed when it is dissolved in aqueous surfactant solutions (SDS FR and SDS ON). It is clear from **Table 5.10** that fluorescence of Karanjin is significantly quenched in an aqueous medium. In the presence of SDS, the lifetime shows a significant increase presumably due to the shielding of Karanjin from the aqueous medium. The tendency to form higher order aggregates may be a reason for the quenched fluorescence of Karanjin in an aqueous medium. However, more detailed investigations are needed to confirm this

interpretation. The results obtained are found to be similar to the previous finding of lifetime determination of flavone as described by Guharay et al. (1999). Similar observation was also recorded by Mishra et al. (2001) showed a high lifetime of aminostyryl pyridinium in viscosity solvents like glycerol and surfactants.

5.5. Conclusion

This chapter highlights the application of absorption and fluorescence spectroscopic methods in the investigation of photophysical properties of Karanjin in different solvent and solvent mixtures. Attention is focused on an intrinsic property of flavonoid as their own 'signature' for characterizing their interactions with the solvents and solvent mixtures. Change in absorbance and fluorescence properties as a function of the solvatochromic parameters was studied. Karanjin in MeOH has the highest molar extinction coefficient followed by SDS and EtOAc. Furthermore, the dimerization of fluorophores and formation of higher order aggregates in solution can induce changes of the extinction coefficient. Karanjin has high transition dipole moment and oscillator strength in aqueous micellar solutions and MeOH. The reduced fluorescence intensity after 50% water fraction may be attributed due to reduced solubility and crystallization of Karanjin in water and water-MeOH mixtures which were demonstrated by UV-Vis absorbance, fluorescence, and microscopic study. Karanjin fluorescence decays in all the solvents are bi-exponential with decay times ranging from 1.3 to 3.4 ns. The mean lifetimes are highest in SDS and least in water. There is a significant improvement of photophysical property of Karanjin in micellar solution due to shielding from water inside the micelle and inaccessibility of solvent molecules around the fluorophore molecule in surfactants. All experimental results suggest that Karanjin binds strongly with the SDS micelles and reside at micellar interior. We hope that the photophysical characterization of Karanjin could provide initial insight into other potential applications in different areas.

Chapter 6

Bioactivity of crude extract and purified compounds against bacteria

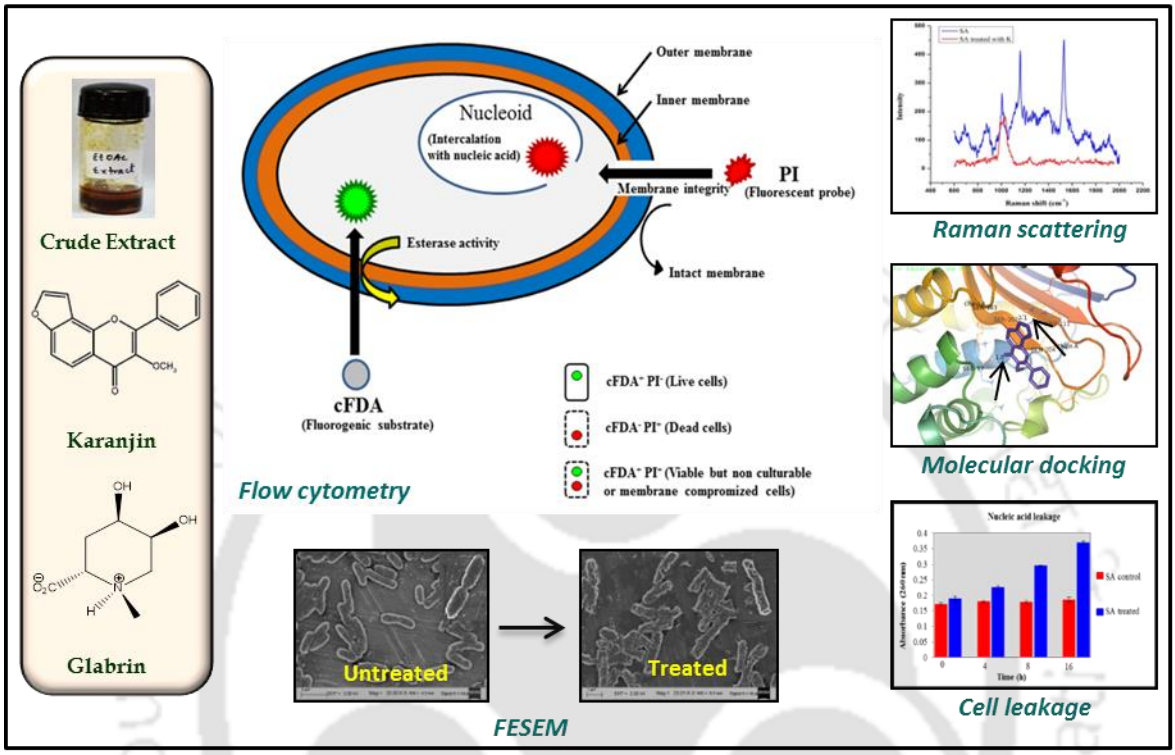

The chapter describes the efficacy of *P. pinnata* crude extract and purified compounds against bacteria. The mode of action of the compounds on the bacteria was also studied.

Chapter 6

Bioactivity of crude extract and purified compounds against bacteria

6.1. Introduction

Medicinal plants being rich source of bioactive constituents have encouraged researcher and scientists towards the utilization of natural products and investigate its pharmacological properties. Several human health problems including life-threatening and deadly infectious disease can be targeted to reduce mortality and morbidity rates. Infectious diseases caused by bacteria have become the main concern for humanity. Plant extracts are found to be very useful in eradicating these infections and exhibit antibacterial property against a wide range of Gram-negative and Gram-positive bacteria (Arote et al., 2009; Bajpai et al., 2009; Chandrashekar and Prasanna, 2010; Kesari et al., 2010). Several compounds have been discovered from *Pongamia* and found to deliver diversified biological efficacy either *in vitro* or *in vivo* against a range of diseases. Seed oil of *Pongamia* exhibits antibacterial activity against *Staphylococcus aureus* and *Pseudomonas aeruginosa* (Wagh et al., 2007; Kesari et al., 2010). Several compounds have been isolated from this species such as quercetin (Mirzoeva et al., 1997; Plaper et al., 2003), pongaglabol (Alam et al., 2004), rutin (Bernard et al., 1997), pongamol (Baki et al., 2007), lupeol (Erazo et al., 2008; Ahmed et al., 2010), methylkarranjic acid (Baki et al., 2007) and others that are used as potent antibacterial therapeutics. Among various phytoconstituents, furanoflavonoid like Karanjin is the main constituent of Karanj seed possessing different biological effect both *in vivo* and *in vitro* (Sapna et al., 2007; Tamrakar et al., 2008; Vismaya et al., 2011).

About, 250 non-protein amino acids have been identified in the plant kingdom and are noteworthy in many ways such as being the intermediates in biosynthetic pathways and possess a physiological role or functioning as natural, semi-synthetic and synthetic pharmacological compound (Swain, 1977; Vranova et al., 2011; Yokoo et al., 2015). These compounds represent a vast array of diverse structural component for the development of new therapeutic drug. Glabrin is a nonproteinogenic α-amino acid isolated from Karanj seeds. However, the antibacterial effect of the compound and its mechanism of action is unexplored yet. Therefore, the isolated compounds were investigated to unveil the mechanism of action as an antibacterial agent by *in silico* and *in vitro* approaches.

In silico study includes structure-based virtual screening, Lipinski's rule of five and docking study are routinely used for understanding drug-like property, drug-receptor interaction, and to predict the binding orientation of drug candidate to its protein target so as to predict the affinity and activity of ligand (Bachwani and Kumar, 2011; Vijesh et al., 2013). *In vitro* study includes susceptibility test (Langfield et al., 2004), Raman scattering (Das et al., 2013), cell leakage assay (Oonmetta-aree et al., 2006), flow cytometry (Leonard et al., 2016) and electron microscopy (Ghosh et al., 2013) which are routinely used for assessing antibacterial property.

Flow cytometry is emerging as a leading technology of bacterial population in food biotechnology (Bunthof et al., 2001), industrial biotechnology (Looser et al., 2001) and environmental samples (Hoefel et al., 2003). It offers a powerful tool for analyzing a cell population at the single-cell level and is helpful in the characterization of functional property, biochemical parameter of the individual cell (Sincock and Robinson, 2001), therefore, offering significant information on the dynamics and physiological heterogeneity of a bacterial population (Hewitt and Nebe-von-Caron, 2001). It relies on

the application of fluorescence probe with suitable target specificity (e.g., nucleic acid, membrane probe or enzyme activity) and optical properties (e.g., fluorescence excitation and emission spectra of fluorescent dyes). This methodology uses commercially available dyes (carboxyfluorescein diacetate, cFDA, and propidium iodide, PI) that allow quantification of different population within the bacterial sample (Antolinos et al., 2014). cFDA is a cell-permeable non-fluorescent ester that undergoes hydrolysis by non-specific esterase activity resulting in accumulation of a green fluorescence compound, carboxyfluorescein inside the cell, thereby offering a means for rapid detection of metabolically active bacteria (Hoefel et al., 2003). PI is a red fluorescent nucleic acid specific dye which enters only in cell with damaged or compromised membrane (**Figure 6.1**).

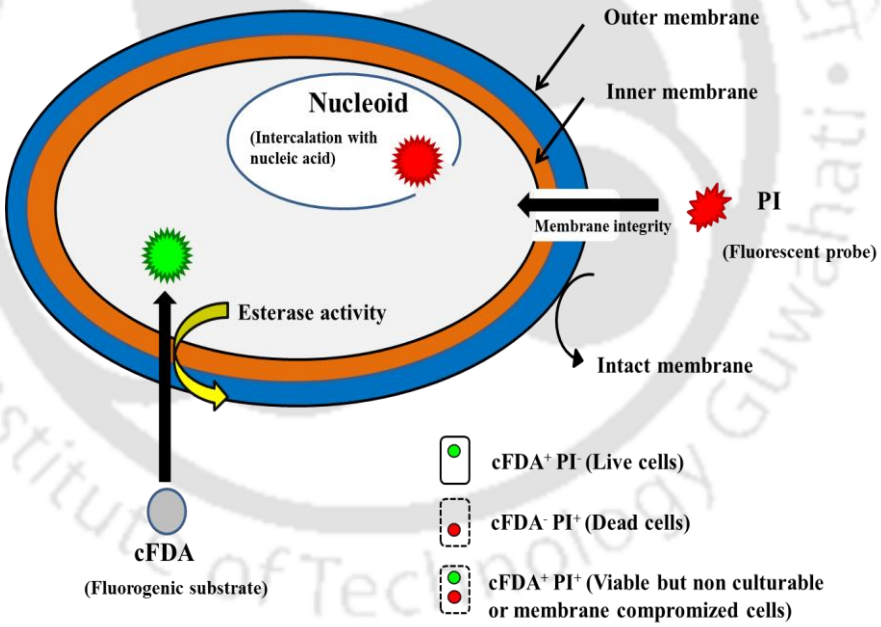

Figure 6.1 Cellular target sites for viability assessment of pathogenic bacteria by flow cytometry.

In the current chapter, the physicochemical parameters of isolated compounds were determined by *in silico* drug-likeness property prediction using OSIRIS Property Explorer based on the structure of the compound. Further, molecular docking study has

been undertaken to screen the possible target of action of purified compounds among common target sites of bacteria. Finally, *in vitro* study of antibacterial action has been studied using microbroth dilution assay, Raman spectroscopy, flow cytometry, and electron microscopy. The effect of purified compounds on the pathogenic bacteria was assessed by measurement of cell leakage and vibrational mode using Raman scattering.

6.2. Materials and methods

6.2.1. Study material and reagents

The organic crude extracts (EE and ME) and purified compounds (Karanjin and Glabrin) were subjected to biological studies.

6.2.2. Bacterial strains

The antibacterial activity were evaluated against two bacteria, *viz. Staphylococcus aureus*, SA (ATCC 6538) and *Escherichia coli* enterotoxic, ETEC (MTCC 723). All the tested bacteria were grown and maintained on nutrient agar (NA) as described earlier (Kesari et al., 2010).

6.2.3. *In silico* drug-likeness and toxicity prediction

OSIRIS Property Explorer was used to estimate the risk of side effects, such as mutagenic, tumorigenic, irritant and reproductive effect, as well as drug-relevant properties including cLogP (lipophilicity), LogS (solubility), molecular weight, drug-likeness, overall drug-score and percentage of absorption (http://www.organic-chemistry.org/prog/peo/) (Ayati et al., 2012).

6.2.4. Lipinski's rule

The pharmacological property and drug likeliness of molecule were examined by Lipinski's rule of five using Molinspiration server (http://www.molinspiration.com/). For a

drug to be orally active it must fulfill all of the following criteria; <10 hydrogen bond acceptors, <5 hydrogen bond donors, molecular weight <500 Dalton and partition coefficient logP to be <5 (Lipinski et al., 1997).

6.2.5. Molecular docking study

6.2.5.1. Protein and ligand retrieval

The set of proteins selected for this study are common target site for evaluation of antibacterial property of ligand. The three-dimensional structure of the common bacterial protein was retrieved from Protein data bank (PDB) (http://www.rscb.org/pdb). Three-dimensional structures of Karanjin and Glabrin were obtained in standard delay format (SDF) from PubChem and converted to PDB format using online SMILES translator (http://cactus.nci.nih.gov/translate/).

6.2.5.2. Binding site determination

The binding site of the bacterial protein, as well as its area and volume, was predicted by computed atlas of surface topography of proteins (CASTp) (http://cast.engr.uic.edu) (Dundas et al., 2006).

6.2.5.3. Docking study

Docking studies were carried out using AutoDock 4.2.6. For all receptors undertaken in the present study, heteroatoms (Hetatms) and water molecules were removed, and polar hydrogen atoms and Kollman charges were added. For ligand, Gastieger partial charges were assigned, and nonpolar hydrogen atoms were merged. All torsions of ligand were allowed to rotate during docking run. Grid box was prepared using binding site information retrieved from CASTp. A grid spacing of 0.375Å was used to compute affinity maps and electrostatic maps. Docking search was carried out using a Lamarckian genetic algorithm and all remaining parameters were set as default. The docked

conformations were sorted according to predicted binding energy with the lowest energy conformation considered to be the most reliable one.

6.2.6. Antibacterial property

6.2.6.1. Determination of MIC by microbroth dilution assay

Minimum inhibitory concentration (MIC) is the lowest concentration of an antimicrobial agent inhibiting the visible growth of a microorganism. The MIC was determined using the microdilution method, in 96 wells microtitre plates (0.3 mL volume, Axiva) (Camporese et al., 2003; Bajpai et al., 2014). Karanjin was dissolved in dimethyl sulfoxide (DMSO) at a concentration of 1 mg/mL, and this concentration was further used to make compound concentration up to 1.95 µg/mL by two-fold dilution method. Test strains were suspended in 0.8% (w/v) NaCl to obtain a cell density of 1×10^8 colony forming unit per milliliter (CFU/mL). These cell suspensions were diluted to obtain a final density of 5×10^5 CFU/mL in each well. Proper growth control, vehicle control (DMSO treated cells) and negative control were adjusted on to the plate. The maximum concentration of compound tested was 500 µg/mL. Microtitre plates were incubated at 37ºC in the moist dark chamber for 24 h, and MIC recorded spectrophotometrically (*Tecan, Infinite M 200 Pro, Switzerland*) at 600 nm (the concentration at which there is a sharp decline in the absorbance value). Kanamycin (5 µg/mL) was used as positive control. The experiment was performed in triplicates and MIC recorded as the mean concentration of triplicate values.

6.2.6.2. Antibacterial study by Raman spectroscopy

Characterization of the bacterial cells before and after exposure of Karanjin was performed on SA and ETEC using Raman spectroscopy (*Horiba LabRAM HR* spectrometer) in the backscattering mode using Argon-ion laser at 514 nm wavelength as

the excitation source at room temperature. Untreated bacterial cells were used as a negative control. About 3 mL of bacterial cultures at exponential growth phase with an appropriate concentration of 10^6 CFU/mL were centrifuged at 3,000 rpm for 5 min. Cells were washed and suspended in 1 mL sterile distilled water. Sample was dried at 37ºC, and then the spectrum was recorded for the changes in intensity and shift in Raman spectrum (Dutta et al., 2011). Spectral data for generating Raman signals were taken from the sample at specific wavenumbers (600 to 2,000 cm^{-1}).

6.2.6.3. Effect of compounds on bacterial cell membrane

Bacterial cell membrane damaging efficacy by purified compounds was performed by cell leakage analysis. Absorbance of respective cell supernatants at 260 and 280 nm was recorded to assess the efflux of cellular components such as proteins and nucleic acids. Briefly, SA and ETEC cells that had been incubated overnight were centrifuged (10,000 rpm; 10 min) and resuspended in sterile NaCl solution (0.9%). Subsequently, each bacterial culture was treated with pure compound at their MIC and incubated for 0, 4, 8 and 16 h respectively. After incubation, samples were centrifuged (10,000 rpm; 5 min) to separate the bacterial cells (pellet) from low molecular weight metabolites (supernatant) which are known to leak from cells after stress exposure. Finally, the absorbance of released materials from cells was determined by measuring the optical density (OD) of the supernatant at 260 and 280 nm using a UV/VIS spectrophotometer (*Varian Carry 50, USA*) (Ghosh et al., 2013). Mean OD values of the respective treatment and vehicle control were compared independently at each time points.

6.2.6.4. Filed emission electron microscopy (FESEM) study

Field emission scanning electron microscopy (FESEM) was used to visualize the changes in the morphology of the SA and ETEC cells before and after treatment with

Karanjin and Glabrin. Healthy, active and untreated bacterial cells were used as negative control for this study. The bacterial samples were washed with 50 mM phosphate buffer solution (PBS, pH 7.2), fixed with 2.5% glutaraldehyde in PBS and rinsed with the same buffer. The specimen was sequentially dehydrated using different ethanol concentration ranging from 30% to 100% as described in detail previously by Ghosh et al. (2013). Finally, the specimen were coated with gold and analyzed through FESEM (*Carl Zeiss, Ultra 55*).

6.2.6.5. Determination of antibacterial action by flow cytometry

The ability to distinguish different physiological states is essential for assessing and validating the survival and virulence of any pathogenic microorganism. To determine the antibacterial action, mid-log phase culture of pathogenic bacteria (*E. coli* enterotoxic and *S. aureus*) were treated with EE, ME and pure compounds at different concentration ranging from 1 mg/mL to 0.001 mg/mL in DMSO. It was subsequently incubated for 24 h along with the vehicle control (cells treated with 1% DMSO). Bacterial suspension were centrifuged (10,000 rpm; 10 min) at room temperature followed by washing with PBS (50 mM, pH 7.0). Cells were resuspended in PBS, and cell density of approximately 10^4 cells/mL was maintained. Heat-killed cells (95°C for 15 min) were taken as positive control. Samples were first stained by adding 10 µL cFDA (0.25 µM, Sigma Aldrich) and incubated at 37°C for 30 min in the dark. All the stained samples were then subsequently washed with PBS to remove residual dye. Samples were then stained with 10 µL PI (10 µg/mL, Sigma Aldrich) (Mahato et al., 2016). Analysis was carried out by fully integrated and multiparametric *BD (Becton Dickinson) FACSCalibur* system equipped with an air-cooled argon ion laser emitting 15 mW blue light at 488 nm and with the standard filter set up. The FC analysis of the cell sample was performed using

FACS Flow solution (BD) as the sheath fluid. Samples were kept at a low flow rate (12 µL/min ± 3 µL/min) up to a total of 10,000 events per sample. Bacterial cells were analyzed by forward (FSC), and side (SSC) light scatter. Viability in term of membrane integrity and functional cytoplasmic enzyme was examined by staining with cFDA detected by FL1 channel, which has 530 nm bandpass filter and the red fluorescence signal of PI collected in the FL3 channel with >600 nm long pass filter depicting the membrane permeability. The fluorescence signals of individual cell were collected in both log and bi-exponential mode. Gating was done in dot-plot of FSC-SSC (forward scatter-side scatter) to discriminate bacteria from noise and artifacts. Data were acquired by BD CellQuest Pro software and were analyzed and refined by FloJo software (*Tree Star, Stanford, USA*).

6.2.6.6. Statistical analysis

All experiments were set up in a completely randomized design and repeated thrice with a minimum of three replicates. Similarly, in cell leakage experiment and flow analysis, significance analysis for mean values of each treatment was compared to the mean of corresponding vehicle control at respective time point using one-way ANOVA followed by Tukey's test. Differences were considered significant at a value of $p < 0.05$.

6.3. Results and discussion

6.3.1. *In silico* drug-likeness and toxicity prediction

Structure and activity relationship was predicted by OSIRIS Property Explorer because of its speed, flexibility, low cost and less time-consuming efforts in comparison to *in vitro* and *in vivo* approaches. Analysis suggests that Karanjin and Glabrin may have low risk to human health considering the four main parameters of the analysis (mutagenic, tumorigenic, irritant and reproductive effectiveness) and can be a potential candidate for

future drug discovery and development (**Figure 6.2**). According to the known structure and activity relationship, it is considered that certain small heterocyclic molecules act as highly functionalized scaffold and known pharmacophores of some biologically active and medicinally useful molecules (Martins et al., 015). The logarithm of this coefficient, log Po/w, has been shown to be one of the key parameter in quantitative structure-activity/property relationship (QSAR/QSPR) study (Bayat and Nassab, 2010). It is also responsible for the activity differences (Alves et al., 2000). The log Po/w of Karanjin and Glabrin are found to be less than 5.0 indicating high lipophilicity and higher absorption and permeation. The aqueous solubility of Karanjin and Glabrin are found to be -4.96 and 0.18 respectively which significantly affect its absorption and distribution characteristics. It was reported that more than 80% of the drugs in the market have aqueous solubility value greater than -4 (Sander et al., 2009). It is also known that the total sum of all polar region of a molecule's surface correlates well with various bioavailability related properties, such as intestinal absorption, and blood-brain barrier penetration. Moreover, the percentage of absorption (ABS) was estimated using the equation as represented earlier by Zhao et al. (2002).

$$\%ABS = 109 - (0.345 \times TPSA)$$

Karanjin and Glabrin showed 92.20 and 81.05% of intestinal absorption capacity and are classified under high absorption group. A positive value of drug-likeness score (Karanjin: 0.52 and Glabrin: 2.87) states that the purified compounds contain a fragment of the compound which are frequently present in commercial drugs. The drug score combines drug-likeness, cLogP, logS, molecular weight, and toxicity risks. It is one handy value that may be used to judge the compound's overall potential to qualify for a drug. The calculation data of purified compounds showed nontoxic behavior with highly desirable physicochemical parameters disclosing its potential as a promising therapeutic

agent (**Table 6.1**). Thus, further experimental testing of these predictions will be required to support the *in silico* data.

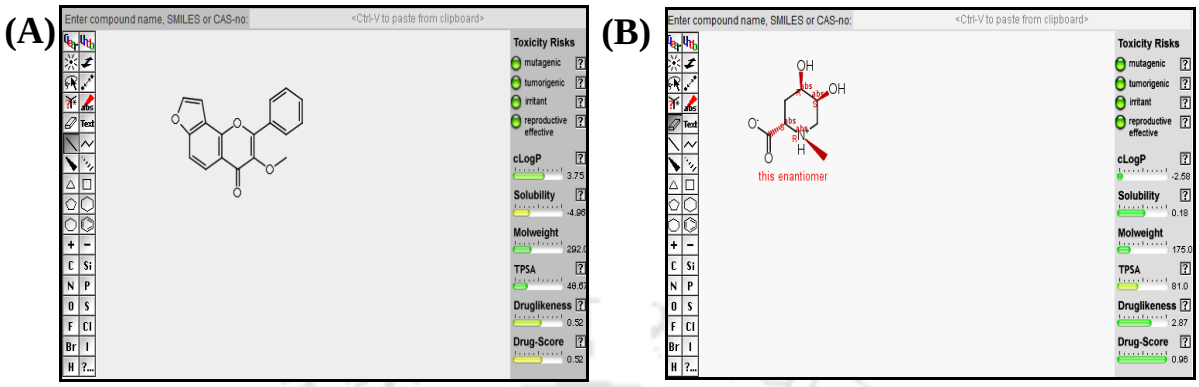

Figure 6.2 OSIRIS Property Explorer of (**A**) Karanjin and (**B**) Glabrin. The results are valued and color coded. Green: safe or drug-like behavior; red: unsafe or undesirable property.

Table 6.1 Physiochemical properties of Karanjin and Glabrin.

Compound	cLogP[a]	LogS[b]	MW[c]	TPSA[d]	Drug likeness[e]	Drug score[f]	%ABS[g]
Karanjin	3.75	-4.96	292	48.67	0.52	0.52	92.20
Glabrin	-2.58	0.18	175	81	2.87	0.96	81.05

[a] **cLogP:** compound's lipophilicity expressed as the logarithm of the partition coefficient between water and 1-octanol. A modified range of Lipinski log*P* value is ranging from -0.4 to +5.6.

[b] **LogS:** solubility (value should be greater than -4)

[c] **MW:** Molecular weight, less than 500

[d] **TPSA:** total polar surface area present in the molecule and should not exceed 90 Å for efficient penetration of drug molecule through the blood-brain barrier.

[e] **Drug likeness:** positive range shows that the molecule contains fragments of the compound which are frequently present in commercial drugs.

[f] **Drug score:** calculated by multiplying contribution of the individual property (cLogP, LogS, MW and toxicity risks)

[g] **% ABS:** absorption percentage (high: 100-67%; medium: 66-33% and low: 32-0%).

6.3.2. Lipinski's rule of five

Lipinski's rule of 5 evaluates whether a given compound can be administered as an orally active drug (Lipinski et al., 1997). The analyzed data show that the compounds

meet the Lipinski's rule of the five, suggesting that the compound theoretically would not have problem with oral bioavailability (**Table 6.2**).

Table 6.2 Lipinski's rule of five.

Compound	logP[a]	MW[b]	H acceptor[c]	H donor[d]	Lipinski's violation
Karanjin	4	292.08	4	0	0
Glabrin	-3.04	175.18	3	5	0

[a] **log*P*:** lipophilicity

[b] **MW:** molecular weight

[c] **Hydrogen bond acceptor (H acceptor):** less than 10

[d] **Hydrogen bond donor (H donor):** less than 5

6.3.3. Antibacterial activity of Karanjin

6.3.3.1. Antibacterial activity by microbroth dilution assay

The MIC for bacterial strains was in the range of 1.95 µg/mL-1 mg/mL. MIC values observed were 125 µg/mL for *S. aureus* and 250 µg/mL for *E. coli* enterotoxic, when treated with pure Karanjin. The lipopolysaccharide in cell wall structure of Gram-negative bacteria blocks the penetration of compound and prevents its accumulation in the cell membrane (Bezic et al., 2003). This in turn blocks several antibiotics which would usually damage the peptidoglycan layer of bacteria. The thin layer of peptidoglycan of Gram-positive bacteria is considerably more accessible to Karanjin to permeate through the membrane to target site. Therefore, Gram-positive bacteria were found to be more sensitive to Karanjin than Gram-negative bacteria. The reactive structures of flavonoid are a pyrogallol group, catechol group, 2, 3-double bond in conjugation with 4-oxo group, 3-hydroxyl group and some additional resonance-effective substituents (Yang, 2001). The antimicrobial effectiveness is thought to come from flavonoid for its ability to form complex with both extracellular and soluble proteins as well as bacterial membrane (Cowan, 1999; Fowler et al., 2011). The five-

membered heterocycle like furan constitutes a vast and differentiated group with a broad spectrum of biological activity (Kharb et al., 2011). The activity of Karanjin could be due to the presence of a hydrophilic substituent in the furan and flavonoid moieties which is very important for antimicrobial effect (Xu and Lee, 2001; Jeong et al., 2009).

6.3.3.2. Antibacterial activity by Raman spectroscopy

Raman spectroscopy is a non-invasive, non-destructive and rapid identification analytical tool for the biological material (Popp, 2007; Das et al., 2013). Antibacterial activity of the Karanjin has been evaluated against SA and ETEC at its MIC values (**Figure 6.3**). Raman spectroscopy provided a fingerprint region below the wavenumber of 1,800 cm^{-1}, which reflects detailed information about the composition of bacterial cells. A high-intensity peak at 1007 cm^{-1} is observed due to C-C stretching of the aromatic ring. Furthermore, another strong peak signal observed at 1525 cm^{-1} which can be attributed to pigments of carotenoid family and peak at 1162 cm^{-1} due to the presence of C-C conjugated stretching in carotenoid. Peaks at 1455, 1606 and 1614 cm^{-1} in bacterial cells are assigned to vibrations of tyrosine and phenylalanine of protein (Naumann, 2001). The bands at 1289 and 1342 cm^{-1} are assigned to L-glutamate and glycine, respectively whereas the band at 1628 cm^{-1} is assigned to pyruvate in ETEC. The band at 1009 cm^{-1} present in the spectra of L-tryptophan can be assigned to the trigonal ring breathing of benzene ring. On the other hand, the Raman spectra of linear saturated fatty acids present in ETEC cells show the band at 1438 cm^{-1} along with few smaller bands (Naumann, 2001). The bands at 1598 cm^{-1} and 1320 cm^{-1} in SA are assigned to phenylalanine and guanine respectively (Maquelin, 2002; Movasaghi, 2007) Moreover, SA and ETEC bacterial cells signifies the cell lysis with a sharp decline in almost all prominent peak intensity after treatment with Karanjin.

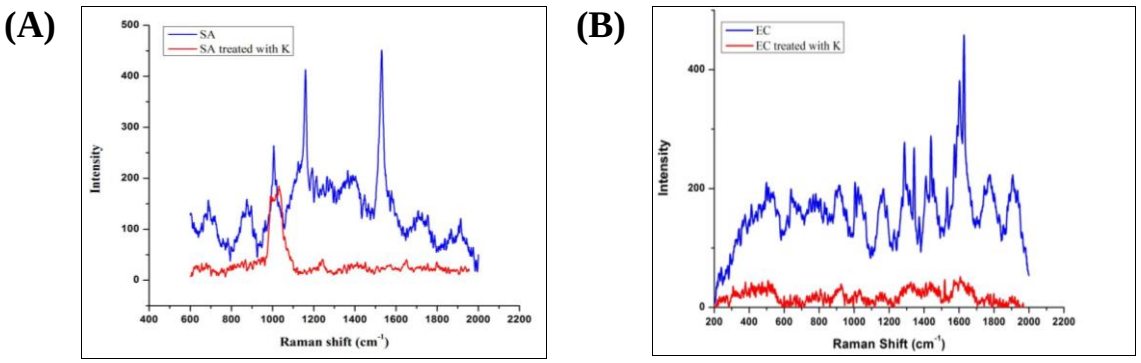

Figure 6.3 Raman spectra of studied bacteria before and after treatment with Karanjin at their respective MICs. Effect of Karanjin on (**A**) *S. aureus*, SA and (**B**) *E. coli* enterotoxic, ETEC.

6.3.3.3. Docking study

The current investigation aims at *in silico* analysis of the interaction between common bacterial proteins and Karanjin at catalytic sites as predicted by CASTp (**Table 6.3**).

Table 6.3 Active site residues of few selected bacterial proteins as predicted by CASTp.

PDB ID	Area ($Å^2$)	Volume ($Å^3$)	Residues
1AJ2	1212	1639.4	ILE20, ASN22, ASP56, GLY58, GLU60, SER61, THR62, ARG63, PRO64, ASP96, THR97, SER98, MET148, GLN149, GLY189, PHE190
1KAS	650.6	934.8	PHE202, ALA205, ARG206, ASP227, GLY228, PHE229, HIS268, MET269, THR270, SER271, PRO272, HIS303, GLY304, GLY310
1KE4	1745.5	2110.9	ILE78, ALA79, ARG80, ILE83, LYS84, LEU85, ASN237, LEU238, LYS239, PRO240, PRO304, THR305, PRO306, ALA307, VAL308
1LTB	2988.6	5565.1	ASP22, LYS23, TYR76, LEU77, THR78, GLU79, THR80, LYS81, LYS102, ASN103
1S16	4453.1	13315	GLY1024, MET1025, TYR1026, THR1027, ARG1031, ASN1033, HIS1034, PRO1257, GLY1258, GLU1261, MET1274
1AD1	992.5	1586.5	ILE9, LEU10, ASN11, VAL12, THR13, ASP15, SER16, PHE17, SER18, GLY48, VAL49, SER50, HIS55, GLU56, GLY169, ILE170, GLY171
1ZOW	1569.2	3089.9	PHE8, GLY9, ALA10, TYR11, ALA12, PRO13, GLU14, LYS14, ILE16, ILE17, ASP18, ASP47, ASP48, VAL60, LYS61
3BLM	146.4	127.7	TYR40, ALA42, ALA242, ARG244, THR265, ASN266, LYS267, PRO274, ASN275, LEU278, ILE279
3FRB	562.4	838.3	LEU5, VAL6, ALA7, ILE14, GLY15, PHE16, ASN18, GLN19, LEU20, ASP27, LEU28, PHE92, GLY93, GLY94, GLN95, THR96, THR121
3G7B	762.4	2010.4	GLN66, ILE67, GLU68, LYS78, THR80, ASP81, ASN82, HIS143, LYS173, THR171, GLY172, THR173, VAL222, ARG223

On performing the molecular docking of Karanjin with all target structure, the calculated binding energy falls within the range of 5-10 kcal/mol with the highest

binding affinity of -9.51 kcal/mol for 1KAS and lowest binding affinity of -5.36 kcal/mol of 3BLM as shown in **Table 6.4**. The intermolecular interaction between receptors and Karanjin is shown in **Figure 6.4** and **6.5.**

Table 6.4 Binding energy of Karanjin with common targets for the antibacterial property.

Sr. No.	Name of protein	PDB ID	Binding energy (kcal/mol)
S. aureus			
1	Dihydropteroate synthase	1AD1	-5.73
2	β-ketoacyl-acyl carrier protein synthase III (KAS III or FabH)	1ZOW	-8.65
3	β- lactamase	3BLM	-5.36
4	Dihydrofolate reductase	3FRB	-5.4
5	DNA gyrase subunit B	3G7B	-5.65
E. coli enterotoxic			
1	Dihydropteroate synthase	1AJ2	-7.92
2	β-ketoacyl-acyl carrier protein synthase II (KAS II or FabF)	1KAS	-9.51
3	β- lactamase	1KE4	-7.9
4	Heat labile enterotoxin (LT)	1LTB	-7.94
5	DNA topoisomerase 4 subunit A	1S16	-7.29
5	DNA gyrase subunit B	3G7B	-5.65

Although Karanjin showed highest binding affinity when docked with β-ketoacyl-acyl carrier protein synthase II (1KAS) of *E. coli*, i.e., 9.51 kcal/mol, the docked conformation lacked hydrogen bond between the ligand and protein. The amino acid residues involved at the binding site are ASP265, HIS268, MET269, THR270, and SER271 (**Table 6.5**). Similarly, Karanjin showed highest binding affinity with β-ketoacyl-acyl carrier protein synthase III or KAS III (1ZOW) of *S. aureus* with the formation of one hydrogen bond between carbonyl oxygen atom of A ring to the nitrogen of atom of residue ALA12 of protein. **Table 6.6** shows the amino acid residues involved at active site ALA12, GLU14, GLU14, and LYS15 which are similar to the binding pocket of isoniazid, a well-known potent inhibitor of these enzymes (Campbell and Cronan, 2001). β-ketoacyl acyl carrier protein synthase (KAS) is a member of the

condensing enzyme family, which is a crucial catalyst in bacterial fatty acid biosynthesis. It represents an attractive target for novel antibiotics related to the elongation of unsaturated fatty acids in the bacterial system (Chen et al., 2007). Heat-labile enterotoxin (1LTB) having second highest binding affinity (-7.94 kcal/mol) showed similar binding pocket when docked with inhibitor 4-nitrophenyl α-D-galactopyranoside (Zhang et al., 2010). On the other hand, DNA topoisomerase 4 subunit A (1S16) showed the least binding affinity of -7.29 kcal/mol among the target selected for *E. coli*. However, dihydropteroate synthase (1AJ2) and β- lactamase (1KE4) showed the binding energy of -7.29 and -7.9 kcal/mol respectively. There is no formation of a hydrogen bond between Karanjin and any of the target proteins of *E. coli*. On the other hand, all target proteins of *S. aureus* showed the formation of one or more hydrogen bonds between the best active site of protein as predicted by CASTp and Karanjin molecule. The binding energy of -5.73 kcal/mol was observed by docking of dihydropteroate synthase (1AD1) with Karanjin. Hydrogen bond formation occurred between nitrogen atom of ASN10 residue and the carbonyl group of Karanjin. Dihydrofolate reductase (3FRB) with the binding energy of -5.4 kcal/mol along with the formation of hydrogen bond between the carbonyl oxygen atom of A ring in Karanjin with the hydrogen atom of residue GLN19. The least binding energy of -5.36 kcal/mol was observed when β-lactamase (3BLM) was docked with Karanjin along with the formation of two hydrogen bonds. For 3BLM, the hydrogen bond acceptor atoms in Karanjin were between the oxygen atom in C ring of Karanjin with the hydrogen atom of residue ARG211 and a carbonyl group in Karanjin with the hydrogen atom of residue SER97. The amino acid residues involved at binding sites are ILE1680, THR1681, GLU1682, GLU1683, LEU1705, GLY1709, LYS1711, GLN1779, TRP1782, GLN1785 and LEU1786 of DNA gyrase subunit B (3G7B) showed binding energy of -5.65 kcal/mol when docked with Karanjin. For this protein, GLU43 formed a

hydrogen bond with the oxygen atom of 3-methoxy group of Karanjin. From docking result, Karanjin showed better binding affinity than the corresponding inhibitors like 1KAS, 1AJ2, 1LTB, 1ZOW, 1KE4 and 1S16.

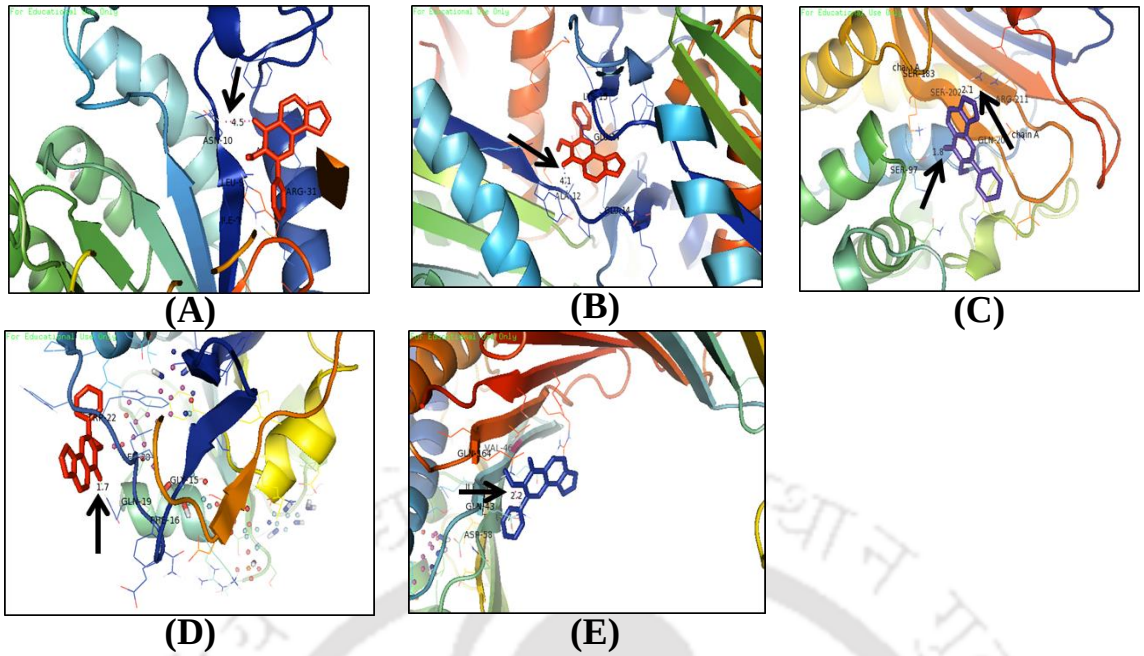

Figure 6.4 Predicted docked conformation of Karanjin against common *S. aureus* proteins. (**A**) Dihydropteroate synthase; (**B**) β-ketoacyl-acyl carrier protein synthase III or KAS III or FabH; (**C**) β- lactamase; (**D**) Dihydrofolate reductase and (**E**) DNA gyrase subunit B.

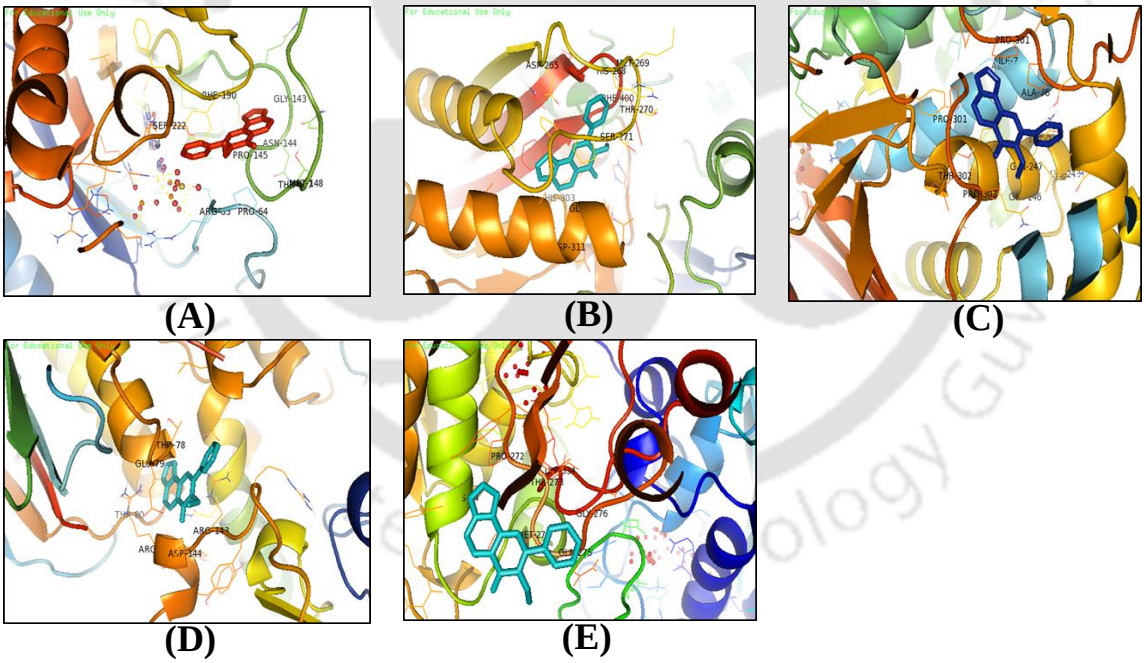

Figure 6.5 Predicted docked conformation of Karanjin against common *E. coli* proteins. (**A**) Dihydropteroate synthase; (**B**) β-ketoacyl-acyl carrier protein synthase II (KAS II or FabF); (**C**) β- lactamase; (**D**) Heat-labile enterotoxin (LT) and (**E**) DNA topoisomerase 4 subunit A.

Table 6.5 Docking result of Karanjin and well known potent inhibitors with common bacterial proteins.

Protein IDs	Ligands	Binding energy (kcal/mol)	Intermolecular Energy (kcal/mol)	Inhibition constant (μM)	Ligand efficiency (kcal/mol)	H-bonds	Residues involved in H-Bonding
1AJ2	Karanjin	-7.92	-8.51	1.57	-0.36	-	-
	Sulfamethoxazole	-5.25	-6.44	142.6	-0.31	1	ARG63:HH21
1KAS	Karanjin	-9.51	-10.1	107.43 (nM)	-0.43	-	-
	Isoniazid	-6.27	-6.86	25.46	-0.63	1	ASP265:OD2
1KE4	Karanjin	-7.9	-8.5	1.61	-0.36	-	-
	Clavulanic acid	-5.0	-6.2	214.7	-0.36	3	SER254:HG SER254:HG ALA304:HN
1LTB	Karanjin	-7.94	-8.54	1.51	-0.36	-	-
	4-Nitrophenyl α-D-galactopyranoside	-6.95	-9.34	8.02	-0.33	3	THR78:O THR78:O ARG145:HH12
1S16	Karanjin	-7.29	-7.88	4.55	-0.33	-	-
	Norfloxacin	-6.34	-7.53	22.49	-0.28	3	ARG31:HE ARG31:HH21 ARG183:HH21
1AD1	Karanjin	-5.73	-6.23	63.48	-0.26	1	ASN10:HN
	Sulfamethoxazole	-6.33	-7.52	22.85	-0.37	3	ARG51:HE GLN104:HE22 LYS202:HZ1
1ZOW	Karanjin	-8.65	-9.25	455.76 (nM)	-0.39	1	ALA12:HN
	Isoniazid	-5.79	-6.39	56.99	-0.58	3	ILE16:HN ALA12:HN TYR266:OH
3BLM	Karanjin	-5.36	-5.95	118.56	-0.24	2	SER97:HG; ARG211:HH21
	Clavulanic acid	-5.11	-6.3	179.8	-0.37	1	LYS234:HZ3
3FRB	Karanjin	-5.4	-6.0	109.55	-0.25	1	GLN19:HE22
	Trimethoprim	-5.72	-7.81	64.38	-0.27	3	PHE16:O GLN19:HE22 LEU20:O
3G7B	Karanjin	-5.65	-6.25	71.97	-0.26	1	GLN43:HE22
	Ciprofloxacin	-5.73	-6.93	62.78	-0.24	1	ASP172:OD2

Table 6.6 Amino acids involved at docking site between ligands (Karanjin and common inhibitors) and proteins.

Protein	Ligand	Nearby amino acid residue
1AJ2	Karanjin	PRO64, ARG63, GLY143,ASN144,THR147,MET148, PHE190, SER222
	Sulfamethoxazole	ASN22, GLU60, SER61, THR62, ARG63, ASP96
1KAS	Karanjin	ASP265, HIS268, MET269, THR270, SER271, HIS303, GLY310, ASP311, PHE400
	Isoniazid	ASP265, HIS268, MET269, THR270, GLY399
1KE4	Karanjin	ILE7, ALA74, ALA76, LYS243, THR244, GLN246, GLN247, PRO301, THR302, PRO303
	Clavulanic acid	LEU251, SER254, PRO303, ALA304
1LTB	Karanjin	THR78, GLU79, THR80, ARG143, ASP144, ARG145
	4-Nitrophenyl α-D-galactopyranoside	GLN30, GLU79, THR80, ARG145
1S16	Karanjin	HIS34, PRO272, MET274, PRO272, THR273, GLY275, GLY276, LYS334
	Norfloxacin	ARG31, HIS34, GLN37, MET274, THR333, GLU335
1AD1	Karanjin	ILE8, LEU9, ASN10, ALA28, ARG31
	Sulfamethoxazole	ILE8, ILE9, LEU10, ASN11, ASP83, ARG51, ASP83, GLN104
1ZOW	Karanjin	ALA12, GLU14, GLU14, LYS15
	Isoniazid	ALA12, ILE16, ASP18, TYR266, LYS265, LYS283,
3BLM	Karanjin	SER97, SER183, SER202, GLN204, ARG211
	Clavulanic acid	LYS240, ASN242, LYS234
3FRB	Karanjin	GLY15, PHE16, GLN19, LEU20, TRP22
	Trimethoprim	ILE14, PHE16, LEU20, TRP22
3G7B	Karanjin	GLN43, ILE44, VAL46, THR57, ASP58, GLN164
	Ciprofloxacin	ASP51, ARG171, ASP172, GLU173

Natural products like flavonoid are capable of binding to multiple targets primarily due to their mode of generation as proposed by Ji et al. (2009). From the docked conformations we can deduce that the carbonyl group, 3-methoxy group and oxygen atom in C ring in Karanjin is biologically vital for forming hydrogen bond interactions with receptors. However, it is pertinent to mention that *in vitro* and *in vivo* experiments often lay the foundation stone and complement or confirm docking analyses.

6.3.3.4. Cell leakage assay

Bacterial homeostasis is vital for its survival. This is carried out by maintaining the functional roles of membrane-coupled and energy-dependent cellular processes such as metabolite transport, turgor pressure balance, metabolism regulation and cells motility (Cox et al., 2001). Therefore, even slight change in the structural integrity of the cell membrane can adversely affect the synthesis of macromolecule and cause cell death. Nucleotide building blocks (purines, pyrimidines, pentose, and inorganic phosphate) and proteins are known to leak from compromised bacterial cells, and the level of leakage determined by measuring the optical density (OD) using UV/Vis spectrophotometer. It was observed that the amount of low molecular weight metabolites in supernatant increased with increasing time of exposure due to the continuous release of cellular material through the compromised cell membrane of treated bacterial strains as compared to controls (**Figure 6.6**). The results showed that Karanjin effectively induce cell damage in both Gram-positive as well as Gram-negative bacteria, although the effect is more pronounced against SA. Therefore, the release of intracellular components is a good indicator of membrane integrity. Similar observations of bacterial cell damage and subsequent leakage have been reported previously (Bajpai et al., 2014). Our findings are in agreement with an earlier published report describing the role of plant-derived bioactive compounds towards cell membrane damage of diverse pathogenic bacteria (Cushnie and Lamb, 2005).

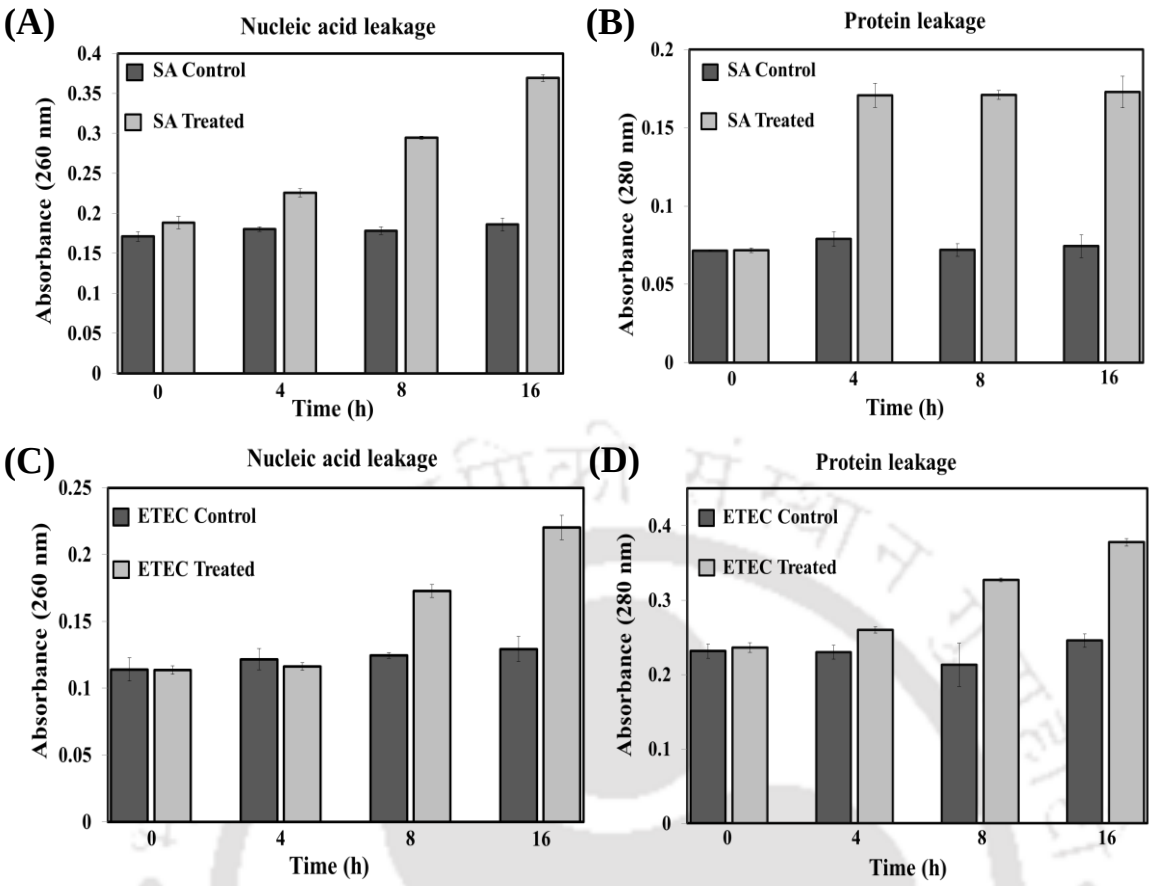

Figure 6.6 Cell leakage analysis.

The absorbance of the cell materials at 260 and 280 nm after treatment with Karanjin at 0, 4, 8 and 16 h incubation period, where SA- **A**, **B,** and ETEC- **C**, **D**. The data are expressed as mean ± standard error.

6.3.3.5. FESEM study

The bacteria SA and ETEC were examined by FESEM to observe physical and morphological changes caused by treatment with Karanjin (**Figure 6.7**). FESEM images of untreated SA and ETEC showed intact, smooth cell surface with defined cell features (**Figure 6.7 A** and **C**) indicating absence of morphological alteration whereas shrinkage, membrane disintegration and noticeable damage of the cell wall were observed in bacterial cells treated with the compound (**Figure 6.7 B** and **D**). These findings indicate that Karanjin caused lysis of SA and ETEC by degrading bacterial cell wall and affecting cell membrane permeability (Dutta, 2011). Changes in membrane fluidity usually occur

due to alterations in membrane lipid composition (Sikkema et al., 1995) and these results are supported by the similar observation when bacteria were treated with terpenes causing changes in membrane property and function (Denyer, 1990).

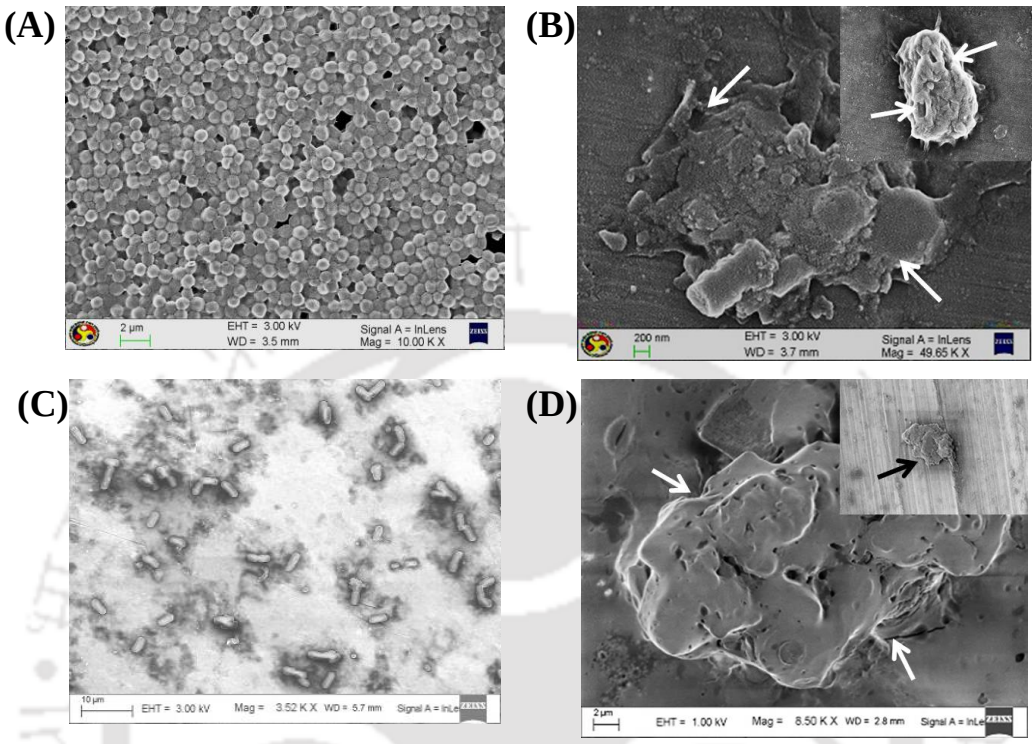

Figure 6.7. Field emission scanning electron micrographs of *S. aureus* (**A** and **B**) and *E. coli* enterotoxic (**C** and **D**). **A** and **C** untreated bacterial cells; **B** and **D** cells treated with Karanjin.

6.3.4. Antibacterial activity of Glabrin

6.3.4.1. Docking study

The current investigation aims at *in silico* analysis of the interaction between common bacterial proteins and Glabrin at the catalytic sites as predicted by CASTp (**Table 6.3**). On performing the molecular docking of Glabrin with all target structures, the calculated binding energy falls within the range of 3-5 kcal/mol with a highest binding affinity of -5.49 kcal/mol for 1ZOW and lowest binding affinity of -3.8 kcal/mol for 3BLM as shown in **Table 6.7**.

Table 6.7 Binding energy of Glabrin and common targets for the antibacterial property.

Sr. No.	Name of protein	PDB ID	Binding energy (kcal/mol)
S. aureus			
1	Dihydropteroate synthase	1AD1	-4.16
2	β-ketoacyl-acyl carrier protein synthase III (KAS III or FabH)	1ZOW	-5.49
3	β- lactamase	3BLM	-3.8
4	Dihydrofolate reductase	3FRB	-4.04
5	DNA gyrase subunit B	3G7B	-4.06
E. coli enterotoxic			
1	Dihydropteroate synthase	1AJ2	-4.43
2	β-ketoacyl-acyl carrier protein synthase II (KAS II or FabF)	1KAS	-4.36
3	β- lactamase	1KE4	-4.32
4	Heat labile enterotoxin (LT)	1LTB	-5.3
5	DNA topoisomerase 4 subunit A	1S16	-5.04
5	DNA gyrase subunit B	3G7B	-4.43

Glabrin showed highest binding affinity of -5.3 kcal/mol when docked with heat labile enterotoxin (1LTB) of *E. coli* with five hydrogen bonds between Glabrin and TYR, ARG and THR residues of the protein (**Table 6.8**). The docked conformation between β-ketoacyl-acyl carrier protein synthase III (1ZOW) and Glabrin has three hydrogen bonds. Amino acid residues involved at the binding site are ALA12, ILE16, TYR11, GLU14, ASP279, and LYS283 which are similar to the isoniazid. All target proteins of *S. aureus* and *E. coli* showed the formation of one or more hydrogen bonds between the best active site of the protein (predicted by CASTp) and Glabrin. The least binding energy of -3.8 kcal/mol was observed when β-lactamase (3BLM) was docked with Glabrin along with the formation of three hydrogen bonds between the oxygen atom of Glabrin with residues PHE257, MET254, and TYR196. The intermolecular interactions between receptors and Glabrin are shown in **Figure 6.8** and **6.9**. Amino acids involved at docking site are given in **Table 6.9**. From the docked conformations we can deduce that the carboxyl group, hydroxyl group and nitrogen atom in Glabrin is biologically vital for forming hydrogen bond interactions with receptors.

Table 6.8 Docking result of Glabrin and well known potent inhibitors with common bacterial proteins. (Docking study of selected proteins with well-known inhibitors is shown in Table 6.5).

Protein (IDs)	Binding energy (kcal/mol)	Inter molecular Energy (kcal/mol)	Inhibition constant (µM)	Ligand efficiency (kcal/mol)	H-bonds	Residues involved in H-Bonding
1AJ2	-4.43	-5.62	567.31	-0.37	3	GLN142:O; LYS192:HN; GLN142:O
1KAS	-4.36	-5.56	633.14	-0.36	1	THR307:HG1
1KE4	-4.32	-5.51	681.18	-0.36	3	TYR256:HH; PRO301:O; PRO301:O
1LTB	-5.3	-6.5	129.73	-0.44	5	TYR147:O; ARG1:HE; ARG1:HH21; THR87:OG1; THR87:HN
1S16	-5.04	-6.23	202.21	-0.42	4	GLU335:HN; ARG336:HH21; GLU335:OE1; ARG336:HN
1AD1	-4.16	5.35	890.9	-0.35	4	ARG51:HH22; ARG51:HE; VAL48:O; VAL48:O
1ZOW	-5.49	-6.69	93.88	-0.46	3	ALA12:HN; LYS283:HZ2; ILE16:HN
3BLM	-3.8	-4.99	1.64 (mM)	-0.32	3	PHE257:OXT; MET254::O; TYR196:HH
3FRB	-4.04	-5.23	1.1 (mM)	-0.34	4	LEU24:HN; LEU20:HN; HIS23:HD1; GLN19:HE22
3G7B	-4.06	-5.26	1.05 (mM)	-0.34	3	THR125:OG1; LYS124:HZ2; THR125:OG1

Table 6.9 Amino acids involved at docking site between ligands and protein.

Protein	Ligands	Nearby amino acid residues
1AJ2	Glabrin	GLN142, GLN143, ASN143, PRO145, ALA151, GLY189, PHE190, GLY191, LYS192
	Sulfamethoxazole	ASN22, GLU60, SER61, THR62, ARG63, ASP96
1KAS	Glabrin	THR270, SER271, PRO272, HIS303, THR307, ALA309, PHE400
	Isoniazid	ASP265, HIS268, MET269, THR270, GLY399
1KE4	Glabrin	ALA252, GLN253, SER254, TYR256, PRO301
	Clavulanic acid	LEU251, SER254, PRO303, ALA304
1LTB	Glabrin	ARG1, ALA86, THR87, TYR 122, TYR142, TYR147, ARG148
	4-Nitrophenyl α-D-galactopyranoside	GLN30, GLU79, THR80, ARG145
1S16	Glabrin	GLN275, THR333, GLU335, ARG336
	Norfloxacin	ARG31, HIS34, GLN37, MET274, THR333, GLU335
1AD1	Glabrin	ASN10, VAL48, ARG51, ILE57, ASP83, ASN102, GLN104, ARG238
	Sulfamethoxazole	ILE8, ILE9, LEU10, ASN11, ASP83, ARG51, ASP83, GLN104
1ZOW	Glabrin	ALA12, ILE16, GLU14, ASP279, LYS283
	Isoniazid	ALA12, ILE16, ASP18, TYR266, LYS265, LYS283,
3BLM	Glabrin	PRO193, TYR196, LYS 251, MET254, LYS255, GLU256, PHE257
	Clavulanic acid	LYS240, ASN242, LYS234

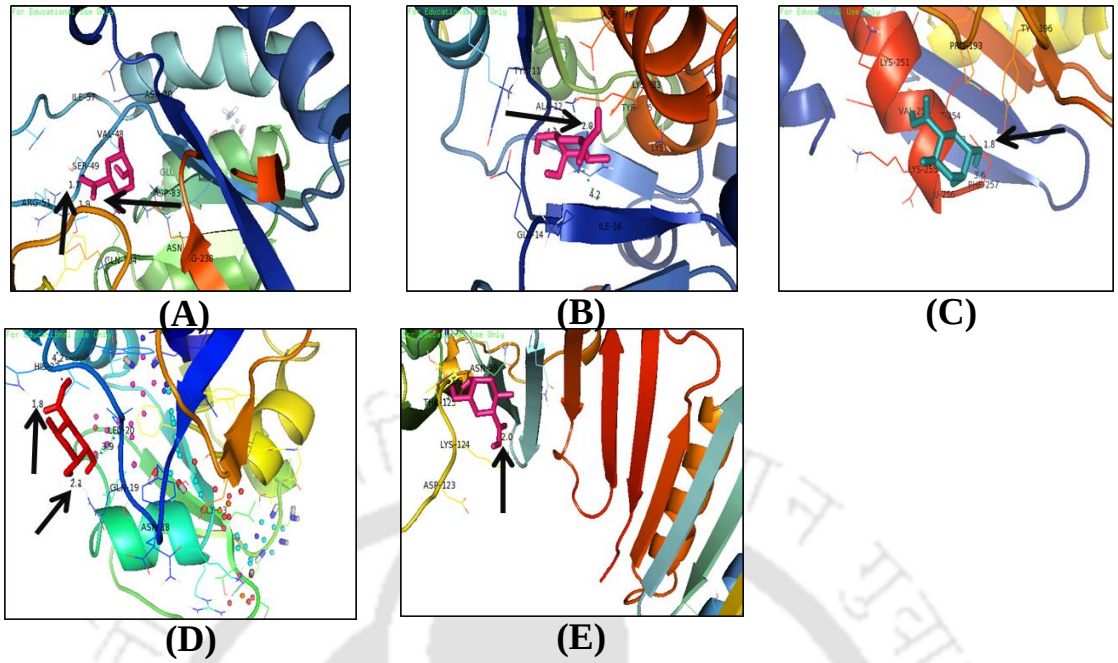

Figure 6.8 Predicted docked conformation of Glabrin against common *S. aureus* proteins. (**A**) Dihydropteroate synthase; (**B**) β-ketoacyl-acyl carrier protein synthase III or KAS III or FabH; (**C**) β- lactamase; (**D**) Dihydrofolate reductase and (**E**) DNA gyrase subunit B.

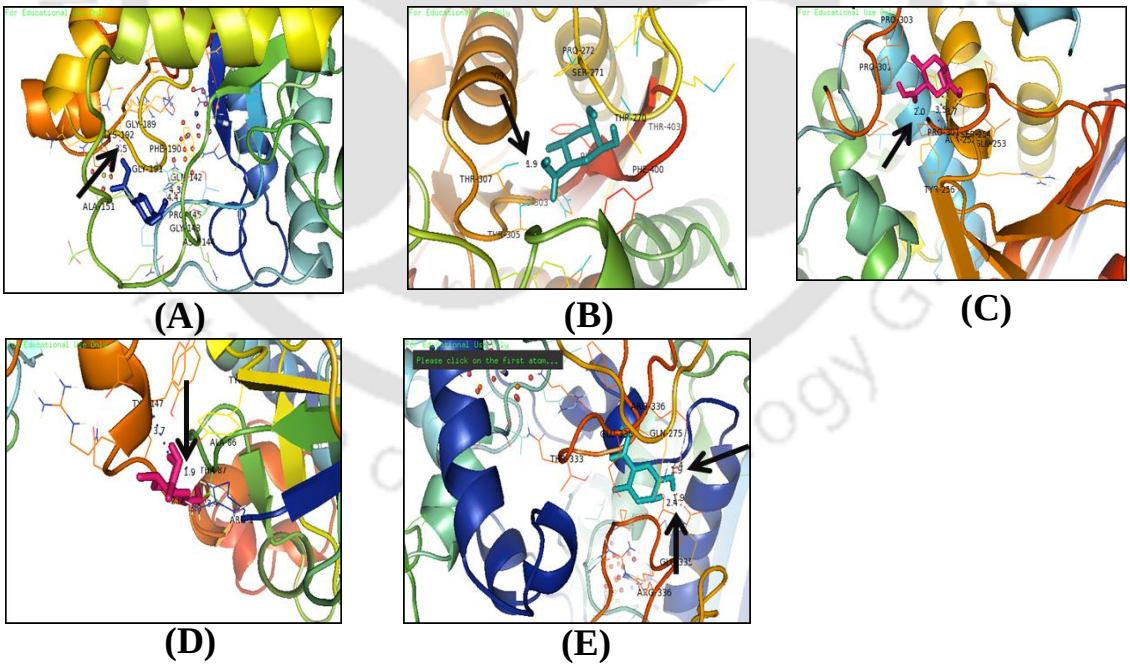

Figure 6.9 Predicted docked conformation of Glabrin against common *E. coli* proteins. (**A**) Dihydropteroate synthase; (**B**) β-ketoacyl-acyl carrier protein synthase II (KAS II or FabF); (**C**) β- lactamase; (**D**) Heat-labile enterotoxin (LT) and (**E**) DNA topoisomerase 4 subunit A.

6.3.4.2. Cell leakage

The cytoplasmic membrane of bacteria acts as a barrier between cytoplasm and extracellular medium by maintaining the chemiostatic balance which is necessary for the survival and metabolism of the cell. The leakage of low molecular weight cytoplasmic constituents often leads to the leakage of larger cellular contents either due to further damage of the membrane or gradual breakdown of proteins and nucleic acids by autolytic enzymes of the cell (Johnston et al., 2003). It was observed that the amount of low molecular weight metabolites increased with increasing time of exposure due to the continuous release of cellular materials through the compromised cell membrane of treated bacterial strains as compared to controls (**Figure 6.10**). The leakage of cellular material could be an indication of a disturbance and disorganization of the cytoplasmic membrane integrity when the concentration of antimicrobials was bacteriostatic. At high antimicrobial dose, it would cause lethality to microbial cells. The results shows that Glabrin effectively induces the cell damage in both Gram-positive as well as Gram-negative bacteria, although the effect is more pronounced against SA. Finally, cell lysis occurs due to pores formation or disruption of cell membrane causing loss of metabolic activity and ultimately cellular leakage resulting to the cell death. Similar observations of cell membrane damage and subsequent leakage caused due to bioactive compounds was reported earlier (Cushnie and Lamb, 2005).

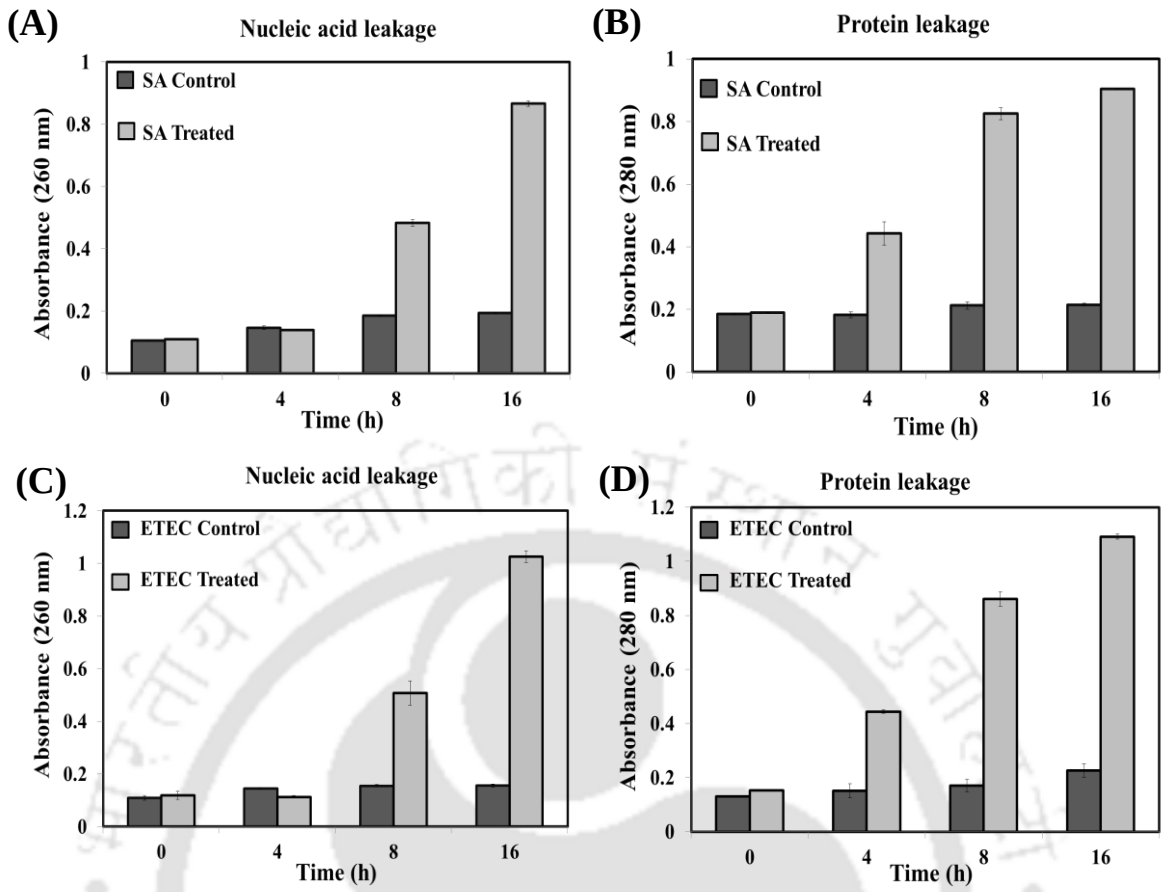

Figure 6.10 Cell leakage analysis.

The absorbance of the cell materials at 260 and 280 nm released after treatment with Glabrin at 0, 4, 8 and 16 h incubation period, where SA- **A**, **B,** and ETEC- **C**, **D**. The data are expressed as mean ± standard error.

6.3.4.3. FESEM study

The bacteria ETEC and SA were examined by FESEM to observe morphological changes caused by treatment with Glabrin (**Figure 6.11**). FESEM images of untreated ETEC and SA exhibited intact, well-defined cellular contents and were normal in size (**Figure 6.11 A** and **C**) whereas Glabrin is more likely to have direct contact with the cell membrane through damaged cell wall after treatment of compound (**Figure 6.11 B** and **D**). These findings indicate that Glabrin cause lysis of SA and ETEC by weakening peptidoglycan layers thereby rupturing cell wall and leading to pores formation. These

damaging effects inturn trigger the leakage of ions and cellular materials ultimately causing the cell death (Cowen, 1999).

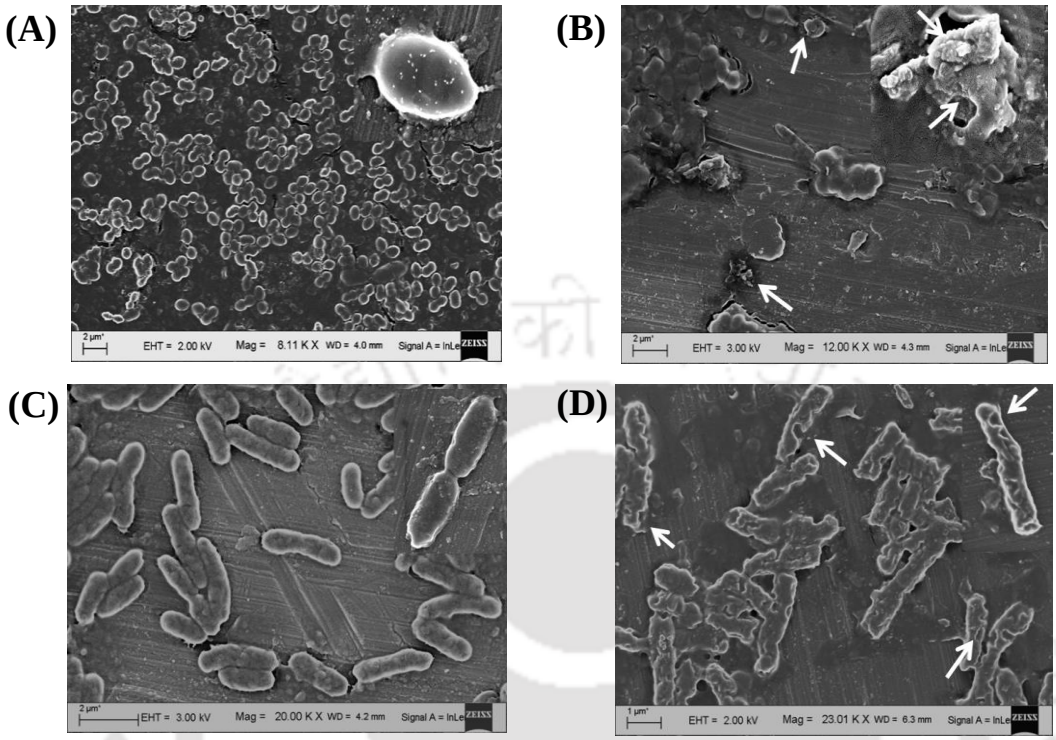

Figure 6.11 Field emission scanning electron micrographs of *S. aureus* (**A** and **B**) and *E. coli* enterotoxic (**C** and **D**). **A** and **C** untreated bacterial cells; **B** and **D** cells treated with Glabrin.

6.3.5. Flow cytometry study

The mean fluorescence intensity for live cells (MFI of FL 1) and dead cells (MFI for FL 3) was measured. The vehicle control (DMSO) and untreated bacterial cells showed minimum relative fluorescence intensity of PI. But, the positive control (heat-killed) showed a significant increase in relative fluorescence intensity in tested bacteria concerning vehicle control and confirmed the significant cell populations as dead (**Figure 6.12 A** and **B**). Interestingly, it was observed that PI relative fluorescence intensity was maximum when the cells were subjected to heat treatment indicating significant damage and depolarization of the bacterial cell membrane.

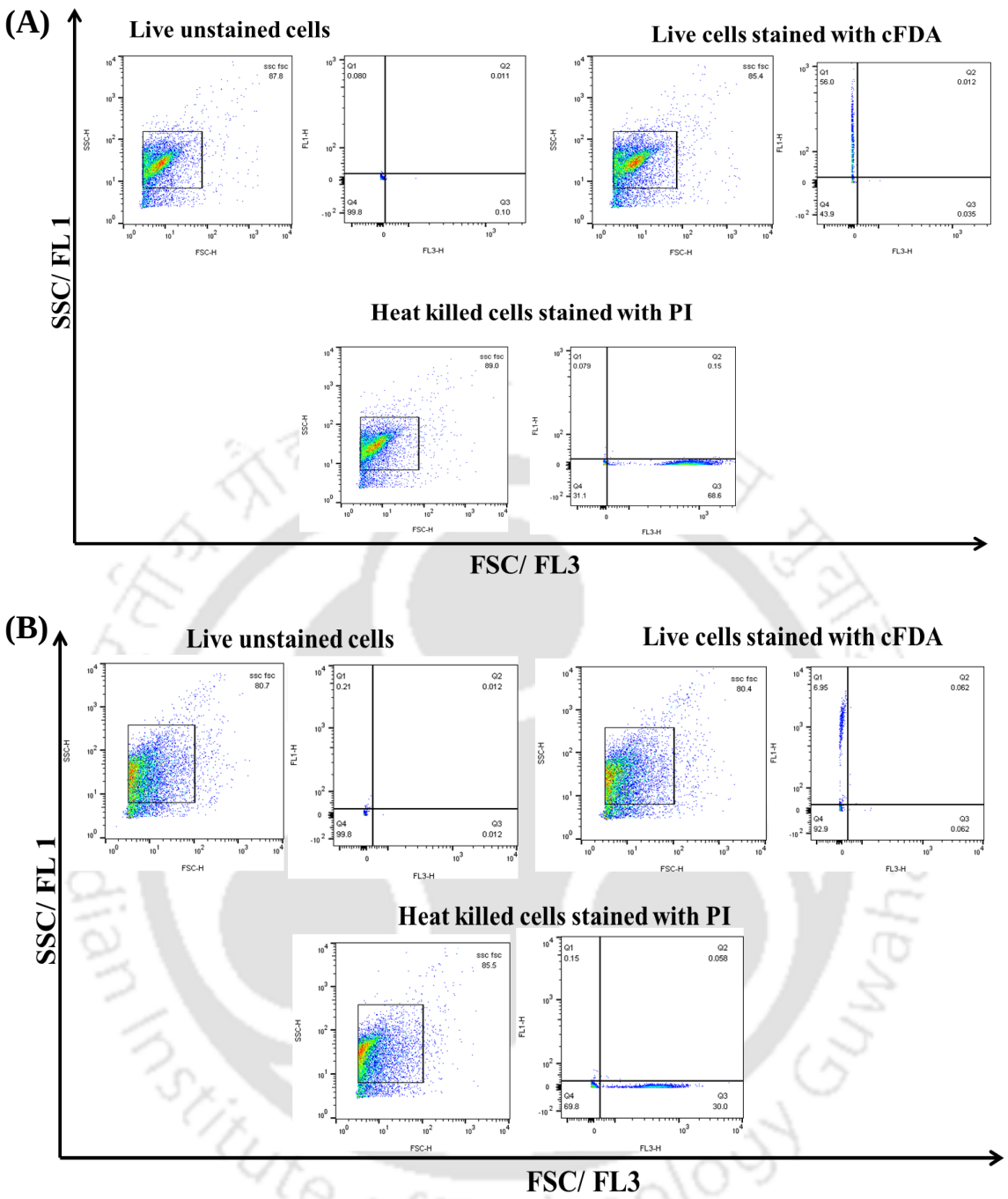

Figure 6.12 Proper control of tested bacteria for detector set up. (**A**) SA and (**B**) ETEC. Live unstained cells ($cFDA^-$ PI^-) serve as negative experimental control, live cells stained with cFDA ($cFDA^+$ PI^-) as positive control for cFDA and heat-killed cells stained with PI ($cFDA^-$ PI^+) as a positive control for PI.

The antimicrobial effect of crude extracts and compounds are represented in terms of MFI of fluorescent dyes, cFDA (as live population) and PI (as dead cell population) as shown in **Figure 6.13**. At high concentration of extract and purified

compounds, MFI of cFDA also decreases in both test bacteria (**Figure 6.13 A** and **C**). It also shows dynamic changes of the membrane integrity and indicates the existence of three main subpopulations of treated bacteria. These are identified as live, dead and membrane-compromised bacteria based on their differential staining characteristics with PI and cFDA. Thus, cells were simultaneously stained with cFDA and PI revealed a striking physiological heterogeneity within the stressed bacterial population. **Figure 6.13** (**B** and **D**), shows that the potency of the extract and compounds increase with increase in concentration as reflected from MFI of FL 3. ME is active against *S. aureus*, but EE is more potent against *E. coli* enterotoxic. Karanjin is found to be more potent against *E. coli* enterotoxic (**Figure 6.13 B** and **D**) whereas Glabrin is active against both the bacteria. The hydrophilic nature of MeOH crude extract and Glabrin allows it to penetrate microbial cells and induce alterations in structure and function of the bacterium. These changes possibly resulted in the loss of microbial viability.

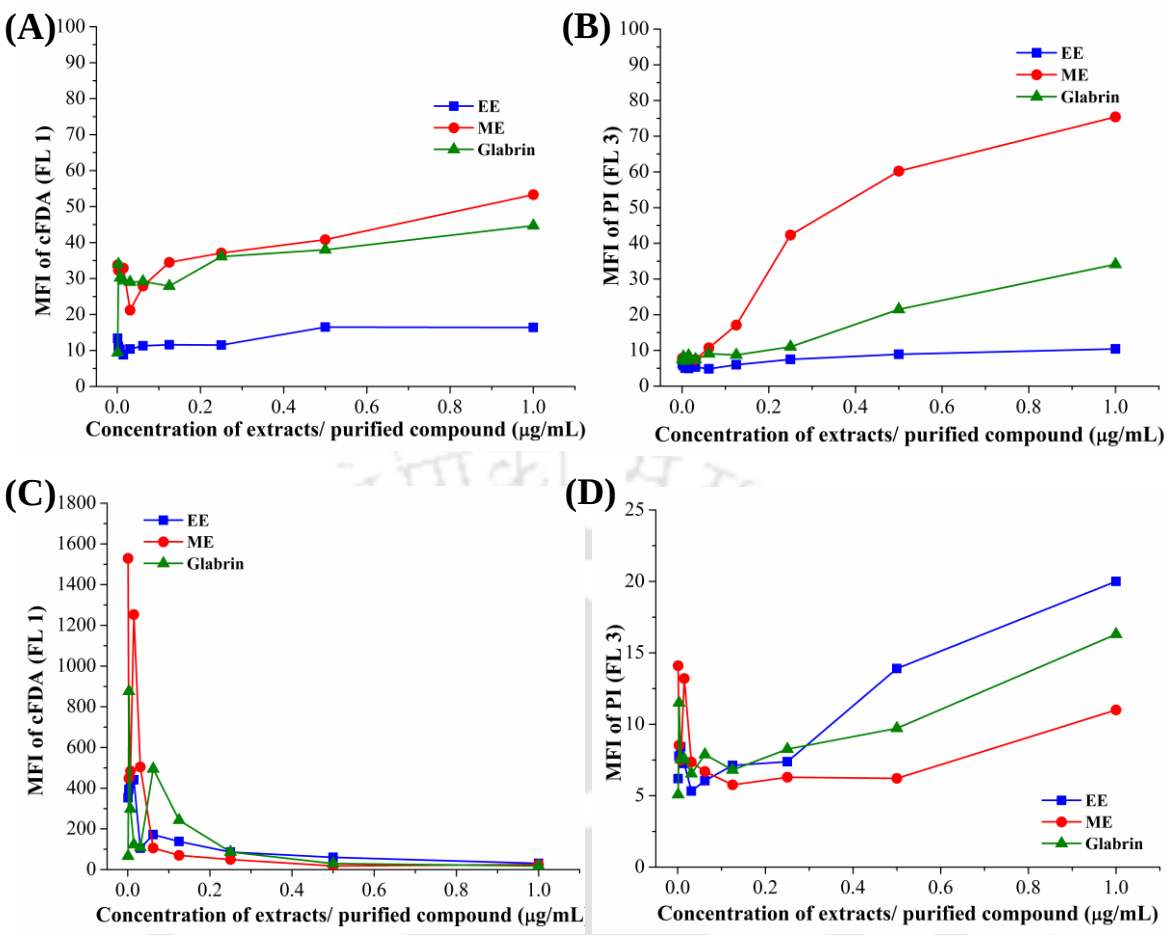

Figure 6.13 Viability assessments of pathogenic bacteria against crude extracts (EE and ME) and purified compounds (Glabrin).

(**A**) MFI of cFDA of *S. aureus*; (**B**) MFI of PI of *S. aureus*; (**C**) MFI of cFDA of *E. coli* enterotoxic and (**D**) MFI of PI of *E. coli* enterotoxic.

MFI = mean fluorescence intensity; FL 1 = filter channel 1 for cFDA (live cells) and FL 3 = filter channel 3 for PI (dead cells).

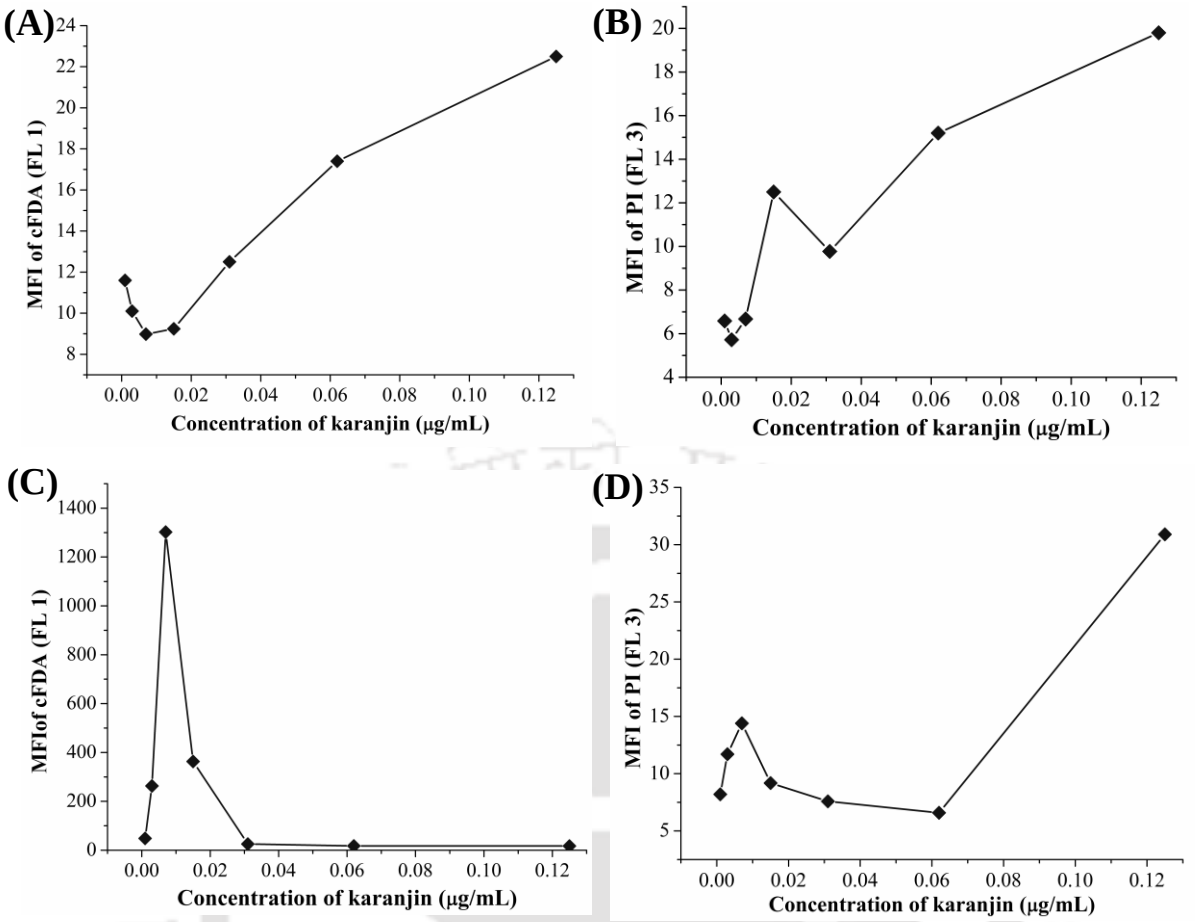

Figure 6.14 Viability assessments of pathogenic bacteria against Karanjin. (**A**) MFI of cFDA of SA; (**B**) MFI of PI of SA; (**C**) MFI of cFDA of ETEC and (**D**) MFI of PI of ETEC.

The percent double-stained cells ($cFDA^+$ PI^+) showed a subtle increase revealing 'viable but non-culturable' (VBNC) and cryptobiotic states along with the active and dead subpopulations in the heterogeneous sample (Leonard et al., 2016). In the current study, the percentage of VBNC subpopulation is high when cells were treated with ME as compared to EE and purified compounds (**Figure 6.14**). Crude extract and purified compounds were found to be more potent against ETEC at low concentration in inducing VNBC state in bacterial population.

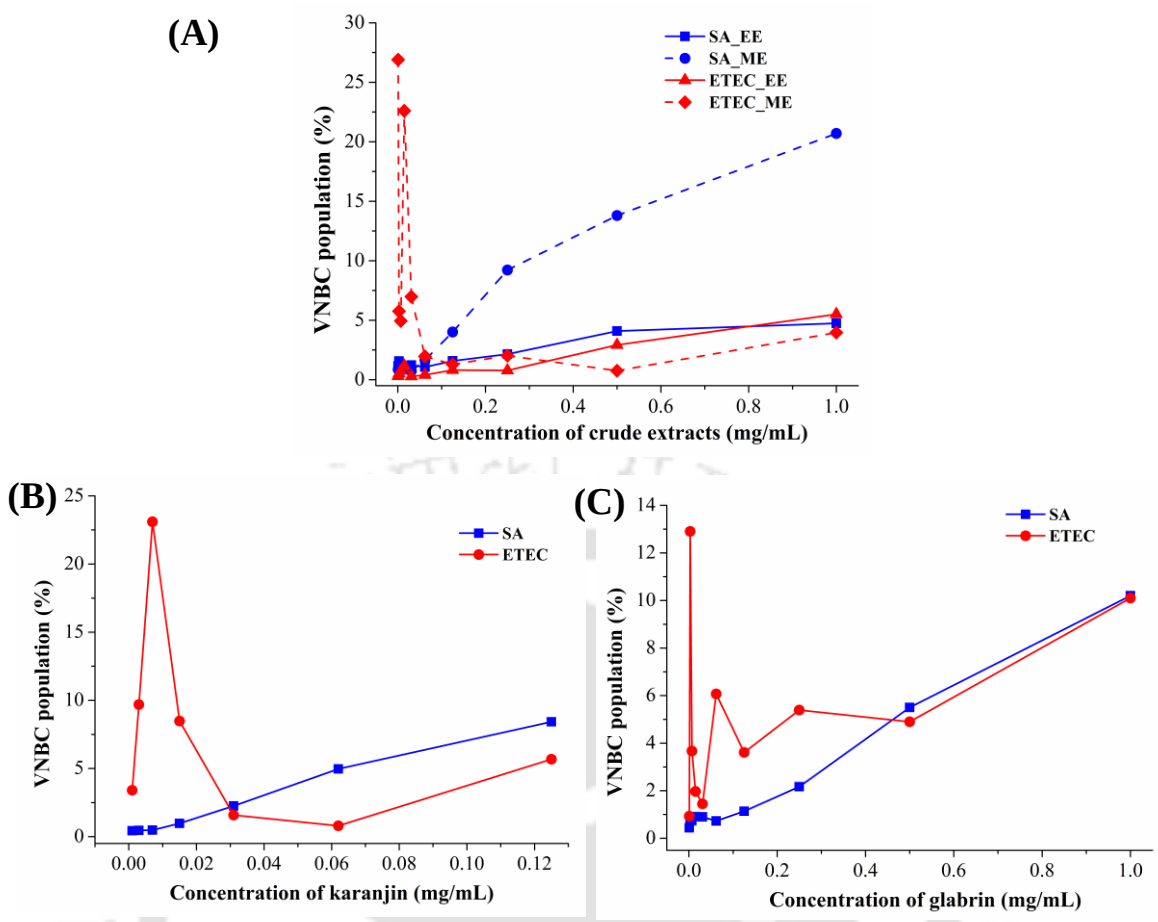

Figure 6.15 VBNC population of SA and ETEC after exposure of crude extracts and pure compounds at different concentrations. (**A**) Effects of ME and EE; (**B**) Karanjin and (**C**) Glabrin.

In 1982, Xu et al. first reported about VBNC bacteria, including *E. coli*. Subsequently, many investigators have reported about VBNC state, with more than 60 species of bacteria showing the phenomenon, including many human pathogens (Oliver, 2010). It is believed that VBNC pathogens are incapable of inducing disease despite the retention of virulent factors and are considered to be in a stage preceding cell death or adaptation to stress (Sachidanandham and Gin, 2009; Zhao et al., 2017). During this period, VBNC cells often exhibit dwarfing, and some significant metabolic changes occur, including reduction in nutrient transport, respiration rate, change in membrane fatty acid composition and macromolecular synthesis as clearly discussed by Trevors et

al. (2012). **Table 6.10** differentiates the physiological and metabolism processes between actively dividing cells and VBNC bacteria.

Table 6.10 Comparison of cytoplasm in actively growing/dividing bacterial cells to VBNC cells (Trevors et al., 2012).

Actively growing/dividing	VBNC physiological state
Molecularly crowded cytoplasm	Less molecular crowding
Optimal diffusion	Minimal diffusion
Higher total protein concentration	Lower total protein concentration
More organization of molecules such as cell division proteins	Less molecular organization such as cell division proteins
Optimal protein oscillations	Fewer to no protein oscillations
High ribosome numbers	Fewer ribosomes
Optimal gene expression	Minimal to no gene expression
Higher number of transcripts	Minimal transcripts
High tRNA content	Minimal tRNA
Optimal cytoplasmic membrane fluidity	Cytoplasmic membrane may be less fluid with leakage from cytoplasm (e.g., K+)
Optimal ATP pool	Minimal ATP pool
More nonspecific molecule interactions	Fewer nonspecific molecule interactions
Optimal cytoplasm volume just before cell division	Minimal cytoplasm volume
Replicating DNA	Condensed DNA
Optimal Mg2+	Less Mg2+

Moreover, cells also showed high complexity upon exposure of crude extract and pure compounds (**Figure 6.15** and **6.16**). It can be described by the change in their morphological characteristics such as cell surface roughness, cell membrane disruption, nucleus, and internal granular material, rupture of cell organelles, etc. At high concentration of stress exposure, cells showed high SSC profile that can be correlated with changes in cell's molecular composition.

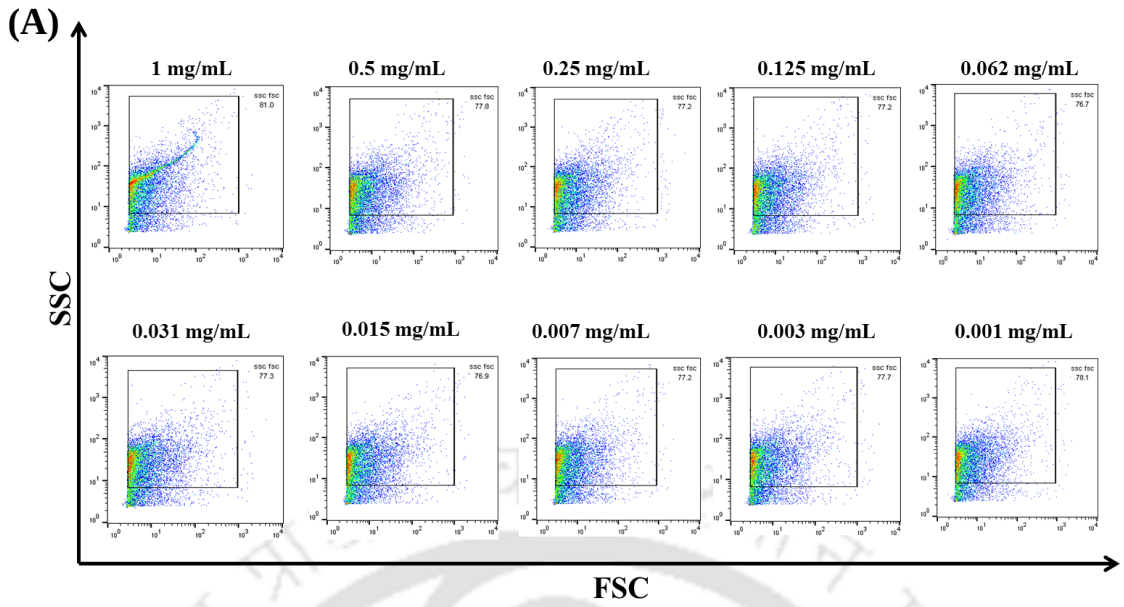

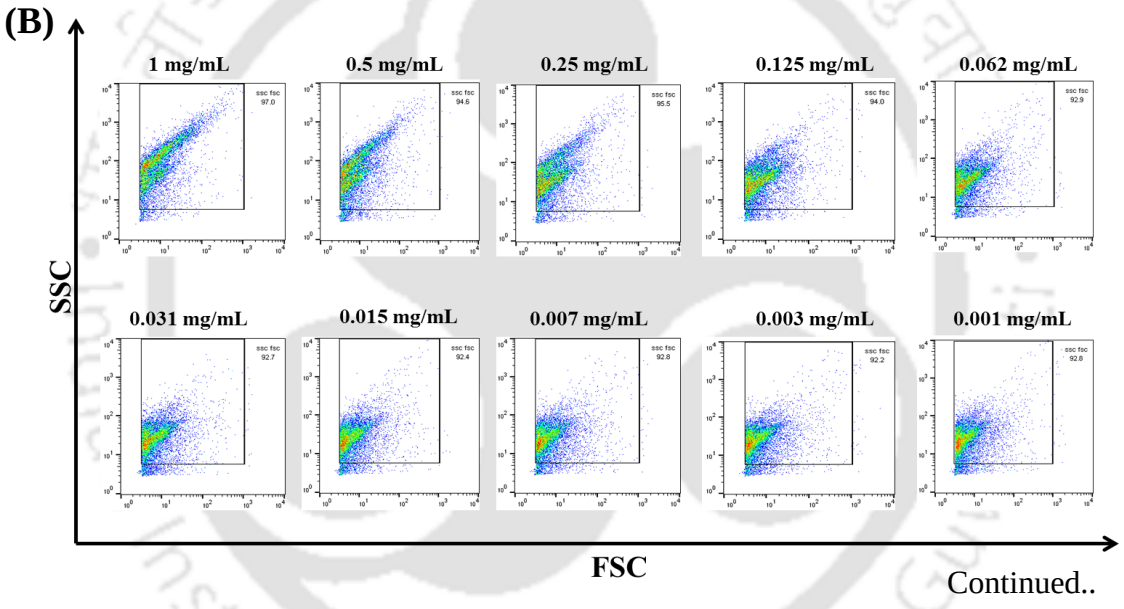

Continued..

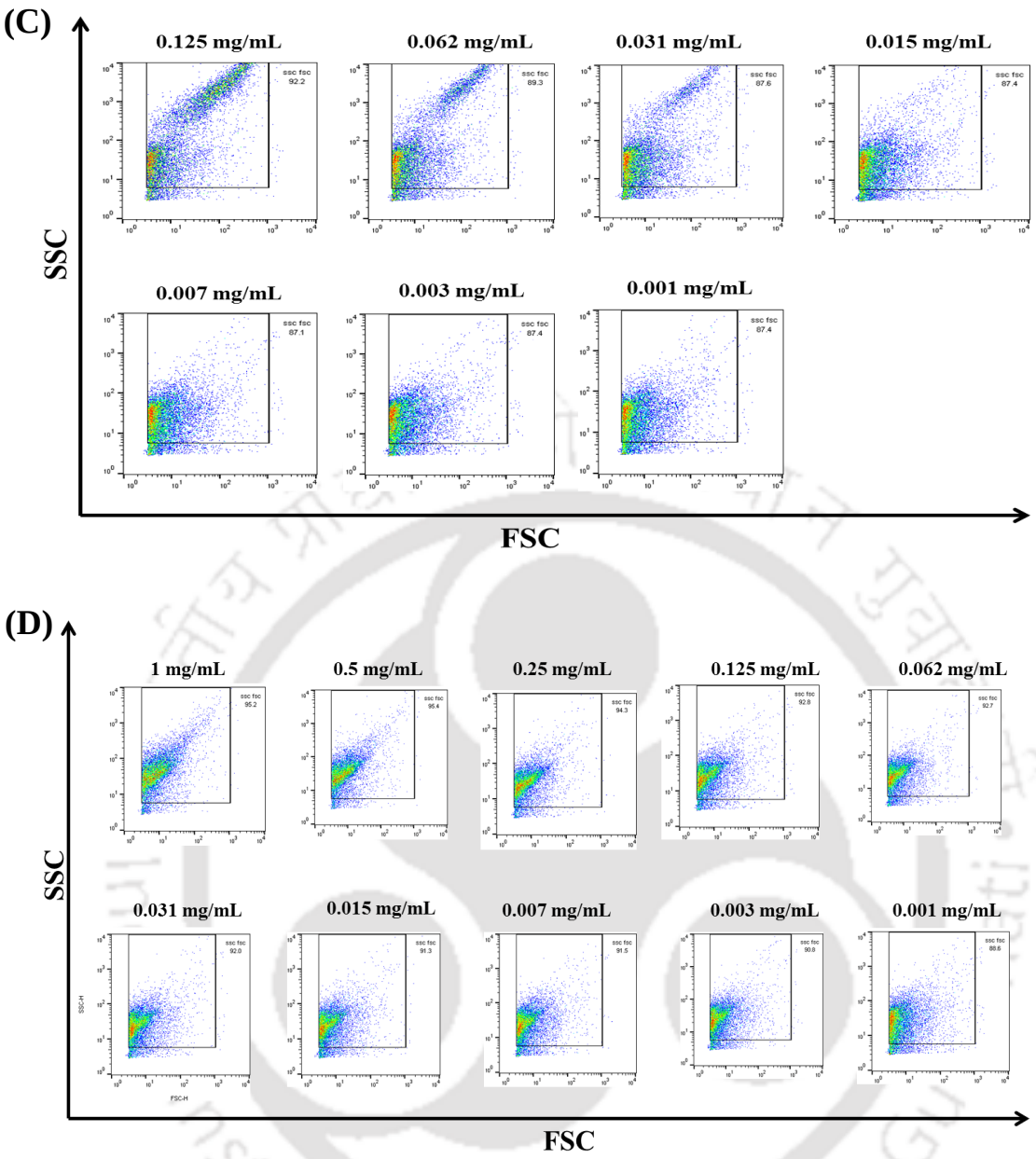

Figure 6.16 SSC FSC profiles of SA upon treatment with different concentration of (**A**) EE; (**B**) ME; (**C**) Karanjin and (**D**) Glabrin.

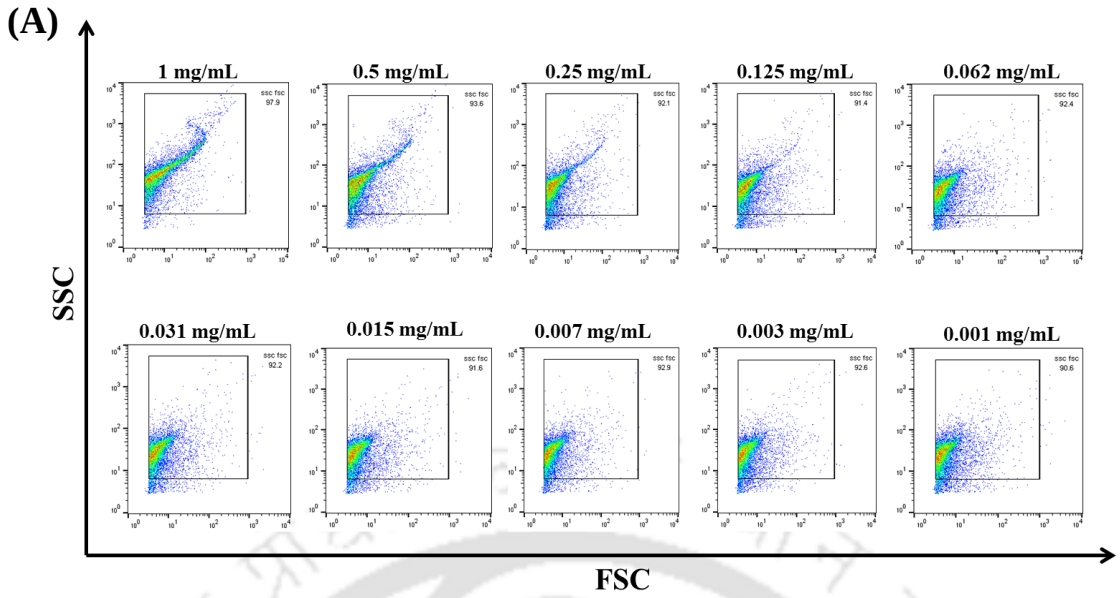

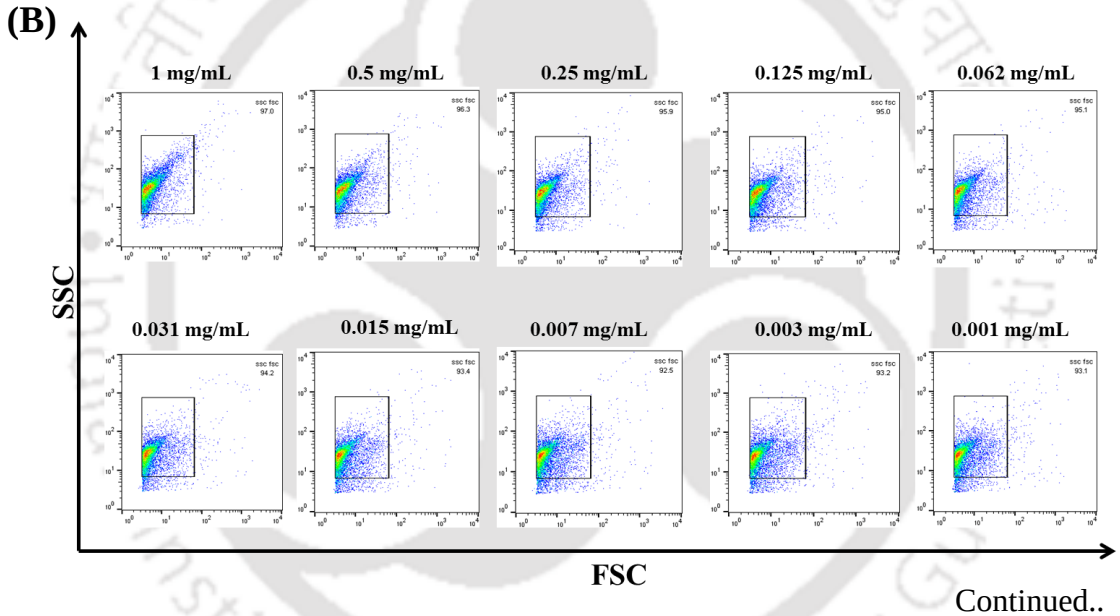

Continued..

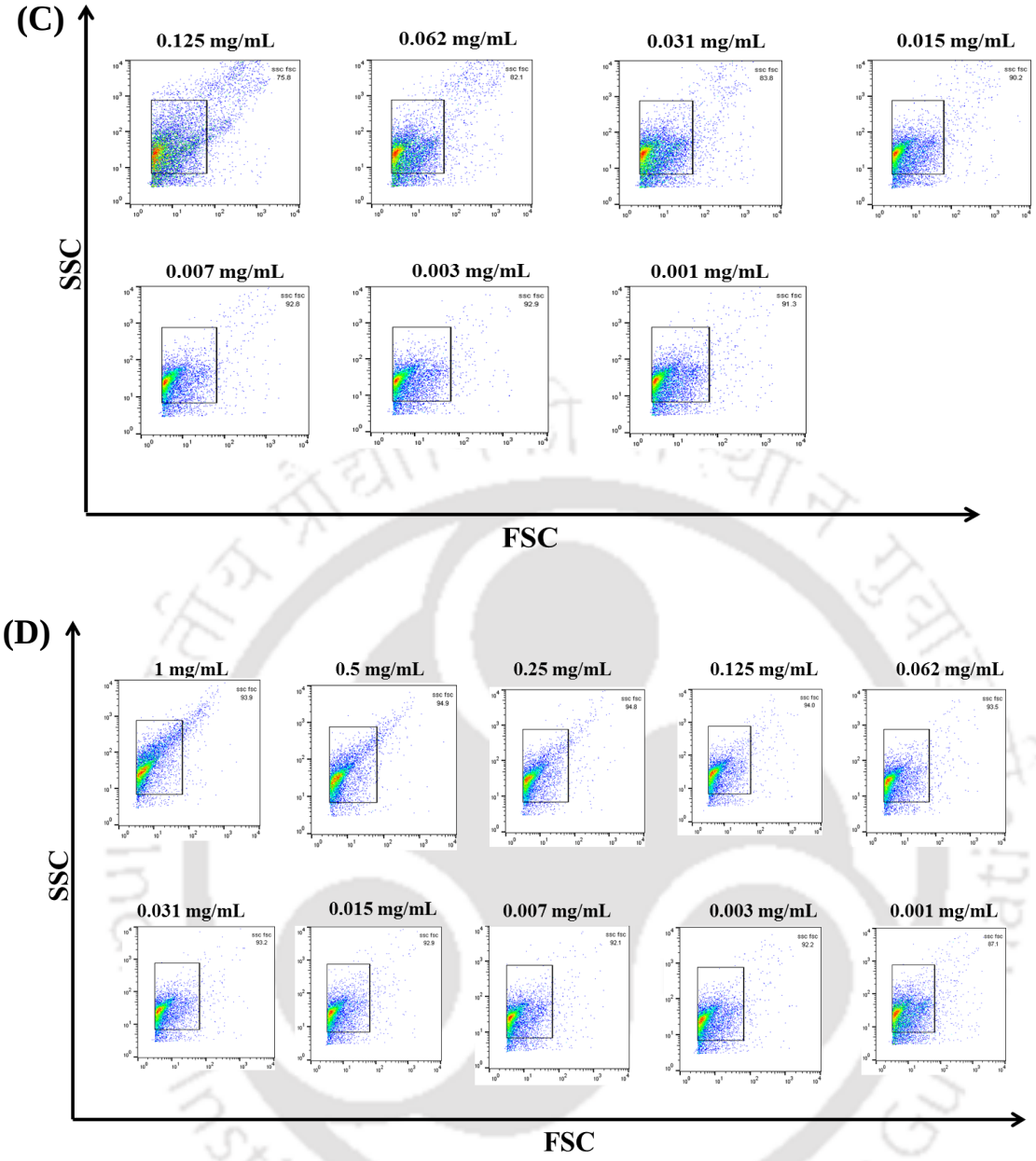

Figure 6.17 SSC FSC profiles of ETEC upon treatment with different concentration of (**A**) EE; (**B**) ME; (**C**) Karanjin and (**D**) Glabrin.

The attenuation of growth indicates the disorganization of the cell membrane when the concentration of antimicrobials was bacteriostatic although, the cells can grow, albeit at a lower rate. One explanation for this effect is that at high cell density, more substantial amount of the antimicrobials are required for bactericidal activity for pronounced lethality caused by the antimicrobial agents (Broxton et al., 1983). On the

other hand, conventional methods like optical density, dry cell weight, microscopy, and manual cell count indicate reproductive growth but do not provide information on cell physiological status. In the presence of a stressed population of cells that maintain cell metabolic activity, as determined by the fluorescent dye point towards the advantage of flow cytometry over the above mentioned conventional methods (Falcioni et al., 2008; Khan et al., 2010). Therefore, the potential application of multiparametric flow cytometry as a rapid, sensitive and easy-to-operate technique for detection of the VBNC state will help in understanding the discrepancies between culturability and viability of pathogen in medically relevant areas.

6.4. Conclusion

In this chapter, crude extract and purified compounds were evaluated for their antibacterial activity against pathogenic bacteria using *in vitro* and *in silico* approaches. The application of *in silico* technology offers significant potential for reducing the number of experimental studies required for compound selection during drug designing. PI incorporation and associated loss of esterase activity and other cellular functions seem to suggest that the primary mechanism of action of Karanjin and Glabrin is membrane damage, which leads to cell death as confirmed by flow cytometry, cell leakage assay, and FESEM micrographs. The results demonstrate the potential of combining flow cytometry and FESEM as a rapid and accurate technique for the detection and understanding the physiology of bacteria. It further encourages the use of purified compounds in antibacterial formulations as the compound effectively kills pathogenic bacteria related to foodborne diseases and nosocomial infections. Also, experimental study and evaluation of structure-activity relationship could help in the development of potential inhibitors against pathogenic bacteria that may serve as leads in the development of new pharmaceutical drugs.

Chapter 7

Concluding remark

7.1. Significance and salient features of the study

Medicinal plant extract or fractions are used as therapeutic to combat various diseases due to its efficacy, lesser side effects, and wide acceptability. *Pongamia pinnata*, a member of Leguminaceae family, is well-known for its high medicinal value and multipurpose pharmaceutical applications.

In the present study, two compounds were isolated and purified from seeds of *P. pinnata*. Structure of the isolated compounds was elucidated and characterized by various analytical and spectroscopic techniques. The compounds were identified as furanoflavonoid Karanjin (IUPAC: 3-methoxy-2-phenylfuro[2,3-h]chromen-4-one) and a cyclic amino acid Glabrin (IUPAC: 4,5-dihydroxy-1-methylpiperidine-2-carboxylic acid). The vibrational frequencies of the compound were also calculated using DFT for better understanding of the structure. Based on the structure of Karanjin, it is proposed that the conjugated ring system is responsible for its electronic transition as demonstrated by UV-Visible and fluorescence spectroscopic studies. The molecular structure of Karanjin was found to be very sensitive to a slight change in its immediate microenvironment, thereby, altering the photophysical property and photobiological behavior.

The potency of crude extracts and isolated compounds were investigated for their antibacterial property against pathogenic indicator by various *in silico* and *in vitro* approaches. The study reveals the mechanism of antibacterial action of Karanjin and Glabrin against both Gram-positive and Gram-negative bacteria. Moreover, the important physicochemical parameters of the compound were determined by *in silico* drug-likeness property prediction and Lipinski's rule of five based on the structure of the

compound. Molecular docking study has been undertaken to screen the possible target of action of purified compounds among common target sites of bacteria. *In vitro* study of antibacterial activity has been studied using microbroth dilution assay, cell leakage assay, Raman spectroscopy, flow cytometry, and electron microscopy. The viability of bacteria was also assessed by flow cytometry highlighting the application of PI and cFDA to study the different physiological status of bacteria.

Taking into all consideration, this is the first report describing the structure and photophysical property of the compound. The study also highlights the promising antibacterial potential of the isolated compounds which can certainly help in the development of the new drug in the area of herbal medicine research.

The salient features of the study are;

- Three organic crude extracts (HE, EE and ME) were obtained by hot solvent extraction method using Soxhlet apparatus. Crude extracts clearly showed thermal stability towards high temperature which is an important and determining parameter during its extraction, processing, and storage. Two compounds were isolated from EE and ME; named as PPS-E and PPS-M, respectively. Each compound was further purified to achieve analytically pure crystals.

- The structure of isolated compounds (PPS-E and PPS-M) were characterized and identified as Karanjin and Glabrin.

- Spectroscopic methods were used in the investigation of photophysical properties of Karanjin as a function of solvatochromic parameters. Attention is focused on the intrinsically fluorescent flavonoid as their own ‘signature’ for characterizing their interaction with the solvent. The physical parameters of Karanjin, such as molar extinction coefficient (ϵ), oscillator strength (*f*), transition dipole moment also changed with the fluctuation in polarity of the microenvironment. It was observed

that the dimerization of fluorophores and formation of higher order aggregates in solution induce changes of the fluorescence emission efficiency. Karanjin crystal formation in water-MeOH was demonstrated by UV-Vis absorbance, fluorescence, and microscopic study. The solvation dynamics in heterogeneous microenvironment like micelles was also studied, and the strong influence was observed on the photophysical property of Karanjin. Karanjin fluorescence decay in all the solvents is bi-exponential with decay time ranging from 1.3 to 3.4 ns. The mean lifetimes (τ) are highest in SDS and least in water.

- Crude extracts and purified compounds were evaluated for their antibacterial activity against pathogenic bacteria using *in vitro* and *in silico* approaches. PI incorporation and associated loss of esterase activity and other cellular functions seem to suggest that the primary mechanism of action of Karanjin and Glabrin is membrane damage, which leads to cell death; confirmed by flow cytometry, cell leakage assay, and FESEM micrographs. The results demonstrate the potential of combining flow cytometry, Raman scattering, and FESEM as a rapid and accurate technique for the detection and understanding the physiology of bacteria. It further affirms the use of the purified compound in the antibacterial formulation as the compound effectively kills pathogenic bacteria related to foodborne disease and nosocomial infection. Also, experimental study and evaluation of structure-activity relationship can aid in the development of potential inhibitor against pathogenic bacteria that may serve as leads in the development of new pharmaceutical drug.

7.2. Future scope

The current research activity has enabled the identification and characterization of two compounds from seeds of *P. pinnata*. The study shows the structural and photophysical property of a compound in the different microenvironment. The high analytical sensitivity and specificity of spectroscopic techniques provide an advantage over other physical methods and offers a powerful approach for real-time monitoring and understanding the compound in the different local environment at physiologically relevant concentrations (micromole range), from both qualitative and quantitative perspectives. Spectroscopic techniques could help in designing and executing various spectroscopic assay involving its binding to various macromolecules signifying its potential as a 'fluorescent reporter' molecule.

Bioactive compounds were evaluated for antibacterial action by various *in vitro* approaches that revealed cell wall disruption as supported by flow cytometry and FESEM imaging. Docking study revealed strong binding to β-ketoacyl-acyl carrier protein synthase III (KAS III or FabH) which is a crucial catalyst in bacterial fatty acid biosynthesis. It represents an attractive target for a novel antibiotic which is related to the elongation of unsaturated fatty acids in the bacterial system. KAS III could provide the primary lead for elucidating the mechanism of their action. Based on their activity and biological targets, various compound derivatives could be synthesized to improve their specificity and selectivity. It could help in the development of a potential inhibitor with chemically interesting and biologically more effective drug candidate against pathogenic bacteria. However, further exploration will be needed for better knowledge and understanding the aspect of bioactivity of the compounds in combating infectious disease.

References

Abraham JP, Joe IH, George V, Nielsen OF, Jayakumar VS (2003). Vibrational spectroscopic studies on the natural product, columbianadin. Spectrochim Acta A Mol Biomol Spectrosc; 59(1):193-199.

Aguiar J, Carpena P, Molina-Bolivar JA, Ruiz CC (2003). On the determination of the critical micelle concentration by the pyrene 1:3 ratio method. J Colloid Interface Sci; 258:116-122.

Ahmed SA, Obi-Egbedi N, Bamgbose JT, Adeogun AI (2016). Solvent enhancement of electronic intensity in acridine and 9-aminoacridine. J Saudi Chem Soc; 20:S286-S292.

Ahmed Y, Sohrab MH, Al-Reza SM, Tareq FS, Hasan CM, Sattar MA (2010). Antimicrobial and cytotoxic constituents from leaves of *Sapium baccatum*. Food Chem; 48:549-552.

Akansha, Sirvastava AK, Maurya R (2010). Antihyperglycemic activity of compounds isolated from Indian medicinal plants. Indian J Exp Biol; 48:294-298.

Al Muqarrabun LMR, Ahmat N, Ruzaina SAS, Ismail NH, Sahidin I (2013). Medicinal uses, phytochemistry and pharmacology of *Pongamia pinnata* (L.) Pierre: A review. J Ethnopharmacol; 150:395-420.

Alam S, Sarkar Z, Islam A (2004). Synthesis and studies of antibacterial activity of pongaglabol. J Chem Sci; 116:29-32.

Alston RW, Urbanikova L, Sevcik J, Lasagna M, Reinhart GD, Scholtz JM, Pace CN (2004). Contribution of single tryptophan residues to the fluorescence and stability of Ribonuclease Sa. Biophys J; 87(6):4036-4047.

Alves CN, Pinheiro JC, Camargo, AJ, Ferreira MMC, Silva ABF (2000). A structure activity relationship study of HEPT-analogue compounds with anti-HIV activity. J Mol Struc-Theochem; 530:39-47.

Androutsopoulos V, Wilsher N, Arroo RR, Potter GA (2009). Bioactivation of the phytoestrogen diosmetin by CYP1 cytochromes P450. Cancer Lett; 274:54-60.

Androutsopoulos VP, Spandidos DA (2013). The flavonoids diosmetin and luteolin exert synergistic cytostatic effects in human hepatoma HepG2 cells via CYP1A-catalyzed metabolism, activation of JNK and ERK and P53/P21 up-regulation. J Nutr Biochem; 24(2):496-504.

Aneja R, Khanna RN, Seshadri TR (1963). 6-Methoxyfuroflavone, a new component of the seeds of *Pongamia glabra*. J Chem Soc; 163-168.

Anouar EH, Osman CP, Weber JFF, Ismail NH (2014). UV/Visible spectra of a series of natural and synthesised anthraquinones: experimental and quantum chemical approaches. Springerplus; 3:233.

Antolinos V, Esteban M-D, Ros-Chumillas M, Huertas J-P, Periago PM, Palop A, et al. (2014). Assessment of the of acid shock effect on viability of *Bacillus cereus* and *Bacillus weihenstephanensis* using flow cytometry. Food Res Int; 66:306-312.

Anuradha R, Krishnamoorthy P (2011). Antioxidant activity of methanolic extract of *Pongamia pinnata* on lead acetate induced hepatic damage in rats. Afr J Biochem Res; 5:348-351.

Arote SR, Dahikar SB, Yeole PG (2009). Phytochemical screening and antibacterial properties of leaves of *Pongamia pinnata* Linn. (Fabaceae) from India. Afr J Biotechnol; 8:6393-6396.

Arote SR, Dahikar SB, Yeole PG (2009). Phytochemical screening and antibacterial properties of leaves of *Pongamia pinnata* Linn. (Fabaceae) from India. Afr J Biotechnol; 8:6393-6396.

Arshad N, Rashid N, Absar S, Abbasi MSA, Saleem S, Mirza B (2013). UV-absorption studies of interaction of karanjin and karanjachromene with ds. DNA: Evaluation of binding and antioxidant activity. Cent Eur J Chem; 11(12):2040-2047.

Ayati A, Falahati M, Irannejad H, Emami S (2012). Synthesis, *in vitro* antifungal evaluation and *in silico* study of 3-azolyl-4-chromanone phenyl hydrazones. DARU J Pharm Sci; 20:46.

Bachwani M, Kumar R (2011). Molecular docking: A review. Int J Res Ayurveda Pharm; 2(6):1746-1751.

Badole SL, Bodhankar SL (2009a). Investigation of antihyperglycaemic activity of aqueous and petroleum ether extract of stem bark of *Pongamia pinnata* on serum glucose level in diabetic mice. J Ethnopharmacol; 123:115-120.

Badole SL, Bodhankar SL (2009b). Concomitant administration of petroleum ether extract of the stem bark of *Pongamia pinnata* (L.) Pierre with synthetic oral hypoglycaemic drugs in alloxan-induced diabetic mice. Eur J Integr Med; 1:73-79.

Badole SL, Bodhankar SL, Raut CG (2011). *In vitro* antioxidant and antimicrobial activity of cycloart-23-ene-3β, 25-diol (B2) isolated from *Pongamia pinnata* L. Pierre. Asian Pac J Trop Biomed; 4:910-916.

Badole SL, Mahamuni SP, Bagul PP, Khose RD, Joshi AC, Ghule AE, Bodhankar SL, Raut CG, Khedkar VM, Coutinho EC, Wagh NK (2013). Cycloart-23-ene-3b,25-diol stimulates GLP-1(7–36) amide secretion in streptozotocin-nicotinamide induced diabetic Sprague Dawley rats: A mechanistic approach. Eur J Pharmacol; 698:470-479.

Badole SL, Zanwar AA, Ghule AE, Ghosh P, Bodhankar SL (2012). Analgesic and anti-inflammatory activity of alcoholic extract of stem bark of *Pongamia pinnata* (L.) Pierre. Biomed Aging Pathol; 2:19-23.

Bagga S, Straney D (2000). Modulation of cAMP and phosphodiesterase activity by flavonoids which induce spore germination of *Nectria haematococca* MP VI (*Fusarium solani*). Physiol Mol Plant Path; 56(2):51-61.

Bahri MA, Hoebeke M, Grammenos A, Delanaye L,Vandewalle N, Seret A (2006). Investigation of SDS, DTAB and CTAB micelle microviscosities by electron spin resonance. Colloids Surf A; 290:206-212.

Bajpai VK, Rahman A, Shukla S, Mehta A, Shukla S, Arafat SMY, Rahman MM, Ferdousi Z (2009). Antibacterial activity of leaf extracts of *Pongamia pinnata* from India. Pharm Biol; 47:1162-1167.

Bajpai VK, Sharma A, Baek KH (2014). Activity of essential oil against foodborne pathogens. Food Technol Biotechnol; 52(1):109-118.

Baki MA, Sadik G, Mondal KAMSH, Mosaddik MA, Rahman MM (2007). Methylkarranjic acid and pongamol from *Derris indica* seeds and their antibacterial activity. Dhaka University J Pharm Sci; 6:9-13.

Baki MA, Sadik G, Mondal KAMSH, Mosaddik MA, Rahman MM (2007). Methylkarranjic acid and pongamol from *Derris indica* seeds and their antibacterial activity. Dhaka University J Pharm Sci; 6:9-13.

Bala M, Nag TN, Kumar S, Vyas M, Kumar A, Bhogal NS (2011). Proximate composition and fatty acid profile of *Pongamia pinnata*, a potential biodiesel crop. J Am Oil Chem Soc; 88:559-562.

Balabhadrapathruni S, Thomas TJ, Yurkow EJ, Amenta PS, Thomas T (2000). Effects of genistein and structurally related phytoestrogens on cell cycle kinetics and apoptosis in MDAMB-468 human breast cancer cells. Oncol Rep; 7:3-12.

Banerjee D, Bagchi S, Mondal S, Ghosh S (1995). Fluorometric study of solvation characteristics of ketocyanine dyes in mixed binary solvents. J Photochem Photobiol; 90:171-176.

Bayat Z, Nassab SQ (2010). Computational approaches to the prediction of the 1-octanol/water partition coefficient of benzimidazole derivatives drugs. J Chem Pharm Res; 2(6):306-315.

Bednarek P (2012). Sulfur-containing secondary metabolites from *Arabidopsis thaliana* and other Brassicaceae with function in plant immunity. Chembiochem; 13(13):1846-59.

Bedoya LM, Bermejo P, Abad MJ (2009). Anti-infectious activity in the Cistaceae family in the Iberial Peninsula. Mini Rev Med Chem; 9(5):519-525.

Bell EA (1962). The isolation of L-homoarginine from seeds of *Lathyrus cicera*. Biochem J; 85:91-93.

Bell EA, Fellows LE (1966). Occurrence of 5-hydroxytryptophan as a free plant amino acid. Nature; 210: 529.

Bell EA, Fellows LE, Qureshi MY (1976). 5-Hydroxytryptophan: taxonomic character and chemical defence in *Griffonia*. Phytochemistry; 15:823.

Bell EA, Fellows LE, Qureshi MY (1976). 5-Hydroxytryptophan: taxonomic character and chemical defence in *Griffonia*. Phytochemistry; 15:823.

Benito I, Garcia MA, Monge C, Saz JM, Marina ML (1997). Spectrophotometric and conductimetric determination of the critical micellar concentration of sodium dodecyl sulfate and cetyltrimethylammonium bromide micellar systems modified by alcohols and salts. Colloids Surf A: Physicochem Eng Aspects; 125:221-224.

Berezin MY, Achilefu S (2010). Fluorescence lifetime measurements and biological imaging. Chem Rev; 110(5):2641-2684.

Bergan RC, Waggle DH, Carter SK, Horak I, Slichenmyer W, Meyer M (2001). Tyrosine kinase inhibitors and signal transduction modulators: rationale and current status as chemopreventive agents for prostate cancer. Urol; 57:77-80.

Berlim LS, Bezerra AG, Pazin WM, Ramin TS, Schreiner WH, Ito AS (2018). Photophysical properties of flavonoids extracted from *Syngonanthus nitens*, the golden grass. J Lumin; 194:394-400.

Bernard FX, Sable S, Cameron B (1997). Glycosylated flavones as selective inhibitors of topoisomerase IV. Antimicrob Agents Chemother; 41:992-998.

Bernhoft A (2010). Bioactive compounds in plants-Benefits and risks for man and animals. The Norwegian Academy of Science and Letters, Oslo.

Beutler JA (2009). Natural products as a foundation for drug discovery. Curr Protoc Pharmacol; 46: 9.11.1-9.11.21.

Bevington PR (1969). Data reduction and error analysis for the physical sciences. McGraw-Hill Inc., New York.

Beyaz A, Oh WS, Reddy VP (2004). Ionic liquids as modulators of the critical micelle concentration of sodium dodecyl sulphate. Colloids Surf B Biointerfaces; 35(2):119-124.

Beynon JH (1959). Advances in high resolution mass spectrometry, Vol. 1, Pergamon Press, London.

Bezic N, Skocibusic M, Dinkic V, Radonic A (2003). Composition and antimicrobial activity of *Achillea clavennae* L. essential oil. Phytother Res; 17:1037-1040.

Bhatia G, Puri A, Maurya R, Yadav PP, Khan MM, Khanna AK, Saxena JK (2008). Anti-dyslipidemic and antioxidant activities of different fractions of *Pongamia pinnata* (lin.) fruits. Med Chem Res; 17:618-620.

Bhattacharya A, Sood P, Citovsky V (2010). The roles of plant phenolics in defence and communication during *Agrobacterium* and *Rhizobium* infection. Mol Plant Pathol; 11(5):705-719.

Bhattacharyya K, Bagchi B (2000). Slow dynamics of constrained water in complex geometries. J Phys Chem A; 104:10603-10613.

Bi S, Qiao C, Song D, Tian Y, Gao D, Sun Y, Zhang H (2006). Study of interactions of flavonoids with DNA using acridine orange as a fluorescence probe. Sens Actuators B; 119:199-208.

Bitis L, Kultur S, Melikoglu G, Ozsoy N, Can A (2010). Flavonoids and antioxidant activity of *Rosa agrestis* leaves. Nat Prod Res; 24(6):580-589.

Bitis L, Sen A, Ozsoy N, Birteksoz-Tan S, Kultur S, Melikoglu G (2017). Flavonoids and biological activities of various extracts from *Rosa sempervirens* leaves. J Biotechnol Biotechnol Equip; 31(2):299-303.

Blom MN, Compagnon I, Polfer NC, von Helden G, Meijer G, Suhai S, Paizs B, Oomens J (2007). Stepwise solvation of an amino acid: The appearance of zwitterionic structures. J Phys Chem A; 111:7309-7316.

Borchardt JK (1996). A short history of quinine. Drug News Persp; 9:116-120.

Breton RC, Reynolds WF (2013). Using NMR to identify and characterize natural products. Nat Prod Rep; 30:501-524.

Brijesh S, Daswani PG, Tetali P, Rojatkar SR, Antia NH, Birdi TJ (2006). Studies on *Pongamia pinnata* (L.) Pierre leaves: understanding the mechanism(s) of action in infectious diarrhea. J Zhejiang University Science B; 7:665-674.

Broxton P, Woodcock PM, Gilbert P (1983). A study of the antibacterial activity of some polyhexamethylene biguanides towards *Escherichia coli* ATCC 8739. J Appl Bacteriol; 54:345-353.

Buchweitz M, Kroon PA, Rich GT, Wilde PJ (2016). Quercetin solubilisation in bile salts: A comparison with sodium dodecyl sulphate. Food Chem; 211:356-364.

Bunthof CJ, van Schalkwijk S, Meijer W, Abee T, Hugenholtz J (2001). Fluorescent method for monitoring cheese starter permeabilization and lysis. Appl Environ Microbiol; 67:4264-4271.

Butler MS (2008). Natural products to drug: natural product derived compounds in clinical trials. Nat Prod Rep; 25(3):475-516.

Calica PN (2017). Nodulation and nitrogen fixation of *Pongamia pinnata*. J Trop Crop Sci; 4(1):1-12.

Campbell JW, Cronan Jr JE (2001). Bacterial fatty acid biosynthesis: Targets for antibacterial drug discovery. Annu Rev Microbiol; 55:305-332.

Camporese A, Balick MJ, Arvigo R, Esposito RG, Morsellino N, De Simone F, Tubaro A (2003). Screening of anti-bacterial activity of medicinal plants from Belize (Central America). J Ethnopharmacol; 87:103-107.

Camuria IJ, Costa AB, Ito AS, Pazin WM (2018). Optical absorption and fluorescence spectroscopy studies of Artepillin C, the major component of green propolis. Spectrochim Acta A Mol Biomol Spectrosc; 198:71-77.

Canamares MV, Lombardi JR, Leona M (2009). Raman and surface enhanced Raman spectra of 7-hydroxylfavone and 3', 4'-dihydroxyflavone. e-PS; 6:81-88.

Cannell R J P (1998). Natural products isolation. New Jersey: Human Press Inc; pp. 165-208.

Carcache-Blanco EJ, Kang YH, Park EJ, Su BN, Kardono LBS, Riswan S, Fong HHS, Pezzuto JM, Kinghorn AD (2003). Constituents of the stem bark of *Pongamia pinnata* with the potential to induce quinone reductase. J Nat Prod; 66:1197-1202.

Carcache-Blanco EJ, Kang YH, Park EJ, Su BN, Kardono LBS, Riswan S, Fong HHS, Pezzuto JM, Kinghorn AD (2003). Constituents of the stem bark of *Pongamia pinnata* with the potential to induce quinone reductase. J Nat Prod; 66:1197-1202.

Chandel HS, Singhai A, Nayak S (2005). Preparation and estimation of metal complexes of glabrin from *Pongamia glabra* Linn. seeds. Anc Sci Life; 25(1):42-46.

Chandrashekar KS, Prasanna KS (2010). Antimicrobial activity of *Pongamia pinnata* leaves. Int J Med Res; 1:18-20.

Chen JC, Huang LJ, Wu SL, Kuo SC, Ho TY, Hsiang CY (2007). Ginger and its bioactive component inhibit enterotoxigenic *Escherichia coli* heat-labile enterotoxin-induced diarrhea in Mice. J Agric Food Chem 55: 8390-8397.

Cheon BS, Kim YH, Son KS, Chang HW, Kang SS, Kim HP (2000). Effects of prenylated flavonoids and biflavonoids on lipopolysaccharide-induced nitric oxide production from the mouse macrophage cell line RAW 264. Planta Med; 66:596-600.

Chi YS, Jong HG, Son KH, Chang HW, Kang SS, Kim HP (2001). Effects of naturally occurring prenylated flavonoids on enzymes metabolizing arachidonic acid: cyclooxygenases and lipoxygenases. Biochem Pharmacol; 62:1185-1191.

Cho H, Yun CW, Park WK, Kong JY, Kim KS, Park Y, Lee S, Kim BK (2004). Modulation of the activity of pro-inflammatory enzymes, COX-2 and iNOS, by chrysin derivatives. Pharmacol Res; 49:37-43.

Chowdhry BZ, Dines TJ, Jabeen S, Withnall R (2008). Vibrational spectra of α-amino acids in the zwitterionic state in aqueous solution and the solid state: DFT calculations and the influence of hydrogen bonding. J Phys Chem A; 112:10333-10347.

Christoff M, Toscano VG, Baader WJ (1996). Influence of methoxy substitution on flavonoid photophysics: a steady state and laser flash photolysis study. J Photochem Photobiol A Chem; 101:11-20.

Cifuentes A, Bernal JL, Diez-Masa JC (1997). Determination of critical micelle concentration values using capillary electrophoresis instrumentation. Anal Chem; 69(20):4271-4274.

Cirin DM, Posa MM, Krstonosic VS, Milanovic ML (2012). Conductometric study of sodium dodecyl sulphate-nonionic surfactant (Triton X-100, Tween 20, Tween 60, Tween 80 or Tween 85) mixed micelles in aqueous solution. Hem ind; 66(1):21-28.

Clardy J, Walsh C (2004). Lessons from natural molecules. Nature; 432:829-837.

Corredor C, Teslova T, Canamares MV, Chen Z, Zhang J, Lombardi JR, Leona M (2009). Raman and surface-enhanced Raman spectra of chrysin, apigenin and luteolin. Vib Spectrosc; 49:190-195.

Cowan MM (1999). Plant products as antimicrobial agents. Clin Microbiol Rev; 12:564-586.

Cox SD, Mann CM, Markhan JL, Gustafson JE, Warmington JR, Wyllie SG (2001). Determining the antimicrobial action of tea tree oil. Molecules; 6:87-91.

Cragg GM, Grothaus PG, Newman DJ (2009). Impact of natural products on developing new anti-cancer agents. Chem Rev; 109(7):3012-43.

Cragg GM, Newman DJ (2005). Biodiversity: A continuing source of novel drug leads. Pure Appl Chem; 77:7-24.

Cragg GM, Newman DJ (2013). Natural products: a continuing source of novel drug leads. Biochim Biophys Acta; 1830:3670-3695.

Critchfield JW, Butera ST, Folks TM (1996). Inhibition of HIV activation in latently infected cells by flavonoid compounds. AIDS Res Hum Retrovir; 12:39-46.

Crozier A, Jaganath IB, Clifford MN (2006). Plant secondary metabolites: occurrence, structure and role in the human diet. Crozier A, Clifford MN, Ashihara H (Eds.), Blackwell Publishing Ltd. ISBN-13:978-1-4051- 2509-3.

Cushnie TP, Lamb AJ (2005). Antimicrobial activity of flavonoids. Int J Antimicrob Ag; 26(5):343-356.

Damodaran M, Ramaswamy R. (1937). Isolation of l-3:4-dihydroxyphenylalanine from the seeds of *Mucuna pruriens*. Biochem J; 31(12):2149-52.

Das A, Kesari V, Nath A, Khare A, Rangan L (2013). Antimicrobial and micro Raman spectroscopy of selected Zingiberaceae species from Northeast India. J Crop Sci Biotechnol; 16(1):75-81.

Dash N, Mishra A, Krishnamoorthy G (2013). Alkyl chain dependent interactions of ligands with bovine serum albumin. J Pharm Biomed Anal; 77:55-62.

Demissie H, Duraisamy R (2016). Effects of electrolytes on the surface and micellar characteristics of sodium dodecyl sulphate surfactant solution. J Sci Innov Res; 5(6):208-214.

Denyer SP (1990). Mechanisms of action of biocides. Int Biodeter; 26:89-100.

Deshmukhe P, Hooli AA, Holihosur SN (2009). Screening of cold ethyl alcohol extract of *Pongamia pinnata* for insecticidal properties against *Spodoptera litura* Fabricius. J Oil Seeds Res; 26:181-182.

Dezhampanah H, Firouzi R (2012). Thermodynamic investigation of the interaction between anionic dye and cationic surfactant in aqueous solution. Int J Res Phys Chem; 2:45-48.

Dolomanov OV, Bourhis LJ, Gildea RJ, Howard JAK, Puschmann H (2009). OLEX2: a complete structure solution, refinement and analysis program. J Appl Crystallogr; 42:339-341.

Dominguez A, Fernandez A, Gonzalez N, Iglesias E, Montenegro L (1997). Determination of critical micelle concentration of some surfactants by three techniques. J Chem Edu; 74:1227-1231.

Donovalova J, Cigan M, Stankovicova H, Gaspar J, Danko M, Gaplovsky A, Hrdlovic P (2012). Spectral properties of substituted coumarins in solution and polymer matrices. Molecules; 17:3259-3276.

Dsouza D, Braz LN (2018). Antibacterial activity of 3,3′,4′-trihydroxyflavone from *Justicia wynaadensis* against diabetic wound and urinary tract infection. J Microbiol; 49(1):152-161.

Duke SO (2007). The emergence of grass root chemical ecology. Proc Nat Acad Sci; 104(43):16729-16730

Dundas J, Ouyang Z, Tseng J, Binkowski A, Turpaz Y, Liang J (2006). CASTp: computed atlas of surface topography of proteins with structural and topographical mapping of functionally annotated residues. Nuc Acid Res; 34:116-118.

Dunford CL, Smith GJ, Swinny EE, Markham KR (2003). The fluorescence and photostabilities of naturally occurring isoflavones. Photochem Photobiol Sci; 2:611-615.

Dutta RK, Sharma PK, Pandey AC (2011). Assessing the conformational and cellular changes of ZnO nanoparticles impregnated *Escherichia coli* cells through molecular fingerprinting. Adv Mat Lett; 2(4):268-275.

Dzotam JK, Simo IK, Bitchagno G, Celik I, Sandjo LP, Tane P, Kuete V (2018). *In vitro* antibacterial and antibiotic modifying activity of crude extract, fractions and 3′,4′,7-trihydroxyflavone from *Myristica fragrans* Houtt against MDR Gram-negative enteric bacteria. BMC Complement Altern Med; 18:15.

Egorov AV, Lyubartsev AP, Laaksonen A (2011). Molecular dynamics simulation study of glycerol water liquid mixtures. J Phys Chem B; 115:14572-14581.

Elanchezhiyan M, Rajarajan S, Rajendran P, Subramanian S, Thyagarajan SP (1993). Antiviral properties of the seed extract of an Indian medicinal plant, *Pongamia pinnata*, Linn., against herpes simplex viruses: *in vitro* studies on Vero cells. J Med Microbiol; 38:262-264.

Emerson MF, Holtzer A (1965). On the ionic strength dependence of micelle number. J Phys Chem; 69:3718-3721.

Erazo S, Rocco G, Zaldivar M, Delporte C, Backhouse N, Castro C (2008). Active metabolites from *Dunalia spinosa* resinous exudates. Z Naturforsch C; 63:492-496.

Ertl P, Roggo S, Schuffenhauer A (2008). Natural product-likeness score and its application for prioritization of compound libraries. J Chem Inf Model; 48:68-74.

Essa MM, Subramanian P (2006). Protective role of *Pongamia pinnata* leaf extract on tissue antioxidant status and lipidperoxidation in ammonium chloride-induced hyperammonemic rats. Toxicol Mech Meth; 16:477-483.

Essa MM, Subramanian P, Suthakar G, Manivasagam T, Dakshayani KB (2005). Protective influence of *Pongamia pinnata* (Karanja) on blood ammonia and urea levels in ammonium chloride-induced hyperammonemia: antihyperammonemic effect of the leaf extract. J Appl Biomed; 3:1-6.

Evale BG, Hanagodimath SM, Khan IA, Kulkarni MV (2009). Estimation of dipole moments of some biologically active coumarins by solvatochromic shift method based on solvent polarity parameter, E(T)(N). Spectrochim Acta A Mol Biomol Spectrosc; 73(4):694-700.

Exarchou V, Krucker M, Beek TA, Vervoort J, Gerothanassis IP, Alert K (2005). LC-NMR coupling technology: recent advancements and applications in natural products analysis. Magn Reson Chem; 43(9):681-687.

Fabricant DS, Farnsworth NR (2001). The value of plants used in traditional medicine for drug discovery. Environ Health Perspect; 109:69-75.

Fain VY, Zaitsev BE, Ryabov MA (2006). Tautomerism of anthraquinones: IV. 1-Hydroxy-9,10-anthraquinone and its substituted derivatives. Russ J Org Chem; 42:1484-1487.

Falcioni T, Papa S, Campana R, Manti A (2008). State transitions of *Vibrio parahaemolyticus* VBNC cells evaluated by flow cytometry. Cytometry B Clin Cytom; 74(5):272-281.

Fendler JH (1980). Microemulsions, micelles, and vesicles as media for membrane mimetic photochemistry. J Phys Chem; 84(12):1485-1491.

Ferreira LMB, Kobelnik M, Regasini LO, Dutra LA, Bolzani VS, Ribeiro CA (2017). Synthesis and evaluation of the thermal behavior of flavonoids. Thermal decomposition of flavanone and 6-hydroxyflavanone. J Therm Anal Calorim; 127:1605-1610.

Fischer G, Cao X, Cox N, Francis M (2005). The FT-IR spectra of glycine and glycylglycine zwitterions isolated in alkali halide matrices. Chem Phys; 313:39-49.

Foti M, Piattelli M, Baratta MT, Ruberto G (1996). Flavonoids, coumarins, and cinnamic acids as antioxidants in a micellar system. structure-activity relationship. J Agric Food Chem; 44:497-501.

Fowler Z, Baron GM, Panepinto JG, Koffas MA (2011). Melanization of flavonoids by fungal and bacterial laccase. Yeast; 28:181-188.

Friedhoff P, Schneider A, Mandelkow EM, Mandelkow E (1998). Rapid assembly of Alzheimer-like paired helical filaments from microtubule-associated protein tau monitored by fluorescence in solution. Biochemistry; 37(28):10223-10230.

Garidel P, Hildebrand A, Neubert R, Blume A (2000). Thermodynamic characterization of bile salt aggregation as a function of temperature and ionic strength using isothermal titration calorimetry. Langmuir; 16:5267-5275.

Gates M, Tschudi G (1956). The synthesis of morphine. J Am Chem Soc; 78:1380-1393.

Gaussian 03, Revision C.02, Frisch MJ et al. (2004).

George S, Bhalerao SV, Lidstone EA, Ahmad IS, Abbasi A, Cunningham BT, Watkin KL (2010). Cytotoxicity screening of Bangladeshi medicinal plant extracts on pancreatic cancer cells. BMC Complement Altern Med; 10:52-62.

Ghosh S, Indukuri K, Bondalapati S, Saikia, AK, Rangan L (2013). Unveiling the mode of action of antibacterial labdane diterpenes from *Alpinia nigra* (Gaertn.) B. L. Burtt seeds. Eur J Med Chem; 66:101-105.

Ghufran A, Prem P, Maurya R (2004). Furanoflavonoid glycosides from *Pongamia pinnata* fruits. Phytochemistry; 65:921-924.

Gill PS, Sauerbrunn SR, Crowe BS (1992). High resolution thermogravimetry. J Therm Anal; 38:255-266.

Giri MA, Bhalke RD, Pal SC (2010). Gastro protective effect of hydroalcoholic leaves extract of *Pongamia pinnata*. Int J Pharm BioSci; 1:1-6.

GmbH P (2018). Time-resolved Fluorescence|*PicoQuant*. [online] Picoquant.com. Available at:https://www.picoquant.com/applications/category/life-science/time-resolved-fluorescence#tab-5 [Accessed 5 Jun. 2018].

Gouveia de Souza A, Oliveira Santos JC, Conceicao MM, Dantas Silva MC, Prasad S (2004). A thermoanalytic and kinetic study of sunflower oil. Braz J Chem Eng; 21(2):265-273.

Graham PH, Vance CP (2003). Legumes: importance and constraints to greater use. Plant Physiol; 131: 872-877.

Grinvald A, Steinberg IZ (1974). On the analysis of fluorescence decay kinetics by the method of least-squares. Anal Biochem; 59:583-598.

Guharay J, Dennison SM, Sengupta PK (1999). Influence of different environments on the excited-state proton transfer and dual fluorescence of fisetin. Spectrochim Acta A Mol Biomol Spectrosc; 55(5):1091-1099.

Guharay J, Sengupta PK (1997). Excited-state proton-transfer and dual fluorescence of robinetin in different environments. Spectrochim Acta A Mol Biomol Spectrosc; 53:905-912.

Gulland JM, Robinson R (1923). The morphine group. Part I. A discussion of the constitutional problem. J Chem Soc; 123:980-998.

Gupta, MP, Solis PN, Calderon AJ, Guinneau-Sinclair F, Correa M, Gladames C, Guerra C, Espinosa A, Alvenda GL, Robles G, Olampo R (2005). Medical ethnobotany of the tribes of Bocas del Toro, Panama. J Ethnopharmacol; 96: 389-401.

Gustavsson T, Sarkar N, Banyasz A, Markovitsi D (2007). Solvent effects on the steady-state absorption and fluorescence spectra of uracil, thymine and 5-fluorouracil. Photochem Photobiol; 83(3):595-599.

Halkier BA, Gershenzon J (2006). Biology and biochemistry of glucosinolates. Annu Rev Plant Biol; 57:303-333.

Hammond JH, Powley CR, Cook KD, Nieman TA (1980). Determination of critical micelle concentrations by bipolar pulse conductance. J Colloid Interface Sci; 76(2):434-438.

Handa AK, Nandini D, Uma (2005). An alternative source of biofuel, seed germination trials of *Pongamia pinnata*. Int J Forest Usufructs Manage; 6:75-80.

Hernandez I, Alegre L, Munne-Bosch S (2004). Drought-induced changes in flavonoids and other low molecular weight antioxidants in *Cistus clusii* grown under Mediterranean field conditions. Tree Physiol; 24:1303-1311.

Hesse M (2002). Alkaloids: nature's curse or blessing? Wiley VCH, New York.

Hewitt CJ, Nebe-von-Caron G (2001). An industrial application of multiparameter flow cytometry: assessment of cell physiology state and its application to the study of microbial fermentations. Cytometry; 44:179-187.

Hirose C, Sepulveda I (1981). Transfer Free Energies of p-alkyl-substituted benzene derivatives, benzene, and toluene from water to cationic and anionic micelles and to n-heptane. J Phys Chem; 85(24):3689-3694.

Hoefel D, Grooby WL, Monis PT, Andrews S, Saint CP (2003). A comparative study of carboxyfluorescein diacetate and carboxyfluorescein diacetate succinimidyl ester as indicators of bacterial activity. J Microbiol Methods; 52:379-388.

Hofener S, Kooijman PC, Groen J, Ariese F, Visscher L (2013). Fluorescence behavior of (selected) flavonols: a combined experimental and computational study. Phys Chem Chem Phys; 15:12572-12581.

Horn-Ross PL, Hoggatt KJ, Lee MM (2002). Phytoestrogens and thyroid cancer risk: the San Fransisco Bay area thyroid cancer study. Cancer Epidemiol Biomarkers Prev; 11:43-49.

Hunter MD, Hull LA (1993). Variation in concentrations of phloridzin and phloretin in apple foliage. Phytochemistry; 34:1251-1254.

Husain MM, Sindhu R, Tandon HC (2012). Photophysical properties and estimation of ground and excited state dipole moments of 7-diethylamino and 7-diethylamino-4-methyl coumarin dyes from absorption and emission spectra. Eur J Chem; 3(1):87-93.

Isely D (1982). Leguminosae and *Homo sapiens* I. Econ Bot; 36(1):46-70.

Iwashina T (2003). Flavonoid function and activity to plants and other organisms. Biol Sci Space; 17(1):24-44.

Jeong MR, Park PB, Kim DH, Jang YS, Jeong HS, Choi SH (2009). Essential oil prepared from *Cymbopogon citratus* exerted an antimicrobial activity against plant pathogenic and medical microorganisms. Mycobiology; 37(1):48-52.

Ji HF, Li XJ, Zhang HY (2009). Natural products and drug discovery. EMBO Rep; 10(3):194-200.

Johnston MD, Hanlon GW, Denyer SP, Lambert RJW (2003). Membrane damage to bacteria caused by single and combined biocides. J Appl Microbiol; 94(6):1015-1023.

Junquera E, Pefia L, Aicart E (1994). Influence of temperature on the micellization of sodium dodecylsulfate in water from speed of sound measurements. J Solution Chem; 23(3):421-430.

Kandaswami C, Lee LT, Lee PP, Hwang JJ, Ke FC, Huang YT, Lee MT (2005). The antitumor activities of flavonoids. In Vivo; 19(5):895-909.

Kanwal Q, Hussain I, Siddiqui HL, Javaid A (2015). Antifungal activity of flavonoids isolated from mango (*Mangifera indica* L.) leaves. Nat Prod Res; 24(20):1907-1914.

Kaplan F, Kopka J, Haskell DW, Wei ZK, Schiller C, Gatzke N, Sung DL, Guy CL (2004). Exploring the temperature-stress metabolome of *Arabidopsis*. Plant Physiol; 136:4159-4168.

Karthikeyan S (2013). Chemopreventive potential of chrysin in 7,12-dimethylbenz(a)anthracene-induced hamster buccal pouch carcinogenesis. Int J Nutr Pharmacol Neurol Dis; 3(1):46-53.

Karukstis KK, Litz JP, Garber MB, Angell LM, Korir GK (2010). A spectral approach to determine location and orientation of azo dyes within surfactant aggregates. Spectrochim Acta A Mol Biomol Spectrosc; 75(4):1354-1361.

Kasala ER, Bodduluru LN, Barua CC, Madhana RM, Dahiya V, Budhani MK, Mallugari RR, Maramreddy SR, Gogoi R (2016). Chemopreventive effect of chrysin, a dietary flavone against benzo(a)pyrene induced lung carcinogenesis in Swiss albino mice. Pharmacol Rep; 68(2):310-318.

Katekhaye SD, Kale MS, Laddha KS (2012). A simple and improved method for isolation of karanjin from *Pongamia pinnata* Linn. seed oil. Indian J Nat Prod Resour; 3(1):131-134.

Kazemipoor M, Radzi CW, Cordell GA, Yaze I (2012). Safety, efficacy and metabolism of traditional medicinal plants in the management of obesity: a review. Int J Chem Eng Appl; 3(4):288-92.

Keating G J, O'Kennedy R (1997). The chemistry and occurrence of coumarins. In: O'Kennedy R, Thornes R D, editors. Coumarins: biology, applications and mode of action. New York, John Wiley & Sons, Inc. p 348.

Kempinski C, Jiang Z, Bell S, Chappell J (2015). Metabolic engineering of higher plants and algae for isoprenoid production. Adv Biochem Eng Biotechnol; 148:161-199.

Kesari V, Das A, Rangan L (2010). Physico-chemical characterization and antimicrobial activity from seed oil of *Pongamia pinnata*, a potential biofuel crop. Biomass Bioenergy; 34:108-115.

Kesari V, Krishnamachari A, Rangan L (2008). Systematic characterisation and seed oil analysis in candidate plus trees of biodiesel plant, *Pongamia pinnata*. Ann Appl Biol; 152(3):397-404.

Kesari V, Rangan L (2010). Development of *Pongamia pinnata* as an alternative biofuel crop-current status and scope of plantations in India. J Crop Sci and Biotechnol; 13(3):127-137.

Khan MMT, Pyle BH, Camper AK (2010). Specific and rapid enumeration of viable but nonculturable and viable-culturable Gram-negative bacteria by using flow cytometry. Appl Environ Microbiol; 76(15):5088-5096.

Khan MR, Omoloso AD, Barewai Y (2006). Antimicrobial activity of the *Derris elliptica*, *Derris indica* and *Derris trifoliate* extractives. Fitoterapia; 77:330.

Khanna RN, Seshadri TR (1963). Pongaglabrone, a new component of the seeds of *Pongamia glabra*: its constitution and synthesis. Tetrahedron; 19:219-225.

Kharb R, Shama P, Yar MS (2011). Pharmacological significance of triazole scaffold. J Enzyme Inhib Med Chem; 26:1-21.

Khare CP (2004). Encyclopedia of Indian medicinal plants. Springer, New York; 378-379.

Klymchenko AS, Duportail G, Ozturk T, Pivovarenko VG, Mely Y, Demchenko AP (2002). Novel two-band ratiometric fluorescence probes with different location and orientation in phospholipid membranes. Chem Biol; 9:1199-1208.

Klymchenko, AS, Ozturk T, Pivovarenko VG, Demchenko AP (2001). A 3-hydroxychromone with dramatically improved fluorescence properties. Tetrahedron Lett; 42:7967-7970.

Kong LY, Wang P (2013). Determination of the absolute configuration of natural products. Chin J Nat Med; 11(3):0193-0198.

Kubo I, Muroi H, Kubo A (1994). Naturally occurring anti-acne agents. J Nat Prod; 57:9-17.

Kumar S, Jain SK, Rastogi RC (2001). An experimental and theoretical study of excited-state dipole moments of some flavones using an efficient solvatochromic method based on the solvent polarity parameter, E_T^N. Spectrochim Acta A; 57(2):291-298.

Kumar V, Chandrashekar K, Sidhu OP (2006). Efficacy of karanjin and different extracts of *Pongamia pinnata* against selected insect pests. J Entomol Res; 30:103-108.

Lahlou M (2013). The success of natural products in drug discovery. Pharmacol Pharm; 4:17-31.

Lakhsmi G, Srimannarayana G, Rao NVS (1974). Pongaflavone, a new chromenochromone and an analog of karanjin isolated from *Pongamia pinnata* (Linn.) Pierre (syn. *Pongamia glabra*). Indian J Chem; 12:8.

Lakowicz JR (1999). Principles of fluorescence spectroscopy. Second edition, Kluwer Academic/Plenum Publishers, New York.

Lakowicz JR (2006). Principles of Fluorescence Spectroscopy. Springer, New York.

Lambein F, Kuo YH, Ikegami F, Murakoshi I (1990) Toxic and non-toxic nonprotein amino acids in the Vicieae. In: Lubec G., Rosenthal G.A. (eds) Amino Acids. Springer, Dordrecht.

Lampert RA, Chewter LA, Phillips D (1983). Standards for nanosecond fluorescence decay time measurements. Anal Chem; 55:68-73.

Langfield RD, Scarano FJ, Heitzman ME, Kondo M, Hammond GB, Neto CC (2004). Use of a modified microplate bioassay method to investigate antibacterial activity in the Peruvian medicinal plant *Peperomia galioides*. J Ethnopharmacol; 94:279-281.

Lanjhiyana S, Garabadu D, Ahirwar D, Bigoniya P, Rana AC, Patra KC, Lanjhiyana SK, Karuppaih M (2011). Hypoglycemic activity studies on aerial leaves of *Pongamia pinnata* (L.) in alloxan-induced diabetic rats. Der Pharmacia Lettre; 3:55-70.

Lanot A, Morris P (2005). Elicitation of isoflavan phytoalexins. In Marquez AJ (ed.), *Lotus japonicus* handbook. Springer, The Netherlands; 355-361.

Lemos MA, Sarnikova K, Bot F, Anese M, Hungerford G (2015). Use of time-resolved fluorescence to monitor bioactive compounds in plant based foodstuffs. Biosensors; 5:367-397.

Leonard L, Chibane LB, Bouhedda BO, Degraeve P, Oulahal N (2016). Recent advances on multi-parameter flow cytometry to characterize antimicrobial treatments. Front Microbiol; 7:1225.

Li HB, Jiang Y, Chen F (2004). Separation methods used for *Scutellaria baicalensis* active components. J Chromatogr B; 812:277-290.

Li L, Li X, Shi C, Deng Z, Fu H, Proksch P, Lin W (2006). Pongamone A-E, five flavonoids from the stems of a mangrove plant *Pongamia pinnata*. Phytochemistry; 67:1347-1352.

Limaye DB (1925). Karanjin part I: a crystalline constituent of the oil from *Pongamia glabra*. In: Proceedings of the 12th Indian Academy and Science Congress, India.

Lin CE, Huang HC, Chen HW (2001). A capillary electrophoresis study on the influence of β-cyclodextrin on the critical micelle concentration of sodium dodecyl sulfate. J Chromatogr A; 917:297-310.

Lin CE, Lin WC, Chiou WC (1996). Migration behaviour and selectivity of dichlorophenols in micellar electrokinetic capillary chromatography influence of micelle concentration and buffer pH. J Chromatogr A; 722:333-343.

Lipinski CA, Lombardo F, Dominy BW, Feeney PJ (1997). Experimental and computational approaches to estimate solubility and permeability in drug discovery and development settings. Adv Drug Deliv Rev; 23:4-25.

Lirdprapamongkol K, Sakurai H, Abdelhamed S, Yokoyama S, Maruyama T, Athikomkulchai S, Viriyaroj A, Awale S, Yagita H, Ruchirawat S, Svasti J, Saiki I (2013). A flavonoid chrysin suppresses hypoxic survival and metastatic growth of mouse breast cancer cells. Oncol Rep; 30(5):2357-2364.

Liu B, Shi Y, Peng W, Zhang O, Liu J, Chen N, Zhu R (2016). Diosmetin induces apoptosis by upregulating p53 via the TGF-β signal pathway in HepG2 hepatoma cells. Mol Med Rep; 14(1):159-164.

Liu H, Liu K, Huang Z, Park CM, Thimmegowda NR, Jang JH, Ryoo IJ, He L, Kim SO, Oi N, Lee KW, Soung NK, Bode AM, Yang Y, Zhou X, Erikson RL, Ahn JS, Hwang J, Kim KE, Dong Z, Kim BY (2013). A chrysin derivative suppresses skin cancer growth by inhibiting cyclin-dependent kinases. J Biol Chem; 288(36):25924-25937.

Liu HB, Yu D, Shin SC, Park HR, Park JK, Bark KM (2009). Spectroscopic properties of quercetin derivatives, quercetin-3-O-rhamnoside and quercetin-3-O-rutinoside, in hydro-organic mixed solvents. Photochem Photobiol; 85(4):934-942.

Liu W, Guo R (2005). The interaction between morin and CTAB aggregates. J Colloid Interface Sci; 290:564-573.

Liu X, Xu Z, Cole JM (2013). Molecular design of UV-vis absorption and emission properties in organic fluorophores: toward larger bathochromic shifts, enhanced molar extinction coefficients, and greater stokes shifts. J Phys Chem C; 117:16584-16595.

Lo HM, Wu MW, Pan SL, Peng CY, Wu PH, Wu WB (2012). Chrysin restores PDGF-induced inhibition on protein tyrosine phosphatase and reduces PDGF signaling in cultured VSMCs. J Nutr Biochem; 23(6):667-678.

Lockemann G, Serturner FW (1951). The discoverer of morphine. J Chem Ed; 28:279.

Looser V, Hammes F, Keller M, Berney M, Kovar K, Egli T (2005). Flow cytometric detection of changes in the physiological state of *E. coli* expressing a heterologous membrane protein during carbon-limited fed batch cultivation. Biotechnol Bioeng; 92:69-78.

Madagundi SD, Pawadshetter MK, Sholar HP, Habbu P and Biradar SM (2012). A comparative study of isolated flavonoid and different extracts of *Caesalpinia pulcherrima* (L) SW. for *in-vitro* immunomodulatory effects on human neutrophils. Asian J Tradit Med; 7(4):159-167.

Mahato S, Singh A, Rangan L, Jana CK (2016). Synthesis, *in silico* studies and *in vitro* evaluation for antioxidant and antibacterial properties of diarylmethylamines: A novel class of structurally simple and highly potent pharmacophore. Eur J Pharm Sci; 88:202-209.

Mahli SS, Basu SP, Sinha KP and Banerjee NC (1989). Pharmacological effects of karanjin and pongamol from seed oil of *Pongamia pinnata*. Ind J of Anim Sci; 59:657-660.

Mani R, Natesan V (2018). Chrysin: Sources, beneficial pharmacological activities, and molecular mechanism of action. Phytochemistry; 145:187-196.

Manigauha A, Patel S (2010). Anticonvulsant study of *Pongamia pinnata* Linn. against pentylenetetrazole induced convulsion in rats. Int J Pharm and BioSci; 1:1-4.

Manigauha A, Patel S, Monga J, Ali H (2009). Evaluation of anticonvulsant activity of *Pongamia pinnata* Linn in experimental animals. Int J Pharm Tech Res; 1:1119-1121.

Manikannan M, Balamurugan R, Varatharajan R, Dinesh S, Manickan E (2011). Nitric oxide induce IL-10, a CD4+ T Helper Type-2 (Th-2) cytokines in human PBMC. J Pharma Biomed Sci; 7:1-6.

Mannina L, Luchinat C, Emanuele MC, Segre AL (1999). Acyl positional distribution of glycerol tri-esters in vegetable oils: a ^{13}C NMR study. Chem Phys Lipids; 103:47-55.

Maquelin K, Kirschner C, Choo-Smith LP, van den Braak N, Endtz HP, Naumann D, Puppels GJ (2002). Identification of medically relevant microorganisms by vibrational spectroscopy. J Microbiol Methods; 51:255-271.

Marcolongo JP, Mirenda M (2011). Thermodynamics of sodium dodecyl sulfate (SDS) micellization: An undergraduate laboratory experiment. J Chem Educ; 88:629-633.

Martins P, Jesus J, Santos S, Raposo LR, Roma-Rodrigues C, Baptista PV, Fernandes AR (2015). Heterocyclic anticancer compounds: Recent advances and the paradigm shift towards the use of nanomedicine's tool box. Molecules; 20: 16852-16891.

McNally DJ, Wurms KV, Labbe C, Belanger RR (2003). Synthesis of C-glycosyl flavonoid phytoalexins as a site-specific response to fungal penetration in cucumber. Physiol Mol Plant path; 63(6):293-303.

Meher N, Chowdhurya SR, Iyer PK (2016). Aggregation induced emission enhancement and growth of naphthalimide nanoribbons via J-aggregation: insight into disaggregation induced unfolding and detection of ferritin at the nanomolar level. J Mater Chem B; 4:6023-6031.

Mehri S, Karami HV, Hassani FV, Hosseinzadeh H (2014). Chrysin reduced acrylamide-induced neurotoxicity in both *in vitro* and *in vivo* assessments. Iran Biomed J; 18(2):101-106.

Michalak A (2006). Phenolic compounds and their antioxidant activity in plants growing under heavy metal stress. Polish J Environ Stud; 15(4):523-530.

Minakawa T, Toume K, Ahmed F, Sadhu SK, Ohtsuki T, Arai MA, Ishibashi M (2010). Constituents of *Pongamia pinnata* isolated in a screening for activity to overcome tumor necrosis factor-related apoptosis-inducing ligand-resistance. Chem Pharm Bull; 58:1549-1551.

Mirzoeva OK, Grishanin RN, Calder PC (1997). Antimicrobial action of propolis and some of its components: the effects on growth, membrane potential and motility of bacteria. Microbiol Res; 152:239-246.

Mishra A, Behera GB, Krishna MMG, Periasamy N (2001). Time-resolved fluorescence studies of aminostyryl pyridinium dyes in organic solvents and surfactant solutions. J Lumin; 92:175-188.

Molan AL, Waghorn GC, Min BR, McNabb WC (2000). The effects of condensed tannins from seven herbages on *Tricho strongylus* colubriformis larval migration *in vitro*. Folia Parasitol (Praha); 47(1):39-44.

Monici M, Mulinacci N, Baglioni P, Vincieri FF (1993). Flavone photoreactivity. UV-induced reactions in organic solvents and micellar systems. J Photochem Photobiol B; 20:167-172.

Moreira da Costa E, Filho JMB, Gomes do Nascimento T, Macedo RO (2002). Thermal characterization of the quercetin and rutin flavonoids. Thermochim Acta; 392-393:79-84.

Movasaghi Z, Rehman S, Rehman IU (2007). Raman spectroscopy of biological tissues. Appl Spectrosc Rev; 42:493-541.

Muthu C, Ayyanar M, Raja N, Ignacimuthu S (2006). Medicinal plants used by traditional healers in Kancheepuram district of Tamil Nadu, India. J Ethnobiol Ethnomed; 2:43-53.

Naeem K, Shah SS, Shah SWH, Monatsh GM (2000). Solubilization of cationic hemicyanine dyesin anionic surfactant micelles: a partitioning study. Monatshefte fur Chemie; 131:761-767.

Naseem B, Sabri A, Hasan A, Shah SS (2004). Interaction of flavonoids with organised molecular assemblies of anionic surfactant. Colloids Surf B Biointerfaces; 35(1):7-13.

Naumann D (2001). FT-infrared and FT-Raman spectroscopy in biomedical research. Appl Spectrosc Rev; 36:239-298.

Newman DJ, Cragg GM (2007). Natural products as sources of new drugs over the last 25 Years. J Nat Prod; 70(3):461-477.

Newman DJ, Cragg GM (2012). Natural products as sources of new drugs over the 30 years from 1981 to 2010. J Nat Prod; 75:311-335.

Newmann DJ, Cragg GM, Snader KM (2000). The influence of natural products upon drug discovery. Nat Prod Rep; 17:215-234.

Niehaus TD, Okada S, Devarenne TP, Watt DS, Sviripa V, Chappell J (2011). Identification of unique mechanisms for triterpene biosynthesis in *Botryococcus braunii*. Proc Natl Acad Sci USA; 108(30):12260-12265.

Nirmal SA, Malwadkar G, Laware RB (2007). Anthelmintic activity of *Pongamia glabra*. Songklanakar J Sci Technol; 29:755-757.

Oberlies NH, Kroll DJ (2004). Camptothecin and Taxol: Historic achievements in natural products research. J Nat Prod; 67:129-135.

Obmann A, Werner I, Presser A, Zehl M, Swoboda Z, Purevsuren S, Narantuya S, Kletter C, Glasl S (2011). Flavonoid C- and O-glycosides from the Mongolian medicinal plant *Dianthus versicolor* Fisch. Carbohydr Res; 346(13):1868-75.

Oliver JD (2010). Recent findings on the viable but non-culturable state in pathogenic bacteria. FEMS Microbiol Rev; 34:415-425.

Oonmetta-aree J, Suzuki T, Gasaluck P, Eumkeb G (2006). Antimicrobial properties and action of galangal (*Alpinia galanga* Linn.) on *Staphylococcus aureus*. LWT; 39:1214-1220.

Pan S, Litscher G, Gao S (2014). Historical perspective of traditional indigenous medical practices: the current renaissance and conservation of herbal resources. Evid Based Complement Altern Med; 2014:1-20.

Pandey AK, Bajpai AK, Kumar A, Pal M, Baboo V, Dwivedi A (2014). Isolation, identification, molecular and electronic structure, vibrational spectroscopic investigation, and anti-HIV-1 activity of karanjin using density functional theory. J Theor Chem Article ID 680987.

Pandey AK, Kumar S (2013). Chemistry and biological activities of flavonoids: an overview. Sci World J; Article ID 162750:16 pages.

Park HR, Daun Y, Park JK, Min Bark K (2013). Spectroscopic properties of flavonoids in various aqueous-organic solvent mixtures. Bull Korean Chem Soc; 34(1):211-220.

Parmar BS (1977). Karanja, *Pongamia glabra*, seed oil assay nergist for pyrethrins. Pyrethrum Post; 14:22-23.

Parveen M, Ghalib RM (2012). Flavonoids and antimicrobial activity of leaves of *Xylosma longifolium*. J Chil Chem Soc; 57(1): 989-991.

Pathak VP, Saini TR, Khanna RN (1983a). Isopongachromene, a chromenoflavone from *Pongamia glabra* seeds. Phytochemistry; 22:308-309.

Pathak VP, Saini TR, Khanna RN (1983b). Glabrachalcone, a chromenochalcone from *Pongamia glabra* seeds. Phytochemistry; 22:1303-1304.

Patil P, Prasad K, Nitin M, Rao KS (2010). Anti-ulcer and anti-secretory properties of the *Pongamia Pinnata* root extract with relation to anti-oxidant studies. Res J Pharm Biol Chem Sci; 1:235-244.

Peer WA, Murphy AS (2006). Flavonoids as signal molecules: Targets of flavonoid action. In Peer WA, and Murphy AS. (eds.), The Science of Flavonoids. Springer, New York; 239-268.

Pena Muniz MA, Ferreira Dos Santos MN, da Costa CE, Morais L, Lamarao ML, Ribeiro-Costa RM, Silva-Junior JO (2015). Physicochemical characterization, fatty acid composition, and thermal analysis of *Bertholletia excelsa* HBK oil. Pharmacogn Mag; 11(41):147-151.

Pengsuparp T, Cai L, Constant H, Fong H H, Lin L Z, Kinghorn A D, Pezzuto J M, Cordell G A, Ingolfsdottir K, Wagner H (1995). Mechanistic evaluation of new plant-derived compounds that inhibit HIV-1 reverse transcriptase. J Nat Prod; 58:1024-1031.

Perrett S, Whitfield PJ, Sanderson L, Bartlett A (1995). The plant molluscicide *Millettia thonningii* (Leguminosae) as a topical antischistosomal agent. J Ethnopharmacol; 47:49-54.

Philip T, Sharma DD (1997). *In vitro* evaluation of leaf and oil cake extracts of *Azadirachta indica* and *Pongamia glabra* on mulberry root rot pathogens. Indian J Sericulture; 36:150-152.

Phillipson JD (2001). Phytochemistry and medicinal plants. Phytochem; 56(3):237-243.

Philomena G (2011). Concerns regarding the safety and toxicity of medicinal plants-An overview. J Appl Pharm Sci; 1(6):40-44.

Pietta P (2000). Flavonoids as antioxidants. J Nat Prod; 63:1035-1042.

Plaper A, Golob M, Hafner I, Oblak M, Solmajer T, Jerala R (2003). Characterization of quercetin binding site on DNAgyrase. Biochem Biophys Res Commun; 306:530-536.

Popp J (2007). Identification of micro-organism by Raman spectroscopy. Newsroom 10:1117.

Posokhov Y, Erten S, Koz O, Anil H, Kirmizigul S, Icli S (2005). UV/VIS spectral properties of novel natural products from Turkish lichens. Int J Photoenergy; 7:27-35.

Prabha T, Dorababu M, Goel S, Agarwal PK, Singh A, Joshi VK, Goel RK (2009). Effect of methanolic extract of *Pongamia pinnata* Linn seed on gastro-duodenal ulceration and mucosal offensive and defensive factors in rats. Indian J Exp Biol; 47: 649-659.

Prabhu TM, Devakumar C, Sastry VRB, Agrawal DK (2002). Quantification of karanjin using high performance liquid chromatography in raw and detoxified Karanj (*Pongamia glabra* vent) seed Cake. Asian-Aust J Anim Sci; 15(3):416-420.

Punitha R, Manoharan S (2006). Antihyperglycemic and anti-lipidperoxidative effects of *Pongamia pinnata* (Linn.) Pierre flowers in alloxan induced diabetic rats. J Ethnopharmacol; 105:39-46.

Punitha R, Vasudevan K, Manoharan S (2006). Effect of *Pongamia pinnata* flowers on blood glucose and oxidative stress in alloxan induced diabetic rats. Indian J Pharmacol; 38:62-63.

Rabe P (1908). Information on the china alcaloide. VIII. Anouncement: The constitution of cinchonines. Ber Deutsch Chem Ges; 41:62-70.

Radwan RM (2007). Electron induced modifications in the optical properties of polypropylene. J Phys D Appl Phys; 40(2):374.

Raghavendra M, Trigunayat A, Singh RK, Mitra S, Goel RK, Acharya SB (2007). Effect of ethanolic extract of root of *Pongamia pinnata* (L) Pierre on oxidative stress, behavioral and hispathological alterations induced by cerebral ischemia- reperfusion and long-term hypoperfusion in rats. Indian J Exp Biol; 45:868-876.

Rameshthangam P, Ramasamy P (2007). Antiviral activity of bis(2-methylheptyl) phthalate isolated from *Pongamia pinnata* leaves against white spot syndrome virus of *Penaeus monodon* Fabricius. Virus Res; 126:38-44.

Ramiro E, Franch A, Castellote C, Andres-lacueva C, Izquierdo-pulido M, Castell M (2005). Effect of theobroma cacao flavonoids on immune activation of a lymphoid cell line. Br J Nutr; 93(6):859-66.

Rani N, Bharti S, Bhatia J, Nag TC, Ray R, Arya DS (2016). Chrysin, a PPAR-γ agonist improves myocardial injury in diabetic rats through inhibiting AGE-RAGE mediated oxidative stress and inflammation. Chem Biol Interact; 250:59-67.

Rao and Rao (1941). A note on glabrin, a new component of the seeds of *Pongamia glabra*. P Indian AS, Section A; 14(2):123-125.

Rao and Rao (1941). A note on glabrin, a new component of the seeds of *Pongamia glabra*. P Indian AS, Section A; 14(2):123-125.

Rao RR, Tiwari AK, Reddy PP, Babu KS, Ali AZ, Madhusudana K, Rao JM (2009). New furanoflavanoids, intestinal a-glucosidase inhibitory and free-radical (dpph) scavenging, activity from antihyperglycemic root extract of *Derris indica* (Lam.). Bioorg Med Chem Lett; 17:5170-5175.

Rao SLN, Ramachandran LK, Adiga PR (1963). The isolation and characterization of L-homoarginine from seeds of *Lathyrus sativus*. Biochemistry; 2:298-300.

Rao YK, Fang SH, Tzeng YM. (2005). Inhibitory effects of the flavonoids isolated from *Waltheria indica* on the production of NO, TNF-alpha and IL-12 in activated macrophages. Biol Pharm Bull; 28(5):912-915.

Rashid N, Abbasi MSA, Tahir MK, Yusof NM, Yamin BM (2008). Isolation and crystal structure of karanjachromene. Anal Sci; 24:21-22.

Rehman MU, Ali N, Rashid S, Jain T, Nafees S, Tahir M, Khan AQ, Lateef A, Khan R, Hamiza OO, Kazim S, Qamar W, Sultana S (2014). Alleviation of hepatic injury by chrysin in cisplatin administered rats: probable role of oxidative and inflammatory markers. Pharmacol Rep; 66(6):1050-1059.

Row LR (1952). New flavones from *Pongamia pinnata* (L.) Merr. Aust J Sci Res; 5:754-759.

Sachidanandham R, Gin K (2009). A dormancy state in nonspore-forming bacteria. Appl Microbiol Biotechnol; 81:927-941.

Sagar MK, Kumar P, Upadhyaya AK (2010). Anti-inflammatory and analgesic activities of methanolic extract of *Pongamia pinnata* stem bark. Int J Pharm Prof Res; 1:5-9.

Saha MM, Mallik UK, Mallik AK (1991). A chromenoflavone and two caffeic esters from *Pongamia glabra*. Phytochemistry; 30:3834-3836.

Saleem M (2009). Lupeol, A novel anti-inflammatory and anti-cancer dietary triterpene. Cancer Lett; 285(2):109-115.

Samuel AJSJ, Radhamani S, Gopinath R, Kalusalingam A, Vimala AGKA, Husain A (2009). *In vitro* screening of anti-lice activity of *Pongamia pinnata* leaves. Korean J Parasitol; 47:377-380.

Sancho MI, Almandoz MC, Blanco SE, Castro EA (2011). Spectroscopic study of solvent effects on the electronic absorption spectra of flavone and 7-hydroxyflavone in neat and binary solvent mixtures. Int J Mol Sci; 12(12):8895-8912.

Sander T, Freyss J, von Korff M, Reich JR, Rufener C (2009). OSIRIS, an entirely in house developed drug discovery informatics system. J Chem Inf Model; 49(2):232-46.

Sangwan, Rao DV, Sharma RA (2010). A review on *Pongamia pinnata* (L.) Pierre: A great versatile leguminous plant. Nat Sci; 8:130-139.

Santos OV, Correa NC, Soares FA, Gioielli LA, Costa CE, Lannes SC (2012). Chemical evaluation and thermal behavior of Brazil nut oil obtained by different extraction processes. Food Res Int; 47:253-258.

Sapna WE, Sindhu Kanya TC, Mamatha AM, Lokesh BR, Appu Rao AG (2007). Karanjin, a flavonoid inhibits lipoxygenases: Proceedings of the National Academy of Science India, CFTRI, Mysore, India.

Sarangi MK, Basu S (2011). Photophysical behavior of acridine with amines within the micellar microenvironment of SDS: a time-resolved fluorescence and laser flash photolysis study. Phys Chem Chem Phys; 13:16821-16830.

Sarkar M, Sengupta PK (1991). Influence of different micellar environments on the excited-state proton-transfer luminescence of 3-hydroxyflavone. Chem Phys Lett; 179:68-72.

Sarkar SD, Latif Z, Gray AI (2006). Natural products isolation methods and protocols, Second edition, Humana Press, Totowa, New Jersey.

Sarma AK, Konwer D, Bordoloi PK (2005). A comprehensive analysis of fuel properties of biodiesel from Koroch seed oil. Energy Fuels; 19:656-657.

Sasidharan S, Chen Y, Saravanan D, Sundram KM, Latha LY (2011). Extraction, isolation and characterization of bioactive compounds from plants' extracts. Afr J Tradit Complement Altern Med; 8(1): 1-10.

Sasirekha V, Umadevi M, Ramakrishnan V (2008). Solvatochromic study of 1,2-dihydroxyanthraquinone in neat and binary solvent mixtures. Spectrochim Acta A Mol Biomol Spectrosc; 69(1):148-155.

Satpati A, Senthilkumar S, Kumbhaka M, Nath S, Maity DK, Pal H (2005). Investigations of the solvent polarity effect on the photophysical properties of coumarin-7 Dye?; Photochem Photobiol; 81:270-278.

Schick MJ (1964). Effect of electrolyte and urea on micelle formation. J Phys Chem; 68(12):3585-3592.

Schwab W, Davidovich-Rikanati R, Lewinsohn E (2008). Biosynthesis of plant-derived flavor compounds. Plant J; 54(4):712-732.

Scott PT, Pregelj L, Chen N, Hadler JS, Djordjevic MA, Gresshoff PM (2008). *Pongamia pinnata*: An untapped resource for the biofuels industry of the future. Bioenerg Res; 1:2-11.

Semalty A, Semalty M, Kumar P, Mir SR, Ali M, Amin S (2012). Isolation and hypoglycemic activity of a novel *Pongamia* flavonyl flavonol from *Pongamia pinnata* pods. Int J Pharmacol; 8:265-270.

Sen S, Chakraborty R, De B (2011). Challenges and opportunities in the advancement of herbal medicine: India's position and role in a global context. J Herb Med; 1:7-75.

Sengupta B, Banerjee A, Sengupta PK (2005). Interactions of the plant flavonoid fisetin with macromolecular targets: Insights from fluorescence spectroscopic studies. J Photochem Photobiol B; 80:79-86.

Sengupta PK, Kasha M (1979). Excited-state proton transfer spectroscopy of 3-hydroxyflavone and quercetin. Chem Phys Lett; 68:382-385.

Shameel S, Usmanghani K, Ali MS, Ahmad VU (1996). Chemical constituents from the seed of *Pongamia pinnata* (L.) Pierre. Pakistan J Pharm Sci; 9:11-20.

Shameel S, Usmanghani K, Ali MS, Ahmad VU (1996). Chemical constituents from the seed of *Pongamia pinnata* (L.) Pierre. Pakistan J Pharm Sci; 9:11-20.

Sharmin E, Ashraf SM, Ahmad S (2007). Synthesis, characterization, antibacterial and corrosion protective properties of epoxies, epoxy-polyols and epoxy-polyurethane coatings from linseed and *Pongamia glabra* seed oils. Int J Biol Macromol; 40(5):407-422.

Shelar D, Shirote P. Nature product in drug discovery: back to future. Biomed Pharmacol J; 4:141-146.

Sheldrick GM (1997). SHELXL97 Program for crystal structure refinement. University of Gottingen, Germany.

Sheldrick GM (2004). SADABS. University of Gottingen, Germany.

Sherif OE (1997). Effect of solvents on the electronic absorption spectra of some substituted diarylformazans. Monatshefte fur Chemie; 128:981-990.

Shirley BW (1998). Flavonoids in seeds and grains: physiological function, agronomic importance and the genetics of biosynthesis. Seed Sci Res; 8:415-422.

Shoba FG, Thomas M (2001). Study of antidiarrhoeal activity of four medicinal plants in castor-oil induced diarrhea. J Ethnopharmacol; 76:73-76.

Sikarwar MS, Patil MB (2012). Antidiabetic activity of *Pongamia pinnata* leaf extracts in alloxan-induced diabetic rats. Int J Ayurveda Res; 1:199-204.

Sikkema J, De Bont JAM, Poolman B (1995). Mechanism of membrane toxicity on hydrocarbons. Microbiol Rev; 59:201-222.

Simonsen HT, Nordskjold JB, Smitt UW, Nyman U, Palpu P, Joshi P, Varughese G (2001). *In vitro* screening of Indian medicinal plants for antiplasmodial activity. J Ethnopharmacol; 74:195-204.

Sincock SA, Robinson JP (2001). Flow cytometric analysis of microorganisms. Methods Cell Biol; 64:511-537.

Singh KP, Dhakre G, Chauhan SVS (2005). Effect of mechanical and chemical treatments on seed germination in *Pongamia glabra* L. Seed Research; 33:169-171.

Singh R (2007). Influence of *Pongamia pinnata* seed extracts and fractions on biology of *Earias vittella*. Indian J Plant Prot; 35:68-72.

Singh RK, Pandey BL (1996). Anti-inflammatory activity of seed extracts of *Pongamia pinnata* in rat. Indian J Physiol Pharmacol; 40(4): 355-358.

Sisa M, Bonnet SL, Ferreira D, Van der Westhuizen JH (2010). Photochemistry of flavonoids. Molecules; 15:5196-5245.

Souza LC, Antunes MS, Filho CB, Del Fabbro L, de Gomes MG, Goes AT, Donato F, Prigol M, Boeira SP, Jesse CR (2015). Flavonoid chrysin prevents age-related cognitive decline via attenuation of oxidative stress and modulation of BDNF levels in aged mouse brain. Pharmacol Biochem Behav; 134:22-30.

Srinivasan K, Muruganandan S, Lal J, Chandra S, Tandan SK, Prakash VR (2001). Evaluation of anti-inflammatory activity of *Pongamia pinnata* leaves in rats. J Ethnopharmacol; 78:151-157.

Stanley FE, Warner AM, Schneiderman E, Stalcup AM (2009). Rapid determination of surfactant critical micelle concentrations using pressure-driven flow with capillary electrophoresis instrumentation. J Chromatogr A; 1216(47):8431-8434.

Steinbeck C (2004). Recent developments in automated structure elucidation of natural products. Nat Prod Rep; 21:512-518.

Stevens CM, Bush JA (1950). New synthesis of α-amino-ϵ-guanidino-*n*-caproic acid (homoarginine) and its possible conversion *in vivo* into lysine. J Biol Chem; 183:139-147.

Summons RE, Bradley AS, Jahnke LL, Waldbauer JR (2006). Steroids, triterpenoids and molecular oxygen. Philos Trans Royal Soc B; 361:951-968.

Sun Y, Bi S, Song D, Qiao C, Mu D, Zhang H (2008). Study on the interaction mechanism between DNA and the main active components in *Scutellaria baicalensis* Georgi. Sens Actuators B; 129:799-810.

Swain T (1977). Secondary compounds as protective agents. Annu Rev Plant Physiol; 28:479-501.

Swain T (1977). Secondary compounds as protective agents. Annu Rev Plant Physiol; 28:479-501.

Swaminathan R, Krishnamoorthy G, Periasamy N (1994a). Similarity of fluorescence lifetime distributions for single tryptophan proteins in the random coil state. Biophys J; 67:2013-2023.

Swaminathan R, Periasamy N, Udgaonkar JB, Krishnamoorthy G (1994b). Molten globule-like conformation of barstar: a study by fluorescence dynamics. J Phys Chem; 98:9270-9278.

Talapatra SK, Mallik AK, Talapatra B (1980). Pongaglabol, a new hydroxyfuranoflavone, and aurantiamideacetate, a dipeptide from the flowers of *Pongamia glabra*. Phytochemistry; 19:1199-1202.

Talapatra SK, Mallik AK, Talapatra B (1980). Pongaglabol, a new hydroxyfuranoflavone, and aurantiamideacetate, a dipeptide from the flowers of *Pongamia glabra*. Phytochemistry; 19:1199-1202.

Talapatra SK, Mallik AK, Talapatra B (1982). Isopongaglabol and 6-methoxy isopongaglabol, two new hydroxyl furanoflavones from *Pongamia glabra*. Phytochemistry; 21:761-766.

Tamrakar AK, Yadav PP, Tiwari P, Maurya R, Srivastava AK (2008). Identification of pongamol and karanjin as lead compounds with antihyperglycemic activity from *Pongamia pinnata* fruits. J Ethnopharmacol; 118:435-439.

Tan CH, Huang ZJ, Huang XG (2010). Rapid determination of surfactant critical micelle concentration in aqueous solutions using fiber-optic refractive index sensing. Anal Biochem; 401:144-147.

Tanaka T, Iinuma M, Yuki K, Fujii Y, Mizuno M (1992). Flavonoids in root bark of *Pongamia pinnata*. Phytochemistry; 31:993-998.

Tanaka T, Iinuma M, Yuki K, Fujii Y, Mizuno M (1992). Flavonoids in root bark of *Pongamia pinnata*. Phytochemistry; 31:993-998.

Tapas AR, Sakarkar DM, Kakde RB (2008). Flavonoids as nutraceuticals: A review. Trop J Pharm Res; 7(3):1089-1099.

Taylor PW (2013). Alternative natural sources for a new generation of antibacterial agents. Int J Antimicrob Agents; 42(3):195-201.

Tehrani-Bagha AR, Holmberg K (2013). Solubilization of hydrophobic dyes in surfactant solutions. Materials; 6:580-608.

Trela BC, Waterhouse AL (1996). Resveratrol:Isomeric molar absorptivities and stability. J Agric Food Chem; 44(5):1253-1257.

Trevors JT, Elsas JD, Bej AK (2012). The molecularly crowded cytoplasm of bacterial cells: dividing cells contrasted with viable but non-culturable (VBNC) bacterial cells. Curr Issues Mol Biol; 15:1-6.

Tulumello DV, Deber CM (2009). SDS micelles as a membrane-mimetic environment for transmembrane segments. Biochem; 48:12096-12103.

Tyler VE (2000). Herbal medicine: From the past to the future. Public Health Nutr; 3:447-452.

Vadivel V, Biesalski HK (2011). Contribution of phenolic compounds to the antioxidant potential and type ii diabetes related enzyme inhibition properties of *Pongamia pinnata* L. Pierre seeds. Process Biochem; 46:1973-1980.

Vargas JE, Puga R, de Faria Poloni J, Timmers LFSM, Porto BN, de Souza ON, Bonatto D, Pitrez PMC, Stein RT (2015). A network flow approach to predict protein targets and flavonoid backbones to treat respiratory syncytial virus infection. Biomed Res Int; 2015: 301635.

Varma YT, Joshi S, Pant DD (2015). Effect of nanosize micelles of ionic and neutral surfactants on the photophysics of protonated 6-methoxyquinoline: Time-resolved fluorescence study. Spectrochim Acta A Mol Biomol Spectrosc; 138:818-826.

Venditti A, Bianco A (2018). Sulfur-containing secondary metabolites as neuroprotective agents. Curr Med Chem; 25:1.

Verpoorte R (2000). Pharmacognosy in the new millennium: lead finding and biotechnology. J Pharm Pharmacol; 52:253-262.

Vijaya K, Ananthan S, Nalini R (1995). Antibacterial effect of theaflavin, polyphenon 60 (*Camellia sinensis*) and *Euphorbia hirta* on *Shigella* spp.- a cell culture study. J Ethnopharmacol; 49:115-118.

Vijesh AM, Isloor AM, Telkar S, Arulmoli T, Fun HK (2013). Molecular docking studies of some new imidazole derivatives for antimicrobial properties. Arab J Chem; 6:197-204.

Vismaya, Belagihally SM, Rajashekhar S, Jayaram VB, Dharmesh SM, Thirumakudalu SKC (2011). Gastroprotective properties of karanjin from karanja (*Pongamia pinnata*) seeds; role as antioxidant and H+, K+-ATPase inhibitor. Evid Based Complement Alternat Med; 2011:747246

Vismaya, Eipeson WA, Manjunatha JR, Srinivas P, Kanya TCS (2010). Extraction and recovery of karanjin: A value addition to karanja (*Pongamia pinnata*) seed oil. Ind Crop Prod; 32:118-122.

Voicescu M, Ionescu S, Gatea F (2014). Photophysical properties of some flavones probes in homogeneous media. J Fluoresc; 24(1):75-83.

Voicescu M, Ionescu S, Gatea F (2014). Photophysical properties of some flavones probes in homogeneous media. J Fluoresc; 24(1):75-83.

Vranova V, Rejsek K, Skene KR, Formanek P (2011). Non-protein amino acids: plant, soil and ecosystem interactions. Plant Soil; 342:31-48.

Wagh P, Rai M, Deshmukh SK, Durate MCT (2007). Bioactivity of oils of *Trigonella foenum-graecum* and *Pongamia pinnata*. Afri J Biotechnol; 6:1592-1596.

Wang M, Lamers RJ, Korthout HA, van Nesselrooij JH, Witkamp RF, van der Heijden R, Voshol P, Havekes LM, Verpoorte R, van der Greef J (2005). Metabolomics in the context of

systems biology: bridging traditional Chinese medicine and molecular pharmacology. Phytother Res; 19:173-182.

Warrier PK, Nambiar VPK, Ramakutty C (1993). Indian medicinal plants: A compendium of 500 species. Orient Longman, India.

Webb AG (2005). Nuclear magnetic resonance coupled microseparations. Magn Reson Chem; 43:688-696.

Williams R, Phillips JN, Mysels KJ (1955). The critical micelle concentration of sodium lauryl sulphate at 25°C. Trans Faraday Soc; 51:728-737.

Willstatter R, Muller W (1898). Ketones of the tropine group. XII. Constitution of ecgonine. Ber Deutsch Chem Ges; 31:2655-2669.

Wink M (2015). Modes of action of herbal medicines and plant secondary metabolites. Medicines (Basel); 2(3):251-286.

Woodman OL, Chan ECH (2004). Vascular and antioxidant actions of flavonols and flavones. Clin Exp Clin Exp Pharmacol Physiol; 3:786-790.

Wu S, Liu B, Zhang Q, Liu J, Zhou W, Wang C, Li M, Bao S, Zhu R (2013). Dihydromyricetin reduced Bcl-2 expression via p53 in human hepatoma HepG2 cells. PloS One; 8(11): e76886.

Xu HS, Roberts N, Singleton FL, Attwell RW, Grimes D, Colwell RR (1982). Survival and viability of non-culturable *Escherichia coli* and *Vibrio cholerae* in the estuarine and marine environment. Microb Ecol; 8:313-23.

Xu HX, Lee SF (2001). Activity of plant flavonoids against antibiotic-resistant bacteria. Phytother Res; 15:39-43.

Yadav PP, Ahmad G, Maurya R (2004). Furanoflavonoids from *Pongamia pinnata* fruits. Phytochemistry; 65:439-443.

Yang B, Huang J, Xiang T, Yin X, Luo X, Huang J, Luo F, Li H, Li H, Ren G (2014). Chrysin inhibits metastatic potential of human triple-negative breast cancer cells by modulating matrix metalloproteinase-10, epithelial to mesenchymal transition, and PI3K/Akt signaling pathway. J Appl Toxicol; 34(1):105-112.

Yang B, Kotani A, Arai K, Kusu F (2001). Estimation of the antioxidant activities of flavonoids from their oxidation potentials. Anal Sci; 17(5):599-604.

Yasuda K, Kizu H, Yamashita T, Kameda Y, Kato A, Nash RJ, Fleet GWJ, Molyneux RJ, Asano N (2002). New sugar-mimic alkaloids from the pods of *Angylocalyx pynaertii*. J Nat Prod; 65:198-202.

Yokoo T, Takata R, Yan J, Matsumoto F, Teraishi M, Okumoto Y, Jander G, Mori N (2015). Identification of β-phenylalanine as a non-protein amino acid in cultivated rice, *Oryza sativa*. Commun Integr Biol; 8(5):e1086045.

Yu XM, Phan T, Patel PN, Jaskula-Sztul R, Chen H (2013). Chrysin activates Notch1 signaling and suppresses tumor growth of anaplastic thyroid carcinoma *in vitro* and *in vivo*. Cancer; 119(4):774-81.

Zhang H, Machutta CA, Peter J, Tonge (2010). Fatty acid biosynthesis and oxidation, Stony Brook University, Stony Brook, NY, USA.

Zhang Z, Li G, Szeto SSW, Chong CM, Quan Q, Huang C, Cui W, Guo B, Wang Y, Han Y, Michael Siu KW, Yuen Lee SM, Chu IK (2015). Examining the neuroprotective effects of protocatechuic acid and chrysin on *in vitro* and *in vivo* models of Parkinson disease. Free Radic Biol Med; 84:331-343.

Zhao X, Zhong J, Wei C, Lin CW, Ding T (2017). Current perspectives on viable but non-culturable state in foodborne pathogens. Front Microbiol; 8:580.

Zhao XD, Sun CJ, Yao QQ, Li WB (2010). Synthesis of 3-hydoxyflavone fluorescent probes and study of their fluorescence properties. Chin Chem Lett; 21:529-532.

Zhao YH, Abraham MH, Le J, Hersey A, Luscombe CN, Beck G, Sherborne B, Cooper I (2002). Rate-limited steps of human oral absorption and QSAR studies. Pharm Res; 19:1446-1457.

Zhu WL, Puah CK, Tanb XJ, Jiang HL, Chen KX, Ji RY (2000). A density functional theory (DFT) calculation of the geometry and vibrational spectrum of natural product, ginkgolide B. J Mol Struc Theochem; 528:193-198.

Zsila F, Bikadi Z, Simonyi M (2003). Probing the binding of the flavonoid, quercetin to human serum albumin by circular dichroism, electronic absorption spectroscopy and molecular modelling methods. Biochem Pharmacol; 65:447-456.

PUBLICATION

Published:

1. **Singh A**, Jahan I, Sharma M, Rangan L, Khare A, Panda AN (2016). Structural characterization, *in silico* studies and *in vitro* antibacterial evaluation of a furanoflavonoid from Karanj. ***Planta Med Lett***; 3(04):e91-e95.
2. Ramesh AM, **Singh A**, Shelke RG, Scott PT, Gresshoff PM, Rangan L (2016). Identification of two genes encoding microsomal oleate desaturases (FAD2) from the biodiesel plant *Pongamia pinnata* L. ***Tress Struct Funct***; 30(4):1351-1360.
3. Mahato S[*], **Singh A**[*], Rangan L, Jana CK (2016). Synthesis, *in silico* studies and *in vitro* evaluation for antioxidant and antibacterial properties of diarylmethylamines: A novel class of structurally simple and highly potent pharmacophore. ***Eur J Pharm Sci***; 88:202-209. ([*]Equal contribution)
4. Baruah PK, **Singh A**, Rangan L, Sharma AK, Khare A (2016). Comparison of surface enhanced Raman scattering of silver and copper nanoparticles on furanoflavanoid karanjin. 13th International Conference on Fiber Optics and Photonics, 4-8 Dec 2016, Kanpur. https://doi.org/10.1364/PHOTONICS.2016.Th4E.2
5. Baruah PK, **Singh A**, Jahan I, Rangan L, Panda AN, Sharma AK, Khare A (2017). Surface-enhanced Raman scattering from copper nanoparticles treated furanoflavonoid karanjin. ***Adv Mater Lett***; 8(10):971-976.
6. Baruah PK, **Singh A**, Rangan L, Sharma AK, Khare A (2018). Optimization of copper nanoparticles synthesized by pulsed laser ablation in distilled water as a viable SERS substrate for karanjin. ***Mater Chem Phys***. (***Accepted***)

Manuscript under review:

1. **Singh A**, Rangan L, Panda AN, Mitra S (2018). Glabrin, a complex unnatural amino acid as antimicrobial product from industrially useful crop *Pongamia pinnata*. ***Phar Rep*** (***Under review***).
2. Baruah PK, **Singh A**, Rangan L, Sharma AK, Khare A (2018). Elucidation of size, structure, surface plasmon resonance and photoluminescence of Ag nanoparticles synthesized by pulsed laser ablation in distilled water and its viability as SERS substrate. ***Colloids Surf A Physicochem Eng Asp*** (***Under review***).

3. **Singh A**, Rangan L, Swaminathan R (2018). UV-Visible absorption and fluorescence spectra of karanjin in different solvents and solvent mixtures (***Communicated***).

PARTICIPATION

Conference:

1. **Singh A**, Rangan L (2013). Isolation, purification, characterization and pharmacological study of bioactive compounds from the seeds of *Pongamia pinnata*. 5th Indian Youth Science Congress, 6-9 Nov 2013, Visva-Bharati University, Shantiniketan, Bolpur.
2. **Singh A**, Rangan L, Khare A, Panda AN (2015). Characterization of bioactive karanjin from seeds of Karanj. International Conference on Medicinal Plants and Herbal Drugs for Human Welfare (ICMP-2015), 28-30 Jan 2015, University of Madras, Chennai, pp 77. (***Awarded as Best Poster***)
3. Rangan L, **Singh A**, Shelke RG, Das R, Ramesh AM, Kesari V, Scott P, Gresshoff P (2015). New positives of biotech research in renewable energy resources-Success story of *Pongamia*. *In*: Proceedings National Seminar on Biofuel A Search for New Fire SIBBR&D, pp 22-25.
4. **Singh A**, Sharma M, Rangan L, Panda AN (2016). Structural characterization and flow cytometric investigation of glabrin, a complex cyclic amino acid from seeds of Karanja. 3rd International Congress Society for Ethnopharmacology, Ethnopharmacology and Evaluation of Medicinal Plants – Global Perspective, 19-21 Feb 2016, Pt. Ravishankar Shukla University (PRSU), Raipur. Peered Reviewed Journal of Ravishankar University, 29(1) Special Issue: 161.
5. Mahato S, **Singh A**, Rangan L, Jana CK (2016). Synthesis, *in silico* studies and *in vitro* evaluation for antioxidant and antibacterial properties of diarylmethylamines: A novel class of structurally simple and highly potent pharmacophore. 9th TCS Annual Event and Flow Cytometry Workshop on "Flow Applications in Basic, Applied and Clinical Biology (FABACTCS 2016)", 3-5 Nov 2016, IIT Guwahati and Dr. B. Barooah Cancer Institute, Guwahati. (***Awarded 2nd best poster***)
6. **Singh A**, Chakrabartty I, Sanjana S (2016). Isolation, identification, vibrational spectroscopic investigation and biological activity of secondary metabolites of medicinal plants of Northeast India, 10 March 2016, IIT Guwahati.

7. Mahato S, **Singh A**, Rangan L, Jana CK (2016). Synthesis, *in silico* studies and *in vitro* evaluation for antioxidant and antibacterial properties of diarylmethylamines: A novel class of structurally simple and highly potent pharmacophore. Research Conclave 2017, pp 98, 16-19 March 2017, IIT Guwahati.
8. **Singh A**, Rangan L, Swaminathan R (2017). UV-Visible absorbance and fluorescence of KARANJIN in different solvents and solvent mixtures. National Workshop on "Fluorescence and Raman Spectroscopy (FCS 2017)", 17-21 Dec 2017, IIT Guwahati.

Workshop:

1. Participated in workshop on Basic and Clinical Flow Cytometry Course" organized by Cachar cancer Hospital and research centre, Silchar and IIT Guwahati, Assam, 2014.
2. Participated in workshop on "Flow cytometry data analysis" organized by Department of Biosciences and Bioengineering, IIT Guwahati, 23-24 Jan, 2015.
3. Organized workshop on "Flow cytometry" in Research Conclave 2017 at Department of Biosciences and Bioengineering, IIT Guwahati, 19 March, 2017.
4. Participated in Sensitization Workshop on "Technological Empowerment of Women" organized by Department of Biosciences and Bioengineering, IIT Guwahati, 3-4 Nov, 2017.
5. Participated in workshop on "Computer Aided Drug Design for Human Pathogens (CADDHP) An International Seminar cum Workshop" organized by Departments of Molecular Biology and Biotechnology, Chemical Sciences and Computer Sciences and Engineering, Tezpur University, 12-17 Feb, 2018.